Extensive Air Showers

Madani, Jamal Hamzah

Extensive Air Showers

BY

Jamal Hamzah Madani, B.Sc.
(King Abdulaziz University, Jeddah)

A thesis submitted to the University of Durham
for the degree of Doctor of Philosophy

Department of Physics,
Durham University, U.K.

August, 1987.

TO MY PARENTS

CONTENTS

Abstract

A computerised 8-channel data acquisition unit constructed by the Durham University Microprocessor Unit is described and the calibration of this unit is given in chapter 2. A test for the data acquisition unit using a Geiger-Muller cosmic ray telescope is described in Chapter 3. In Chapter 4 the main experiment is described. Two plastic scintillation counters each of 0.4 m^2 area and 5cm thick in coincidence were used in this experiment to measure the density spectrum of electrons at sea level in the range 20 - 600 electrons per m^2. The microcomputer data acquisition system is employed to record the scintillator pulse heights. The measured integral density spectrum has been used to calculate the integral size spectrum at sea level.

A brief discription of the theory of electron-photon cascades and the formation of extensive are showers is give in Chapter 5.

A FORTRAN program which uses Monte Carlo method to simulate extensive air showers generated by high energy protons with a given energy is described in Chapter 6. Using the relation between primary energy and average number of electrons arriving at sea level found by Monte Carlo calculation in Chapter 6 an estimate has been made of the integral primary energy spectrum in the range 10^{14}-10^{16}eV, and the result is given in Chapter 7.

Acknowledgements

I am heavily indebted to Dr. F. Ashton for his excellent supervision of this work. I would like to gratefully acknowledge his guidance, assistance, encouragement, and invaluable suggestion throughout the course of this work.

I whish to thank Prof. A.W. Wolfendale and Prof. B.H. Bransden for the use of Physics Department's facilities. I am gratfull to all the members of the group for many constructive discussions. In particular I would like to thank my colleague Mr. T.A. Abbas for his friendly co-operation and assistance. I whish to thank Mr. M. Kolar of the microprocessor centre for his help. The staff of the electronics workshop and the staff of the main workshop are thanked for their help. I would like to thank the staff of the computer centre for their help.

Financial support from King Abdulaziz University, in Jeddah, is gratefully acknowledged. I would like to thank the Saudi Arabian Educational office in London for taking care of my affairs in the U.K.

Finally, from the bottom of my heart I would like to thank my wife for her patience, endurance, and encouragement during this research.

Chapter One

Introduction

1.1 Introduction

By cosmic rays, we mean high energy particles originating in extra-terrestrial sources. A cosmic ray physicist may use his cosmic ray telescope to make a direct detection of these particles as they bombard our planet from all directions. However, one may infer their presence by some indirect astrophysical arguments.

The majority of these particles are protons, but other types of particles also exist.

The discovery of cosmic rays in 1912 activated man's resources to obtain an understanding of what they are, their physical properties and where they come from. The study of cosmic rays provided imformation and helped to form theories of nuclear physics and elementary particle physics. Because the energy spectrum of cosmic rays extends to 10^{20}eV, physicists used them in high energy interaction experiments and to look for new particles. Today the status of cosmic rays as a major entity in both physics and astrophysics is fully established.

1.2 A short history of cosmic ray physics.

It was found about 1900 that electroscopes kept discharging even if they were kept in the dark well away from sources of

natural radioactivity. It was later shown by Rutherford that most of the ionization was due to natural radioactivity, either in rocks or radioactive contamination of the equipment. The real breakthrough came 1912 when Hess and Kolhorster made manned balloon ascents. By late 1912 Hess had flown to 5 km and then Kolhorster by 1914 had made ascents to 9 km. Hess and Kolhorster found the startling result that the average ionization increased from its sea-level value above about 1.5 km altitude. This is clear evidence that there is 'radiation' coming in from above the Earth's atmosphere. Further confirmation came from Millikan and Cameron (1926) who measured the absorption of the radiation in water and found it to be similar to that in an equivalent mass of air. This indicated a radiation which is absorbed by air on its downward path. It was Millikan who first called the radiation 'cosmic radiation'.

In 1929 Skobelzyn noted cloud chamber tracks which were undeflected in his experiment aimed to measure the energies of gamma-particles of radioactive origin. Because they were undeflected they must have had energy greater than 15 MeV. He interpreted the particles as the Compton recoil electrons secondary to the 'Hess ultra-gamma-radiation'. In the same year Bothe and Kolhorstr made use of the invention of the Geiger-Muller counter, which permitted the counting of individual ionizing particles passing through the detector. They found that when two Geiger-Muller counters were placed one above the other, simultaneous discharges of the two detectors occurred very frequently, indicating that charged particles of sufficient

penetrating power to pass through both of the two counters were very common. Bothe and Kolhorster placed gold and lead up to 4 cm thick between the counters and measured the attenuation of the number of coincidences when the absorber was introduced. The mass absorption coefficient agreed very closely with that of the atmospheric attenuation. The experiment strongly suggested that the radiation is corpuscular since it is most unlikely that seperate secondary electrons could be ejected into the two detectors. The authors realized that energies of 10^9 to 10^{10} eV would be needed to give charged particles such long ranges in matter.

It had been noted by Auger et al (1937) and others that 'showers' of particles occurred in the absence of absorber (Rossi in 1935 discoverd this phenomenon in absorbers). This was taken to mean that showers could be initiated in the atmosphere. These were called 'extensive air showers'. The physics of this phenomenon is discussed in Chapter 5.

1.3 Cosmic Rays at the Top of Atmosphere

The total flux of relativistic cosmic rays outside the earth's atmosphere is of the order 2 protons $(m^2\ s\ sr\ MeV)^{-1}$, corresponding to an energy density of about 1 eV/cm^3 (Longair 1981). These particles have very small anisotropy [for example,0.06% for particles with energy around 10^{13} eV (Alexeenko et al 1981)]. As the energy increases the anisotropy increases (see fig.5 in Hillas 1984) and for very high energy (> $3x10^{19}$eV) there is a large excess of particles from high northern galagtic

latitudes (Hillas 1984).

We can classify the primary cosmic rays into three groups, nuclear (ie nuclei), electronic (ie electrons and positrons) and electromagnetic (X-rays and gamma-rays).

1.3.1 Energy spectra of primary cosmic rays

The vast majority of primary cosmic rays are hydrogen nuclei (ie protons). Figure 1.1 shows the characteristic spectra of cosmic hydrogen and helium nuclei from the non-relativistic to the relativistic region. The spectra were estimated from measurements made at solar minimum and so should be least effected by solar modulation.

At relativistic energies the spectrum has a power law form and experiments at higher energies show that the power law form of the spectrum continues up to above 10^{15}eV. The spectrum in the relativistic range can be described well by a differential energy spectrum of the form

$$N(E)\, dE = K\, E^{-2.6} dE \ .$$

The cut-off to the spectrum at low eneregies, $E < 1$ GeV per nucleon, must be investigated more closely. We will find that it is almost certainly due to the effect of the solar wind preventing low energy cosmic rays reaching the Earth.

The spectra of other elements have a similar form to those of hydrogen and helium nuclei. It can be seen that all these spectra are of the same general form: a cut-off at low energies and power law form in the relativistic region.

At the very lowest energies, around 10 MeV per nucleon, the

spectra of protons and helium nuclei seem to be turning up. It is in this very low energy region that solar cosmic ray make a contribution to the total flux but this is highly variable. However, the composition of these low energy cosmic rays includes rare elements such as B,Na and Al in the proportion found in the cosmic rays rather than in the Sun, which may be considered as evidence that this is a real feature of the spectrum of galactic cosmic rays.

For energies greater than $3x10^{15}$eV, the exponent changes to 3.0 (differential spectrum). This 'knee' has been attributed to a number of phenomena. One suggestion is that this is due to the inability of the galactic magnetic fields to contain various types of particles as their containment rigidities are exceeded. However there is evidence that the proton spectrum is steeper at higher rigidities than that for heavy nuclei (Hillas 1979).

On the far end of the cosmic ray energy spectrum, Greisen (1966) and others suggested that there should be cut-off in the spectrum at around 10^{20} eV. This suggestion came after the discovery of the 2.7 K radiation field in 1965. If the highest energy cosmic rays were of universal origin then interaction of the particles with the 2.7 K radiation field would severely modify their energy spectrum. The high energy particles 'see' the microwave photons strongly blue-shifted (Lorentz factor 10^{8}-10^{11}) and pion production by photons sets in above 4×10^{19} eV. So, if cosmic rays with energy above 4×10^{19} eV are observed then we can be confident that their source is relatively local [not further than 3×10^{8} light years]. At Haverah Park about 200 showers

produced by primaries of 10^{19} eV and above have been observed (see Watson 1986) but discordant results were reported by Yakutsk, results which agree with a Greisen cut-off.

1.3.2 Abundances of elements in Cosmic Rays

Apart from the dominant proton component, the primary cosmic radiation contains heavier nuclei. Figure 1.2 (after Lund 1984) shows the relative abundances of elements in cosmic rays and relative galactic abundances. The two curves are normalized so as to correspond to the same abundance of hydrogen. What the local galactic abundances are telling us is the abundances with which elements can be manufactured in stars by normal nuclear processes. It is to be expected that we would not get many of the light elements (Li,Be,B) because they are very fragile nuclei and there are not many ways of making them in the stellar nucleosynthesis. The abundance variation from element to element in the cosmic radiation is much smaller than that in the local galactic sample. The lack of strong abundance variations in the arriving cosmic rays finds a simple explanation, it is believed that this is due to the spallation of heavier nuclei as they pass through the small amount of matter between their source and the Earth. On this basis, the amount of this matter has been estimated as about 5 g cm^{-2} of hydrogen and hence the average travelling time of cosmic ray nuclei is around three million years (Longair 1981) which is significantly smaller than the age of the Universe. Two other features are to be noticed. First that the odd-even effect in the relative stabilities of nuclei according to atomic number is also present in cosmic rays. The second, for elements heavier

than iron there is a good agreement between the rate at which the relative abundances decrease as the atomic number increases.

1.4 Origin of cosmic rays

The fundamental question about cosmic rays is how and where the particles get their tremendous energies. It was first suggested that cosmic rays were created in a single gigantic event. But the existence of heavy nuclei in cosmic rays excludes the possibility that this event was the big-bang because it seems that the radiation from this primeval system would have been in the form of gamma rays, which have suffered an enormous red-shift (Hillas 1972, page 79). Cosmic ray creation in a single event contradicts the experimental evidence based on cosmic ray induced radioactivity especially in meteorites, which tends to indicate that the cosmic ray density has been almost constant over the past 10^9 years (Wolfendale 1978). Furthermore, one can use the relative abundance of radioactive ^{10}Be (half-life = 1.6×10^6 years) produced in the fragmentaion process of heavier cosmic rays, as a cosmic ray clock. Garcia-Munoz et al (1977) found that the ratio of $[^{10}Be]/[^{7}Be+^{9}Be+^{10}Be] = 0.028$ corresponds to a 'confinement age' of 1.7×10^7 years.

At this point we can say that we look for a generation mechanism still at work. There are two major views on that mechanism. The first view originally put forward by Fermi (1949a), holds that cosmic rays are injected into interstellar space and accelerated primarily through collisions with magnetised moving gas clouds. Another mechanism for acceleration is the shock wave

from a supernova explosion.

The second view, and the new one, is the notion of discrete sources, with interstellar space acting only as a diffusive medium. Many types of source have been proposed. If there are discrete sources of cosmic rays it would be possible to pin-point them. But all charged cosmic ray particles are deflected by the magnetic fields in interstellar space, thus the direction of arrival of a cosmic ray particle does not point at the source of this particular cosmic ray particle. However, observing neutral particles could be the answer. Dzikowski et al. at Lodz (1983) reported an excess of air showers detected form the general direction of the Crab Nebula at $>10^{15}$eV (about 10^3 times the energy of previous known gamma-ray sources); however, the Akeno and Haverah Park experiments have failed to see such an excess [Hayashida et al.(1981) and Lambert et al.(1983)]. Samorski and Stamm at Kiel (1983) discoverd that the X-ray binary, Cygnus X-3, emits 10^{16} eV particles, presumably gamma-rays, which are detected at one point of the 4.8-hr binary period. MacKeown and Weekes (1985) believe that Cygnus X-3 is one of the cosmic ray sources. They argued that the gamma rays are only a small part of the total flux of cosmic radiation from Cygnus X-3. The various theoretical models of the object agree that the gamma rays are probably emitted in high-energy interactions of charged nuclei, mainly protons in the source region. These authors estimated the energy flux of charged cosmic ray particles which are emitted from Cygnus X-3 as $6x10^{38}$ ergs/second, 30 times as much energy flux as gamma ray energy flux.

Figure 1.3 (after Watson 1984) gives a summary of the problem of the origin of the cosmic rays. However, this is not final and there are many arguments about it. One may notice that in Figure 1.3 that extragalactic sources are considered for the most energetic cosmic rays, because our galaxy fails to contain them by its magnetic field. Extragalagtic cosmic rays from the local supurcluster have been shown to be consistent with present observations (Wdowczyk and Wolfendale 1979). The problem whether the cosmic ray flux is confined to the galaxy, in whole or in part, is still open for question. Longair (1981) tackled this problem and then gave a summary which is reproduced here as table 1.1. He mentioned that the cosmic ray electrons must be galactic and that all protons and nuclei are isotropic, and he considered these two arguments as 'absolutely concrete' ones. Then he deduced that a single source is not adequate to explain all the cosmic rays.

1.5 Significance of Cosmic Ray Studies

The subject of cosmic rays is a very wide one, having close links with many branches of physics and astrophysics. High energy physics proper had its foundation in experiments with cosmic rays as the only available source of very energetic particles up to the advent of particle accelerators in the early 1950's. After that elementary particle physics and cosmic ray physics began to drift apart. Many elementary particles were discovered by cosmic ray experiments, notably the identification of positrons (Anderson 1933), charged muons (Anderson and Neddermeyer 1938 and Street and

Stevenson 1937), charged pions (Lattes et al 1947), and kaons (Rochester and Butler 1947). The evidence for the existence of the neutral pion was obtained simultaneously in 1950 by Carlson et al (1950) in cosmic ray studies and by Bjorklund et al (1950) at Berkely. Exotic particles like quarks, tachyons and fire-balls are being sought in cosmic rays.

Cosmic rays at energies in excess of 10^{12}eV will remain an important source for very high energy nuclear physics. For example, a comparison of ground level observations with the primary spectrum can be used to extend interaction models to above accelerator energies.

The studies of the origin of cosmic rays, the mechanism by which particles gained their energy and the propagation of cosmic rays enrich astrophysics with experimental observations and theortical ideas. High energy astrophysics is an important branch of astrophysics and has strong links with other branches of this science, because cosmic rays can provide information on the interstellar medium, magnetic fields and the nature of their sources as well as being a probe into the far reaches of our galaxy and beyond.

Evidence	Galactic Theories — Confinement Volume: Disc	Galactic Theories — Confinement Volume: Halo	Extragalactic Theories — Confinement Volume: Supercluster	Extragalactic Theories — Confinement Volume: All Space
1 Cosmic ray electrons	Consistent	Probably consistent	Inconsistent	Inconsistent
2 Chemical composition of light cosmic ray nuclei	Consistent	Consistent	Consistent	Consistent
3 Spectra of cosmic ray sources	Consistent	Consistent	Consistent	Consistent
4 Cosmic ray clocks	Consistent	Consistent	Inconclusive	Inconclusive
5 Transuranic elements	Consistent	Consistent	Inconclusive	Inconclusive
6 γ-rays from π° decays	Consistent	Consistent	Inconclusive	Inconclusive
7 Isotropy of cosmic rays				
10^{11}eV	Consistent	Consistent	Consistent	Consistent
10^{15}eV	Consistent	Consistent	Consistent	Consistent
$\geq 10^{19}$eV	Inconsistent	Inconsistent	Consistent	Consistent
8 Photo-pion and photo-pair production	Consistent	Consistent	Probably consistent	Probably inconsistent for protons. Consistent for Fe nuclei
9 Energy sources for cosmic rays	Consistent with supernovae	Consistent with supernovae	Very powerful sources needed	Extremely powerful sources needed

Table 1.1 : Summary of cosmic ray origin theories (after Longair 1981)

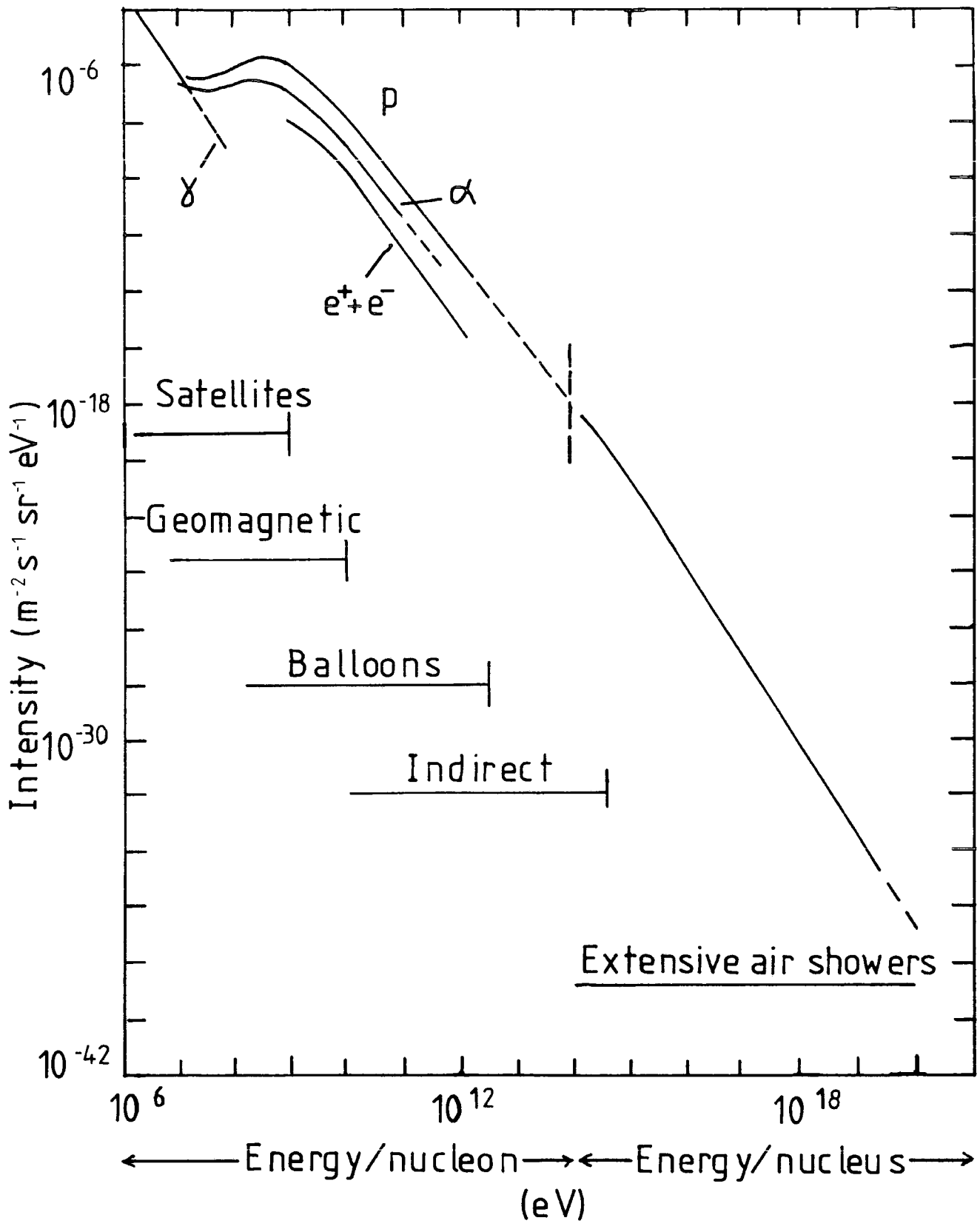

Figure 1.1 : Primary Cosmic Ray Spectra (after Wolfendale 1973)

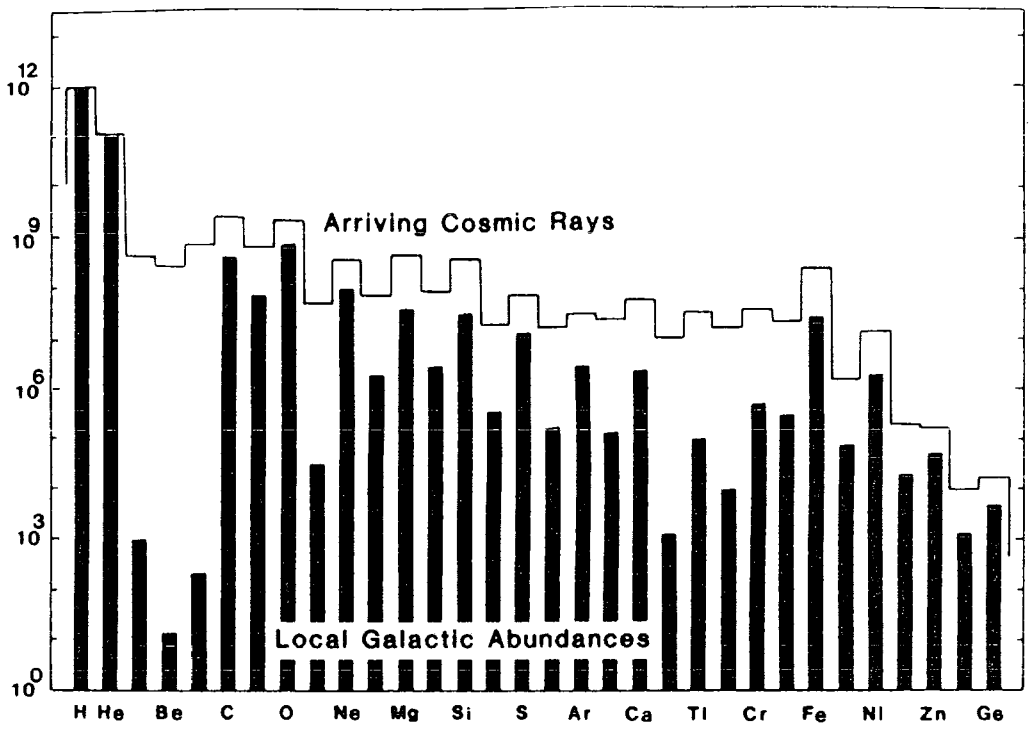

Figure 1.2 : Elemental abundances of arriving cosmic rays (lines) compared with local galactic abundances (bars). The normalization is at hydrogen. After Lund (1984).

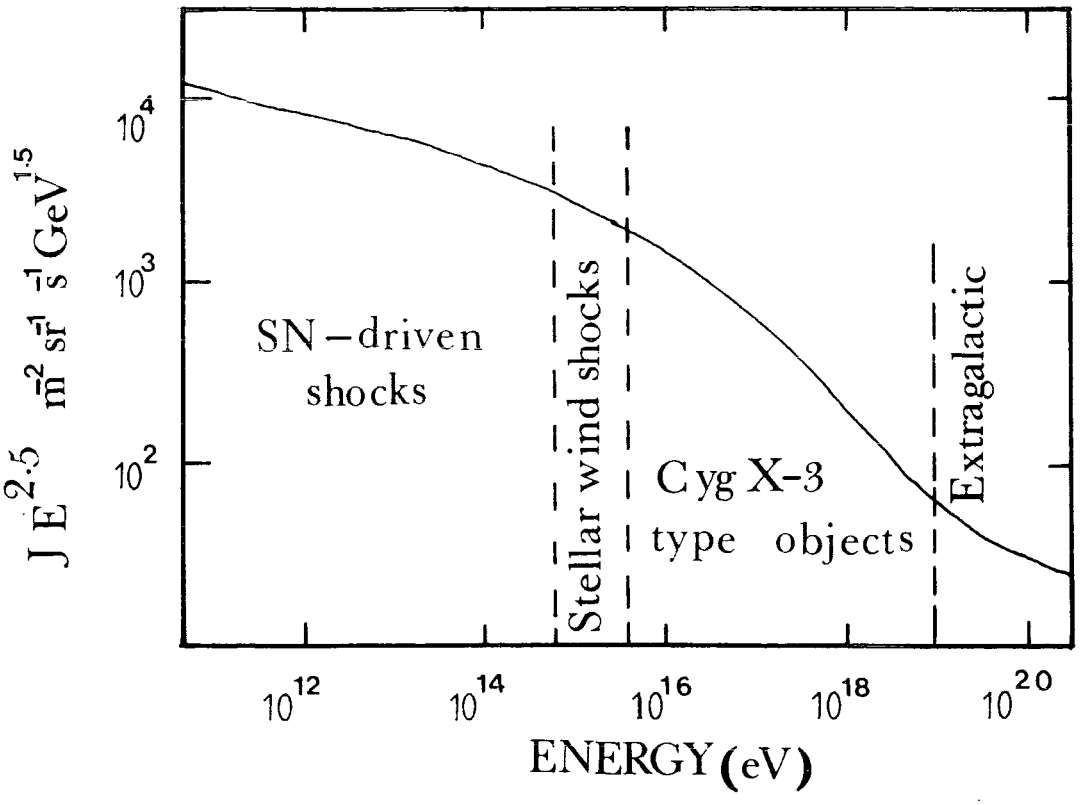

Figure 1.3 : Proposed distribution of dominant cosmic ray sources as a function of energy (after Watson 1984)

Chapter two

The Commodore PET data acquisition unit and its calibration.

2.1 Introduction

In many cosmic ray experiments it is necessary to measure the pulse height recorded by one or more detectors. One way of doing this is to display the pulses to be measured on an oscilloscope sweep using delay lines and photograph the results. However, measuring up the film can be a time consuming process especially if many thousands of events are recorded. A quicker and more flexible approach is to use sample and hold circiuts to store the pulse height information followed by analogue to digital converters which allow the selected pulse heights to be recorded as binary numbers in the store of a microprocessor. These numbers can be transferred to the store of a microcomputer and be available for either immediate print out or subsequent print out after arithmetic operations have been carried out using them. A general purpose 8 channel data acquisition unit operating in conjunction with a Commodore PET microcomputer on the above principles has been constructed by the Durham University Microprocessor Unit. In the following sections the performance of this unit is described.

2.2 Hardware description of the Data Acquisition Unit

The data acquisition unit is a peripheral of the Commodore PET computer which enables it to observe the outputs of any system through its eight input channels. It converts the analogue input information to digital form and sends that information to the PET computer, and that is always done under the control of the PET computer. As Figure 2.1 shows the data acquisition unit consists of four major parts. They are:

a. Analogue part.

b. Trigger control circuitry.

c. PET interface, and

d. Microprocessor subsystem.

(a) Analogue part

The job of the analogue part is to buffer and then convert analogue input signals. The analogue part is made of four parts which are input buffer amplifiers, sample/hold circuits, analogue multiplexer and analogue to digital converter. The input part consists of eight buffer amplifiers which are connected as unit gain inverting ampilfiers. Before each buffer an input protection diode is used to prevent accidental damage to the buffer amplifiers. Each of the eight buffer amplifiers is connected directly to an input of one of eight sample/hold circuits which are operating in the track-and-hold mode, thus reducing the acquisition time. The sample/hold circuit function is to hold the analogue information during the analogue to digital conversion. The outputs of the sample/hold circuits are individually connected

into the input of the analogue to digital converter via an analogue multiplexer.

The analogue to digital converter is a 12 bit converter connected in the bipolar mode with an input voltage range of ±10V.

The analogue part works as follows:

While waiting for a trigger the sample/hold circuits are in the track mode and follow the input signals, and the trigger controlling circuitry is armed and waiting. As soon as the trigger signal is received, the sample/hold circuits are switched into the hold mode. The holding flag flip-flop is set, signalling to the microprocessor, which controls also the start of actual data conversion and data storage, that the trigger has occurred and the conversion should start. The microprocessor then produces a start conversion signal to the A/D converter and waits for the return of a conversion complete signal from the A/D converter. When the conversion is done, the microprocessor switches the A/D to "READ DATA" mode and reads the converted value. After this the microprocessor switches the analogue multiplexer to the next channel and starts conversion again. This is repeated until all the required analogue channels are read. After this the trigger control circuit is again armed to receive the next trigger.

(b) Trigger control circuitry.

As mentioned above the analogue part starts the process of reading and converting data when it receives the trigger signal. There are three sources from which the trigger signal can be derived from. They are :

1. External source
2. Internal signal under program control
3. One of two real times of data acquisition unit.

The microprocessor controls the selection of the particular source of the trigger signal. The selection and setting of the real time timers must be done prior to data convertion itself. In cosmic ray experiment an external trigger is the one of great importance. When a signal is applied to the "EXTERNAL TRIGGER" input of the data acquisition unit, it causes the generation of a trigger signal. The threshold level of the applied signal can be set between $\pm$7 V via the 10 turn potentiometer located next to the "EXTERNAL TRIGGER" input. One can check the setting of the threshold level by the provided "EXTERNAL TRIGGER OUT" socket.

(c) PET interface.

The controlling microprocessor of the data acquisition unit communicates with the PET via an IEEE bus interface. The GPIB interface adapter (MC68488) is used to interface the microprocessor to the PET bus. The physical connection is done by a multicore cable terminated by a socket suitable to be plugged into the bus outlet of the PET. To allow daisy chaining of other devices with the data acquisition unit (e.g. a printer) a PCB outlet similar to PET IEEE bus outlet is provided on the back of the data acquisition unit.

(d) Microprocessor subsystem

The microprocessor subsystem controls the function of the data acquisition unit, including data capture and communication with

the PET. The essential part of the microprocessor subsystem is a 6802 microprocessor running at 1MHz.

2.3 Software description of the Data Acquisition Unit.

When the data acquisition unit is used with the PET computer to collect data from an experimental system and after the required physical connections are made, the experimenter deals entirely with the PET computer. A set of commands was invented by the manufacturer of the data acquisition unit that enables the PET computer to control the data acquisition unit via the IEEE bus. These commands could be sent to the data acquisition unit within a BASIC program by opening a file which is the channel between the program and the data acquisition unit. The following example shows how these commands could be used in a BASIC program.

```
160 OPEN 5,8
170 PRINT#5,"INIT;TRG EXTDH"

... ...........
... ...........
210 CLOSE 5
```

In line number 160 a file is opened and it is numbered as "5" and it is attached to device number "8" which in this case is the data acquisition unit (usually device number 8 is reserved for the disk drive in PET computers). In line 170 two commands, separated by a semi-colon, are sent to the data acquisition unit to be executed. The user may send one command or a series of commands separated by semi-colons as is shown in the example given above. When all

commands are executed the file should be closed as in line 210, this could be because of the end of the program or to open a new file to the data acquisition unit. There are two groups of commands, control commands and data acquisition commands. Table 2.1 summarizes these commands.

It should be mentioned that the material presented here about the hardware and the software descriptions of the data acquisition unit are based mainly on the user manual supplied with the unit.

2.4 Loading and running the PET D.A.U program.

The data acquisition unit works under the control of the PET computer using a BASIC program which sends the required commands to the data acquisition unit. A program was supplied with the unit and is used to operate the system when input pulse heights are required to be recorded. Loading and running the program is as follows.

The data acquisition unit must be connected to the PET computer, via the IEEE488 outlet of the PET. When all required parts of the system are connected together the mains power and individual units can be switched on. After a short time, the PET computer will display a power message and then prompt for a command. At this point everything is ready for loading the program.

Tape with the stored controling program is placed in the cassette drive of the PET and it must be rewound to the beginning of the tape. To load the program on the PET, the phrase (LOAD "PET DACQ") must be typed on the PET keybord, and the program will

be loaded. When loading is compeleted, the cassette drive will stop and a (READY) message appears on the screen of the PET computer. The program tape must be rewound to the start position and it must be removed from the cassette drive as it is now loaded and ready to run.

To run the program, one must type (RUN) on the PET keyboard and then the program will enter the initial dialogue. The user is asked what action must be performed and can then be selectively activated. The first question asked is whether a hard copy of the session is required. The hard copy facilitates identifying information and then data are gathered during the sesion via the PET printer. The next question asked is whether the session should be recorded onto the cassette . If a cassette copy is required the user is asked for an 8 character file name. This file name must uniquely identify the file and can be different to the session identifier. The file created and recorded onto the tape is marked using this file name and can only be recovered using that name. The user is then prompted to rewined the tape data tape to the start position. The cassette starts recording the file header onto the tape. When the file header is recorded, the program will resume its main flow of the initial question session. The user is asked for a session identification, which is an 80 character long string which can be printed via the printer and recorded on the cassette if they are selected. The session identifier is there purely for the convenience of the user to help him record additional information about this session. Some rules are related to the date, which again can be 80 characters long. After the

session identifier and the date the user is asked about the time. The time entered must be six digits first two for hours,then minutes then seconds, in 24 hours notation.

Another question asked is whether to calibrate the zero of the recording channels. The user is asked to connect all inputs to ground and to press D (done) to save the reading as a new zero correction. The last question asked is whether the user wishes to calibrate the gain. To do that, the user is asked to connect all inputs to a positive voltage (in the region of 9500 mV) and to press D when done, then he must enter the exact input voltage to 5 millivolt precision. The user then is also asked to connect all inputs to a negative voltage and do the same as he did for the positive gain correction. Now the program is ready to collect data and record it on the cassette.

2.5 Calibration of the Data Acquisition System

2.5.1 Testing the Data Acquisition Unit.

This test was made with the idea of using the system in cosmic ray experiments in mind. In the proposed cosmic ray experiment, scintillators with fast negative exponential pulses are used. These scintillators give negative exponential pulses with decay time about 10 μs.

The method of this test was as follows. Square negative pulses were generated and the heights were measured simultaneously using a precise oscilloscope and the data acquisition unit. Figure 2.2 illustrates the system used in this test. Negative square pulses with different widths and also negative exponential pulses with

different decay times were applied.

For the negative square pulses, a total agreement between the values of the pulse heights read by the oscilloscope and those read by the data acquisition unit, within the precision of the equipment, was found for any pulse with width greater than about 6.5 μs, see Figure 2.3. However the data acquisition unit failed to read the correct values of any pulse height with width less than 6.5 μs. The curves shown in Figure 2.4 were obtained by fixing the input pulse height and changing the width of the pulses. The result shows how the data acquisition unit ceases to record the correct pulse height as the pulse width becomes narrower than 6.5 μs. The response using exponential negative input pulses was investigated next. The pulse height values which the data acquisition unit recorded are plotted in Figure 2.5 versus the values read on the oscilloscope, and the equality line ($H_{osc} = H_{DAU}$) was drawn for comparison. It is found that the data for long pulses is in conformity with the equality line, but the response which represents the pulses with decay time of 10 μs (which is very similar to the real cosmic ray pulses produced by our scintillator head units) and the equality line are in disagreement. The line which represents the pulses with decay time of 10 μs has a slope of 0.545 which implies that the value that the data acquisition unit reads in this case is the value of the pulse height 6.07 μs after its start time, and that is very close to the delay time (6 μs) between triggering the data acquisition unit and storing the voltage on the sample and hold circuit.

The summary of this test is that the data acquisition unit

only accurately records square pulses with width wider than 6.5 μs and exponential pulses with decay time greater than about 100 μs.

The conclusion reached was that if the output pulses of the scintillator in a cosmic ray experiment are to be monitored by the PET computer via the data acquisition unit, then their pulses should have a long decay time and that could be achieved by using stretcher amplifiers.

2.5.2 Testing the D.A.U. with stretcher amplifier.

A test of the suitability of using stretcher amplifiers with the data acquisition unit was performed using a pulse generator and attenuator, see Figure 2.6. It was found that a diode is required before the input of each stretcher amplifier. Negative exponential pulses with decay time of 10 μs, which is close to the decay time of the real cosmic ray pulses, were produced by the pulse generator and the heights were varied by the attenuator, then passed through the stretcher amplifier. The heights of pulses produced by the stretcher amplifier were measured simultaneously using an oscilloscope and also the data acquisition unit and PET computer. The results of these measurements are plotted in Figure 2.7, which shows that the stretcher amplifier is suitable to be used with the data acquisition unit. The same test was performed with the pulse generator producing negative exponential pulses of 1 μs decay time instead of 10 μs. Results similar to the results which had been obtained previously were achieved as shown in Figure 2.8. At that point it was decided that the stretcher amplifier is the answer of the data acquisition unit problem with

fast exponential pulses. Unfortunately, the stretcher amplifier distorts the pulse heights. The pulse heights at the output of a stretcher amplifier is not the same as the height at the input of the stretcher amplifier. A relation between the pulse heights coming out of the scintillators' head units and the pulse heights at the outputs of the stretcher amplifier read by the data acquisition unit, was needed to know the standard response of the system to a pulse produced by the passage of cosmic ray particles through a scintillator. The arrangement seen in Figure 2.9 was used in these calibration measurements. The decay time used in this work was 10 μs which is close to the 8.5 μs decay time of the scintillator's pulse. The results of this calibration are shown in Figures 2.10 and 2.11. These 'calibration curves' were subsequently used to correct the data collected by the computerized data acquisition system. For completeness, calibration curves were obtained, in the same way, for exponential pulses of 1 μs decay time and square pulses of 1μs in width, and the results of these calibrations are shown in Figure 2.11 and Figure 2.12.

Group	Command	Description
Control Commands	INIT	initialises all internal states of the data acquisition unit reset and reconfigurates the components to the data acquision mode
	TRG INTR	The conversion is started as soon as the data conversion command from PET is received and analysed.
	TRG TMR1	The real timer 1 is used to trigger conversion. Once routing to this timer and the timing period is specifiedby TMR command repeating trigger untill disable by INIT
	TRG TMR2	same as above, but longer periods
	TRG EXTL	the data capture is triggerd by a change of state of the external trigger source. from low to high
	TRG EXTH	as above, but the transition from high to low.
	TRG EXTDL	same as TRG EXTL, but delayed for 6.5µs from the time of external trigger
	TRG EXTDH	as above, but the transition from low to high.
Data acquisition commands	TMR	timer command will set up thetime period of the internal real time timer TMR1 and TMR2
	READ	it waits for the trigger, reads the specified channel, and sends the channel number followed by the appropriat values back to PET.
	CAPT	capture commands consist of two words. The first word specified the type of capture and the number of channel to be read. The second word specifies how many times the capture should be repeated
	FCAPT1	Fast capture command. It captures only the first channel repeatedly in the fast mode

Table 2.1 : The D A U Commands.

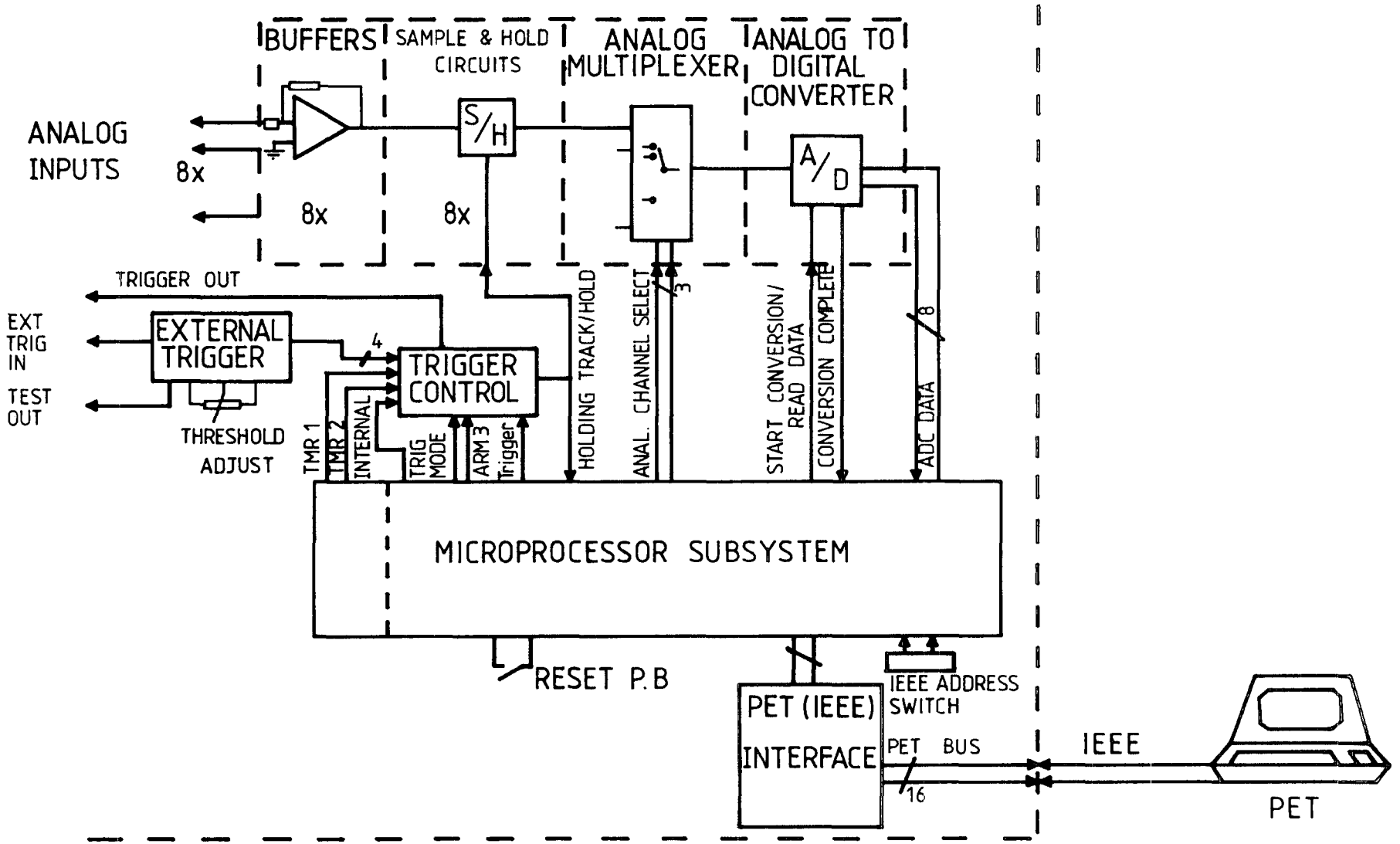

FIG. 2·1 PET DATA AQUISITION UNIT – BLOCK DIAGRAM

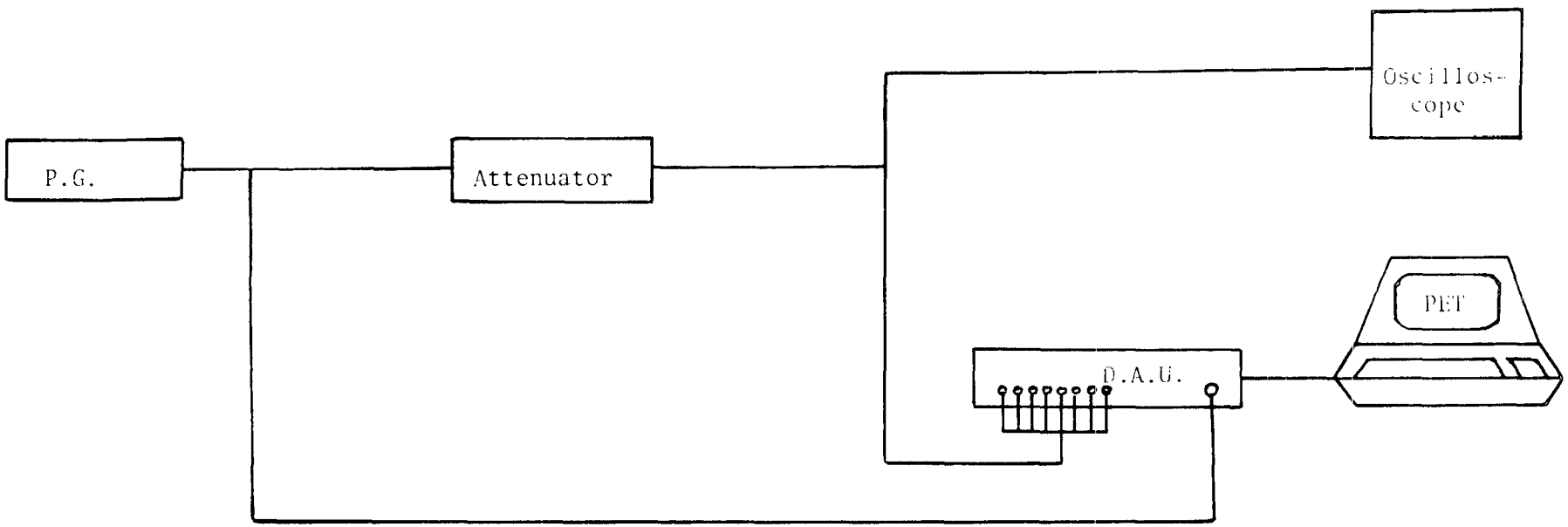

Figure 2.2 : Block diagram of the system used to calibrate the data acquisition unit (D.A.U.) with no stretcher amplifier.

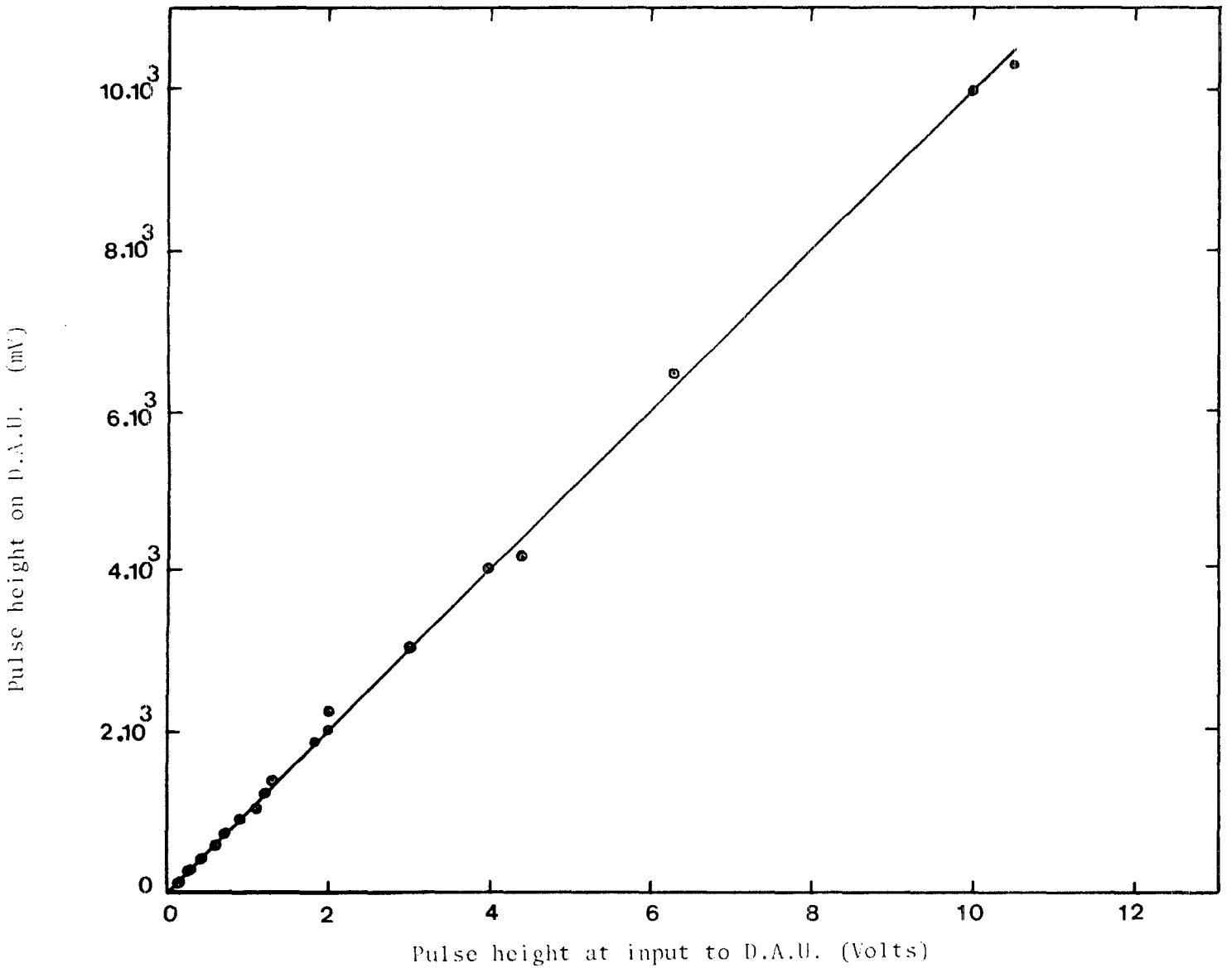

Figure 2.5 : Calibration of the data acquisition unit using 50 μs width input square pulses. Similar results obtained for pulse widths down to 7 μs (see figure 2.4).

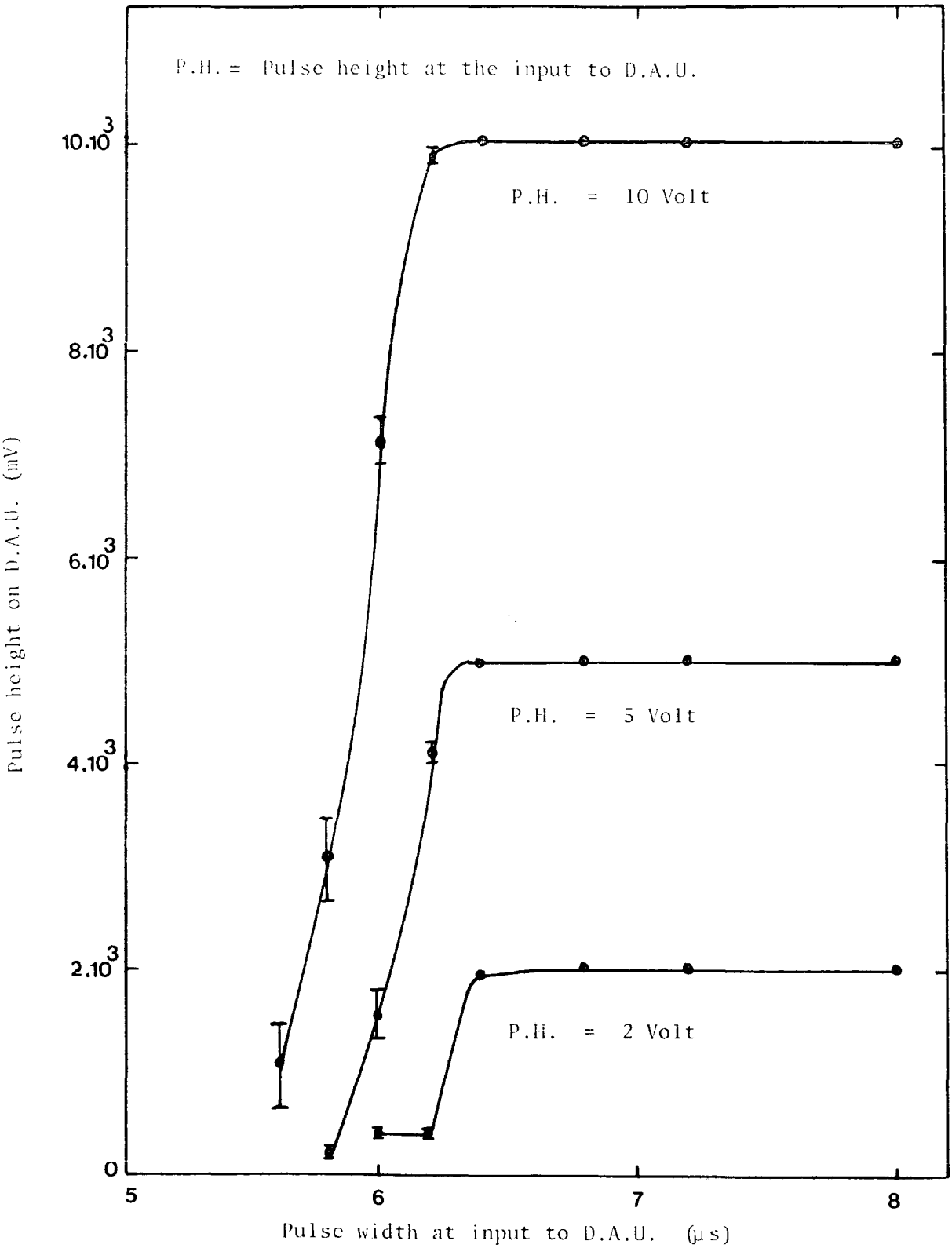

Figure 2.4 : Determination of threshold readable pulse height at the input to the data acquisition unit.

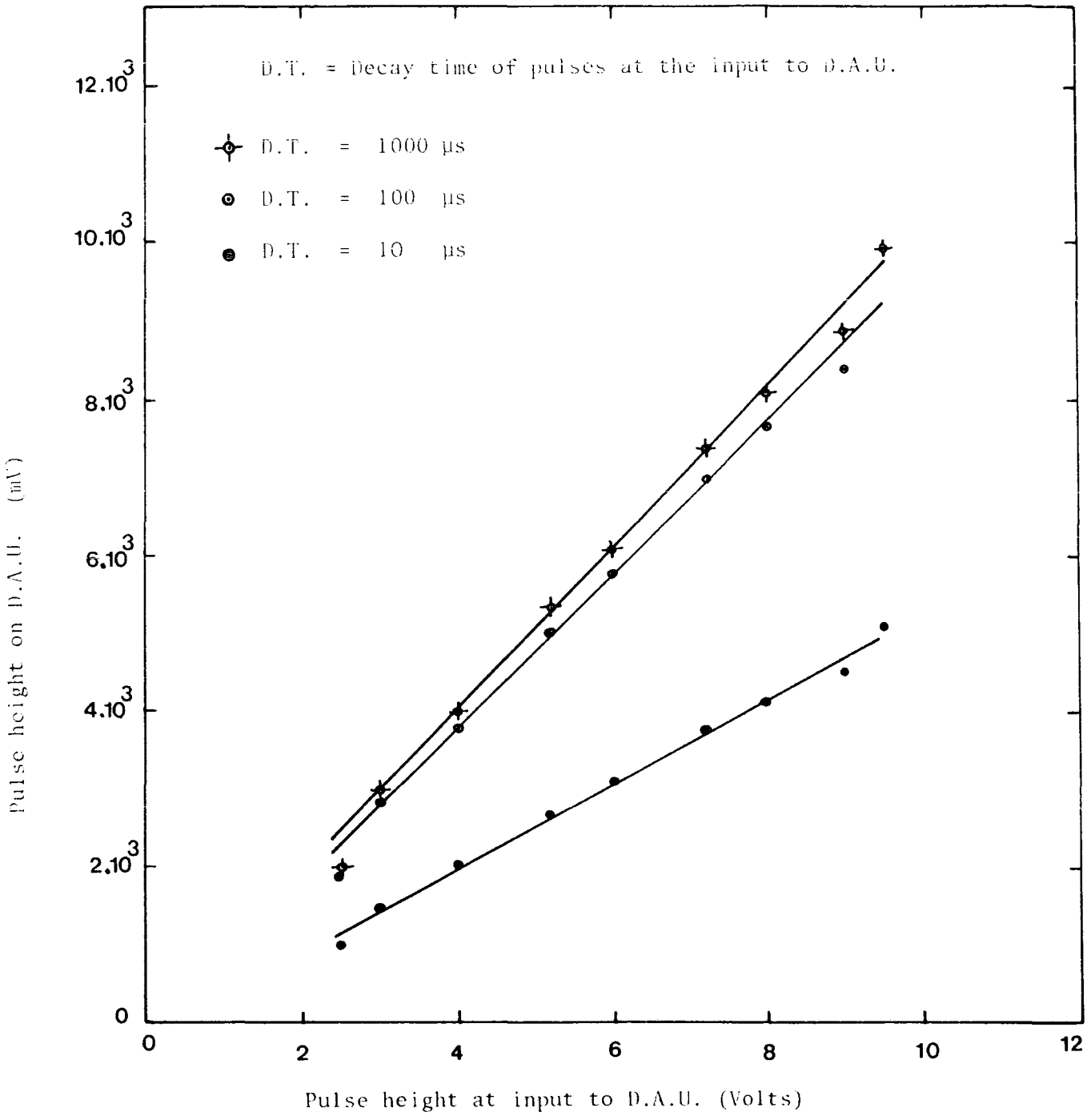

Figure 2.5 : Calibration of the data acquisition unit using negative exponential pulses.

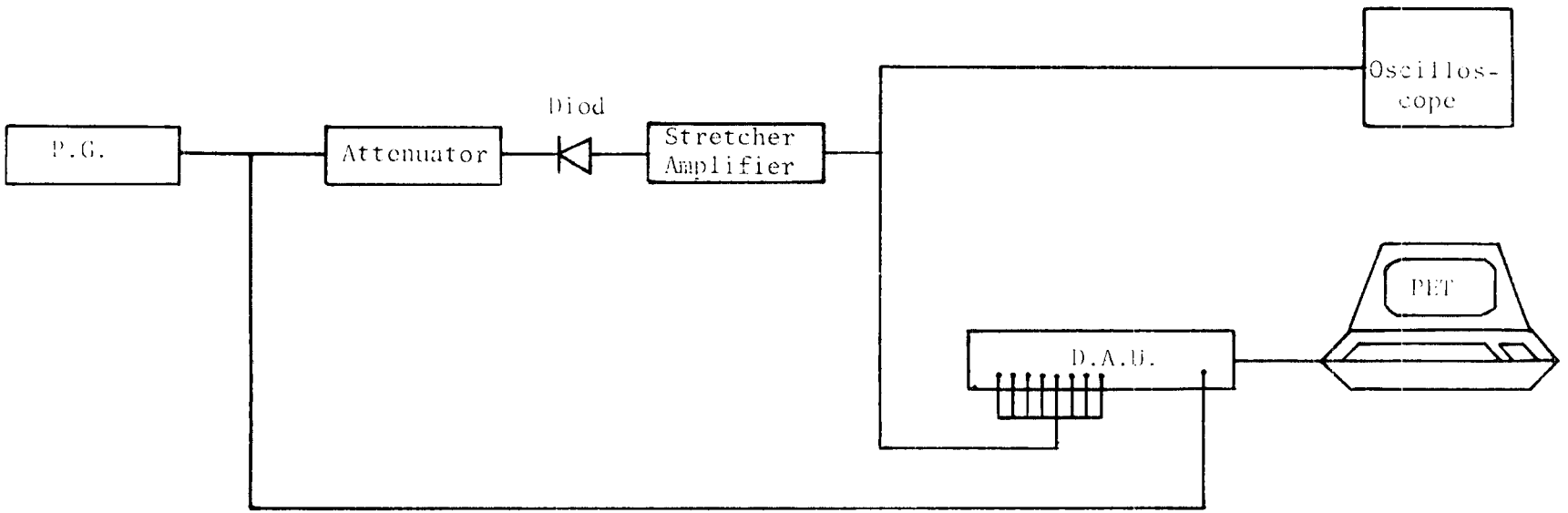

Figure 2.6 : Block diagram of the system used to calibrate the data acquisition unit (D.A.U.) using a stretcher amplifier to generate pulses of different decay time at the input to the D.A.U.

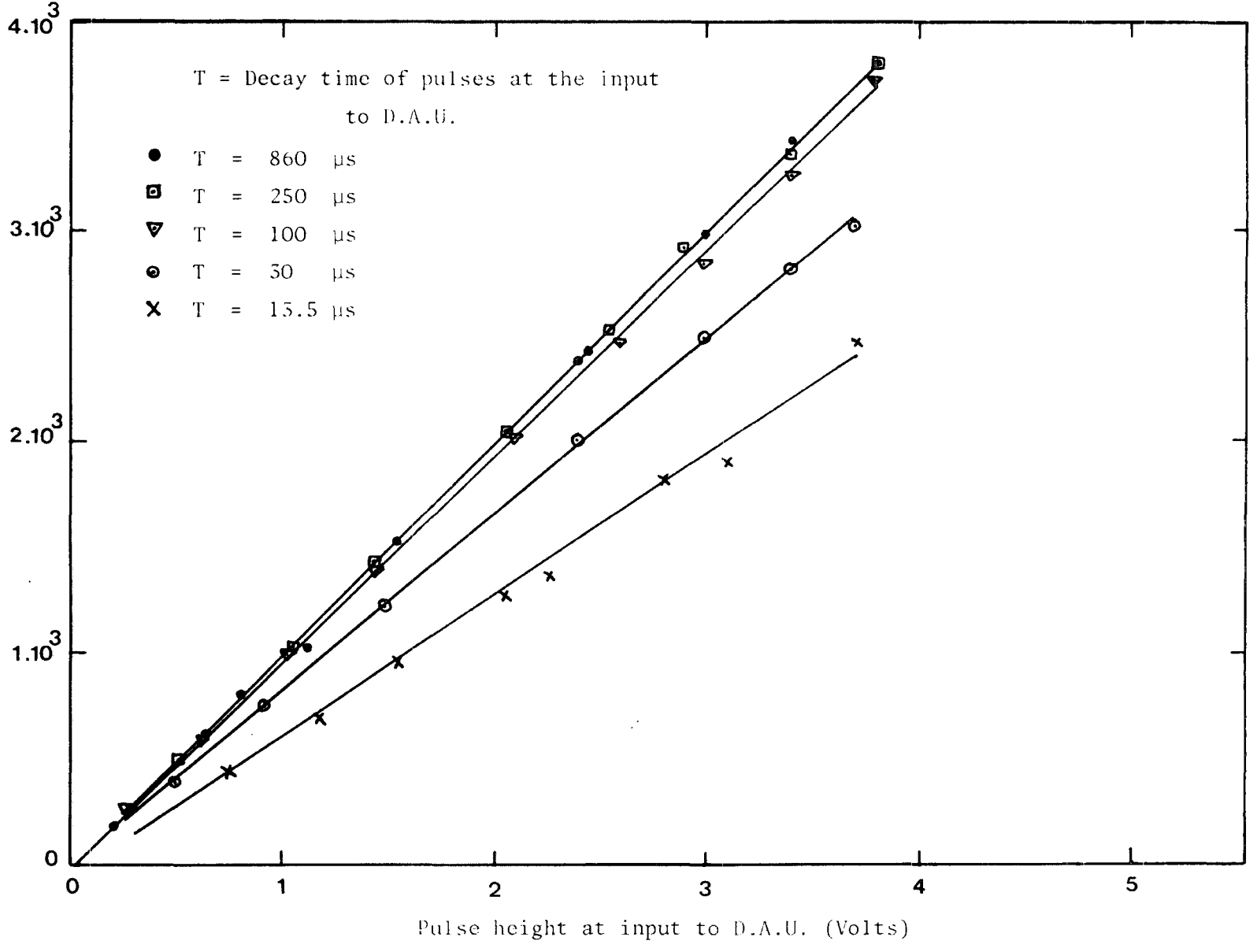

Figure 2.7 : Calibration of the data acquisition unit using a stretcher amplifier to generate pulses of different decay time at the input to the D.A.U. Pulses of decay time 10 µs at the input to the stretcher amplifier were used.

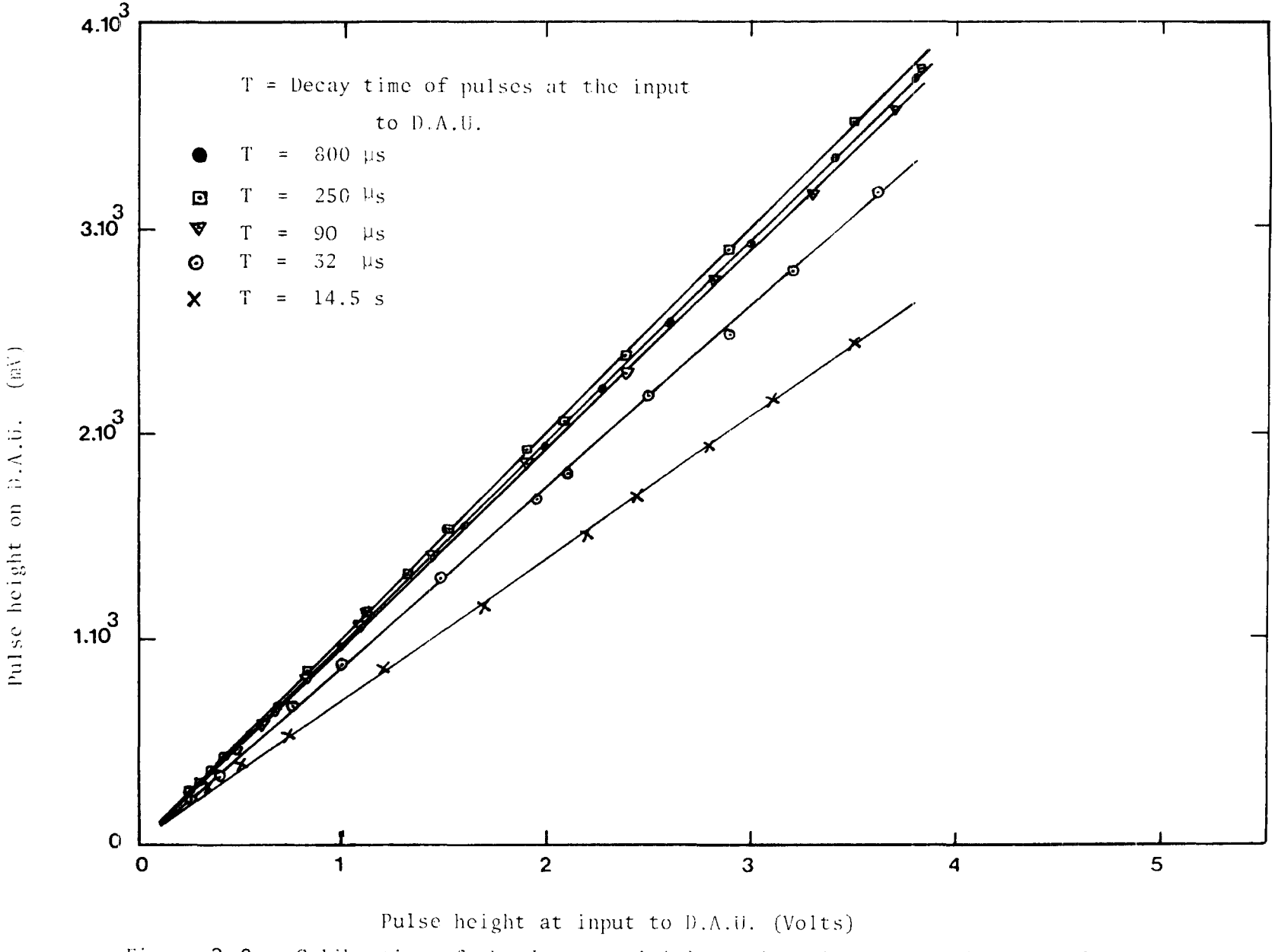

Figure 2.8 : Calibration of the data acquisition unit using a stretcher amplifier to generate pulses of different decay time at the input to the D.A.U. Pulses of decay time 1 µs at the input to the stretcher amplifier were used.

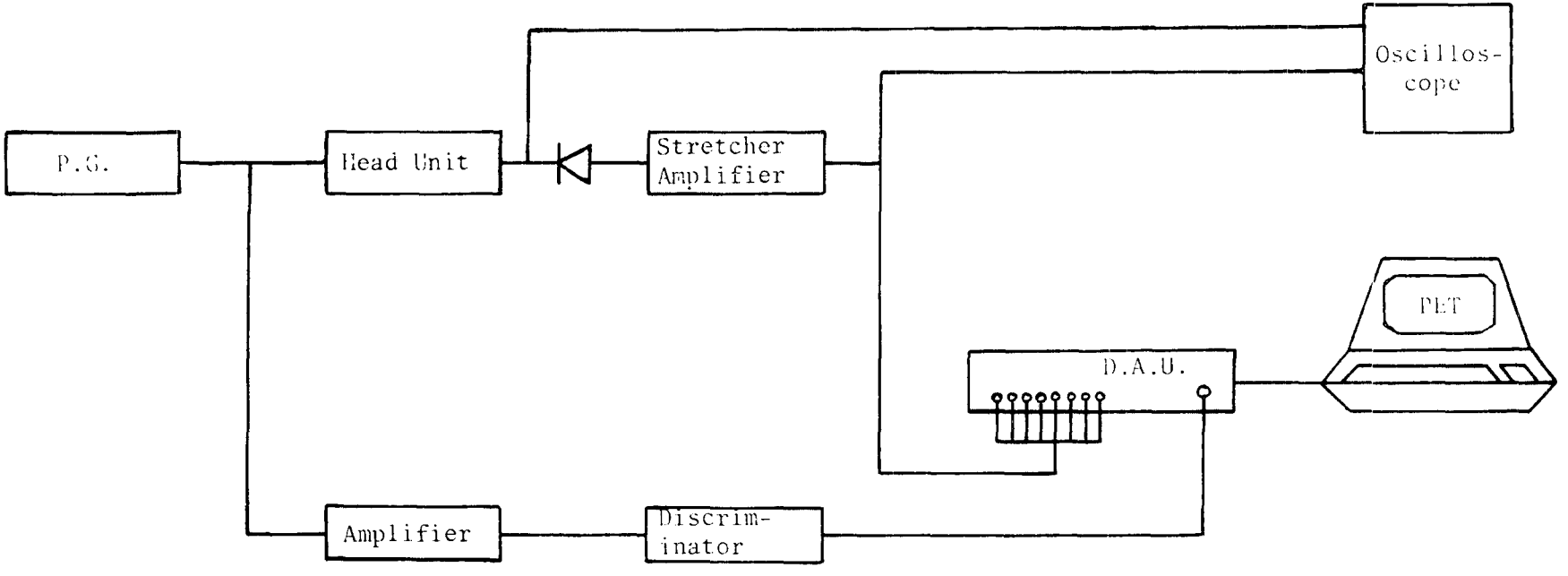

Figure 2.9 : Block diagram of the final workable system used for calibration of the combination of the stretcher amplifier and the data acquisition unit (D.A.U.)

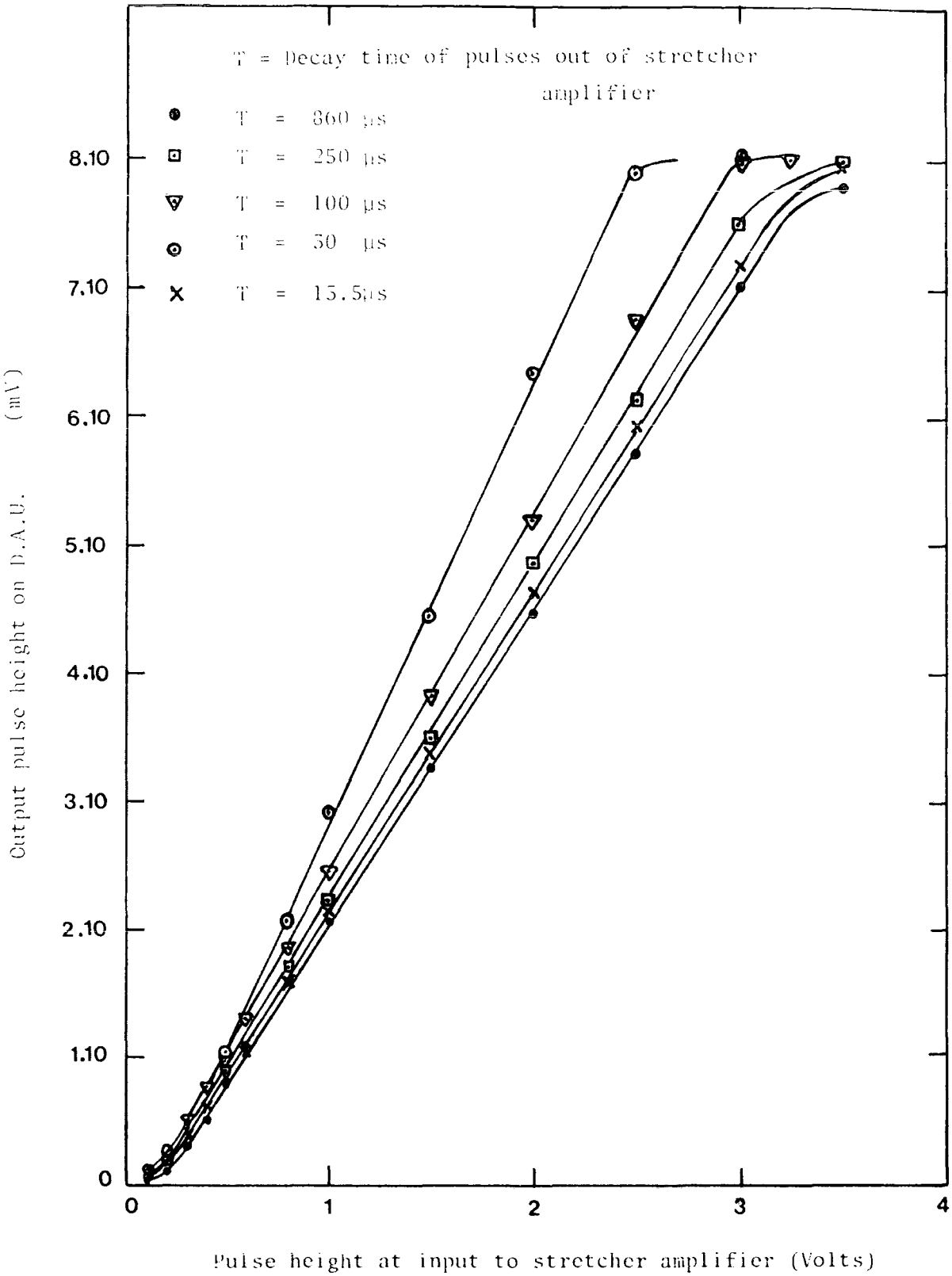

Figure 2.10: Calibration of the combination of stretcher amplifier and the data acquisition unit using 10 μs decay time input exponential pulses.

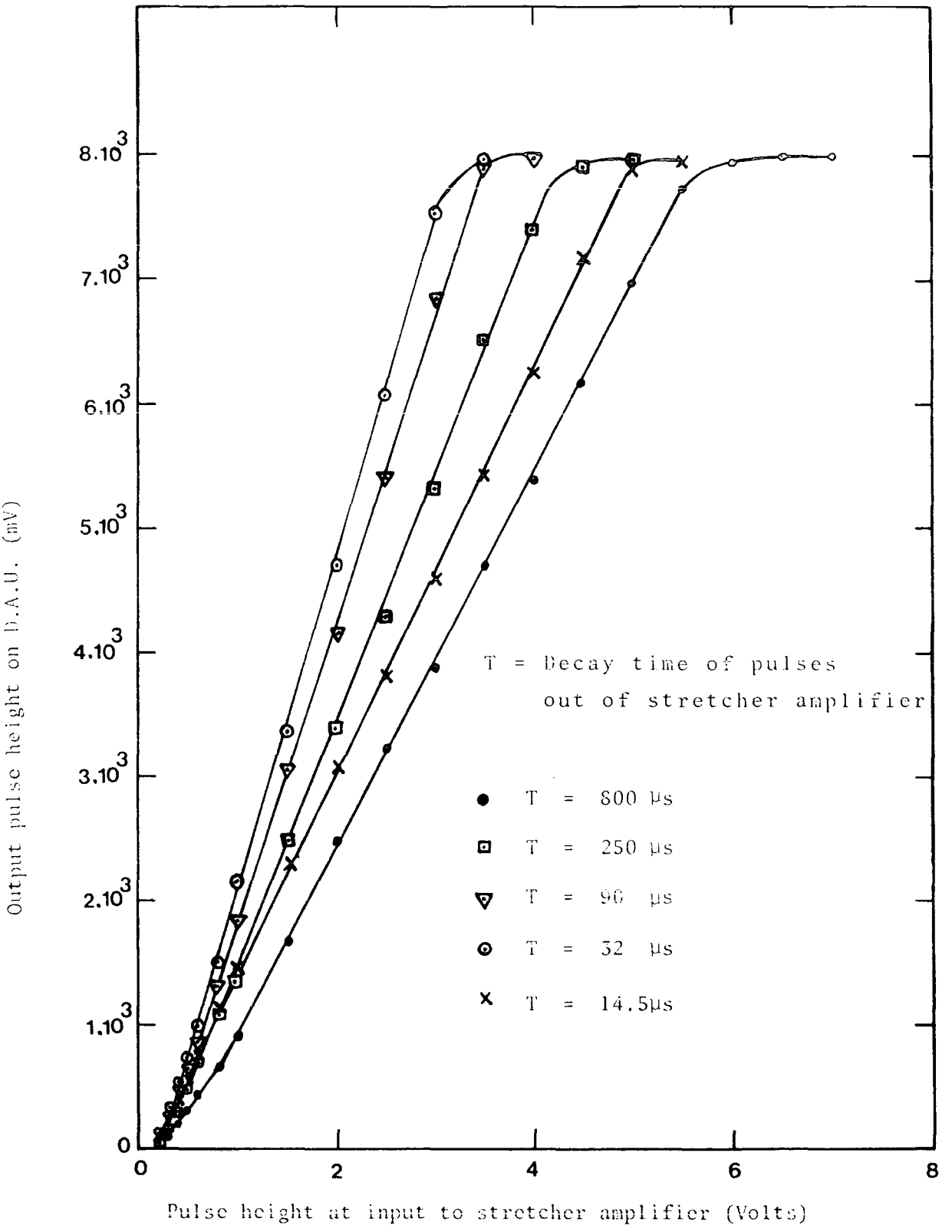

Figure 2.11: Calibration of the combination of stretcher amplifier and the data acquisition unit using 1 µs decay time input exponential pulses.

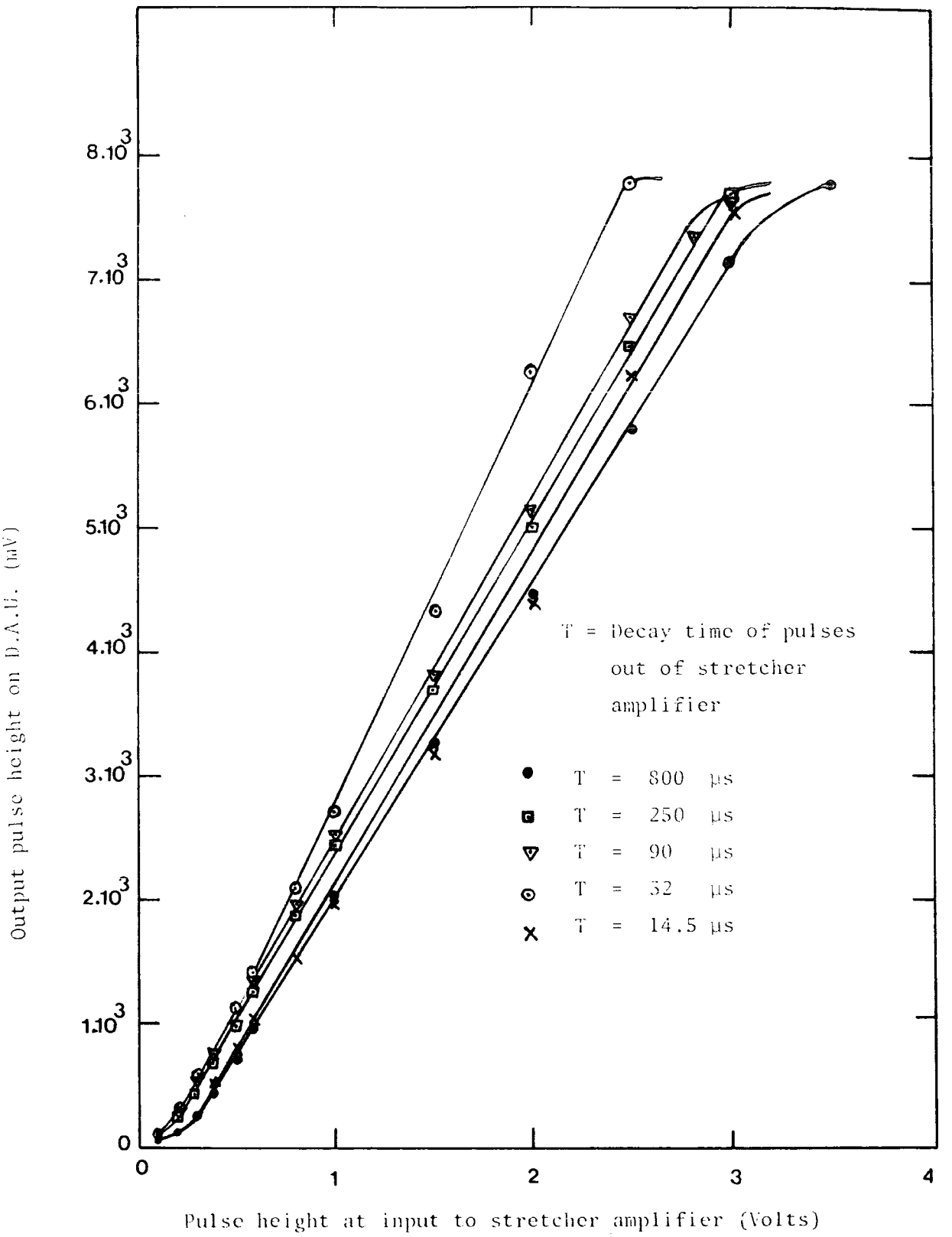

Figure 2.12: Calibration of the combination of stretcher amplifier and the data acquisition unit using 1 µs width input square pulses.

Chapter Three

Testing the data acquisition unit using a Geiger-Müller cosmic ray telescope

3.1 Introduction.

Cosmic ray experiments need a long time to collect data. That is why an automatic recording system is often needed. In the past, as an example, a camera with automatic film drive was used with an oscilloscope to record the information. Computers and especially micro-computers have proved to be very efficient in recording data. In this work the computerised data acquisition system described in the previous chapter is tested operationally using a Geiger-Müller cosmic ray telescope. The zenith angle distribution of the cosmic ray muon flux, east-west effect, barometric effect, and the rate of the cosmic radiation at sea level are studied.

The cosmic radiation flux at sea level consists mainly of secondary particles which owe their origin to the interactions of high energy primary cosmic ray particles near the top of the atmosphere. In these interactions, both charged particles, mainly pions, if they do not interact, decay to muons as do also some of the kaons. The majority of these muons are very penetrating and survive intact to the surface of the earth. Because muons have virtually no nuclear interaction, ionization losses are small (about 2 GeV), and they have a mean life time of 2.2×10^{-6} s in their rest frames of reference. The Lorentz factor for

relativistic time dilation should be about or greater than 20 for muons surviving to sea leve. The vertical flux of the main components of the radiation in the atmosphere is shown in Figure 3.1 (from Hillas 1972, p50).

3.2 The apparatus and the experiment.

The apparatus of the experiment was situated on the first floor in the building of the physics department in Durham University, the roof and the wall of which is mostly made of concrete. This means that cosmic ray electrons from the atmosphere would be absorbed before reaching the cosmic ray telescope so that only muons were detected. That was proved by using layers of lead absorber in the telescope as discussed in section 3.4. The block diagram of the cosmic ray telescope is shown in Figure 3.2. The apparatus used consisted of two layers of Geiger-Müller counters each containing six identical counters, which could be tipped at any desired zenith angle. The distance between the two layers was 56.8 cm so as to give a suitable count rate (see Figure 3.2).

The length of each counter was 73cm, the sensitive length was 67 cm, the internal diameter was 3.5 cm, the diameter of the central anode tungsten wire was 0.01 cm. Figure 3.3 shows the construction of the counter used.

The principal measurements were of the coincidence rate between the counters in the top layer and the counters in the bottom layer. The particles passing any one of the six counters produces a pulse which is fed along coaxial cable to the coincidence unit. Similarly for the other tray of counters a pulse on any of the

counters gives a signal at the coincidence unit. If there is a signal on both inputs to the coincidence unit then there is an output to the PET (through the data acquisition unit) and to a scaler at the same time.

The zenith angles at which measurements were made, were between 0° to 90° to the east and to the west, the axes of the counters being always in the south-north direction. The rate of the events at those different angles have been measured and a graph was obtained of count rate versus angle, which will be described later.

3.3 Performance of the Geiger counters

At first each of the Geiger counters was checked to ensure that it was working correctly and that the voltage on the that particular counter was neither too high nor too low. Hence, by using the switches attached to the tray, one and only one counter could be selected and the number of the particles passing through that counter was counted by switching in only the one input into the coincidence unit. The starting potentials of the counters were checked daily and all counters were operated at exactly the same voltage above the starting potential. Each counter was operated at 50 volts above its starting potential, the starting potentials were around 1300 volts (see Figure 3.4).

With the help of the data acquisition system, the performance of the Geiger-Müller telescope was closely investigated. Only one counter in each of the two layers of the Geiger-Müller telescope was chosen (counters A_1 and B_1), in the arrangement shown in

Figure 3.5. When a particle passes through both counter trays a coincidence triggering pulse is passed to the data acquisition unit which at once reads the pulse heights from both counters, then records them as well as the occurrence time of the event. The mean pulse height and standard deviation (σ) of pulse height distribution about the mean for counters A_1 and B_1 have been found using the microcomputer data acquisition system as shown in Figure 3.6. The measurements were repeated for different runs at different values of operation voltages along the plateau for each counter A_1 and B_1. The distribution in the time separation of the occurrence time of the events has been obtained using the microcomputer data acquisition system. By using a scaler, 240 events were observed in the running time of 41.58 minutes corresponding to an average event rate of $(0.10 \pm 0.01)\ s^{-1}$ or a mean time separation of events of 10 seconds. Figure 3.7 shows the distribution of the separation time between 96 successive events found from the microcomputer data acquisition system and it was found that it is consistent with a distribution of the form

$$n(t) = (63.9 \pm 23.6) \exp[-(0.10 \pm 0.01)\ t] .$$

From this, the average rate of good successive events was found to be $(0.10 \pm 0.0)\ s^{-1}$ or mean time separation of the events of 10 seconds.

The effect of the applied voltage on the Geiger counter pulse height has been found from the results of mean pulse height out of different runs at different values of the operating voltage as shown in Figure 3.8. Dependance of the standard deviation (σ) of

the pulse height distribution about the mean value on the counter operating voltage is shown in Figure 3.9. It is clear from that figure that the standard deviation reached a minimum value at operating voltages along the plateau. Finally, comparison of the variation of the standard deviation (σ) of the pulse height distribution about the mean value with the operating voltage and the variation of the background counting rate with operating vlotage for counters A_1 and B_1 have also been found - Figure 3.10. The summary of all results are shown in Table 3.1.

3.4 Cosmic ray rate at sea level.

Near the base of the atmosphere or under any heavy absorber, almost the entire electron component of cosmic rays must have its origin from decay and collision processes of muons, chiefly from decay. Thus the relative intensity of meson and electrons at low altitude (or under a heavy absorber) may be used to furnish information regarding meson decay. This has been pointed out by Euler and Heisenberg (1938). Rossi (1942) measured the intensities of the hard and of the soft component of cosmic rays as functions of altitude and zenith angle. The directional intensities were calculated on the assumption that all of the multiple coincidences obtained were due to the passage of single particles through the counters. No attempt was made to distinguish sharply between mesons and electrons, but rather the distinction was between particles capable of penetrating only the counter walls and those capable of penetrating also a certain thickness of lead.

Due to difficulties concerning uncertain detector edge effects

and in estimating the overall efficiencies of counter systems many experimenters have normalized their results to a standard intensity point. Until recently this point was that deduced by Rossi (1948) from the data of Greisen (1942). Rossi applied a correction amounting to 4% to the Greisen value to account for the combined effect of showers and scattering in the Greisen apparatus. Alkofer et al (1970), using a scintillation counter telescope which included lead absorber, measured the differential intensity at 1 GeV/c to be

$$(3.09 \pm 0.21)\times10^{-6}\ cm^{-2}\ sr^{-1}\ s^{-1}(MeV/c)^{-1},$$

which is approximately 26% higher than the 1 GeV/c Rossi point. This result is supported by Crookes and Rastin (1971) who measured the intensity at 0.35 GeV/c using a Geiger counter telescope and flash-tube stack. Quantitatively Crookes and Rastin measured an intensity 9% higher than that measured by Greisen.

Measurement of the absolute intensity of muons of higher momenta (above 3.48 GeV/c and 7.12 GeV/c) have been made by Ayre et al (1971) using the Durham spectrogaph MARS. Ayre et al conclude that at the lower momenta the intensity is (7.7 ± 1.3)% greater than those previously given by Aurela and Wolfendale (1967) which were based on the Rossi normalization. Ashton et al (1972) have measured the integral muon intensity above 0.88 GeV/c as $(8.22 \pm 0.04) \times 10^{-3}\ cm^{-2}\ sr^{-1}\ s^{-1}$, which is higher than expected on the basis of the Rossi piont.

The differential response curve of meson detectors (Webber and Quenby 1959) at two different depths in the atmosphere are related approximately in the following way:

$$\frac{dN}{dP}(P,x_1) = \frac{E(x_2)}{E(x_1)} \cdot \frac{dN}{dP}\left(P\,\frac{E(x_2)}{E(x_1)}, x_2\right)$$

If $\int_{P_{min}}^{\infty} \frac{dN}{dP}(P,x_1)=100$, then $\frac{E(x_2)}{E(x_1)} \frac{dN}{dP}\left(P.\frac{(Ex_2)}{(Ex_1)}, x_2\right) = 100$

$\frac{dN}{dP}(P,x_1)$ is the differential response at rigidiy P and depth x_1,

$\frac{E(x_1)}{E(x_2)} \frac{dN}{dP}\left(P.\frac{E(x_2)}{E(x_2)}, x_2\right)$ is the differential response at rigidity

$P \cdot \frac{E(x_2)}{E(x_1)}$ and depth x_2.

If the differential response curve at a depth x is known, then the response curve at another depth can be obtained using the above relation. The differential response curve for sea level meson detectors, calculated in this way from the curve for meson detectors at 312 g cm^{-2} is shown in Figure 3.11.

The cosmic rays detected by the present telescope consisted of two components: a hard component consisting predominantly of muons with a small contamination of soft component which is primarily made up of electrons (negative and positive) and photons. The hard component has great penetrating power while the soft component is easily absorbed out by a few centimetres of lead and this difference in composition of the two types of cosmic rays can easily be shown with the cosmic ray telescope used. A coincidence counting rate was found with and without a layer of wood of about

2 cm thickness, then one layer of lead = 5 cm, and two layers of lead = 10 cm. the result was that no big difference was found between these measurements (see table 3.2).

In the present experiment if we assume the resolving time of the coincidence circuit is 5 μs, the accidental rate at the vertical position for counters A_1 and B_1 when they are connected in coincidence is

$$2\ N_A N_B\ t = 2 \times 10.5 \times 8.6 \times 5\times10^{-6} = 0.9\times10^{-3}\ \text{count/sec},$$

where N_A and N_B are the counting rate per second for counters A_1 and B_1 respectively. This rate is small for all counting rates between zenith angles of 0° and 90°, see Figure 3.13.

3.5 Zenith angle distribution

The zenith angle distribution of the muon component at sea level has previously been measured by Greisen (1942). Representing the angular distribution by $R(\theta) = R_o \cos^n \theta$ Greisen found $n = 2.1$. In the present experiment the cosmic ray angular distribution was found in the range of zenith angle between 0° and 90°. We have described the zenith angle distrbution above where the Geiger-Müller telescope is not pointing in the vertical direction but at some angle, θ, where $R(\theta)$ represent the rate of the cosmic rays at zenith angle θ. R_o is the vertical rate, and the index n is a constant. To find the best estimate of the value of n that describes the zenith angle distribution of the measurements, log $R(\theta)$ versus log $\cos(\theta)$ was plotted and the slope of the best fitted line is the value n. We found that the value of $n = (1.54 \pm 0.01)$ in the range of zenith angle

$\theta = 0^{\circ} - 70^{\circ}$, and $n = (1.82 \pm 0.01)$ in the range of zenith angle $\theta = 0^{\circ} - 40^{\circ}$, see Figure 3.12. The latter value is consistent with previous work. The reason for the decrease of n with increasing range of the zenith angle is believed to be due to the soft component (knock on electron showers etc.) which accompanies the muon component under absorbers. Small vertical electron-photon showers accompaning vertical muons will be registered by the telescope as twofold coincidences at large zenith angles. This will give a smaller value of n than the true value. However, this effect should become decreasingly important as the zenith angle decreases as was found in the present measurements.

3.6 East-west effect

The effect of the earth´s magnetic field on cosmic rays has been known for a long time and a great deal of experimental data has been accumulated on the consequent variations of the flux with respect to inclination to the vertical, latitude and longitude. The basic problem to be considered is the interaction of primary cosmic rays with the earth´s magnetic field as it approaches the earth.

Lemaître and Vallarta, and also Clay and others, made use of the earlier calculations of Størmer, who had developed a theory of the origin of the aurora borealis many years previously, and had shown that there were certain regions around the earth inaccessible to charged particles of a given energy approaching from a distance. Størmer´s theory was then applied to cosmic rays, on the assumption that they were charged particles approaching the

earth from all directions.

Charged particles of sufficiently high energy would only be deflected slightly by the geomagnetic field, but although no general analytical description has been found, Størmer showed that they must lie within certain limits, (see Hillas 1972).

Two groups set up counter telescopes, Johnson (1933) and Alvarez and Compton (1933). Both of the two groups reported in April 1933 that there was an excess of particles coming from west of the zenith compared with easterly directions: at 45° the difference was about 10%. This clearly indicated positively charged particles.

In the present experiment measurements were made in the variation of counting rate with angle to the vertical (zenith angle), and it has been found that there is a difference between the rates when measured with eastward and westward inclination. This phenomenon is called the east-west effected and has been known for many years. The variation is represented in Figure 3.13. It is usual to define the east west effect as

$$\Phi = \frac{R_W(\theta) - R_E(\theta)}{.5\ [R_W(\theta) + R_E(\theta)]}$$

where $R_W(\theta)$ and $R_E(\theta)$ are the rate at zenith angle θ toward the west and east, respectively. It can be seen from table 3.3 that the main results found are that Φ increases with zenith angle up to about 40°, above which it falls off. A typical value for the maximum value of $\Phi(\theta = 40^{\circ})$ is 0.06 ± 0.01.

The explanation of the effect in physical terms is quite

simple. Briefly, since the primary radiation is almost entirely positively charged, there is a higher cut-off rigidity towards the east then towards the west and both rigidities increase with decreasing latitude. At any given latitude the energy lost by the secondaries in getting through the atmosphere increases with increasing θ, i.e. increasing path length in the atmosphere (t sec θ) where t is the depth of the atmosphere. This means that the energy of the primaries responsible for generating the particles arriving at sea level increases with increasing θ. Now the difference in the rigidities between east and west increases with θ so that there are two competing effects occurring, the increasing difference of rigidities causing an increase in Φ and the increasing mean energy trying to produce a decrease in Φ. The result is that Φ goes through a maximum value in the region of $\theta = 40$ as found in the present results.

3.7 Barometric effect.

For extensive air showers the variation in the rate of the showers of a given size with the change of the barometric pressure is of interest because it affords a measurement of the attenuation of the shower, once past its maximum of development in the atmosphere. An increase in pressure effectively corresponds to the apparatus being situated at a greater depth, and hence the rate of showers of a given size will decrease.

The present measurements refer to the low energy muon component. The variation of the rate of any secondary cosmic ray component with atmospheric pressure at the level of observation

can be expressed as follows:

$$R = R_o \exp[-B(p-p_o)] \; m^{-2} \; sec^{-1} \; st^{-1}$$

where R is the cosmic ray rate at pressure p, R_o is the rate at the standard atmospheric pressure p_o (76 cm of Hg). The barometric pressure at Durham during the time this experiment was running varied over the range 75.5 - 77.15 cm.Hg. The measurements of the counting rate variation of cosmic rays due to the pressure was found to be very small during the period of the experiment. In the present work, B is the barometric coefficient defined as the percentage change in the counting rate with atmospheric pressure calculated from the above formula as follows:

$$B = \frac{dR}{Rdp} = (3.40 \pm 0.55)\% \; (cm.Hg)^{-1} \; .$$

The results are shown in Figure 3.14. It is seen that the effect of atmospheric pressure changes on the flux of the low energy muon component is considerably less than on the flux of high energy extensive air showers.

3.8 Conclusion

The aim of this experiment was to test the computerized data acquisition system described in the previous chapter. It was proved in this test that the data acquisition unit functioned as expected and was suitable for use in other cosmic ray experiments.

Counter	Operating voltage (volt)	Mean pulse height (mV)	(σ) (mV)	Coincidence rate	
				Scaler (sec^{-1})	Found from time separation of good successive events (sec^{-1})
A1	1300	2401 ± 13	166 ± 9	.089 ±.005	0.115 ±0.012
B1		2644 ± 17	222 ± 12		
A1	1350	2943 ± 5	58 ± 3	.096 ±.006	.104 ±.013
B1		3252 ± 2.4	29 ± 2		
A1	1400	3122 ± 2.1	24 ± 1.5	.092 ±.006	.113 ±.01
B1		3510 ± 3.3	37 ± 2.4		
A1	1450	3285 ± 2	20 ± 1	.105 ±.006	.082 ±.017
B1		3661 ± 3	34 ± 2		
A1	1500	3360 ± 13	177 ± 9	.090 ±.010	.114 ±.014
B1		3711 ± 16	218 ± 11		

Table 3.1 : Table giving the summary of mean pulse height, standard deviation of pulse height distribution about the mean and two fold coincidence rate for counters A and B at different values of operating voltage.

Absorber	Counting	Time(hr)	$\sqrt{\text{Count}}$	Counting rate ($min.^{-1}$)	σ
Without absorber	135807	12	368.5	188.6	0.512
Board only	202782	18	450.3	187.7	0.417
One layer of Pb 5cm	179685	18	423.9	166.4	0.392
Two layers of Pb 10cm	114522	12	338.4	159.1	0.470

Table 3.2: Dependence of twofold coincidence rate on the amount of absorber inserted in the telescope.

Zenith angle ($\theta°$)	Geographic west rate (R_W) ($min.^{-1}$)	σ_{R_W}	Geographic east rate (R_E) ($min.^{-1}$)	σ_{R_E}	$\frac{R_W}{R_E}$	$\frac{R_E}{R_W}$	$\frac{R_W - R_E}{\frac{1}{2}(R_W + R_E)}$ Φ
0	186.9	1.25	186.9	1.25	1.000 ± 0.009	1.000 ± 0.009	0
10	182.8	1.23	181.4	1.23	1.008 ± 0.010	0.992 ± 0.009	0.008 ± 0.009
20	173.8	1.20	167.7	1.18	1.036 ± 0.010	0.965 ± 0.010	0.036 ± 0.010
30	150.6	1.12	143.4	1.10	1.050 ± 0.011	0.952 ± 0.010	0.049 ± 0.011
40	121.4	1.00	114.5	0.98	1.060 ± 0.013	0.943 ± 0.011	0.058 ± 0.012
50	90.4	0.87	87.6	0.85	1.032 ± 0.014	0.969 ± 0.013	0.031 ± 0.014
60	63.1	0.73	61.7	0.72	1.023 ± 0.017	0.978 ± 0.016	0.022 ± 0.016
70	45.3	0.61	42.1	0.59	1.076 ± 0.021	0.929 ± 0.018	0.073 ± 0.019
80	32.9	0.52	28.4	0.49	1.158 ± 0.027	0.863 ± 0.020	0.147 ± 0.023
90	27.2	0.48	24.4	0.45	1.115 ± 0.028	0.897 ± 0.023	0.109 ± 0.026

Table 3.3: East-west effect. The variation of counting rate when measured with eastward and westward inclinations.

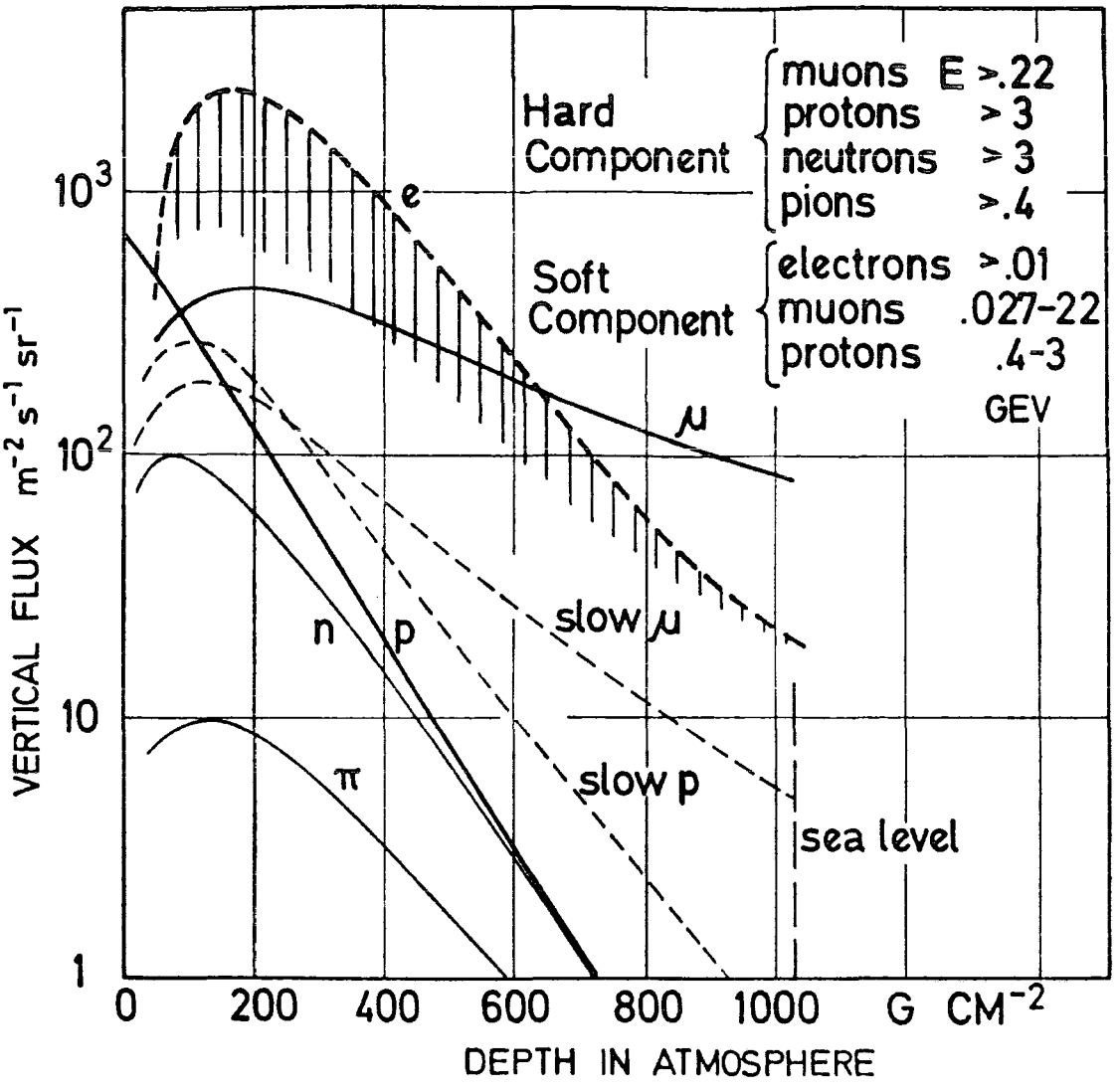

Figure 3.1 : The vertical fluxes of different components of cosmic rays within the atmosphere. (From Hillas, 1972, p. 50.)

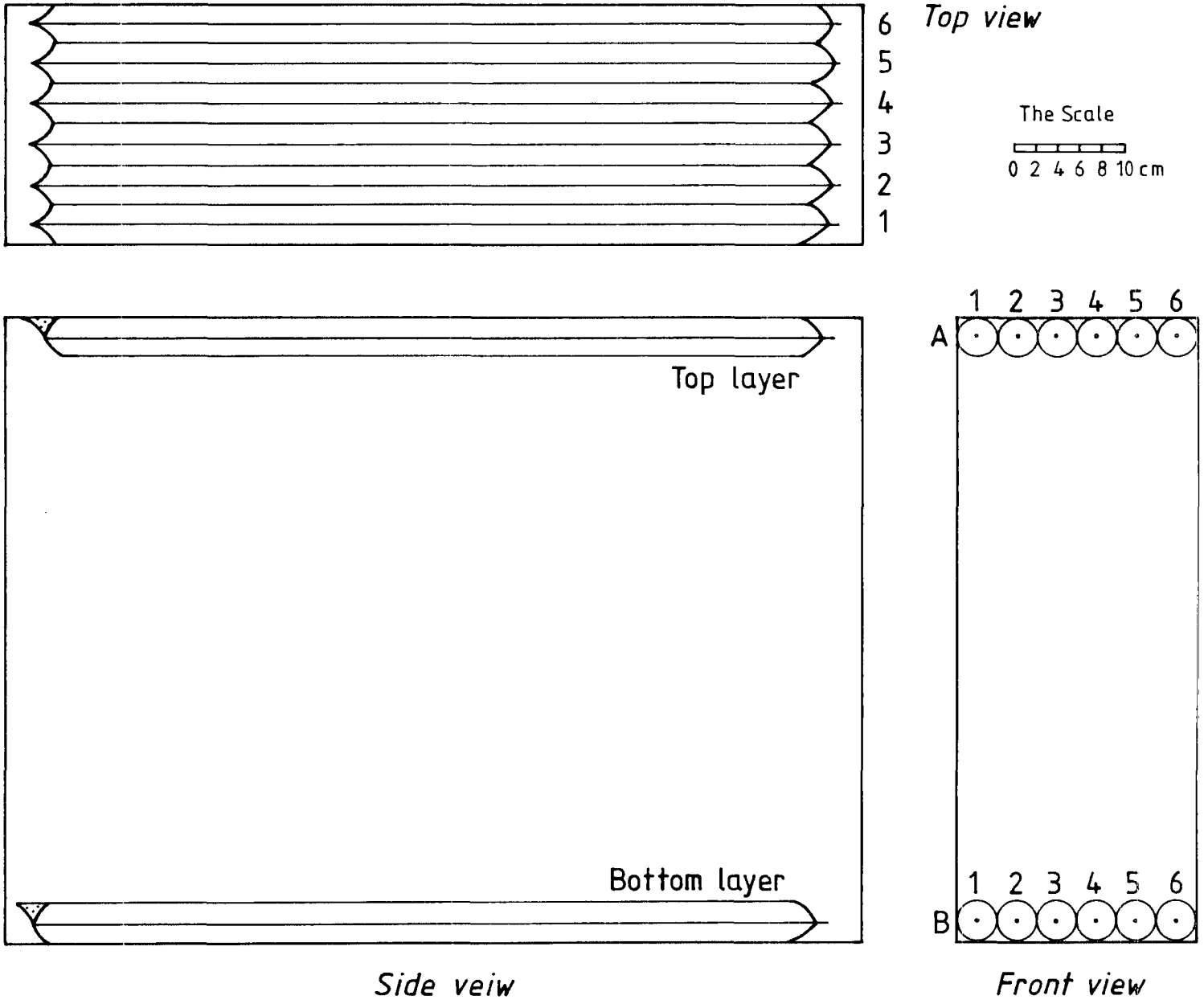

Figure 3.2: The Geiger-Müller cosmic ray telescope.

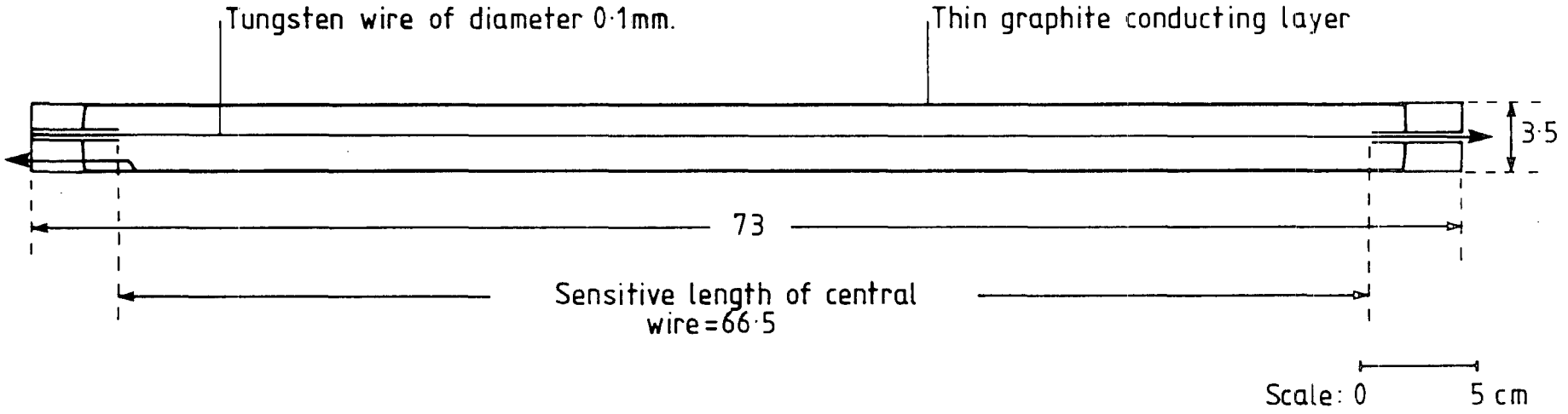

Figure 3.3: Diagram showing Geiger-Müller counter construction.

All dimensions are in centimetres.

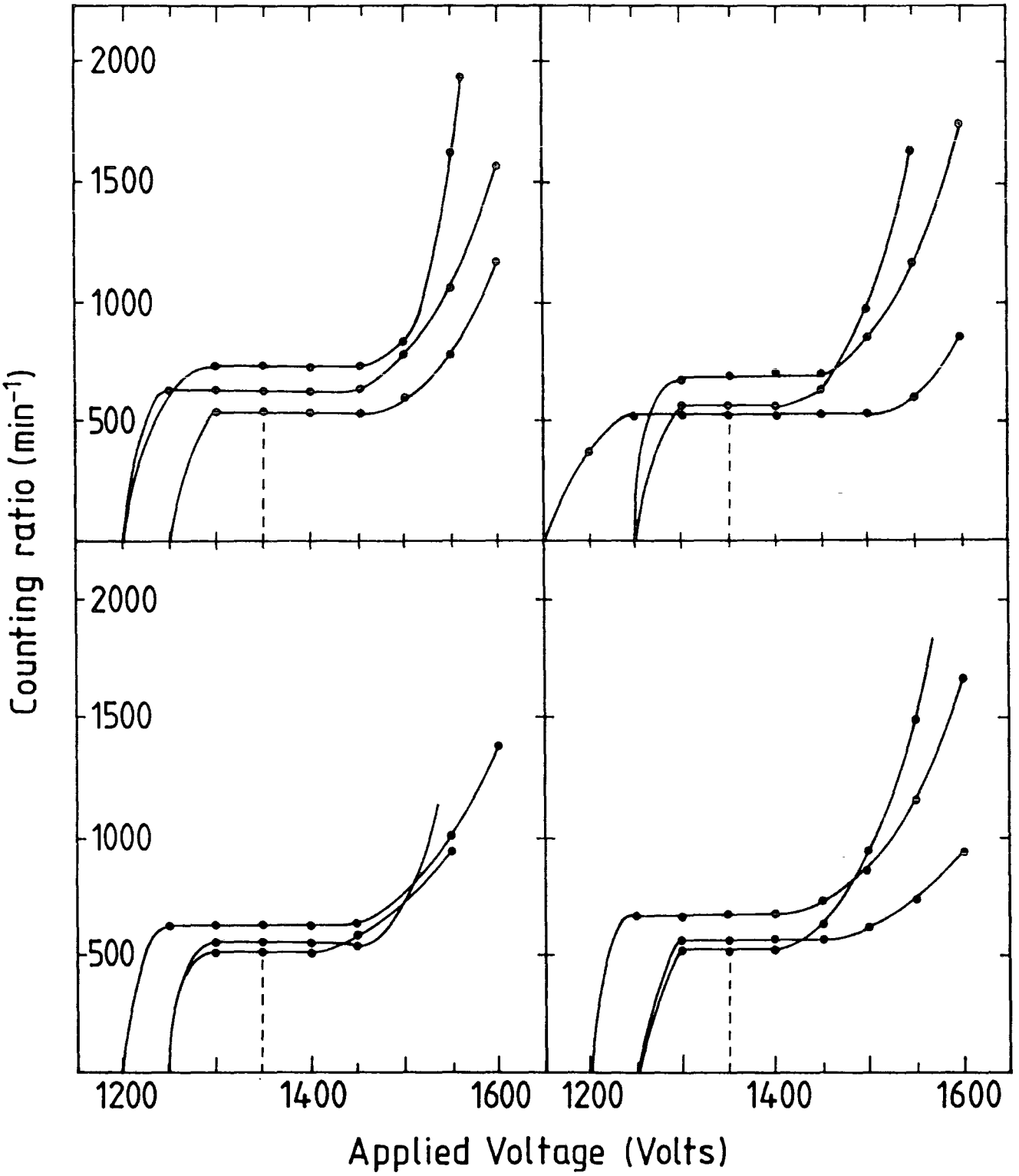

Figure 3.4: Determination of operating voltage of the counters used in the Geiger-Müller cosmic ray telescope.

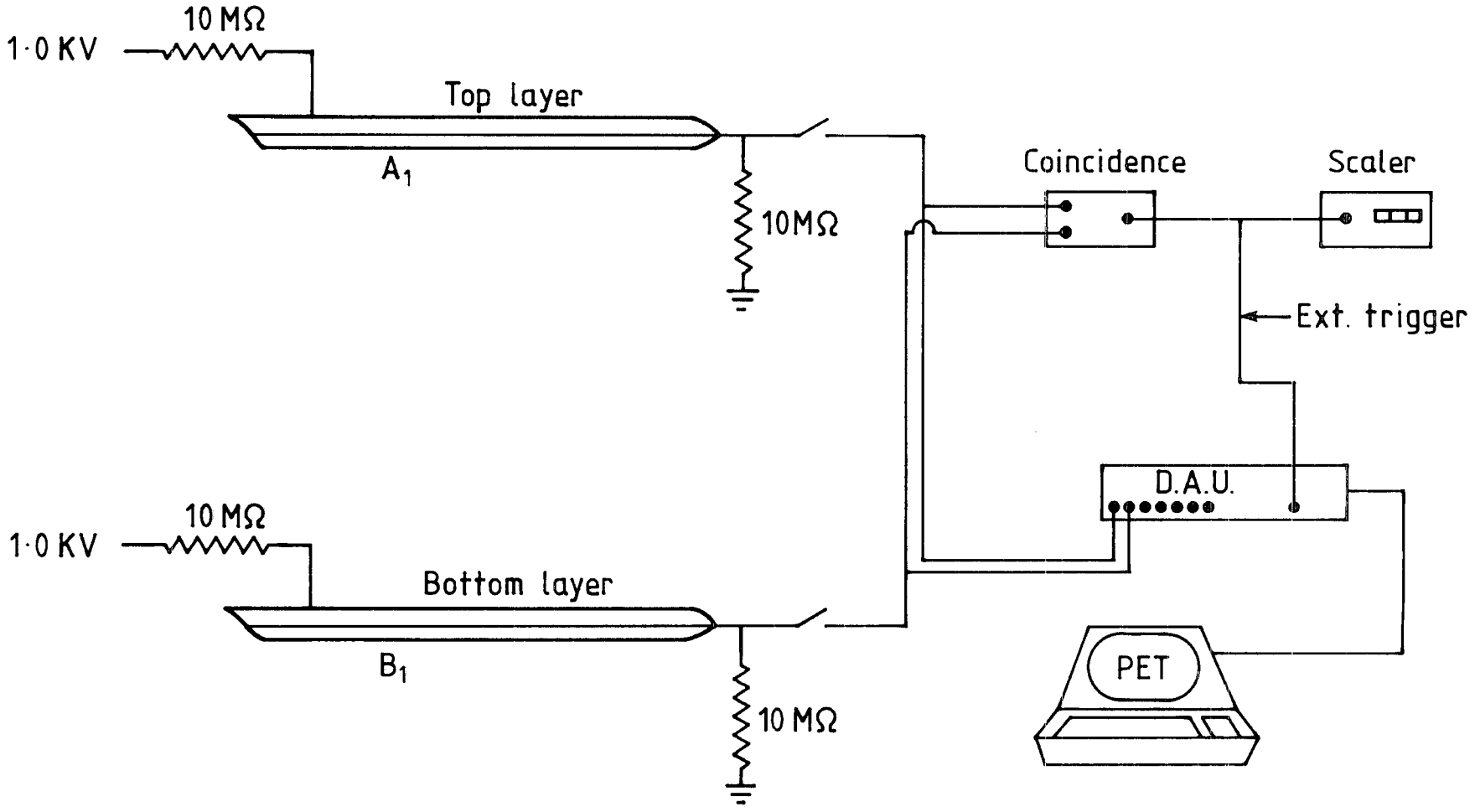

Figure 3.5: Block diagram of Geiger-Müller cosmic ray telescope.

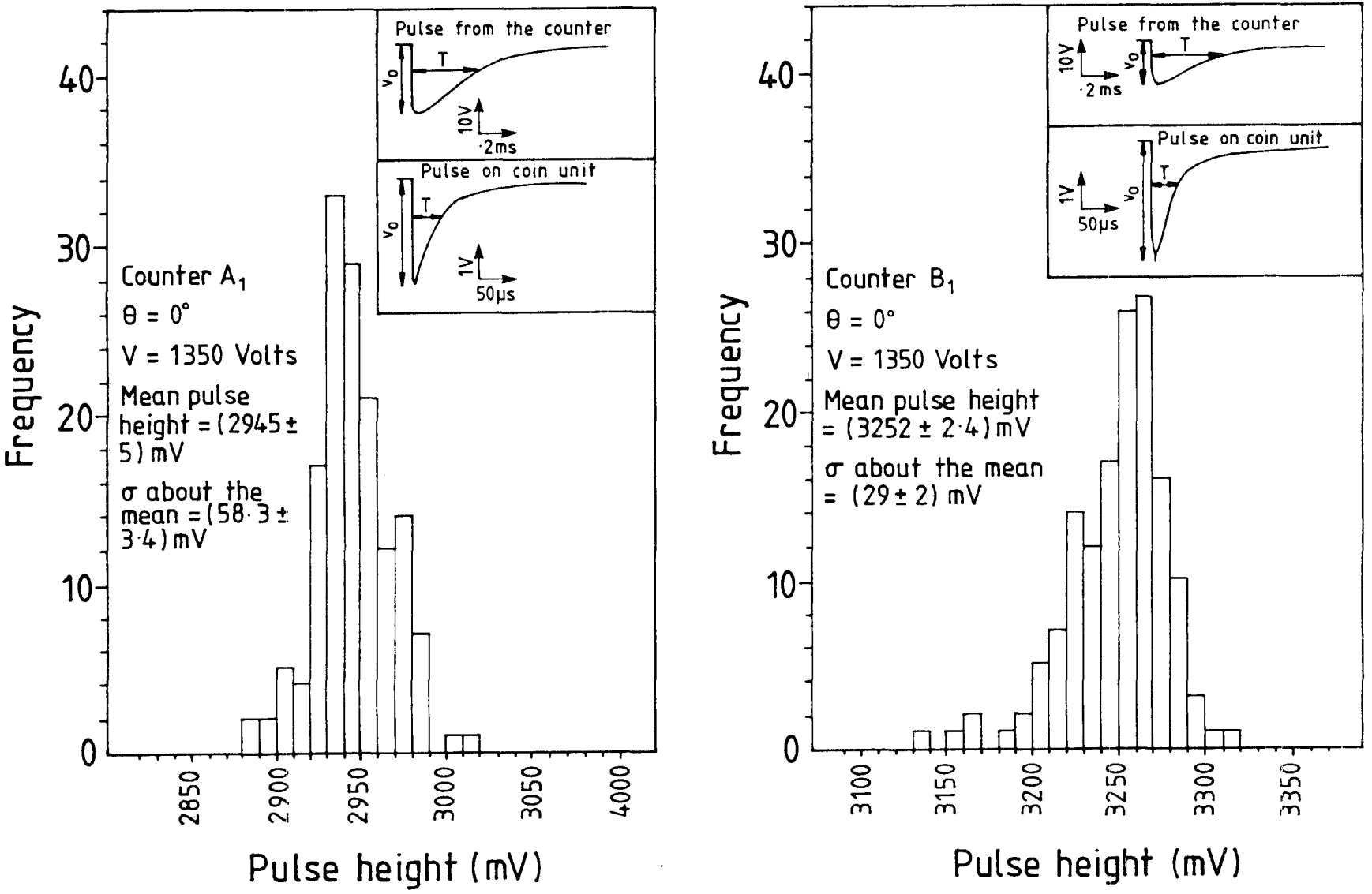

Figure 3.6: Pulse height distribution obtained by Geiger-Müller counters A_1 and B_1.

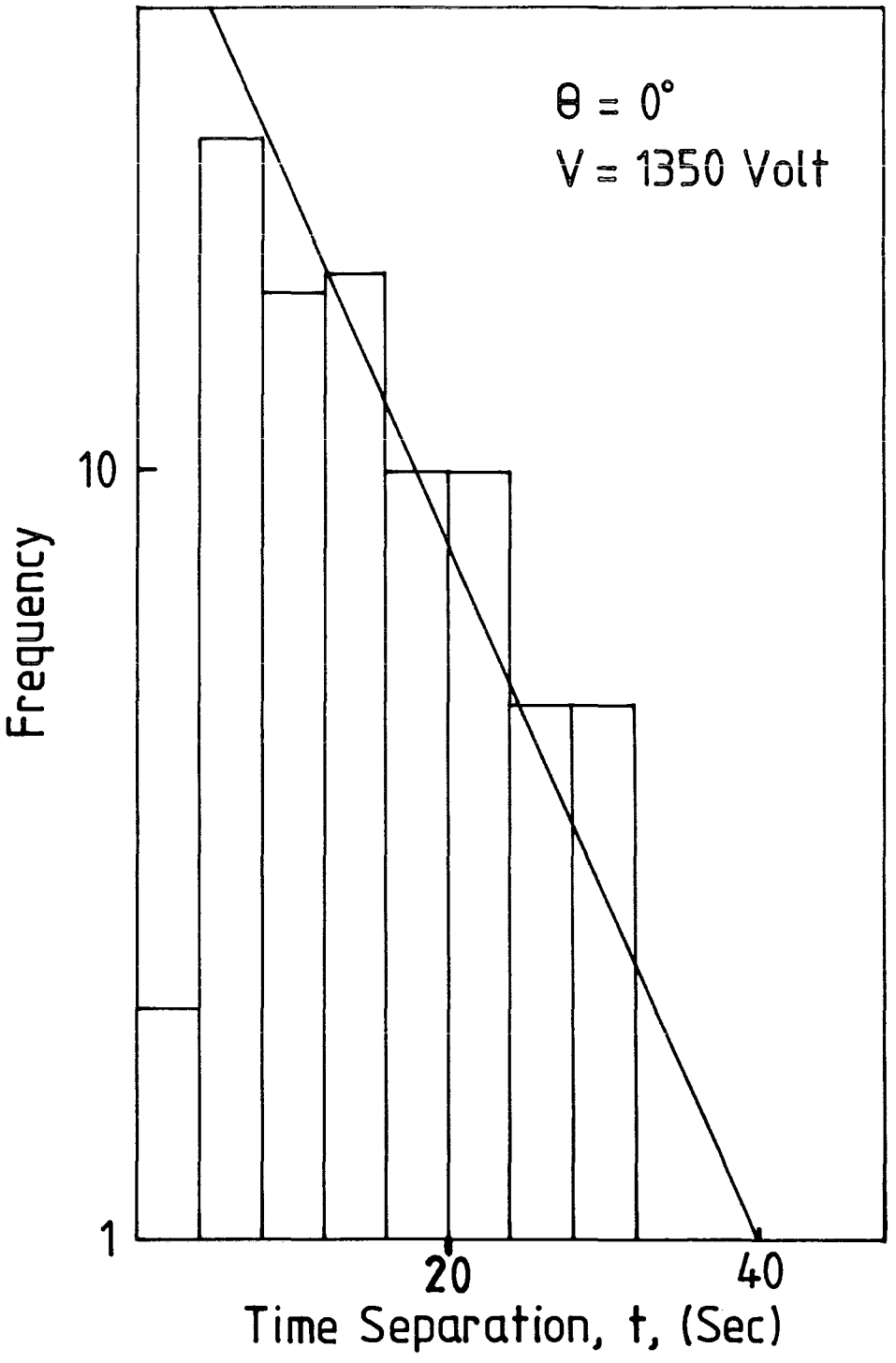

Figure 3.7: Differential distribution of time sepration of 96 successive events for counters A_1 and B_1 in a running time 0.69 hours corresponding to a mean time separation T = 10 seconds. The fitted straight line is of the form $n(t) = n_o e^{-t/T}$.

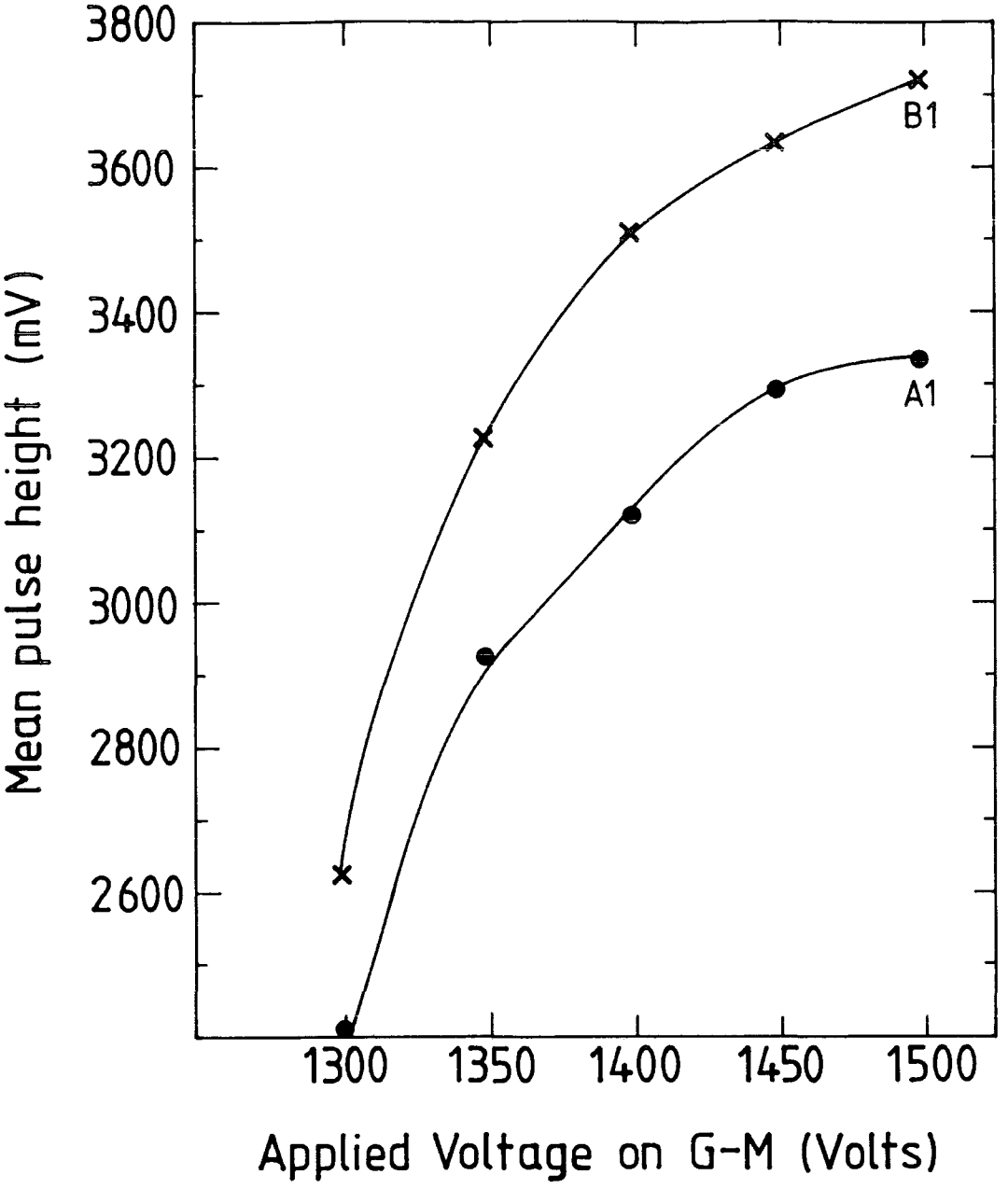

Figure 3.8: Effect of applied voltage on the pulse height of Geiger-Müller counters A_1 and B_1.

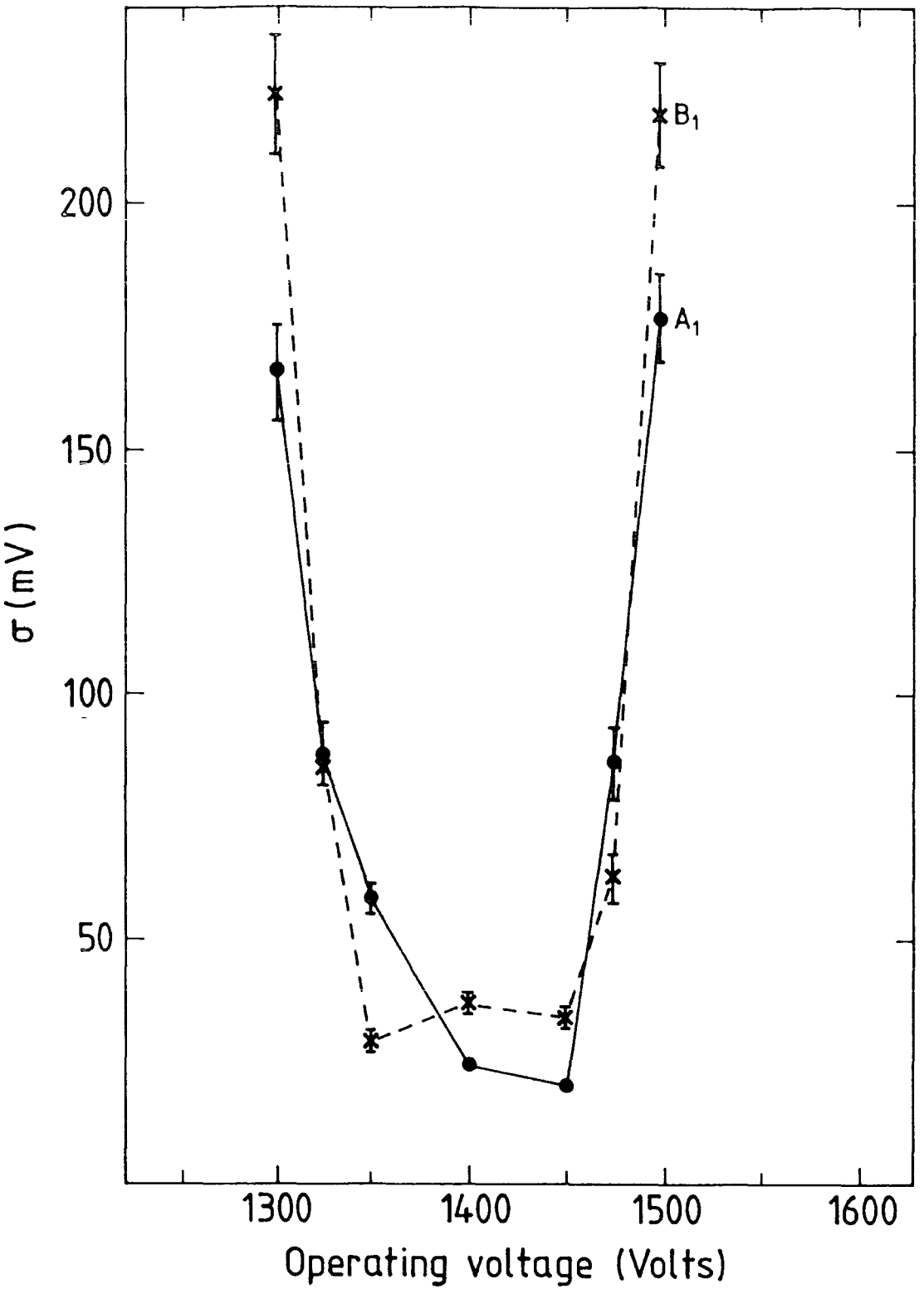

Figure 3.9: Dependence of the standard deviation (σ) of the pulse height distribution about the mean value on the counter operating voltage for counters A_1 and B_1

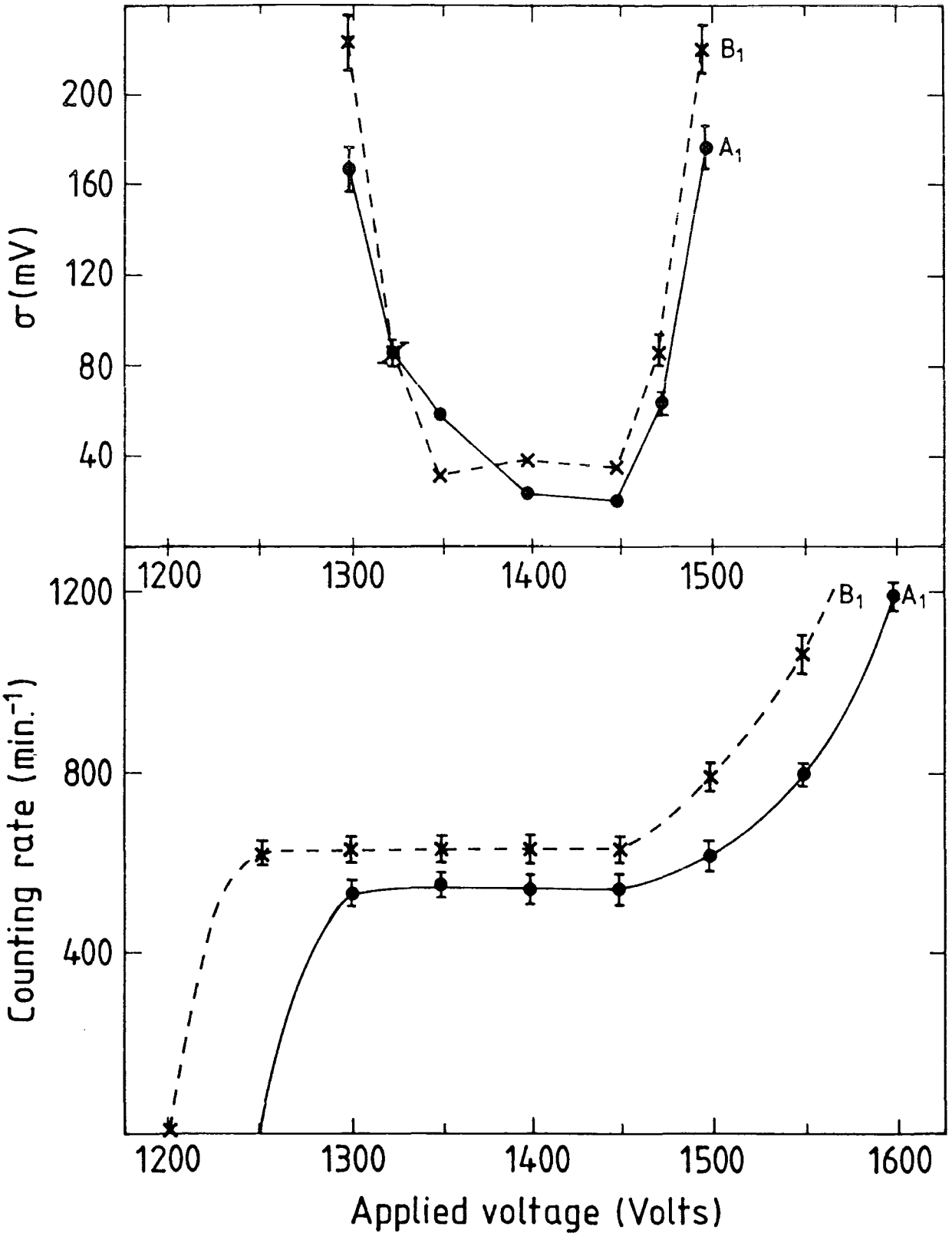

Figure 3.10: Comparison of the variation of the standard deviation (σ) of the pulse height distribution about the mean value with counter operating voltage and the varation of the background counting rate with operating voltage for counters A_1 and B_1.

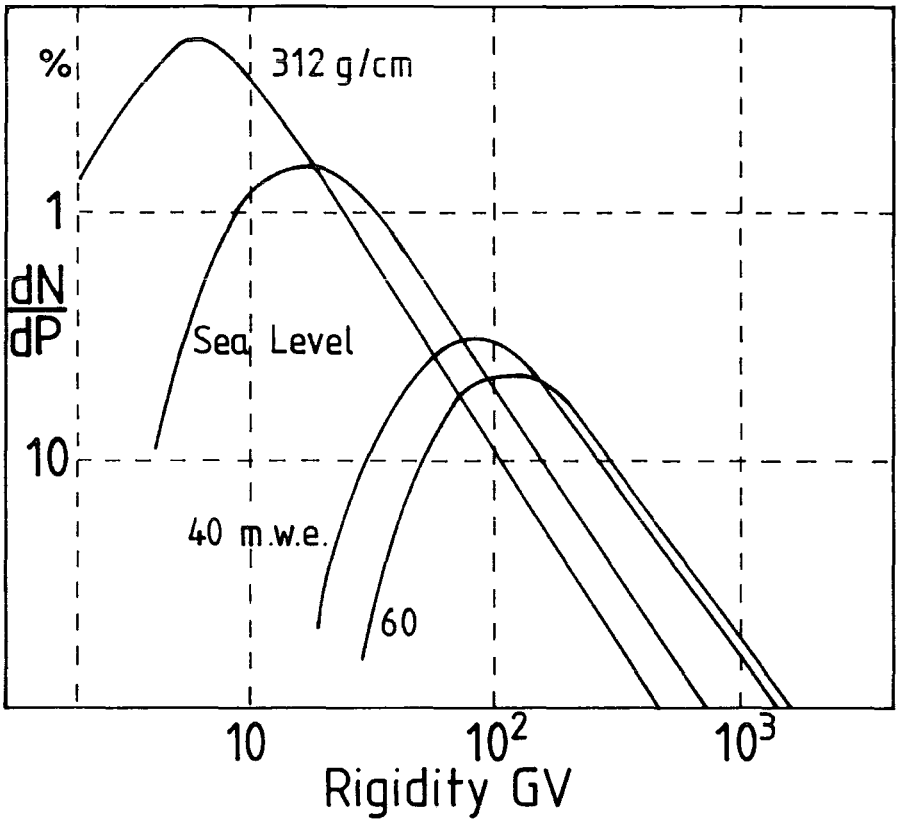

Figure 3.11: Differential response curves for meson monitors (after Webber and Quenby 1959).

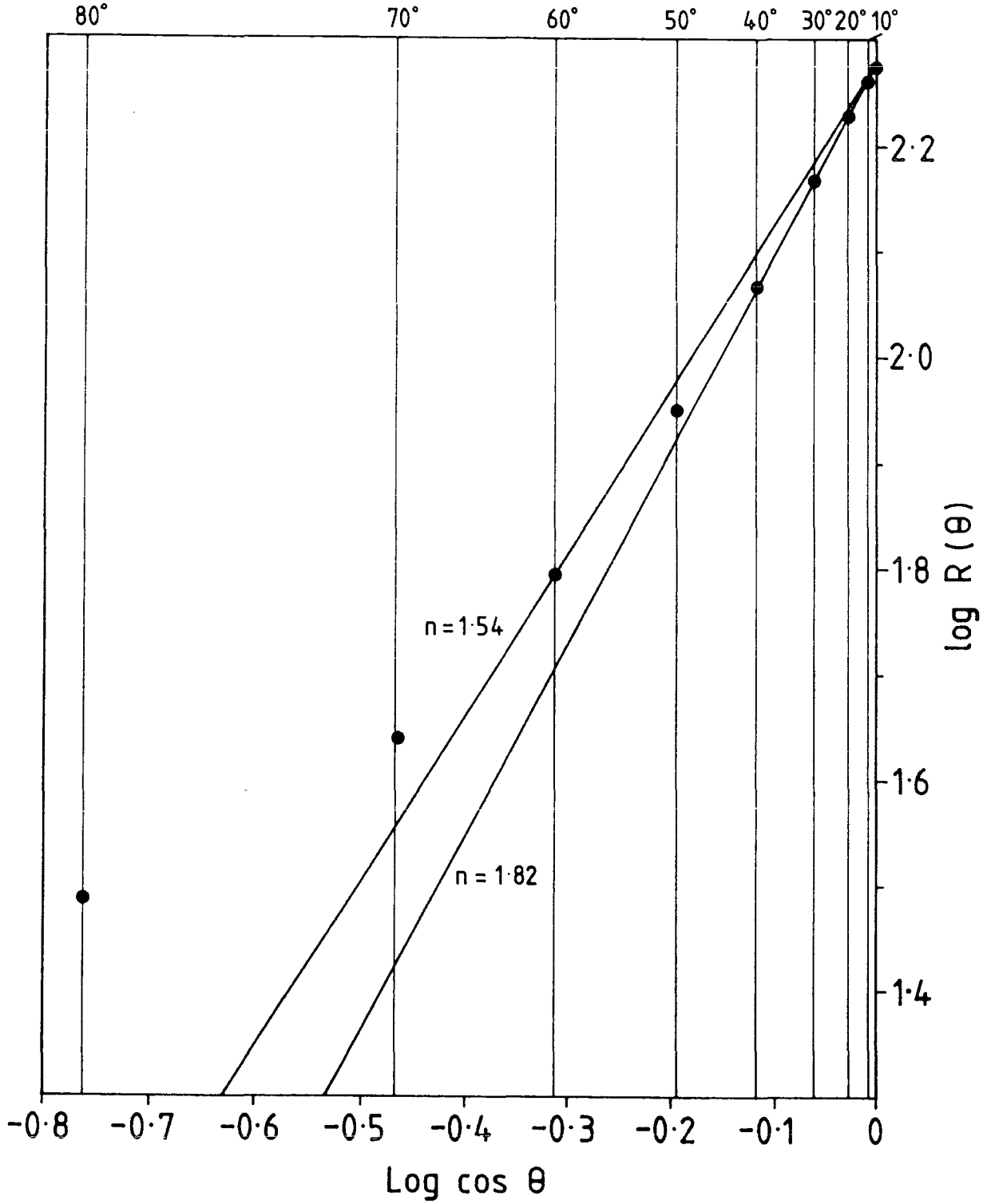

Figure 3.12: log R(θ) - log cos(θ) plot.
(R = counting rate per minute)

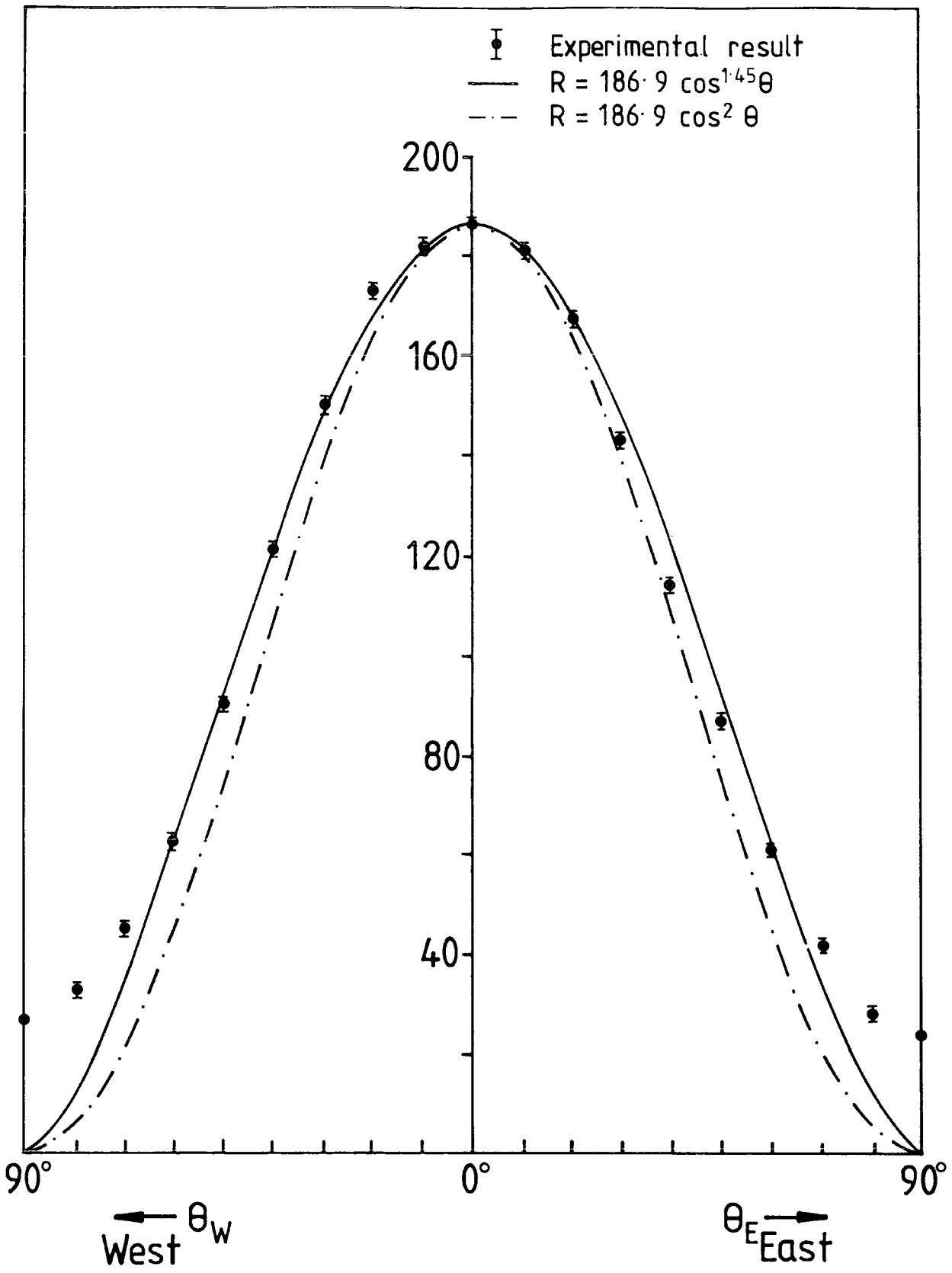

Figure 3.13: East-west effect.
The variation of counting rate with zenith angle.

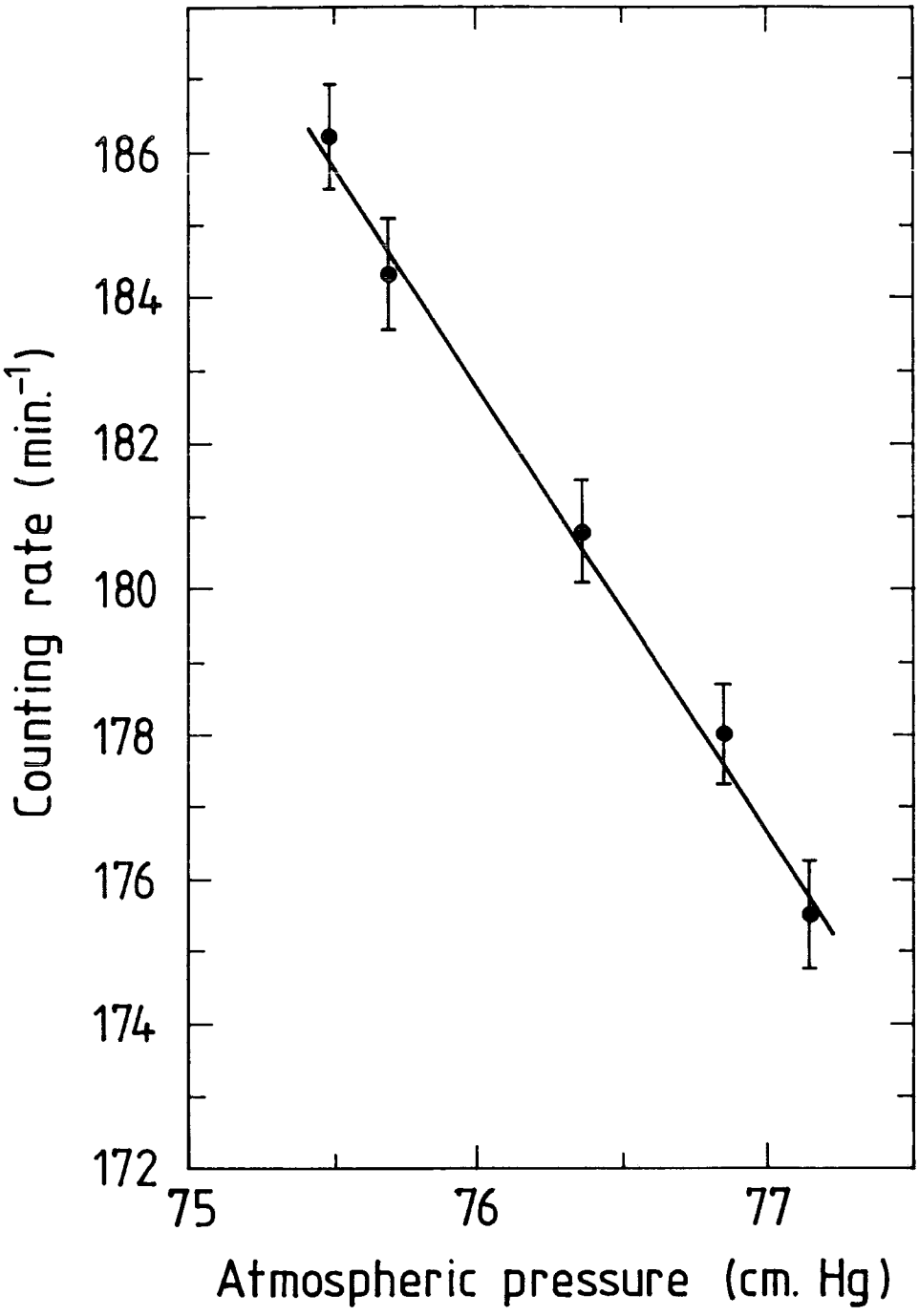

Figure 3.14: Variation of counting rate with atmospheric pressure.

Chapter Four

Measurement of the density spectrum of electrons at sea level and the derived size spectrum

4.1 Introduction

One way of studying extensive air showers is by examining the electron density spectrum for showers at sea level or above. One can gain information about the total number of particles spectrum by assuming that the lateral structure of showers is the same for all showers so that the density of particles at a point depends on the distance from the core of the shower and the total number of particles in this shower. With this information about the number spectrum one can calculate the energy spectrum of primary particles. Moreover, measurements of the density spectrum at various altitudes give an idea about the longitudinal development of showers.

The simplest method of measuring the density spectrum is to use proportional counters. When a shower strikes in the neighbourhood of the detectors, a number of particles simultaneously strike each detector, and this generates a coincident pulse. By analysing a record of such pulse heights, which are proportional to the number of particles traversing the detectors, over a known period of time, the integral density spectrum of the extensive air showers can be obtained.

Experimentally it is convenient to measure the integral density spectrum $R(>\Delta)$ which is defined as the rate that the charged particle density at a fixed point in space exceeds the value Δ.

The present experiment was performed using two scintillation counters, each with 0.4 m^2 area, and using the microcomputer data acquisition system.

Before describing the present experiment, it is convenient to make a few remarks about a number of previous measurements of the density spectrum of extensive air showers.

4.2 Some previous work

4.2.1 R.J. Norman

Norman (1956) measured the integral density spectrum. He used three proportional counters arranged radially in a horizontal plane 60 metres above sea level, at the three corners of a 5 metres equilateral triangle. A three-fold coincidence was used as a method of E.A.S selection. He recorded the pulse heights by taking photographs of them on an oscilloscope. From this record of pulse heights, the integral density spectrum was obtained. In the range of 20 to 500 particles per square metre Norman found that the integral density spectrum is :

$$R(>\Delta) = 540\ \Delta^{-1.39\pm0.04}\ h^{-1}\ ,$$

where R is the rate, Δ is the density of the particles. For $\Delta > 500$ particles per square metre he found that the exponent increases quickly, reaching 2.2 at Δ = 1,000 particles per square metre.

4.2.2 J.R. Prescott (1956)

Prescott used a complementary ionization chamber and Geiger counter system. The two ionization chambers were of cylindrical type 57.6 cm long and 8.8 cm in diameter, filled to 39 atmospheres with nitrogen, both placed at 3 m and 5 m from the master group. The master group is made up of three G-M tubes in coincidences located immediately above one of the chambers to identify the extensive air shower.

The experimental data for coincidence bursts greater than a given size in both chambers at a separation of 5 m obtained in 725.8 hours running time indicated that there is 7% probability that a single line of slope -1.45 fits all the observed data in the range of Δ = 400-500 m^{-2}. Prescott, however, measured the distribution of burst sizes in a single ionization chamber 5 m apart from the master group. In 627.9 hours running time 115 bursts were observed. At densities of $\Delta < 1{,}000\ m^{-2}$ the slope of spectrum was found to be the same as that obtained previously, though its absolute rate was greater by a factor of two compared to the former one. The probability that the experimental results obtained, analysing the results of a single ionization chamber, fit a power law in the whole range of measured densities with exponent -1.45 was found to be 4%. The observation based on the second method showed that the exponent of the integral density spectrum is -1.54 ± 0.14 in the region of Δ = 500 - 1,000 m^{-2} at sea level.

4.2.3. R.J. Reid et al. (1961,1962)

The differential density spectrum of extensive air showers was measured by Reid et al. using a counter controlled cloud chamber. The experiment was carried out at three different stations, Jamaica, Ireland and Sydney. At each station two cloud chambers were employed with their axes at right angles to each other, but only the number of tracks through one of the chambers was counted and related to the density spectrum. The illuminated areas of the chambers at Jamaica, Dublin and Sydney were 540, 360, and 1100 cm^{+2} respectively. A considerable number of triggering criteria were used to trigger the cloud chambers.

Though they found some discrepancy in the observed slope of the density spectrum due to the difference in triggering criteria, the overall results corrected for Poissonian fluctuations of the number of particles crossing the chambers, and also corrected for the triggering probability of the chamber system showed that the exponent of the differential density spectrum is -2.5 in the region of Δ = 50-500 m^{-2} and -3.9 ± 0.5 for $\Delta > 1{,}100\ m^{-2}$.

Further observations were made at the Jamaica station (Reid et al 1962) and it was concluded that the slope of the density spectrum in differential form is -2.6 ± 0.3 for densities in the range of Δ = 200 - 1,000 m^{-2} and -4.0 ± 0.5 for Δ = 1,000 - 5,000 m^{-2}.

4.2.4 T. Gemesy et al (1964)

Gemesy et al employed a cloud chamber to investigate the density spectrum of extensive air shower. A coincidence pulse of four

Geiger counters (of an area of 320 cm^2 each) was placed at the corners of a (10 x 9)m^2 rectangle enclosing the chamber. The chamber was a multiplate one, where only the volume above the upper plate in the chamber was scanned when counting the number of tracks shown on the photographs. The illuminated area of the uppermost plate of the chamber was 150 cm^2 and the observation was carried out at 410 m elevation.

A total of 3,274 coincidences was recorded in the region of Δ = 70 - 13,000 m^{-2}. They found that there was no significant change in the slope of the density spectrum and that the exponent of the integral density spectrum was 1.49 $\pm$ 0.08 in the range 70 -200 m^{-2} and 1.57 $\pm$ 0.03 in the range 70-13,000 m^{-2}.

4.2.5 Ashton and Parvaresh (1975)

A proportional counter of rectangular cross-section was employed initially to measure the density spectrum of extensive air showers. The counter was made of aluminium walls with external dimensions of 15 x 15 x 101 cm filled with a 90% argon and 10% methane gas mixture at atmospheric pressure. Extensive air showers were selected by the simultaneous passage of a predetermined number of particles through each of three liquid scintillators each of an area 1.24 m^2, placed in close proximity of one another. They obtained a density spectrum having the following form:

$$R(>\Delta) = 411\ \Delta^{-(1.50\pm0.05)}\ hr^{-1} \quad \text{for} \quad 40<\Delta<1,000\ m^{-2}$$

$$R(>\Delta) = 1.3 \times 10^4\ \Delta^{-(2.00\pm0.2)}\ hr^{-1} \quad \text{for} \quad 1,000<\Delta<5,000\ m^{-2}$$

where Δ is in the units of particles m^{-2}.

The results indicated that the integral density spectrum of

extensive air shower at sea level has a slope of -1.50 in the density range Δ = 40 - 1000 m^{-2}. This is approximately consistent with most of the other experimental data obtained in this range of density. The slope of the spectrum was found to be -2.0 in for $\Delta > 1000\ m^{-2}$. As a comparison they found that the absolute rate given by Greisen (1960), was higher compared with their experiment with a ratio of 2.0 at Δ = 100 m^{-2}, but they found a better agreement compared with the result given by Cocconi (1949) and Cocconi and Tongiorgi (1949). They concluded that if one takes the average measured rate between their results and those of Greisen it will approximately agree with the absolute rate as given by Cocconi and by Cocconi and Tongiorgi in the range of $40 < \Delta < 1000\ m^{-2}$.

Assuming the lateral structure function of extensive air showers particles is independent of shower size, three different lateral structure functions, the Greisen, the Kiel and the Sydney groups, were used independently to interpret the data. The analytic expression for these function, respectively, are as follows:

$$F_G(r) = \frac{0.4}{r_1^2}\left(\frac{r_1}{r}\right)^{0.75}\left(\frac{r_1}{r+r_1}\right)^{3.25}\left(1+\frac{r}{11.4\ r_1}\right)$$

$$F_K(r) = 1.08\times10^{-2}(r+1.1)^{-1.5}\exp\left(\frac{-r}{120}\right)$$

$$F_G(r) = 2.12\times10^{-3}(r+1.0)^{-1.0}\exp\left(\frac{-r}{75}\right)$$

After measuring a density spectrum, the best estimate of the size spectrum was suggested to be:

$$R(>N) = 3.0 \quad N^{-1.3} \quad m^{-2} \; s^{-1} \; st^{-1} \quad N < 7\times10^{5}$$

$$R(>N) = 36{,}920 \; N^{-2.0} \quad m^{-2} \; s^{-1} \; st^{-1} \quad 7\times10^{5} < N < 3\times10^{7}$$

$$R(>N) = 6.76 \quad N^{-1.5} \quad m^{-2} \; s^{-1} \; st^{-1} \quad N > 3\times10^{7}$$

4.2.6 Previous measurements.

Based on summarised experimental results, Greisen (1960) gives the following expression for the integral density spectrum in the range $1 < \Delta < 10^{4}\ m^{-2}$.

$$R(>\Delta) = 540\ \Delta^{-(1.3 + 0.055 \log \Delta)}\ hr^{-1} \text{ at sea level.}$$

The previous integral density spectra measured at sea level are shown the Figure 4.1, each density spectrum has been normalized so that the rate at $\Delta = \Delta_o$ be identical to the rate given by Greisen, where Δ_o is the minimum density measured in each experiment). One may make some remarks about these spectra. The first is that the exponents of the density spectra are approximately equal. However, there is a notable difference in the absolute rate due to the difference in experimental conditions and the detectors used. It is also remarkable that the slope of the density spectrum does not remain constant throughout the measured density range, this change in the slope has been interpreted in general as due to a change in the characteristic of the nuclear interaction, or as a result of the change of the slope of the primary energy per nucleon spectrum (the knee).

4.3 Introduction to the present experiment.

The object of this experiment is to measure the density spectrum of the extensive air showers at sea level. The density spectrum in the range of 2.7 to 37 particles/m^2 was measured using

two scintillators, a scaler and discriminators. The density spectrum, between 20 and 400 particles/m^2, was obtained by using two scintillators and a PET personal computer, via the data acquisition unit, that recorded the data on a magnetic cassette tape. Beside the main goal of the experiment, the data was analysed to study the correlation between the detected number of particles by each scintillator. Moreover, the muon density was also measured by employing a third scintillator situated under 15 cm lead and 15 cm iron layers, which is equivalent to 288.5 g cm^{-2}.

The design and performance of the two main components of the system used in this experiment which are the thin plastic scintillators and the computerized data acquisition system are described in the next two sections.

4.4 Plastic scintillators

Two thin plastic scintillators were used in the present experiment. Each scintillator consisted of an NE102A phosphor of dimensions 80x50x5cm^2 viewed by two 5 cm diameter photomultipliers (type 53AVP) via perspex light guides. A detailed description of the design and performance of these scintillators was published by Ashton et al (1983). When a relativistic cosmic ray particle traverses the scintillation material, it loses some of its energy by liberating electrons which, in turn, produce photons. The photomultipliers detect this scintillation light and each produces a pulse. The two pulses are added by the head unit. The size of the pulse at the head unit is proportional to the energy deposited

by the traversing cosmic ray particles, since the energy loss per unit length is practically independent of the energy of the particle (see for example Fermi 1949b, page 33), the scintillation material is thin, and most particles have small incident angles, hence the size of the pulse V is proportional to the number of the cosmic ray particles N traversing the scintillator:

$$V = e.N \quad mV$$

where e is the pulse height due to a single relativistic particle traversing the scintillator at a normal incidence. To obtain e, one has to study the response of the scintillator to the global cosmic ray flux, using a pulse height analyzer. This response should yield a distribution with a peak, which is due to the passage of single relativistic cosmic ray particles close to normal incidence. However, the observed distribution is broader than expected, see Figures 4.3 . This is because of different processes, which are Landau fluctuations of ionization loss that are reflected in the number of scintillation photons that arrive at the photomultiplier photocathodes, fluctuations in the number of photoelectrons produced, the non uniformity of response of the phosphor over its area, and that not all incident particles are normal to the plane of the scintillator. The peak of the observed distribution is expected to correspond closely to the average pulse height produced by cosmic ray particles traversing the phosphor at normal incidence. Knowing the relation between the channel number and the pulse height, one could obtain the pulse height produced by single particles. Notice that, this peak should be well resolved from the distribution produced by single thermal

electrons leaving the photocathodes of the photomultipliers of the scintillator.

The response of scintillators A and B to the global cosmic ray flux was examined using a pulse height analyzer . Figure 4.3a and 4.3b show the actual observed distributions of pulse height for scintillators A and B respectively. One may see a recognizable peak for each of these distributions. The most frequent pulse height is considered as the pulse height produced by the passage of single relativistic cosmic ray particles through the scintillators with normal incidence.

The pulse height analyzer was calibrated to interpret the distribution in terms of pulse height and not channel number. The calibration was done by applying negative exponential pulses of 10 μs decay time produced by a pulse generator. Figure 4.4 shows the result of this calibration and the best fit line is drawn in this figure. The equation of this line is as follows:

Pulse height = (0.600 ± 0.004) Channel number + (2.28 ± 0.19) .

4.5 Data acquisition unit.

The data acquisition unit is an electronic analogue to digital device which records the input voltages on its eight channels when it is triggered and then sends the information to a Commodore PET computer. It works under the control of a PET computer after running a long program written in BASIC. This program was supplied with the data acquisition unit on magnetic tape. To operate the system to record pulse heights, one first loads the program from the tape in the usual manner and then runs it. The program will

enter initial dialogue in which the user selects actions, gives a name to the record file, and sets the internal clock. The user may calibrate the zero and the gain if required. Once the dialogue finishes, the system is ready to record whenever it is triggered. In the present experiment, the data were recorded on magnetic tape and then printed using a BASIC program .

The aim of the calibration is to adjust the data acquisition unit to have a standard response to the pulse heights at the scintillator's outputs due to the passage of cosmic ray particles through it to give us the real values of these pulse heights.

Because the cosmic ray pulse is a negative exponential one, the data acquisition unit was calibrated by using an exponential pulse generator to generate negative exponential pulses of different decay time at the input to the data acquisition unit. It was found that using pulses of long decay time there is a linear relation between the pulse height at the input to the data acquisition unit -measured by an oscilloscope- and the pulse height recorded by the data acquisition unit. The slope of the best line through the measurements was found to be approximately one (see Figure 2.3). However, the same agreement was not found when using pulses of short decay time. Unfortunately, the decay time of the cosmic ray pulses at the outputs of the scintillators' head units; is approximately 8.5 μs. This decay time is considered to be short. That explains the necessity to use stretcher amplifiers. When a short pulse is passed to the stretcher amplifier, it produces a readable long pulse. This stretcher amplifier is not linear. The combination of the stretcher amplifier and the data acquisition

unit makes a suitable measuring system for the present experiment. The system was calibrated by using exponential negative pulses of decay time 1 μs and 10 μs at the input to the stretcher amplifier, see Figure 2.9. Figures 2.10, and 2.11 show the results of the calibration.

4.6 Experimental arrangement.

Two thin plastic scintillators A and B (described in section 3 of this chapter) were used in this experiment. The area of each of these is 80x50 cm = 0.4 m^2, placed horizontally with their long sides being parallel and their centers being separated by a distance of 1.7 m. Figure 4.5 shows a schematic diagram of the system used. Each scintillator was calibrated by determining the average pulse height, e, at the head unit outputs, produced by single relativistic cosmic ray particles traversing the phosphor at normal incidence. These scintillators were used as a trigger system as well as proportional detectors. As a trigger system, the arrival of an extensive air shower was identified by a twofold coincidence between the two scintillators, and to select those showers with local density greater than a threshold density, the outputs of each scintillator should be passed, first, through an amplifier and then a discriminator which cuts off all pulse heights smaller than the pulse height corresponding to the given density, before passing to the coincidence unit. The triggering pulse from the coincidence unit was passed through a fan-out to trigger the data acquisition unit and the scaler. For each trigger, each of the pulse heights V_A and V_B, out of scintillators

A and B respectively, was passed through a stretcher amplifier to one of the data acquisition unit channels. The data acquisition unit sent all measurements of this event to the Commodore PET computer, which recorded this information, and the time of each trigger, on a magnetic tape in its cassette drive. The circuit diagrams of the electronics which were used in the experiment are shown in appendix A.

4.7.1 Density spectrum measurement for $2.7<\Delta<37$ m^{-2} by direct counting.

The density spectrum over the range $2.7 < \Delta < 36$ m^{-2} was obtained using the two scintillators (A & B), two discriminators and a coincidence unit, and this system is shown in Figure 4.6. Both discriminators were set on the value corresponding to the same density and then the coincidence rate was counted by scaler for a known interval of time. This was repeated for various discrimination levels. The results of this experiment are given in Table 4.1, and Figure 4.7 shows the plots of these results. This spectrum was found to have the form

$$R(>\Delta) = 2058\ \Delta^{-(1.66\pm0.06)}\ hr^{-1}\ ,$$

where the density Δ is in terms of electrons per m^2.

4.7.2 Density spectrum measurement using the data acquisition system.

Figure 4.5 shows a schematic diagram of the system used in this experiment. The system was run many times and before each run the stability of the system was verified. The total running time was 362 hours. The results of this experiment are given in

Table 4.2 and Figure 4.8 shows the density spectrum obtained in this experiment.

The data were recorded on magnetic tapes by the PET personal computer, via the data acquisition unit (D.A.U) and were corrected using the FORTRAN program 'CALIBRATION' (see Appendix B). As mentioned in Chapter 2, the values of the pulse heights read by the D.A.U were the values after the pulses went through an amplifier and a stretcher amplifier. The correction program 'CALIBRATION' gives the values of the pulse heights as they were given to the D.A.U , then it uses the embedded information about the D.A.U's calibration curves obtained in the laboratory (see Chapter 2) to calculate the the pulse heights out of the scintillators' head units before any modification. The program then converts the calibrated values of the pulse heights to densities and these were stored in a new file ready to be analysed, by using the program 'INTGDST04' (see Appendix C). The idea of this program is that, when it reads the densities as pairs for each pair, the first value represents the density detected by scintillator A, and the second value is for scintillator B. The program then compares these two values to a sequence of preset minimum densities consecutively, if both are larger than the preset density one should be added to the value of the VARIABLE which acts as a counter for events greater than this density level.

The integral density spectrum over the range $20<\Delta<600$ m^{-2}, which was obtained in this experiment, is shown in Figure 4.8. It has the form :

$$R(>\Delta) = (1054 \pm 89)\ \Delta^{-(1.56\pm0.02)}\ hr^{-1}$$

where the density Δ is in terms of electrons per m^2. Figure 4.9 compares the present work with two previous works. One may notice a very good agreement between the present work and the one due to Greisen (1960). The absolute rate of the obtained density spectrum is not in good agreement with the spectrum due to Ashton et al (1975). However, they are almost parallel. The form of the spectrum given by Ashton et al is,

$$R(>\Delta) = 411\ \Delta^{-1.5} hr^{-1}$$

4.7.3 Correlation between the number of particles that traverse scintillators A and B.

The correlation between the number of particles traversing each scintillator was investigated by analysing the data obtained in the density spectrum measurement. Figure 4.10 shows the frequency distribution of the density ratios N_A/N_B and N_B/N_A. It is seen that the most probable value of the frequency ratio is close to unity in both cases and that the distributions show a long tail. The peaking of the density ratio at a value close to unity is consistent with the known slope of the electron density lateral structure function as a function of the core distance and the estimates of the median core distance of showers that produce a local electron density greater than some threshold value are shown in Table 4.3 (Ashton and Parvaresh, 1975).

4.7.4 Density spectrum of penetrating particles

Figure 4.5 shows that a third scintillator of area 1.05 m^2, was used in this experiment. The job of this scintillator was to

detect and count the number of particles which succeeded in penetrating 15 cm of iron and 15 cm of lead (equivalent to 288.5 g cm^{-2}) or the events could be created by a cosmic ray particle that interacted inside the absorption material. The average number of particles recorded by scintillator C is plotted versus the electron density of the shower above the absorbers in Figure 4.11. It is believed that these particles are mainly muons. Their density spectrum is plotted in Figure 4.12, and the experimental results are listed in Table 4.4. The spectrum is also drawn with the electron density spectrum for comparison in Figure 4.13. This spectrum can be represented by,

$$R(>\Delta_c) = (4.2 \pm 0.2)\ \Delta_c^{-(0.76\pm0.03)} \quad hr^{-1} \quad \text{for } \Delta_c < 10\ m^{-2}$$

$$R(>\Delta_c) = (15.4 \pm 6.0)\ \Delta_c^{-(1.3\pm0.1)} \quad hr^{-1} \quad \text{for } \Delta_c > 10\ m^{-2}$$

where Δ_c is in m^{-2}.

4.8 Simulation of the density spectrum

In this section we will discuss the density simulation program MC.DENSITY01, which simulates the present experiment (listed in Figure 4.14). This program assumes that a given number of showers strike in the neighbourhood of the two scintillators used in the experiment and calculates the electron density for each scintillator using the NKG lateral distribution function, with the age parameter 1.2. Each of the simulated showers have a size randomly chosen from the size spectrum due to Hillas (1970) which is as follow:

$$R(>N) = 52\ N^{-1.5}\ m^{-2}\ s^{-1}\ st^{-1} \quad \text{for } N < 5\times10^5$$

$$R(>N) = 36920\ N^{-2}\ m^{-2}\ s^{-1}\ st^{-1} \quad \text{for } N > 5\times10^5$$

The following is the description of the two simulation processes the computer performs.

1. Simulation of the shower size

The shower size, N, is randomly generated from the integral distribution of the form,

$$f(>N) = AN^{-\gamma}$$

where A and γ are constants. The integral method (Knuth, 1981) is used. The actual distribution has a change in the slope, so the size is actually generated from a two component distribution,

$$f_1(>N) = A_1 N^{-\gamma_1} \qquad N_L<N<N_B$$
$$f_2(>N) = A_2 N^{-\gamma_2} \qquad N_B<N<N_U$$

where N_U, N_L are the upper and the lower limits of size generated and N_B is the point where the slope changes.

Firstly the distribution is normalized by dividing by the total area, T, under the distribution, ie.

$$T = A_1 \int_{N_L}^{N_B} N^{-\gamma_1}\, dN + A_2 \int_{N_B}^{N_U} N^{-\gamma_2}\, dN$$

The integral distribution is then formed.

$$I_1 = [A_1 \int_{N_L}^{N} N^{-\gamma_1} dN] \,/\, T \qquad N_L \le N < N_B \qquad \text{(Eq 4.1)}$$

$$I_2 = [A_1 \int_{N_L}^{N_B} N^{-\gamma_1} dN + A_2 \int_{N_B}^{N} N^{-\gamma_2} dN] \,/\, T \qquad N_B \le N<N_U \qquad \text{(Eq 4.2)}$$

If a random number is generated from a uniform distribution between 0 and 1 and equated to the integral, then the relevant random shower size can be determined from equations 4.1 and 4.2. If the random number, R, is greater than,

$$(A_1 \int_{N_L}^{N_B} N^{-\gamma_1} dN) \quad / \ T$$

then I_2 is used, otherwise I_1 is used. This procedure is carried out in the subroutine SIZE. Limits of 1.8×10^4 and 10^9 are placed on the size since outside this region the rate of triggering is very low or non-existent. The integral size spectrum of 1,000 simulated showers using this method is shown in Figure 4.15, together with the integral spectrum given by Hillas (1970). This figure shows that the above simulation procedure gives the correct result for the size spectrum.

2. Simulation of the core distance.

To generate a number of points each representing the core of a shower, uniformly distributed inside a circle with radius R, first generate random points in a square which is concentric with the circle and has side of R, then discard those points that do not lie in the circle (see Cheney and Kincaid 1980). The distance to each scintillator is then calculated.

The results of this program in calculating the expected density spectrum are shown in Figure 4.16 and experimental results are also shown for comparison. The density spectrum produced here was found to have the same exponent as the exponent of the density spectrum measured in the present work, but it has a larger

absolute rate by a factor of 1.4. The spectrum obtained by the simulation program can be described by the analytical form

$$R(>\Delta) = 1475.6 \quad \Delta^{-1.56} \quad hr^{-1}$$

The distribution of the ratio Δ_A/Δ_B is also obtained in this simulation program and the result is shown in Figure 4.17 where it is compared with the average of the two experimental ratios shown in Figure 4.10.

4.9 Derivation of the size spectrum from the density spectrum

The density of electrons in an extensive air shower measured by scintillators depends on the distance from the core of the shower and its size. The relation which gives the density of electrons Δ at distance r is known as the lateral distribution of electrons and is as follows:

$$\Delta(r) = N \frac{f\left(\frac{r}{r_1}\right)}{r_1^2} \quad m^{-2}$$

where N is the size of the shower and r_o is the called the Mollier unit and equals 79 m at sea level. The function $f(r/r_1)$ is called the lateral distribution function (Nishimura-Kamata-Greisen function) where

$$f\left(\frac{r}{r_1}\right) = c(s) \left(\frac{r}{r_1}\right)^{s-2} \left(\frac{r}{r_1} + 1\right)^{s-4.5}$$

c(s) is the normalization constant so that :

$$\int_0^\infty 2\pi r \, \Delta(r) \, dr = 1$$

and the value of it is given in section 5.5. s is called the age parameter and it is a measure of how flat or sharp the lateral electron density distribution is. More discussion about the lateral electron density distribution is given in chapter 5.

To understand the relationship between the sea level density spectrum and the sea level number spectrum consider the following simplified argument. Suppose the sea level integral number spectrum of extensive air showers is $R(>N) = A\ N^{-\gamma}$. Define a lateral distribution function f(r) so that the electron density at distance r from the core is given by $\Delta(r) = N\ f(r)$, then conservation of the total number of particles in the shower gives

$$\int_0^\infty N\ f(r)\ 2\pi r\ dr = N$$

ie

$$\int_0^\infty f(r)\ 2\pi r\ dr = 1$$

For showers falling at distance r from a detector the minimum shower size to produce a density Δ at the detector is

$$N_{min} = \frac{\Delta}{f(r)}$$

Thus the rate of recording showers of density $>\Delta$ is given by

$$R(>\Delta) = \int_0^\infty A \left[\frac{\Delta}{f(r)}\right]^{-\gamma} 2\pi r\ dr$$

$$= \Delta^{-\gamma} \int_0^\infty \frac{A\ 2\pi r}{[f(r)]^{-\gamma}}\ dr$$

$$= K\ \Delta^{-\gamma}$$

if γ and f(r) are independent of N. Thus under these approximations the slope of the density spectrum should be exactly the same as that of the number spectrum.

In the present work the size spectrum was derived in two ways. First by using the density spectrum program, and second by scaling the present work to the similar work by Ashton and Parvaresh (1975).

(1) In the previous section we obtained a density spectrum by simulation assuming that the size spectrum is described by

$$R(>N) = 52\ N^{-1.5} \quad \text{for } N < 5\times10^5$$

$$R(>N) = 36920\ N^{-2} \quad \text{for } N > 5\times10^5$$

(Hillas 1970) and assuming that all showers have the same lateral distribution function. An age parameter of 1.2 was taken for all showers. The results of this program is larger in absolute rate than the measured density spectrum by a factor of 1.4, but it has the same exponent. One can infer that the size spectrum consistent with the present work is in the form

$$R(>N) = 37.1\ N^{-1.5} \quad \text{for } N < 5\times10^5$$

$$R(>N) = 26371\ N^{-2} \quad \text{for } N > 5\times10^5$$

(2) Ashton and Parvaresh (1975) measured a density spectrum of the form

$$R(>\Delta) = 411\ N^{-1.5} \quad hr^{-1}$$

The corresponding size spectrum was found to be

$$R(>N) = 3\ N^{-1.3} \quad m^{-2}\ s^{-1}\ st^{-1}$$

The density spectrum obtained in the present work has an absolute rate larger than that given by them by a factor of 2.56. One may deduce the size spectrum corresponding to the density spectrum

measured in the present work by scaling up the size spectrum given by Ashton and Parvaresh with the same factor. This can be written as follows:

$$R(>N) = 7.7\ N^{-1.3} \qquad m^{-2}\ s^{-1}\ st^{-1}$$

Figure 4.18 shows the two estimates of the size spectra obtained from the present work and the size spectra obtained by both Ashton et al. (1975) and Hillas (1970) are given for comparison.

4.10 Conclusion

A computerized data acquisition system was used to record the output of three scintillation counters. Two of them are thin plastic scintillators each of area of .4 m^2 and 5 cm in thickness and these are used to select the shower. The third scintillator was under heavy absorber. The data recorded by the data acquisition system was analysed and the following results were obtained:

1. The local electron density of the extensive are showers in the range of 20 - 600 m^{-2} was found to be

$$R(>\Delta) = 1054\ \Delta^{-1.56}\ hr^{-1}\ .$$

This result is in very good agreement with Greisen (1960).

2. The correlation between the number of particles traversing each of the two scintillators was investigated. The value of almost unity for the most probable value of the density ratio is consistent with the core distance of most of the showers falling at a distance large compared with the separation of the two counters.

3. The density spectrum of penetrating particles observed

under the absorber was measured and the relation between the density of particles measured under the absorber and the density of the electrons in the shower before the absorber was also found.

The experiment was simulated by the program MC.DENSITY01. The results of this program are compared with the results of the experiment and the size spectrum was derived from the measured density spectrum.

Single pt peaks at output of head unit (mV)		Discrimination levels at output of head unit (mV)		Density threshold Δ (m^{-2})		Run time (hr)	No. of counts	$R(>\Delta)$ (hr^{-1})
A	B	A	B	A	B			
26.5	28	20	20	1.88	1.78	0.45	457	1005±47
26.5	28	30	30	2.83	2.68	1.00	400	400±20
26.5	28	40	40	3.77	3.57	0.94	225	240±16
26.5	28	50	50	4.72	4.46	0.90	160	177±14
26.5	28	60	60	5.66	5.36	0.83	83	100±11
26.5	28	70	70	6.60	6.25	0.85	72	85±10
26.5	28	80	80	7.55	7.14	1.10	77	70±8
26.5	28	100	100	9.43	8.93	1.30	59	46±6
26.5	28	150	150	14.15	13.39	1.10	29	27±5
26.5	28	200	200	18.67	17.86	0.86	15	17.5±4.5
26.5	28	300	300	28.30	26.78	1.11	11	10±3.0
26.5	28	400	400	37.73	35.71	0.96	7	6±2.5

Table 4.1 : Table of basic data for integral density spectrum from counting.

Δ	Exp. 1		Exp. 2		Exp. 3		Exp. 4		TOTAL			
	C(>Δ)	Time	C(>Δ)	Time	C(>Δ)	time	C(>Δ)	time	C(>Δ)	Time	R(>Δ)	Error
20	581	64.94	570	45.95	115	18.91	-	-	1266	129.80	9.753	0.27
30	418	64.94	330	45.95	314	93.64	128	31.24	1190	244.77	4.862	0.14
40	296	64.94	394	81.32	259	114.31	84	31.24	1033	291.81	3.540	0.11
50	219	64.94	282	81.32	199	114.31	59	31.24	759	291.81	2.601	.094
60	148	64.94	210	81.32	150	114.31	45	31.24	553	291.81	1.895	.081
80	91	64.94	137	81.32	93	114.31	28	31.24	349	291.81	1.196	.064
100	62	64.94	98	81.32	112	184.51	23	31.24	295	362.01	0.815	.047
120	47	64.94	67	81.32	92	184.51	16	31.24	222	362.01	0.613	.041
160	26	64.94	41	81.32	65	184.51	9	31.24	141	362.01	0.389	.033
200	16	64.94	26	81.32	45	184.51	6	31.24	93	362.01	0.257	.027
240	11	64.94	23	81.32	35	184.51	3	31.24	72	362.01	0.199	.023
300	10	64.94	14	81.32	24	184.51	1	31.24	49	362.01	0.135	.019
340	10	64.94	12	81.32	19	184.51	-	-	41	330.77	0.124	.019
400	10	64.94	-	-	15	184.51	-	-	25	249.45	0.100	.020
600	-	-	-	-	1	184.51	-	-	1	184.51	.0054	-

Table 4.2: Measurement of the intergral density spectrum by using the microcomputer data acquisition system. Δ is the theshold density in m^{-2}, C(>Δ) is the count of all events of densities greater or equal to Δ. Time is given in hours. R(>Δ) is the rate of all showers with local density greater than or equal to Δ, rate is in $m^{-2}\ hr^{-1}$

Threshold density (m^{-2})	Median core distance (m)	Median shower size	Minimum shower size
1	30	3.5×10^4	8.0×10^2
10	15	1.5×10^5	1.7×10^3
40	11	2.1×10^5	5.5×10^3
300	6	7.0×10^5	3.0×10^4
1,000	3.5	1.5×10^6	8.0×10^4

Table 4.3

The median core distance (in metres) and median shower size producing a given electron density (m^{-2}) calculated using the NKG structure function. The minimum shower size is calculated for showers falling at core distances of $\geq$ 0.1 m. (After Ashton and Parvaresh, 1975).

Density (m^{-2})	Counts	Time hr	Rate hr^{-1}	Error
1	453	114.31	3.963	1.86×10^{-1}
2	291	114.31	2.546	1.49×10^{-1}
3	211	114.31	1.846	1.27×10^{-1}
4	173	114.31	1.513	1.15×10^{-1}
5	145	114.31	1.268	1.05×10^{-1}
6	120	114.31	1.050	9.58×10^{-2}
8	178	195.63	9.099×10^{-1}	6.83×10^{-2}
10	132	195.63	6.747×10^{-1}	5.87×10^{-2}
14	84	195.63	4.294×10^{-1}	4.69×10^{-2}
20	62	195.63	3.169×10^{-1}	4.02×10^{-2}
30	34	195.63	1.738×10^{-1}	2.98×10^{-2}
40	27	195.63	1.380×10^{-1}	2.66×10^{-2}
50	18	195.63	9.201×10^{-2}	2.17×10^{-2}
60	10	195.63	5.111×10^{-2}	1.62×10^{-2}
80	2	195.63	1.022×10^{-2}	7.23×10^{-3}
100	1	195.63	5.111×10^{-3}	5.11×10^{-3}

Table 4.4

The experimental data for the density spectrum of particles observed under absorber of 288.5 g cm^{-2}.

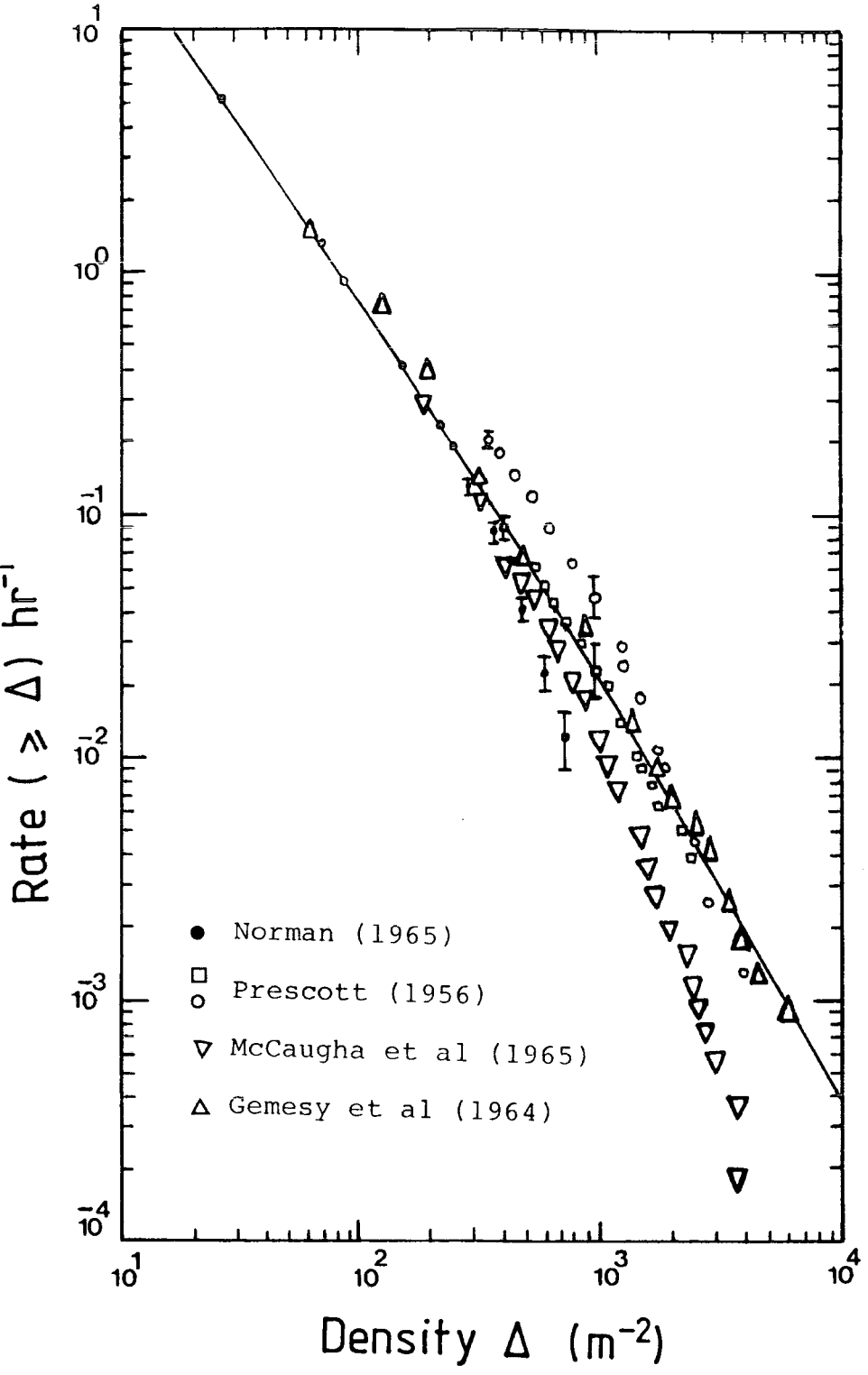

Figure 4.1 : Integral density spectra of E A S measured at sea level. The solid curve is due to Greisen (1960). The experimental observations are normalized to the the solid line such that all spectra give the same rate as obtained by Greisen (1960) at their minimum observed densities.

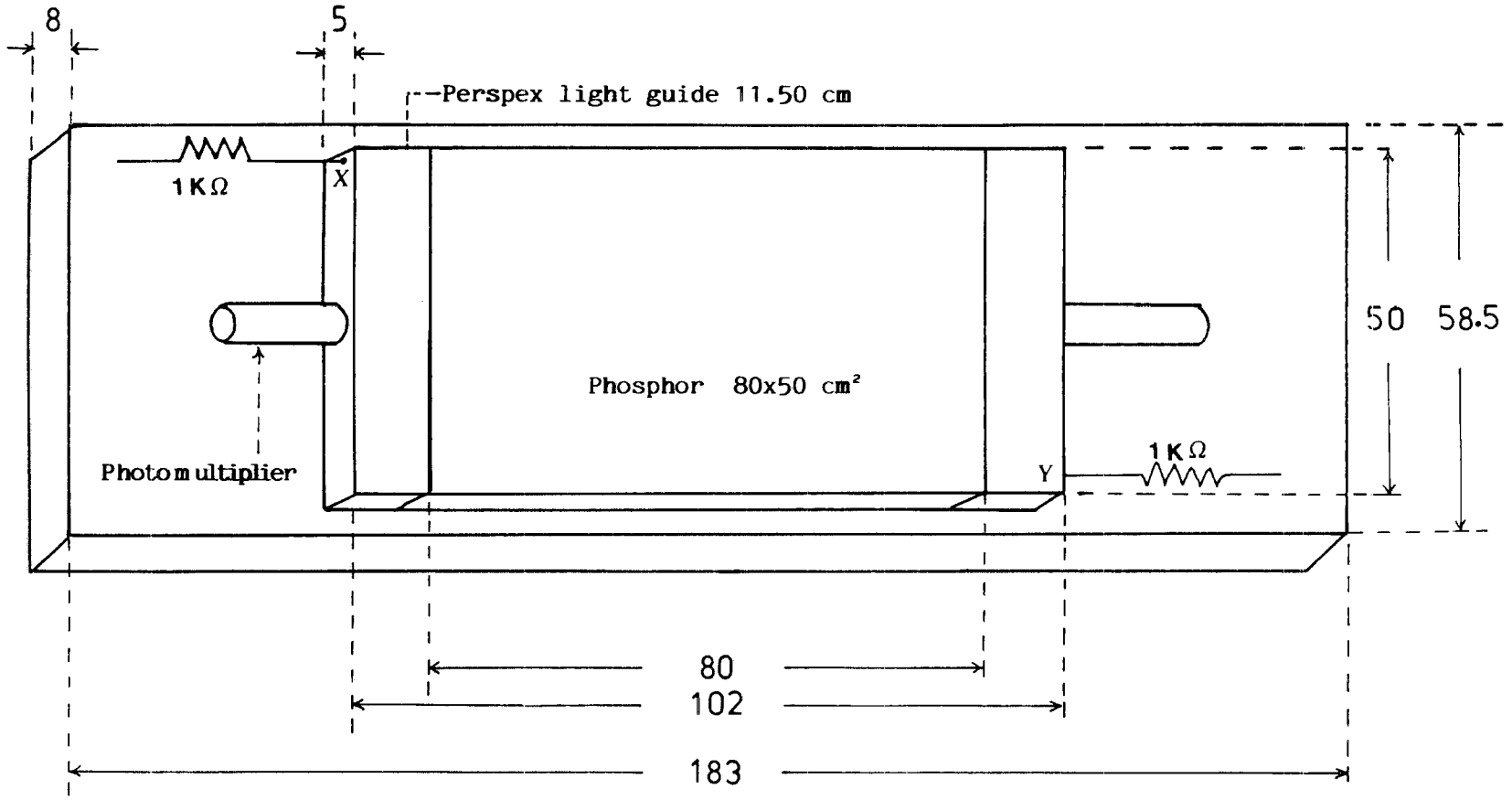

Figure 4.2: Design of plastic scintillation counter.
All dimensions are in centimetres.
X and Y are light emitting diodes.

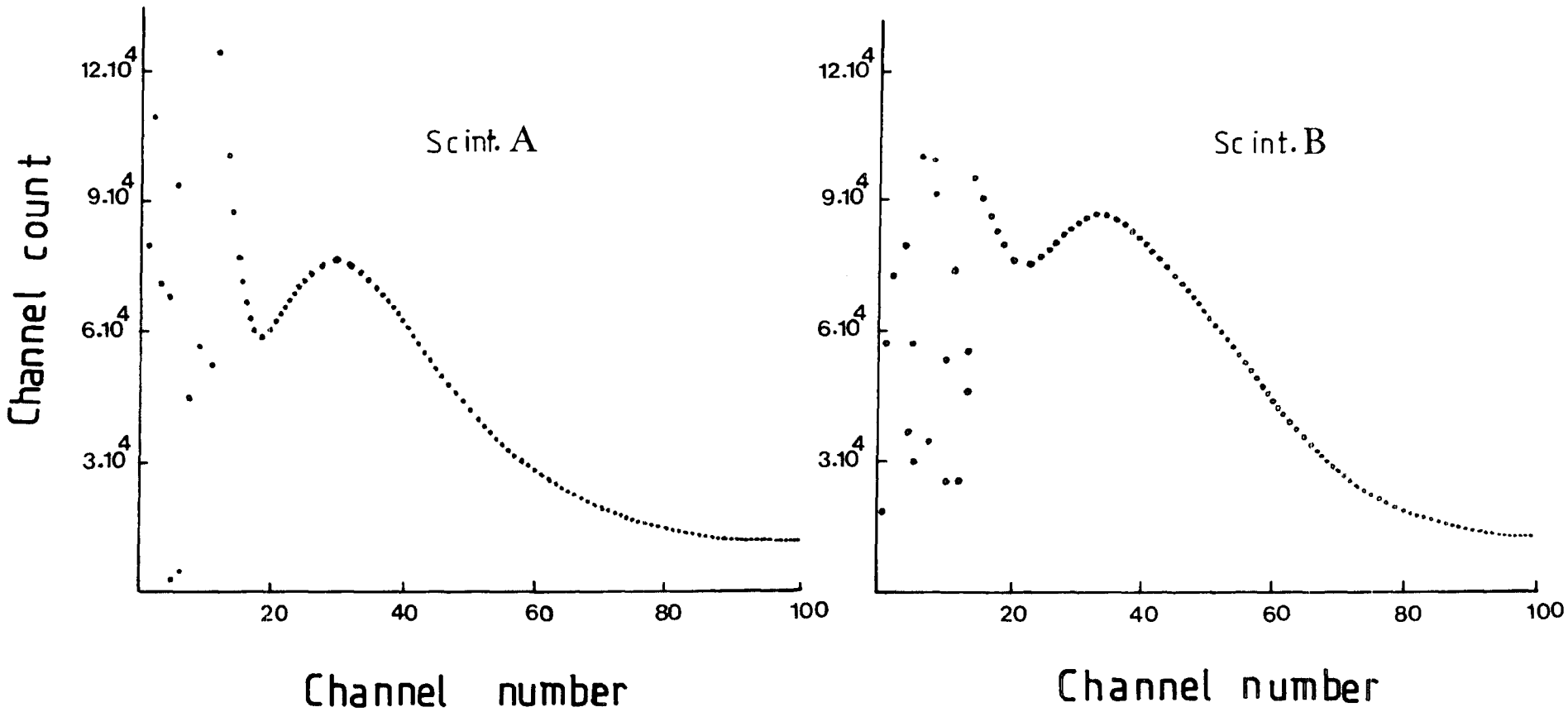

Figure 4.3: Typical single particle cosmic ray peak for each of scintillators A and B as displayed on the pulse height analyser.

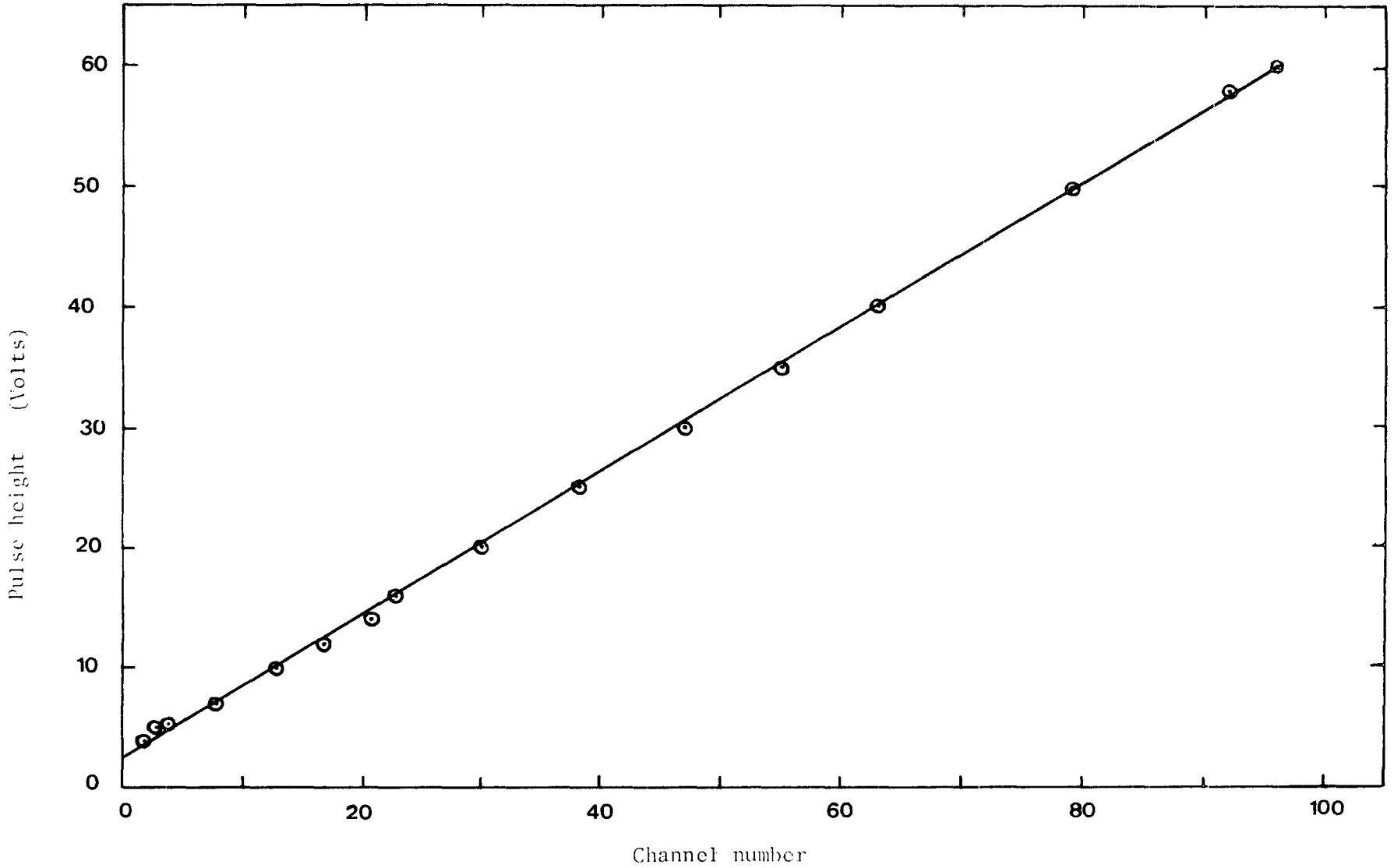

Figure 4.4: Calibration of the pulse height analyser using 1 μs width input exponential pulses.

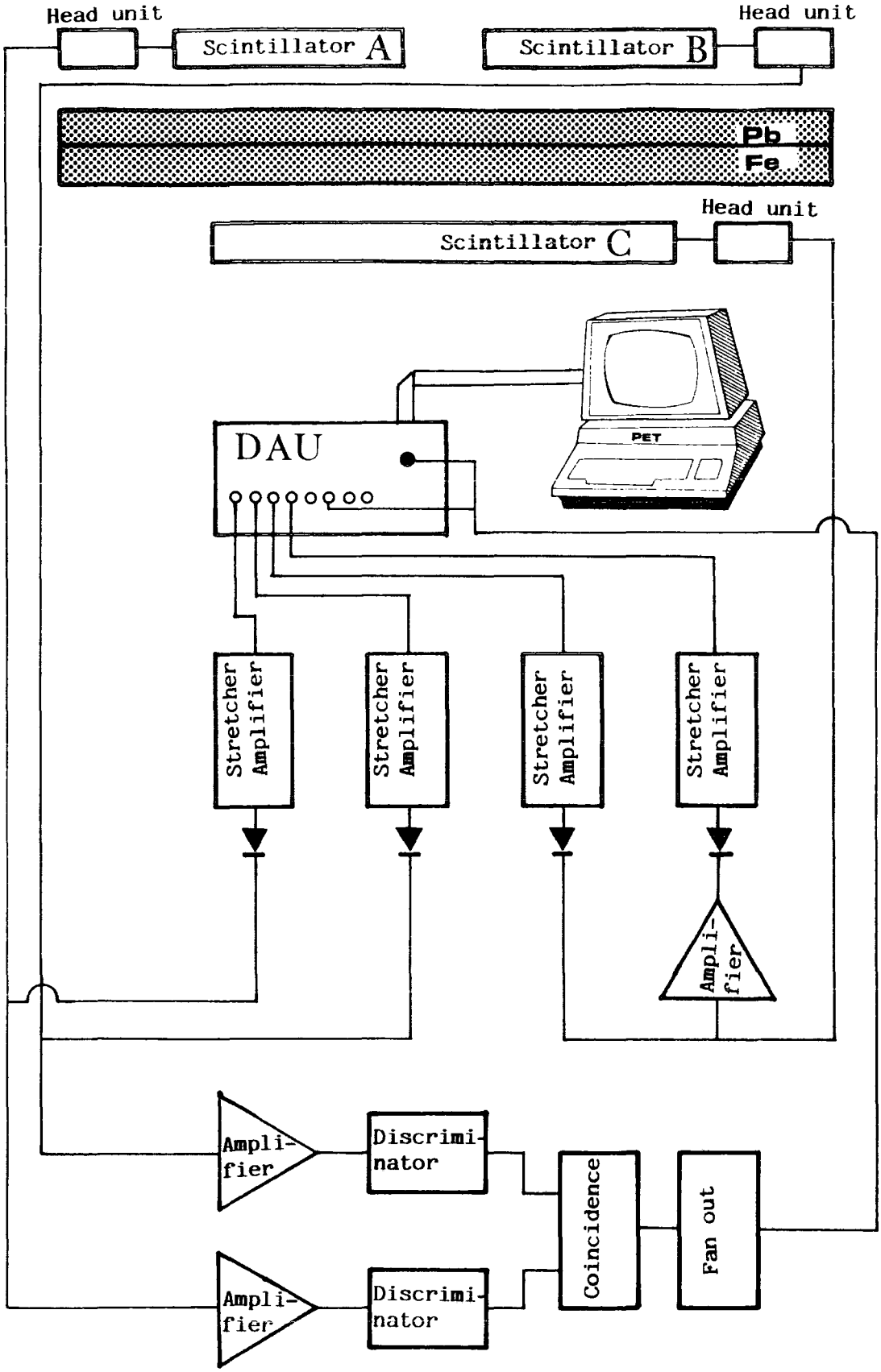

Figure 4.5: Block diagram of the system used in the present experiment.

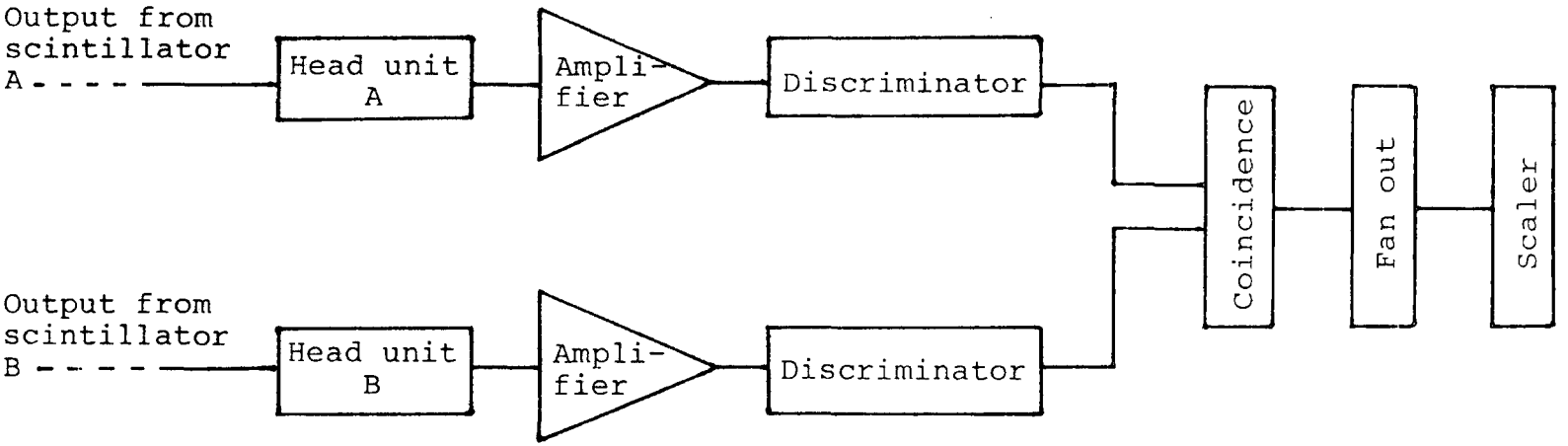

Figure 4.6: Block diagram of the system used to measure the density spectrum in the region 2.7 - 37 m^{-2}.

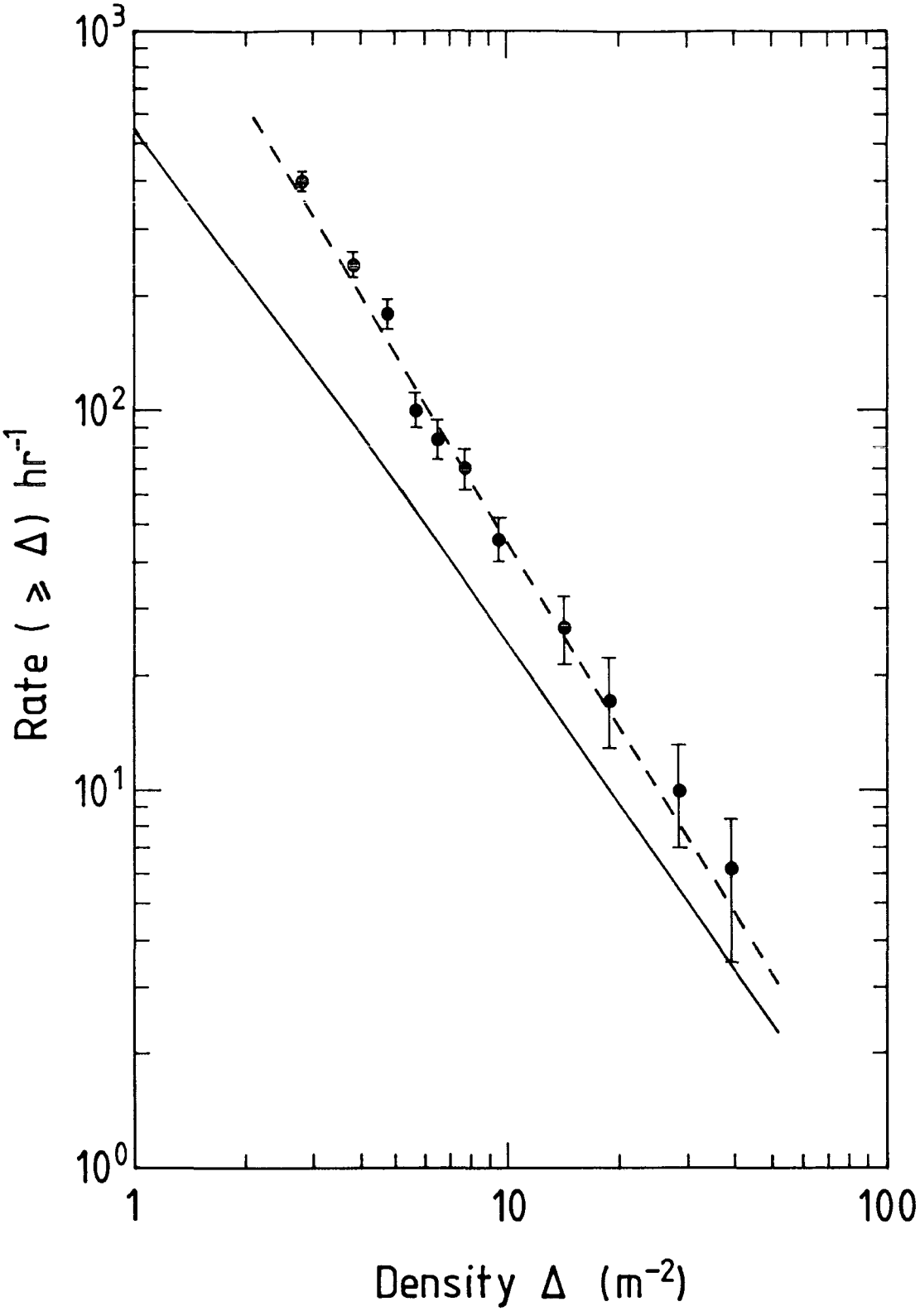

Figure 4.7: The integral density spectrum of electrons at sea level measured by using discriminators, two-fold coincidence and scaler.

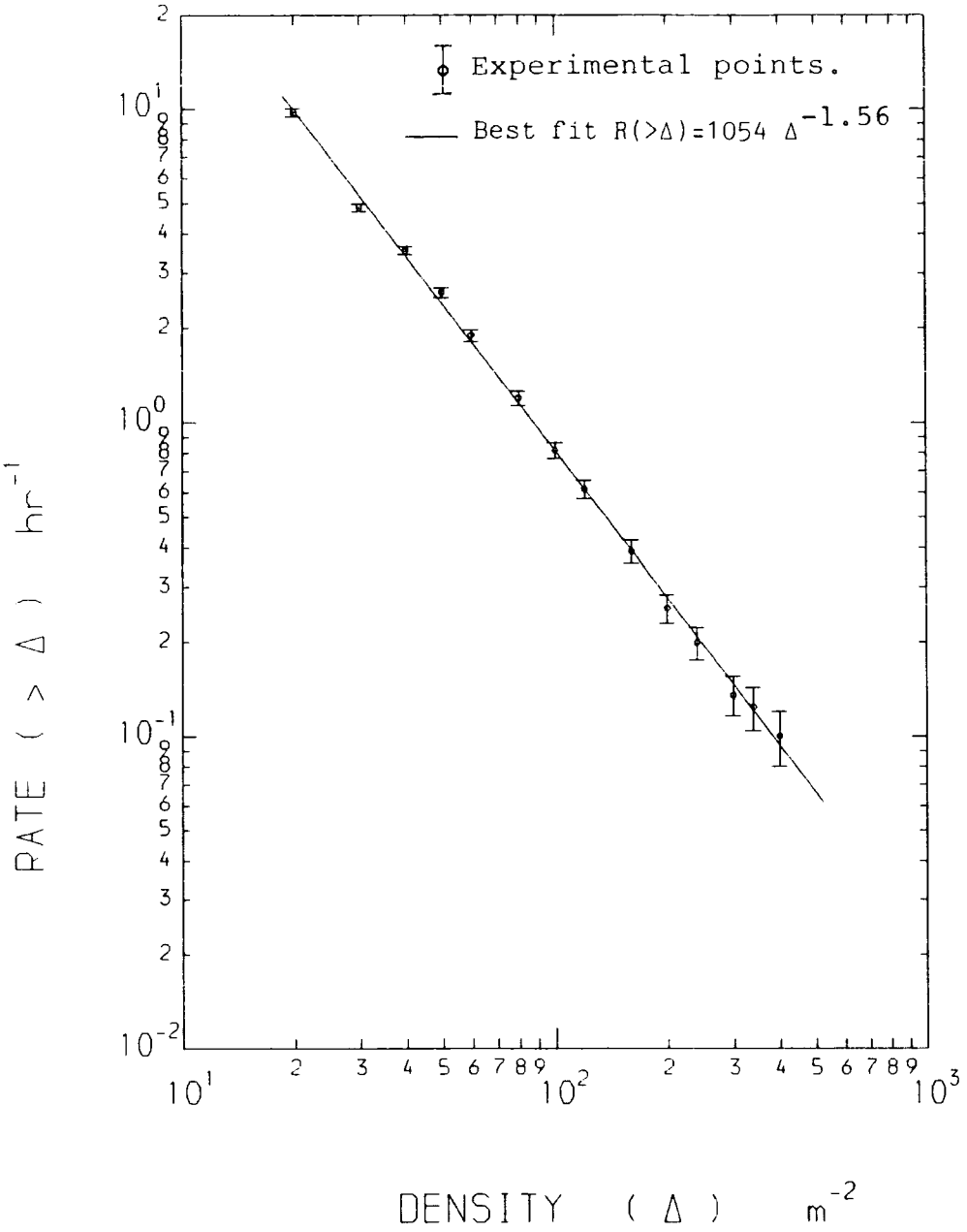

Figure 4.8: The integral density spectrum of electrons at sea level measured by using a microcomputer data acquisition system. The solid line is the best fit line for the experimental points.

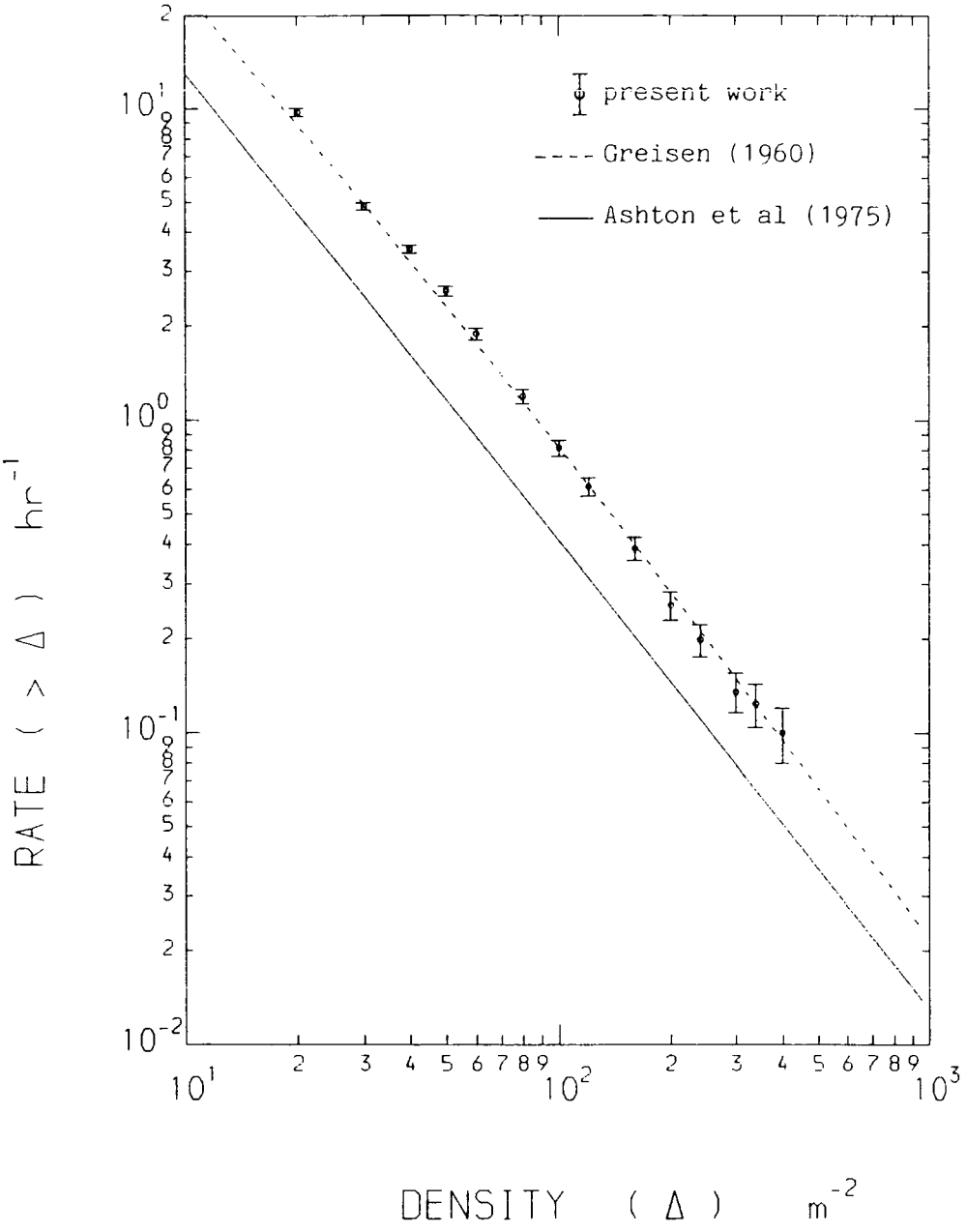

Figure 4.9: The integral density spectrum of electrons at sea level measured by using a microcomputer data acquisition system and compared with the results given by Greisen (1960) and Ashton et al (1975).

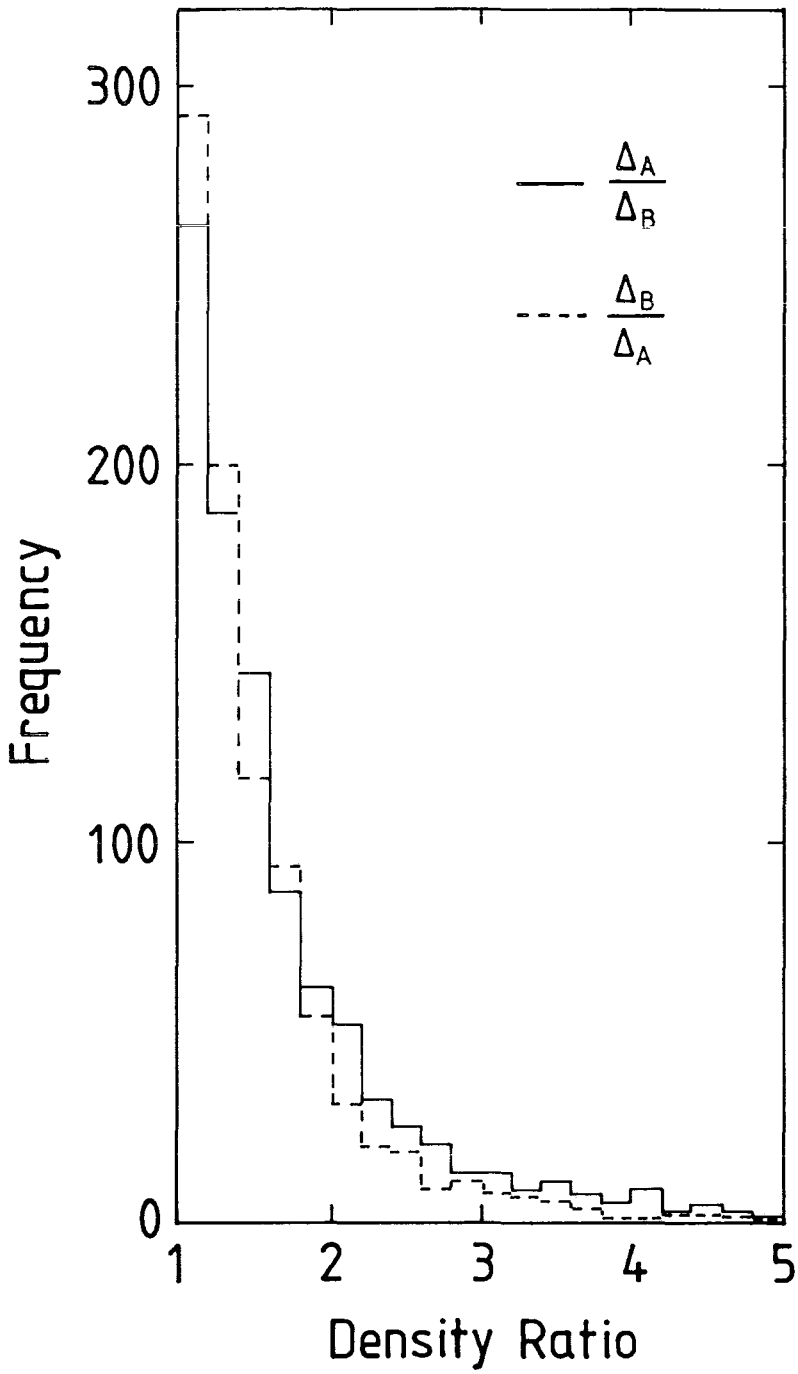

Figure 4.10: The frequency distribution of the ratio of the density of particles through one of scintillators to the other. The number of density ratios = 1816.

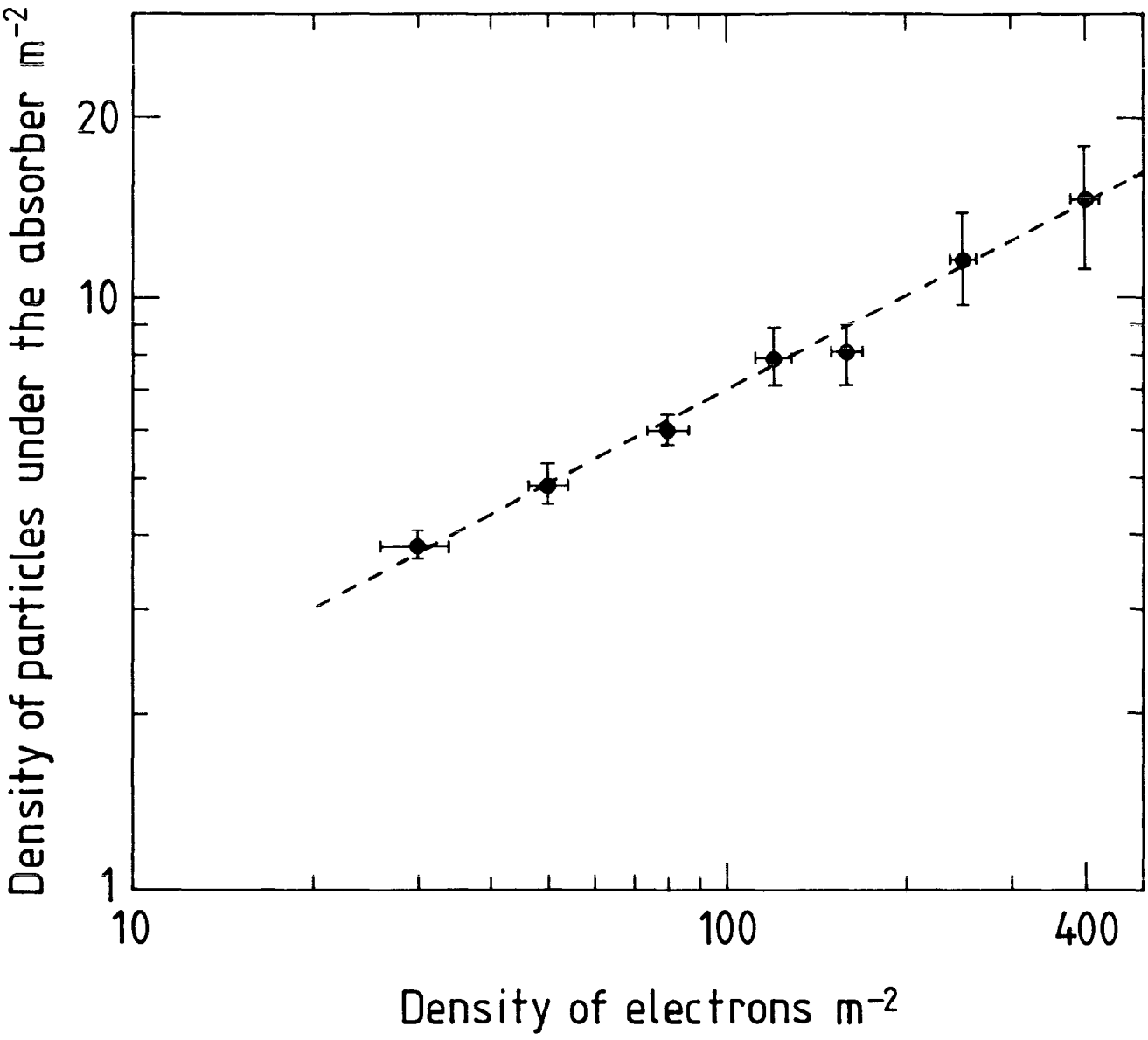

Figure 4.11: The average density of particles under the absorber versus the local density of the shower producing them as measured above the absorber.

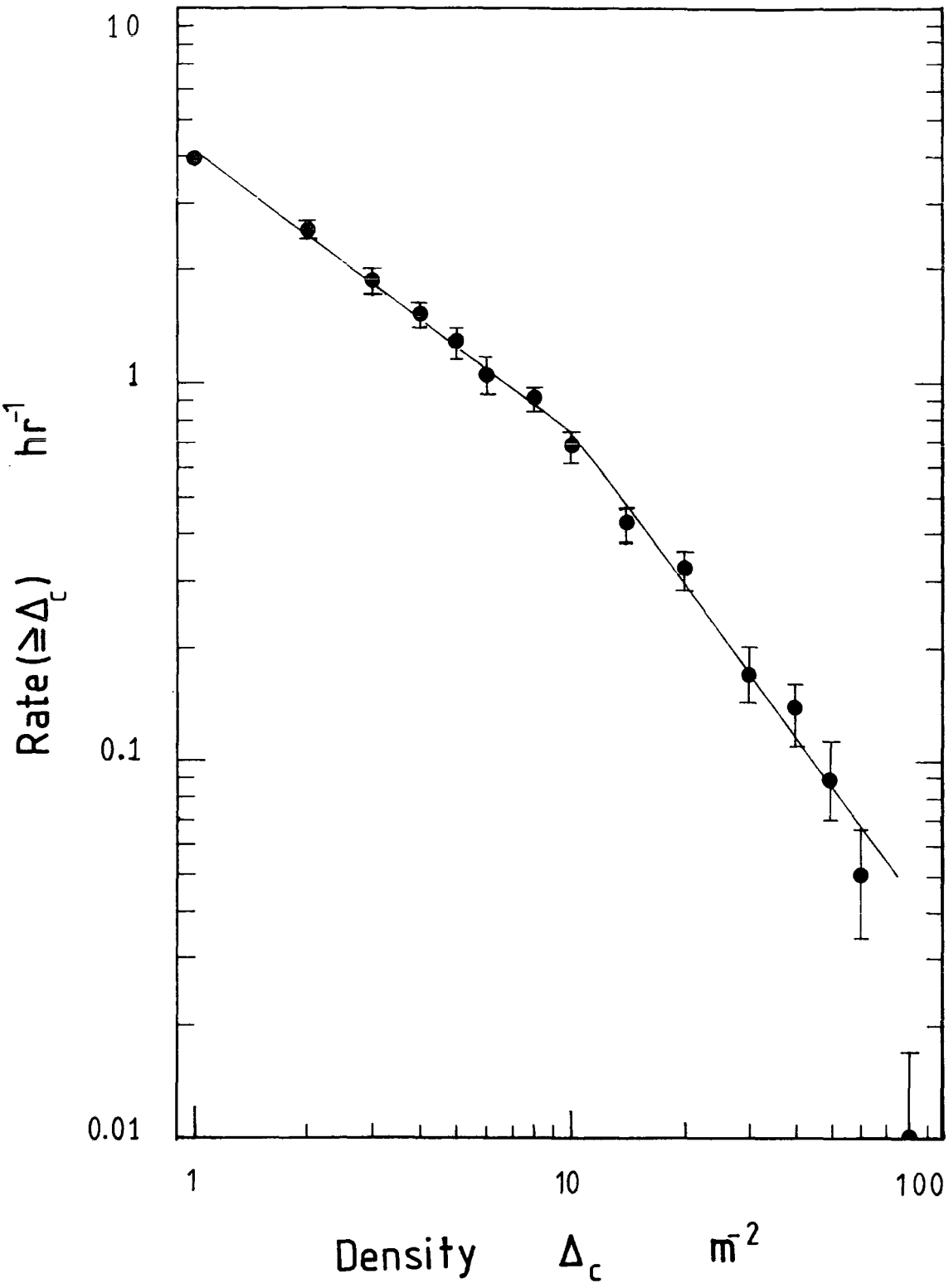

Figure 4.12: Integral density spectra of events in E A S measured at sea level under an absorber of 288.5 g cm^{-2}. The solid lines are best fit lines to the experimental points with a change of slope at a density = 10 m^{-2}.

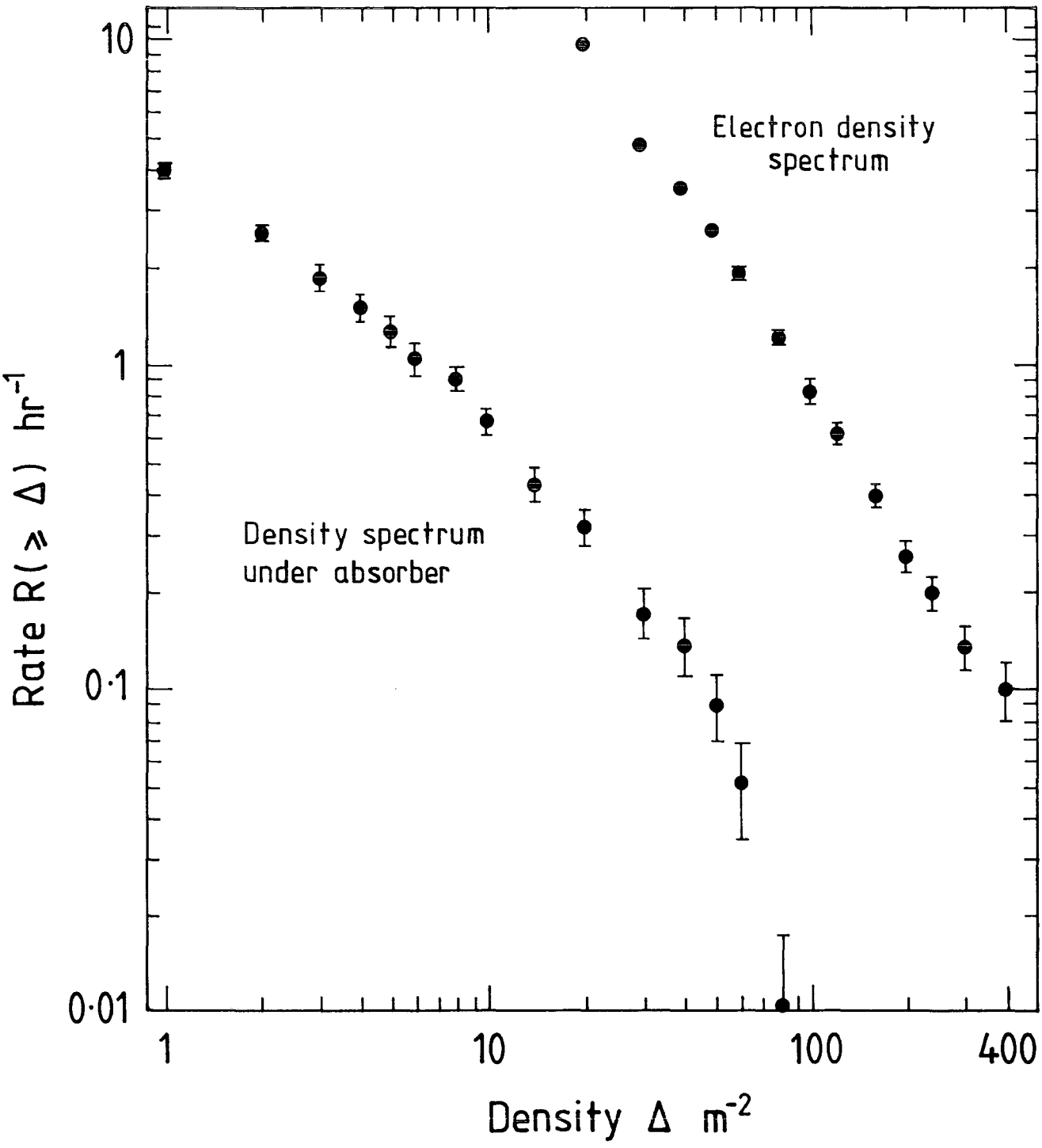

Figure 4.13: The integral density spectrum of the particles observed under the absorber, compared with the electron integral density spectrum.

Figure 4.14: List of the program MC.DENSITY01.

```
1     CCC
2     C  NAME : MC.DENSITY01
3     C         This program simulates
4     C         the density spectrum  experiment.
5     CCC
6           DIMENSION F(50),DENSA(1000),DENSB(1000)
7           REAL*8 Z
8     C
9           NTRIAL = 1000
10          S = 1.2
11          CS= 0.44
12    C--- S = Age parameter, SC = Nornalization Coeffecient
13          KSUM2=0
14    C
15          DO 25 I=1,NTRIAL
16     15   CONTINUE
17          KSUM2=KSUM2+1
18          CALL DIST(RA,RB)
19          CALL SIZE(SZ)
20          DENA=CS*(79./RA)**(2.-S)*(79./(RA+79.))**(4.5-S)
21          DENA=SZ *DENA / (79.*79.)
22          DENB=CS*(79./RB)**(2.-S)*(79./(RB+79.))**(4.5-S)
23          DENB=SZ *DENB / (79.*79.)
24          IF ((DENA .LT. 20.) .OR.(DENB .LT. 20.)) GOTO 15
25          DENSA(I) = DENA
26          DENSB(I) = DENB
27    C     WRITE(7,16)DENA,DENB
28    C16   FORMAT(2(F8.2,2X))
29          IZ=I/100.
30          XZ=I/100.
31          IF (IZ .EQ. XZ) WRITE(8,*) I
32    25    CONTINUE
33    CCCCCCC
34          CALL SPCTRM(NTRIAL,DENSA,DENSE)
35          CALL  RATIO(NTRIAL,DENSA,DENSB)
36          WRITE(6,26)KSUM2
37     26   FORMAT(//'NUMBER OF TOTAL TRIALS =',I8)
38    CCCCCCC
39          STOP
40          END
```

```
41      C
42            SUBROUTINE DIST(RA,RB)
43      C  Simulation of the distance of the shower core.
44      15    Z=G05CAF(Z)
45            X= 160. * Z - 80.
46            Z=G05CAF(Z)
47            Y= 160. * Z - 80.
48            IF ((X*X - Y*Y) .GT. 6400.0) GOTO 15
49            RA = SQRT((X+0.8)*(X+0.8) + Y*Y )
50            RB = SQRT((X-0.8)*(X-0.8) + Y*Y )
51            RETURN
52            END
53      C
54            SUBROUTINE SIZE(X)
55      C Simulation of the shower size.
56            DATA G1,G2/-1.5,-2./
57            DATA A1,A2/52.,36920./
58            DATA SZL,SZB,SZU/1.8E4,5E5,1E9/
59            B=A1*(SZB**G1-SZL**G1)
60            C=B+A2*(SZU**G2 - SZB**G2)
61            R=G05CAF(R)
62            IF((C*R) .LT. B) GOTO  100
63            X=(C*R/A1-SZL**G1)**(1/G1)
64            GOTO 200
65      100   X=((C*R -B)/A2+SZB**G2)**(1/G2)
66      200   CONTINUE
67            RETURN
68            END
69      C
70            SUBROUTINE SPCTRM(N,A,B)
71              INTEGER DELTA(14)
72              DIMENSION A(1000) ,B(1000)
73              DATA DELTA/20,30,40,50,60,80,100,140,200,240,300,400,500,600/
74      C
75             WRITE(8,98)
76        98   FORMAT('DENSITY')
77             KSUM=0
78             WRITE(6,99)
79        99   FORMAT(22HDELTA   COUNTS > DELTA)
80                  DO 200 I=1,14
81                  DO 100 J=1,N
82             IF(A(J) .LT. DELTA(I)) GOTO 100
83             IF(B(J) .LT. DELTA(I)) GOTO 100
84                  KSUM=KSUM+1
85       100    CONTINUE
86       500    CONTINUE
87              WRITE (6,77)DELTA(I),KSUM
88         77   FORMAT(I4,3X,I4)
89                KSUM=0
90       200      CONTINUE
91              RETURN
92              END
```

⟶

```
      C
            SUBROUTINE RATIO(NTRIAL,DENSA,DENSB)
           DIMENSION F(50),DENSA(1000),DENSB(1000)
           WRITE(8,19)
       19  FORMAT('RATIO')
           DO 20 I=1,50
       20  F(I)=0.0
           AMIN=0.0
              N=20
           AMAX=4.
           W= (AMAX - AMIN) / N
      C
           KSAT=0
           BIG=0.0
           KSUM=0
           DO 50 J=1,NTRIAL
           X = DENSA(J)/DENSB(J)
      C    IF(X .LT. 1.0 ) X= 1. / X
           IF(X .GT. AMAX) BIG=BIG+1.
           IF(X .GT. AMAX) WRITE(6,*)X
           IF(X .GT. AMAX)  GOTO 50
           IF(X .EQ. AMAX) F(N)=F(N)+1
           IF(X .EQ. AMAX) GOTO 50
            I = ( X - AMIN ) / W  + 1
            F(I)= F(I)+ 1
           KSUM=KSUM + 1
       50  CONTINUE
           WRITE (6,310)
       310 FORMAT(' INTERVAL       FREQUENCY')
           DO 350 I=1,N
           C = (I-1)*W +AMIN
           D = C+W
           WRITE (6,340)C,D,F(I)
       340 FORMAT(F5.3,2X,F5.3,4X,F7.0)
       350 CONTINUE
           WRITE(6,380)KSUM
       380 FORMAT('TOTAL OF ',I6)
            WRITE(6,392)BIG
       392  FORMAT('GREATER THAN MAX=',F4.0)
      C
          DO 400 I=1,N
          F(I) = F(I)/NTRIAL
      400 CONTINUE
          CALL PAPER(1)
          CALL PSPACE(0.1181,0.9055,0.1181,0.9055)
          CALL MAP(0.0,AMAX,0.0,0.5)
          CALL BORDER
          CALL HISTGM(0.0,0.0,W,F,1,N)
          CALL SCALSI(1.0,0.1)
          CALL PLACE(40,10)
          CALL TYPECS('S=',2)
          CALL TYPENF(S,2)
          CALL GREND
          RETURN
          END
```

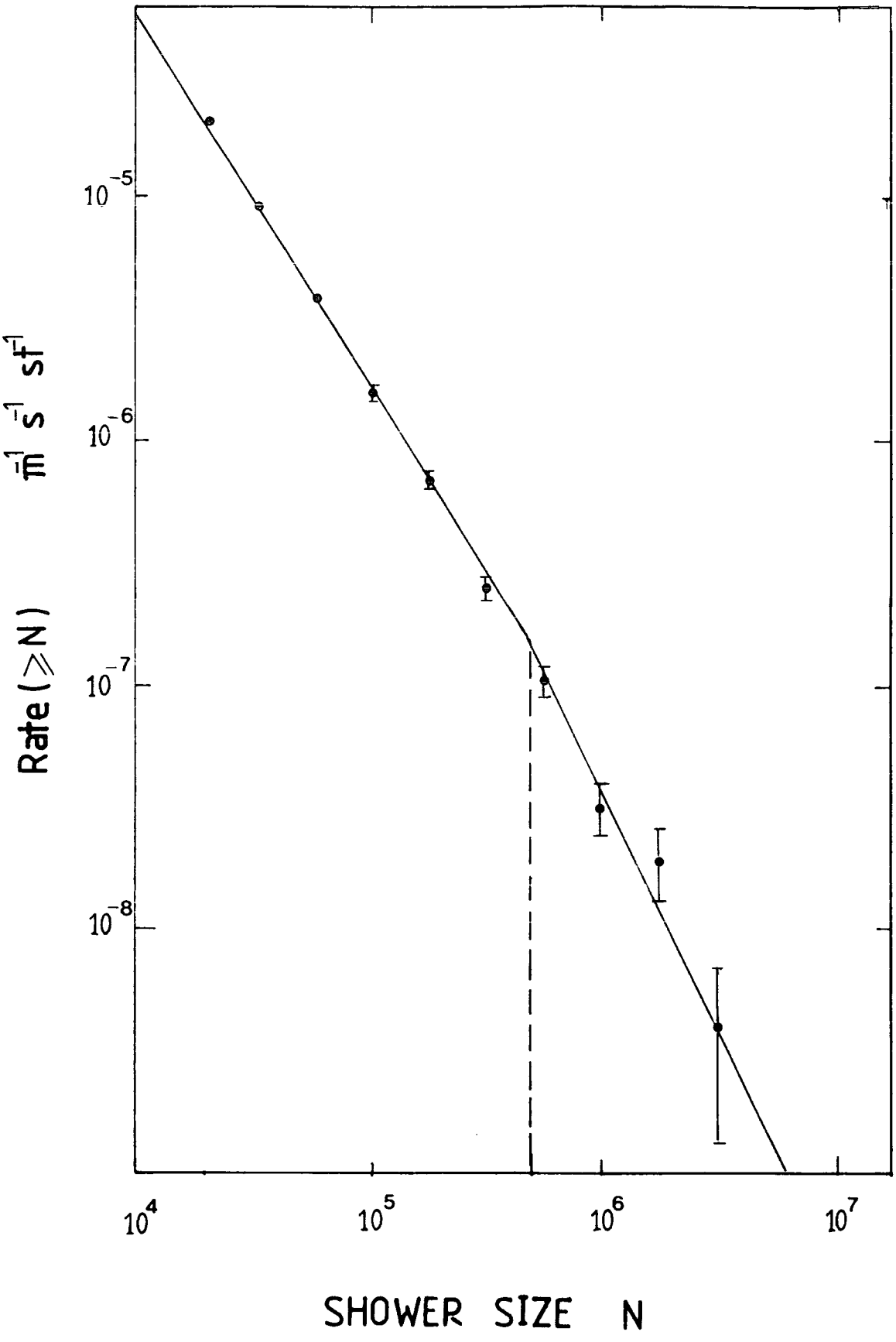

Figure 4.15: Simulated size spectrum by subroutine 'SIZE' produced by simulating 1000 showers. The line is the size spectrum given by Hillas (1970) which was used to generate the shower sizes.

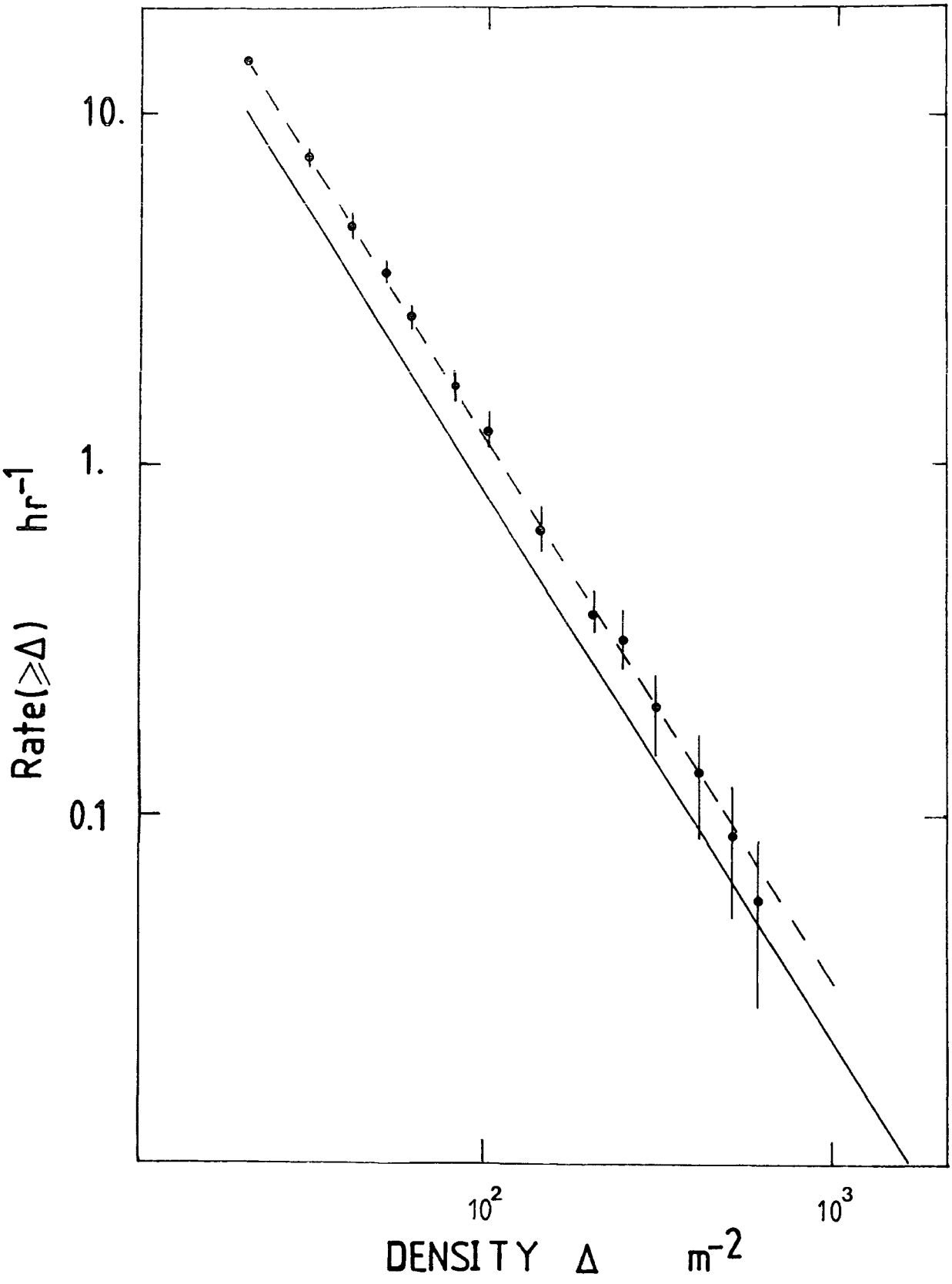

Figure 4.16: Simulated density spectrum by program 'MC.DENSITY01' produced for simulation of 1000 showers. The dashed line is the best fit line and the solid line represents the density spectrum obtained in this work.

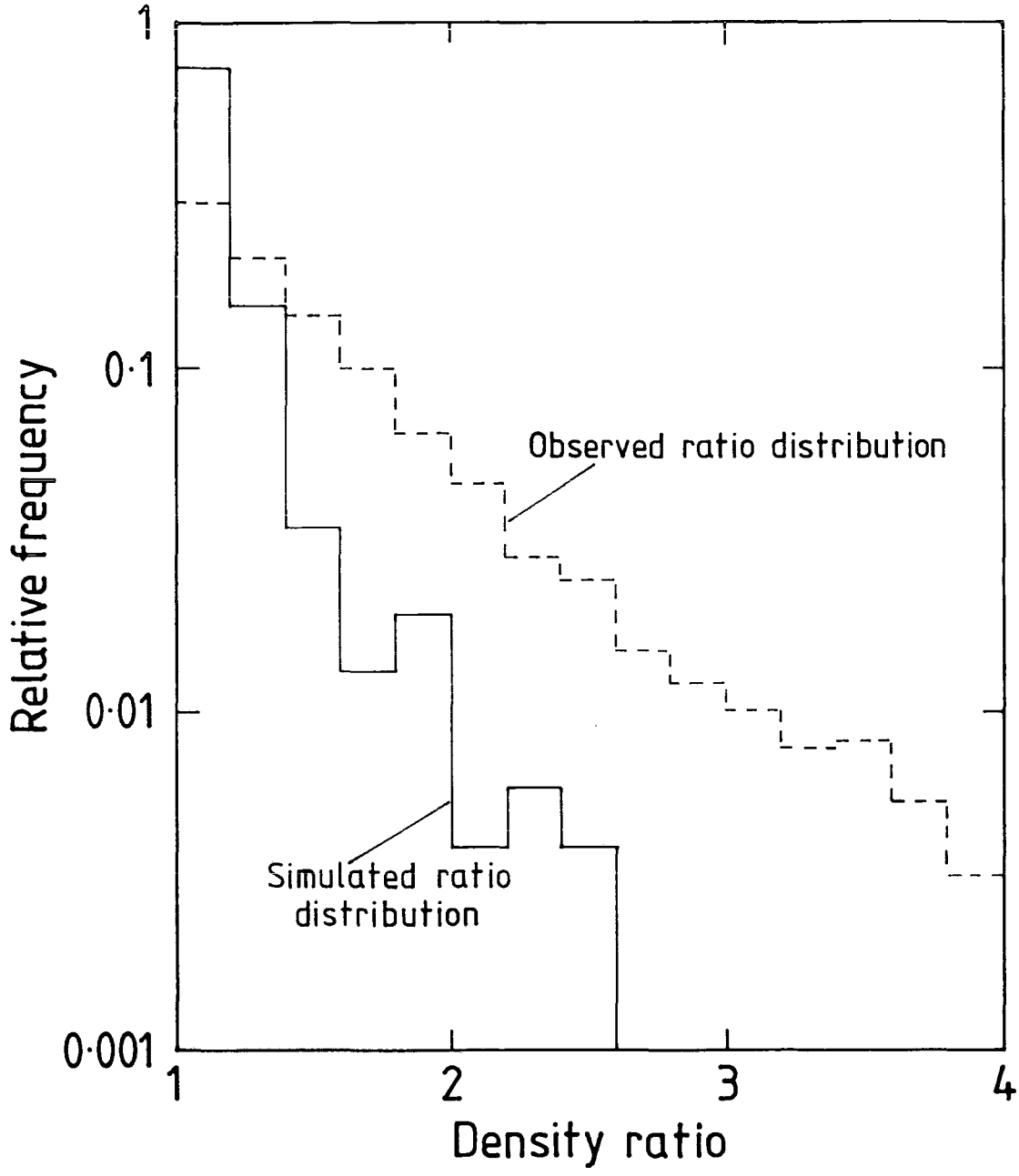

Figure 4.17: The frequency distribution of the ratio of the density of particles through one of scintillators to the other, for 1000 simulated showers by program 'MC.DENSITY01'. The experimental frequency distribution of the ratios is plotted for comparison. The number of experimental density ratios = 1816.

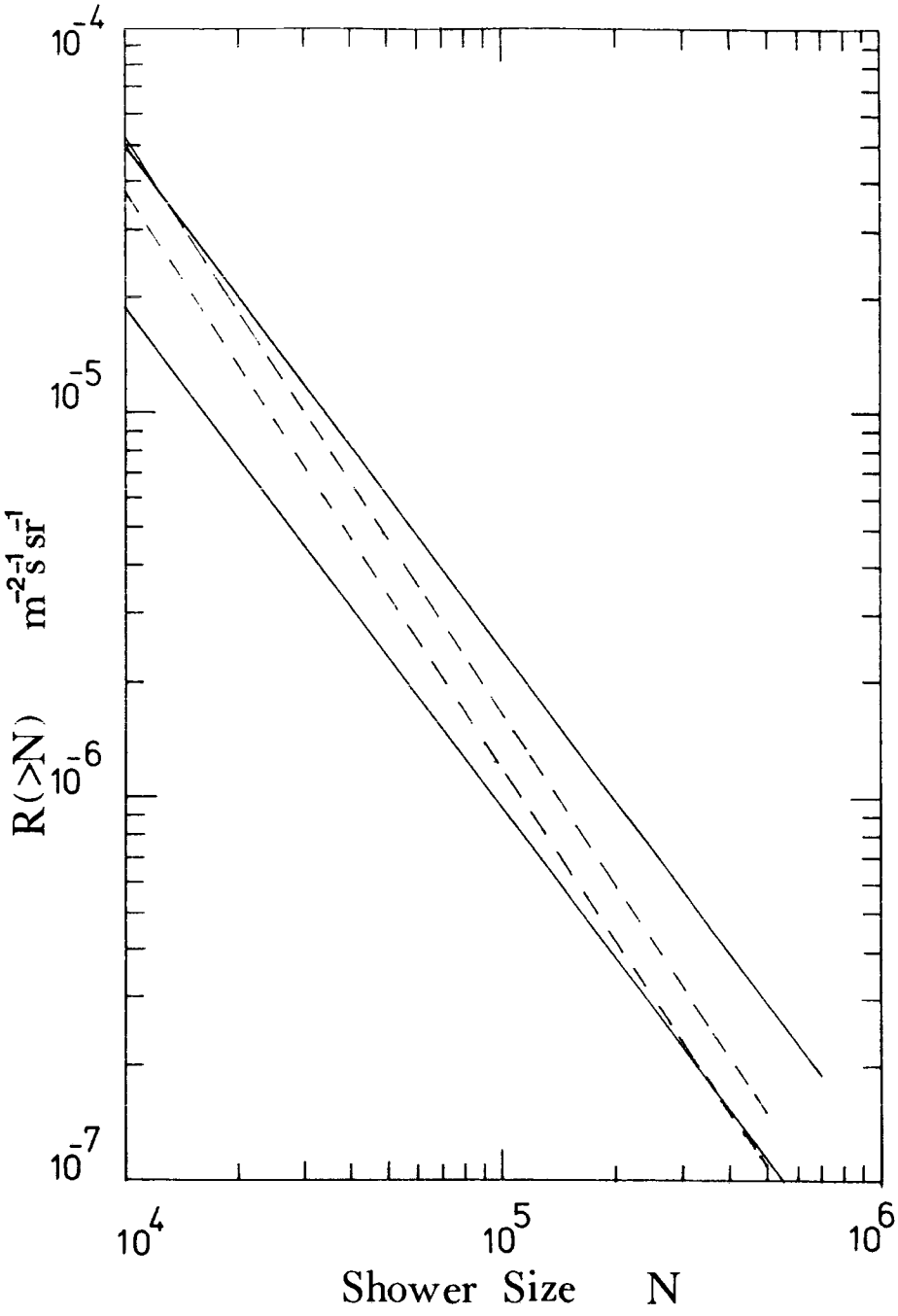

Figure 4.18: Integral number spectrum of E A S at sea level. The lower solid line is due to Ashton et al(1975). The upper solid line is derived from the measured integral density spectrum by scaling the spectrum given by Ashton et al. The upper dashed line is the size spectrum derived from the measured density spectrum using the simulation program, and the lower dashed line is the size spectrum given by Hillas (1970) which was used in the simulation program.

Chapter Five

Electron-photon shower theory and the formation of extensive air showers

5.1 Introduction.

Showers of cosmic rays were noted in some of the earliest cloud chamber experiments but Auger and his colleagues began systematic studies with separated detectors in the late 1930s. They noted coincidences in two or more detectors separated by distances up to 300m and they made the correct inference that these were showers of cosmic rays triggered by a single cosmic ray of very high energy entering the top of the atmosphere. The showers were well described by the photon-electron cascade theory of Bhabha and Heitler (see section 3). Auger made a remarkable conclusion about the initial energy: simply taking the average particle energy to be about the critical energy (87 MeV for air), and considering the energy expended in ionization in atmosphere, he estimated the total energy of the shower, and hence of the primary particle, to be about 10^{15} eV. This discovery extended the energy scale of known radiations by an even greater factor than did the original discovery of cosmic rays, posing new problems with regard to their origin. It was thought first that the shower was initiated by electron or positron or photon. But discovery of other component in the shower (e.g. muons) and that the showers are not attenuated as rapidly as expected from shower theory,

suggested that these electron-photon cascades were generated by another component; some regenerating agent was preventing the showers from being attenuated rapidly. It is known today that the vast majority of particles producing extensive air showers are protons and nuclei.

5.2 Description of the extensive air shower.

The present picture of cosmic rays in the atmosphere is as follows. A primary proton of energy E greater than 10^{13} eV (the minimum for an observable effect at sea-level to be produced), interact with an air nucleus, with mean free path close to 80 g cm^{-2} (see Figure 5.1). Nuclear active particles emerge from the collision with the primary proton (or neutron) retaining about half of the primary energy. Many secondary particles are produced in this interaction. The number of new particles is roughly $3.E^{1/4}$ (with E in GeV). The majority of the new particles are pions; positive, negative, and neutral in equal numbers. Some other hadrons also emerge from the interaction. The neutral pions are unstable and decay within 10^{-15}s into pairs of gamma-rays, which can then initiate electron-photon cascades (see next section). Charged pions have a long life-time due to the time-dilation effect and most, produced near the top of atmosphere, will collide with air nuclei, producing yet more pions and feeding the nucleon cascade. However, in the later stages of a cascade, where the energies are lower and the life-time shorter, they will decay into muons and neutrinos. The muon life-time of $2x10^{-6}$s, dilated by the relativistic effect, means that they are very unlikely to decay

before they reach sea-level, but those that do, produce an electron and two neutrinos. Both muons and neutrinos are weakly interacting and so have no problem in reaching sea level. Finally there is the nuclear-active component. They collide with further air nuclei or decay (in the case of unstable hadrons). Further collision will produce other cascades, similar to the initial one, this process continuing until the energy is too low to produce further secondary particles. Figure 5.1 shows a schematic diagram of this process. The particles produced by these processes add to each other and move downward together. Heavier particles are delayed and the shower reaches sea level in layers, first a 'front' of electrons and photons, of about 2m thickness, and then muons (3 to 4 m). Slower still is the low energy nucleon component.

Coulomb scattering spreads particles, depending on their momentum, which results in the scattering of electrons being greater than muons which, in turn, is greater than nucleons. However the large distances travelled by muons, means that they are found at great distances from the shower core.

5.3 Photon-electron cascade.

Electrons of large energy lose most of their energy by radiation (bremsstrahlung). Hence in the interactions of high-energy electrons with matter only a small fraction of the energy is dissipated, while a large fraction is spent in the production of high energy photons. The secondary photons, in turn, undergo materialization or Compton collision. Either process gives

rise to electrons of energy comparable with that of photons. These new electrons radiate more photons, which again materialise into electron pairs or produce Compton electrons. At each new step the number of particles increases and their average energy decreases. As the process goes on, more and more electrons fall into an energy range where radiation losses cannot compete with collision losses until eventually the energy of the primary electron is completely dissipated in excitation and ionization of atoms. It is clear that a shower can be initiated by a high energy photon as well as by a high energy electron. One can build up a simple model of an electron-photon cascade. Assume that each electron of energy greater than the critical energy undergoes a radiation process at a distance of one radiation length from the place where it has been produced and that, in this process, it loses half of its energy to a secondary photon. Assume that each photon undergoes a materialization process at a distance of one radiation length from the place of production splitting its energy equally between the two secondary electrons. Neglect the Compton effect and neglect collision loss of electrons of energy greater than the critical energy and assume that electrons, when their energy becomes smaller than the critical energy, cease to radiate and are soon brought to rest by collision losses. In the ultrarelativistic limit, the radiation lengths for pair production and bremsstrahlung are the same. Therefore the probability of these process happening is one-half at a distance t, given by

$$e^{-t/t_o} = \tfrac{1}{2}$$

i.e. $$t = R = t_o \ln 2$$

Therefore if we initiate the shower with a gamma-ray of energy E_o, after a distance of, on average, R, an electron-positron pair will be produced and we will assume that the pair share the energy of the gamma-ray, i.e. $E_o/2$ each. In the next radiation length, the electron and positron both lose, on average, half of their energy by bremsstrahlung and, on average, they will each radiate one photon of energy $E_o/4$. Thus, we end up with two particles and two photons, all having $E_o/4$ after two radiation lengths. And so on, as illustrated in Figure 5.2. Thus after a distance $t = nR$, the number of photons + electrons + positrons is 2^n and their average energy is $E_o/2^n$. It is also clear that, on average, the shower consists of 2/3 positrons and electrons; and 1/3 photons. Assuming that cascade multiplication stops when E is equal to the critical energy E_c, then the maximum number of particles is reached at a thickness t_{max} given by

$$E_c = E_o \, e^{-t_{max}}$$

or

$$t_{max} = \ln (E_o / E_c)$$

At the maximum, the number of particles is given by

$$N_{max} = \frac{2}{3} (E_o / E_c)$$

We see that the maximum number of particles in the shower is proportional to E_o, the initial energy, and t_{max} is proportional to the logarithm of E_o.

We expect the build up of the shower to be exponential and once the maximum is reached, the number of particles in the shower decreases, as the shower is absorbed in the atmosphere. We may then assume an exponential absorption beyond the maximum and

write,

$$N(t) \approx N_{max}\, e^{-\lambda (t-t_{max})}$$

where λ is the attenuation coefficient of the shower. This simple model was first assumed by Heitler (1948). We may summarize the important results of the preceding analysis with the following statements, which apply to a shower initiated by either an electron or a photon of energy E_o large compared with the critical energy.

(a) The number of electrons and photons in the initial stages of the shower development increases exponentially with depth.

(b) The shower curve for the total number of shower particles, irrespective of energy, has a maximum at a thickness of about $\ln (E_o / E_c)$.

(c) The total number of shower particles at the maximum is approximately proportional to E_o/E_c.

(d) Beyond the maximum, there is a rapid exponential attenuation of the shower.

To solve the cascade problem in detail, mathematical difficulties will be faced. So I will only write about the general approach to the cascade calculations. The first detailed papers on the theory of the photon-electron cascade presented two independent and different methods of attack. Bhabha and Heitler (1937) computed the growth and decay of the first few generations of particles formed in this way to show that the growth of showers was correctly described, but this approach soon became tedious. Carlson and Oppenheimer (1937) made their approach by writing down

a set of differential equations (the diffusion equations) in which a large cascade is treated as an almost continuous distribution of particles in energy and space, developing in a manner rather like diffusion. For more details the reader is refered to Rossi (1952) or Greisen (1956). Greisen (1956) produced a useful expression which describes the development of the cascade as it passes through the atmosphere, for showers initiated by a single photons of energy E_o, it is as follows,

$$N(E_o,t) = \frac{0.31}{B_o^{\frac{1}{2}}} \exp\left[t\left(1-\frac{3}{2}\ln s\right)\right]$$

where $t = \frac{x}{x_o}$ is the thickness of air in radiation units, $B_o = \ln(E_o/E_c)$ and $s = \frac{3t}{t+2B_o}$ For $E>E_c$, the integral energy spectrum of all the electrons in the shower is given by the expression

$$N(E_o,E,t) = \frac{0.135}{B^{\frac{1}{2}}} \exp\left[t\left(1-\frac{3}{2}\ln s\right)\right]$$

where $B = \ln(E_o/E)$ and $s = \frac{3t}{t+2B}$. Figure 5.3 shows the number of electrons at different thicknesses of air given by the Greisen formula, the points being the result of a simulation carried out by Messel and Grawford (1970). In Figure 5.4 the same relation is given for initial energies from 10^{11} to 10^{19} eV. The parameter, s, is called shower age parameter, which enters into the solution of the diffusion equations representing the showers. At the origin of an event initiated by a single particle, s=0; at the maximum, s=1; and when s=2 the number of particles in the shower has decayed to less than one. The maximum development of the shower is reached when s=1 i.e. at thickness $t_{max} = B_o = \ln(E_o/E_c)$.

5.4 The 'Standard' Model.

The standard model used in the various calculations is that based on the so-called CKP formula. Properties of the model can be summarized as follows (after de Beer et al 1966).

(i) High energy nucleons lose on average 50% of their energy in each collision and have an interaction mean free path in the atmosphere of 80 g cm^{-2}, both these quantities being independent of energy.

(ii) The secondary particles are mainly pions, there being on average equal number of positive, negative, and neutral pions produced.

(iii) The pions have an energy distribution in the laboratory system given by the empirical relation of Cocconi, Koester, and Perkins which, when allowance is made for particles emitted in the 'backward cone' can be written as,

$$S(E,E_o) = \frac{1}{2}\ \frac{n(E_o)}{T}\ \exp(-\frac{E}{T}) + \frac{n(E_o)}{G}\exp\ (-\frac{E}{G})$$

where $n(E_o)$ is the multiplicity of pions produced, E_o is the transferred energy, G is the average energy of pions in the backward cone and $T = 2[E_o - \frac{1}{2}n(E_o)G]/n(E_o)$ is the average in the forward cone.

(iv) It is assumed that the fraction of energy lost by a nucleon which dose not appear as pions is negligible.

(v) The multiplicity of the secondary pions, n_s, is given by $n_s = 2.7\ E_p^{\frac{1}{4}}$ which E_p in GeV for K = 0.5 and $n_s = 2.7 \times 2^{\frac{1}{4}}(KE_p)^{\frac{1}{4}}$ for all K.

(vi) The distribution in transverse momentum, p_t, of the produced pions is given by the expression suggested by Cocconi, Koester, and Perkins,

$$f(p_t) = \frac{p_t}{p_o^2} \exp(-\frac{p_t}{p_o})$$

The mean transverse momentum ($2p_o$) is assumed to be independent of energy and equal to 400 MeV/c.

(vii) Pion interactions are assumed to differ from nucleon interactions in that they are catastrophic with interaction length of 120 g cm^{-2}. The energy spectrum of the pions produced in the pion interactions is taken to be that given by the same relation as for protons but with K=1, in other words $n_s = 3.2E_p^{\frac{1}{4}}$.

(viii) Fluctuations are allowed for in the calculations to the extent that variations in the inelasticity of nucleon air nucleus collisions are included as well as the normal statistical fluctuations in the depth in the atmosphere of the interactions.

The adopted form for the inelasticity distribution is

$$f(K) = (1+a)^2 (1-K)^a \ln(1-K)$$

with a = 1.414.

5.5 Lateral distribution of charged particles.

The lateral distribution of shower particles, i.e. the dependance of particle density on the distance from the shower axis, is of interest for two reasons. Firstly, the shower-particle distribution relative to the direction of motion of primary particle, or the shower axis, reflects the development of the shower during its passage through the atmosphere. Comparison of

the experimental lateral distribution of particles in showers with different total numbers of particles, and at different depths in the atmosphere, with theoretical distributions obtained on the basis of different models, yields some information about the process which gave rise to the deflection of the particles from the shower axis. Secondly, a knowledge of the lateral distribution of shower particles may be used to determined the total number of particles crossing the plane of observation. This number can in turn be employed to estimate the energy of the primary particle initiating the shower, which is important in the analysis of experimental data on extensive air showers. Nishimura and Kamata (1952,1958) have derived the expected lateral structure function of extensive air shower particles. Their derivation was based on a purely electromagnetic cascade shower theory taking into account the multiple scattering of electrons. Greisen (1956) produced a simplified formula representing the lateral distribution of all charged particles in extensive air showers of size N_e at sea level (known as the N.K.G. formula, i.e. Nishimura, Kamata, Greisen) which is plotted in Figure 5.5 for some values of s, and which is given as,

$$\Delta_e(N_e,r) = \frac{N_e}{r_1^2} f(\frac{r}{r_1})$$

where $$f(\frac{r}{r_1}) = c(s) (\frac{r}{r_1})^{s-1}(1 + \frac{r}{r_1})^{s-4.5}$$

and s is the shower age parameter and is a measure of the stage of development for the shower, r is the distance to the shower axis, r_1 is the Moliere unit having a value of 79 metres at sea level

and c(s) is the normalization coefficient, values of which are as follows:

s	= 0.6	0.8	1.0	1.2	1.4	1.6	1.8
c(s)	= 0.22	0.31	0.40	0.44	0.43	0.36	0.25

The age parameter of extensive air showers is practically independent of the number of particles in the shower over the very wide range of number: 10^3 - 10^9 particles. The age parameter over this range is 1.20 to 1.25, (see for example, Greisen 1960).

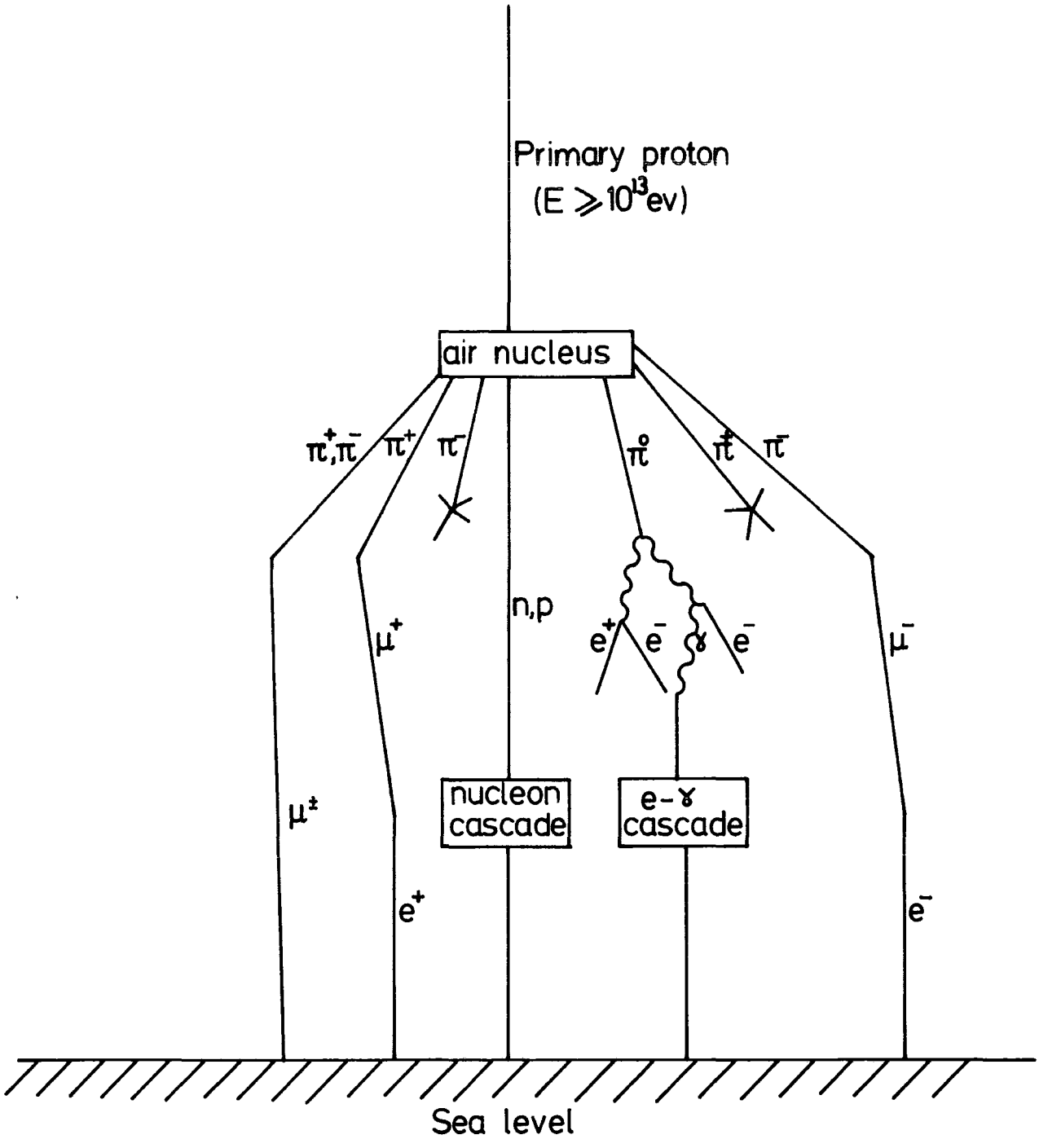

Figure 5.1: Diagram showing the major processes taking place in the atmosphere when an extensive air shower is observed at sea level.

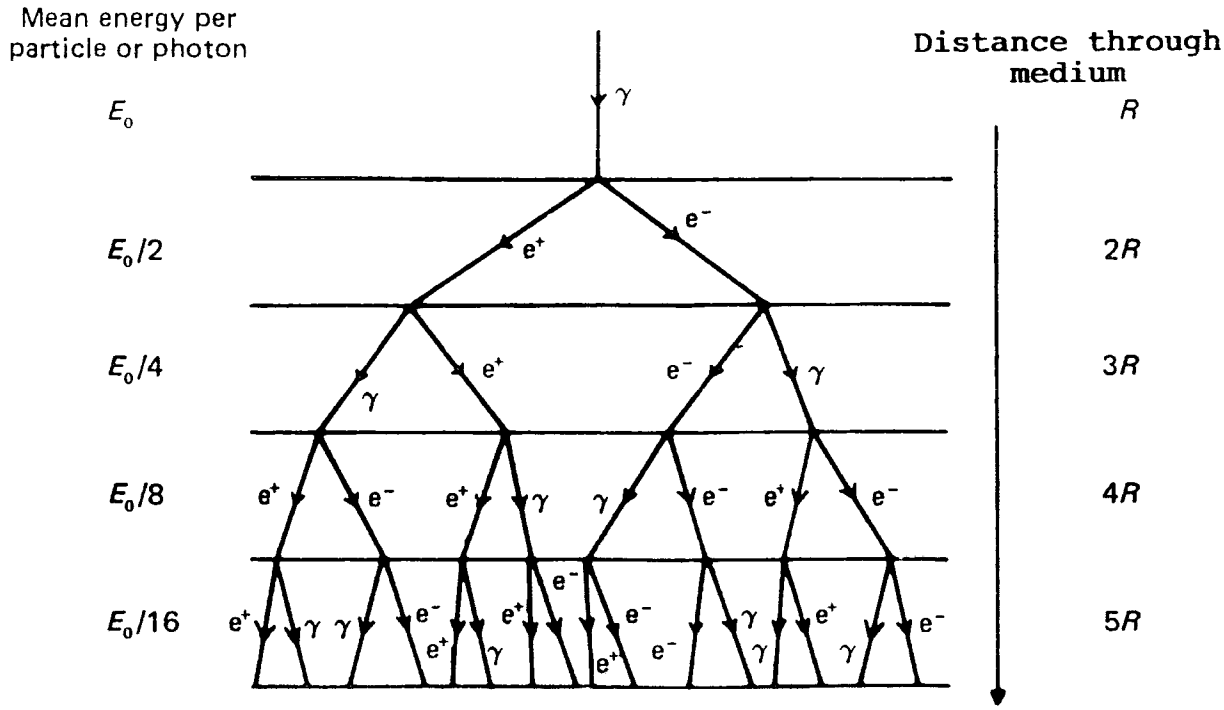

Figure 5.2 : A simple model of an electromagnetic shower.
(after Longair 1981)

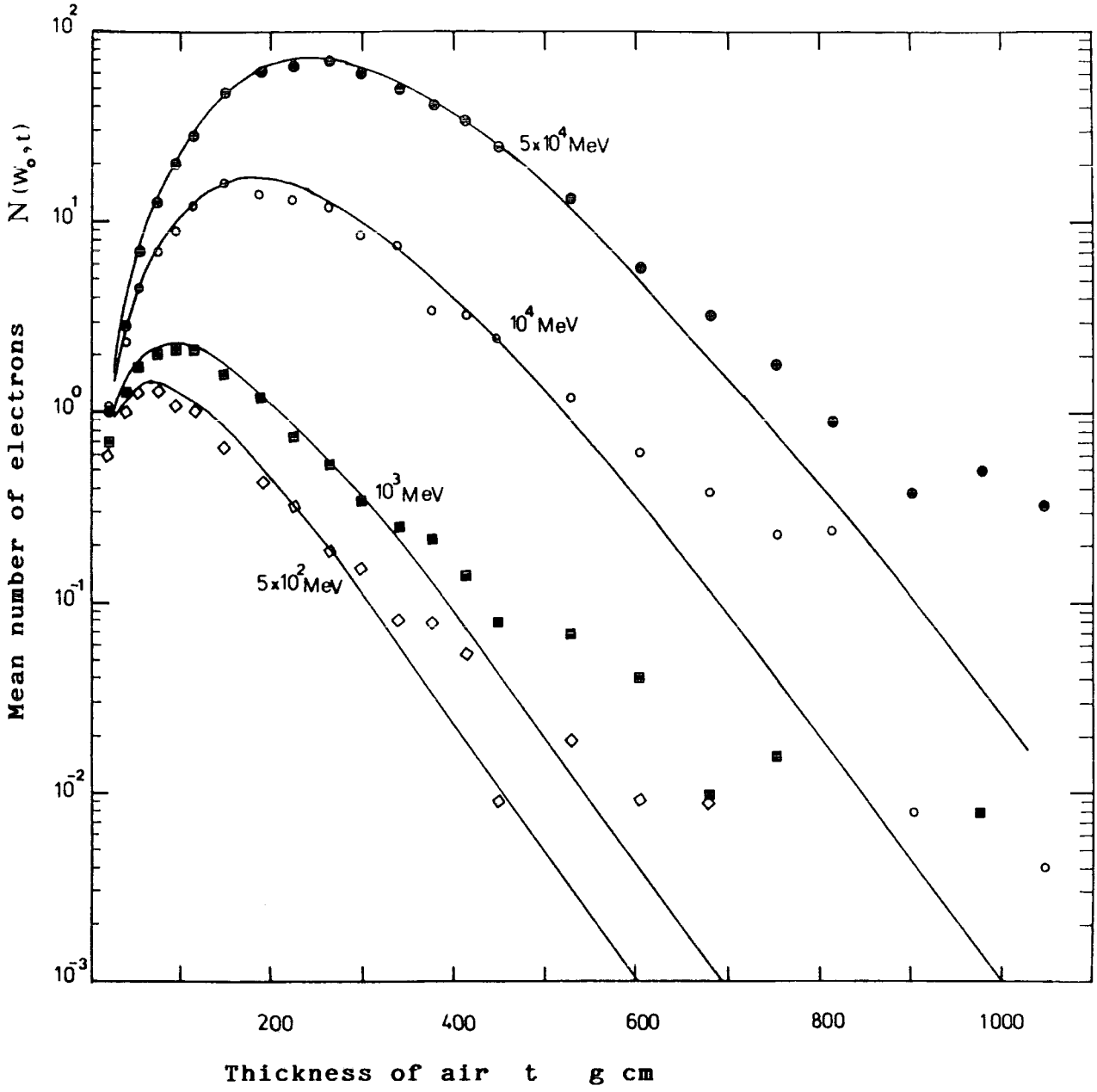

Figure 3.5 Mean number of electrons as a function of air thickness for showers initiated by photons. Photon energies are shown on the graph (in MeV).
Points - Messel and Grawford (1970) simulations.
Curves - Greisen(1956) and Cocconi(1961)

$$N(W_o,t) = \frac{.31}{B_o^{1/2}} \exp[\, t\,(1 - 1.5 \log_e s\,)]$$

t = air thickness in radiation units X_o.

$$B_o = \log_e \frac{W_o}{E_o}$$

$$s = \frac{3t}{t+2B_o} = \text{age parameter}$$

X_o = 1 radiation unit = 37.7 g/cm^2

E_o = critical energy = 84.2 MeV

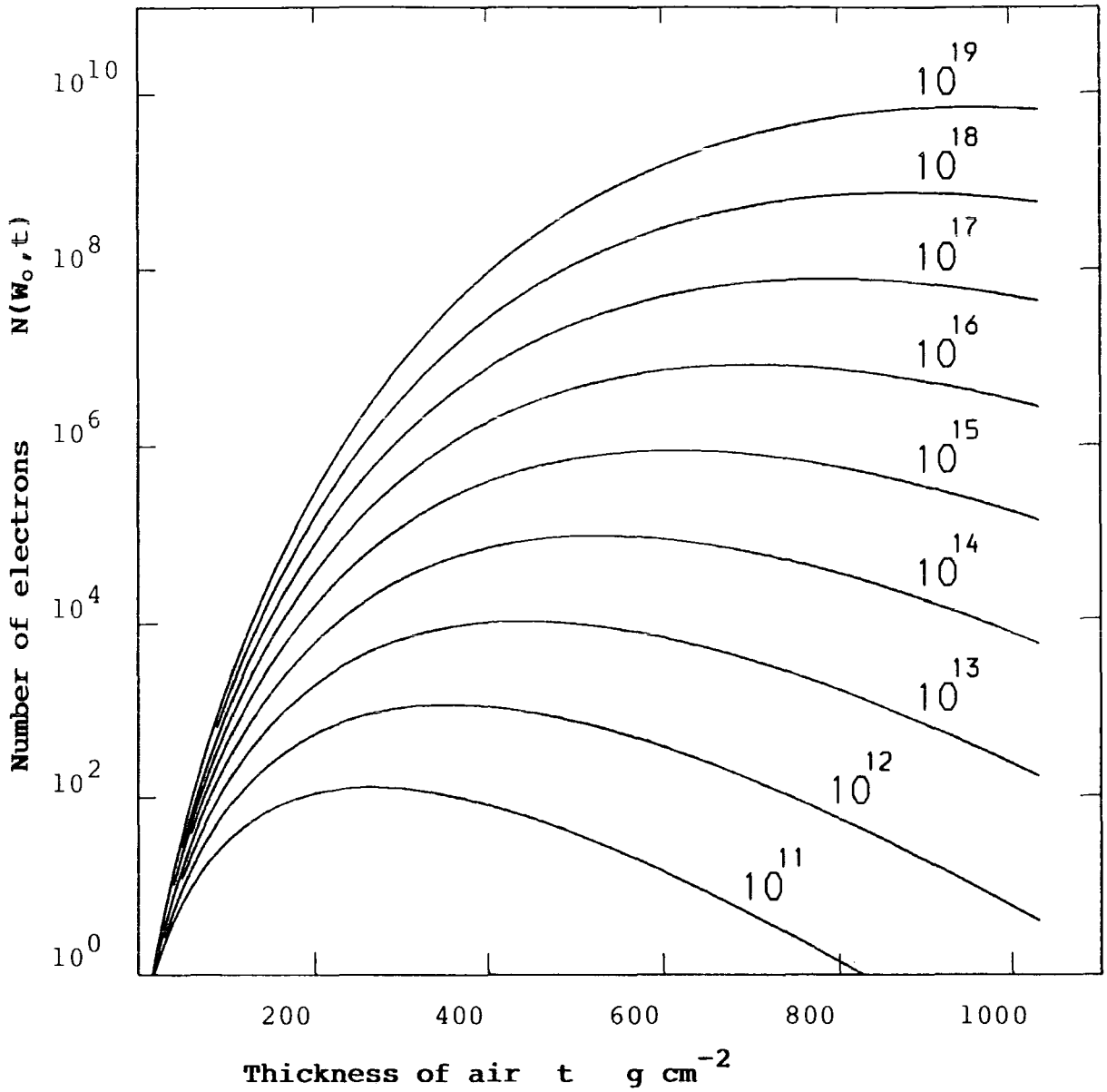

Figure 5.4: Mean number of electrons as a function of air thickness for showers initiated by photons. Photon energies, W_o, are shown on the graph, in eV.

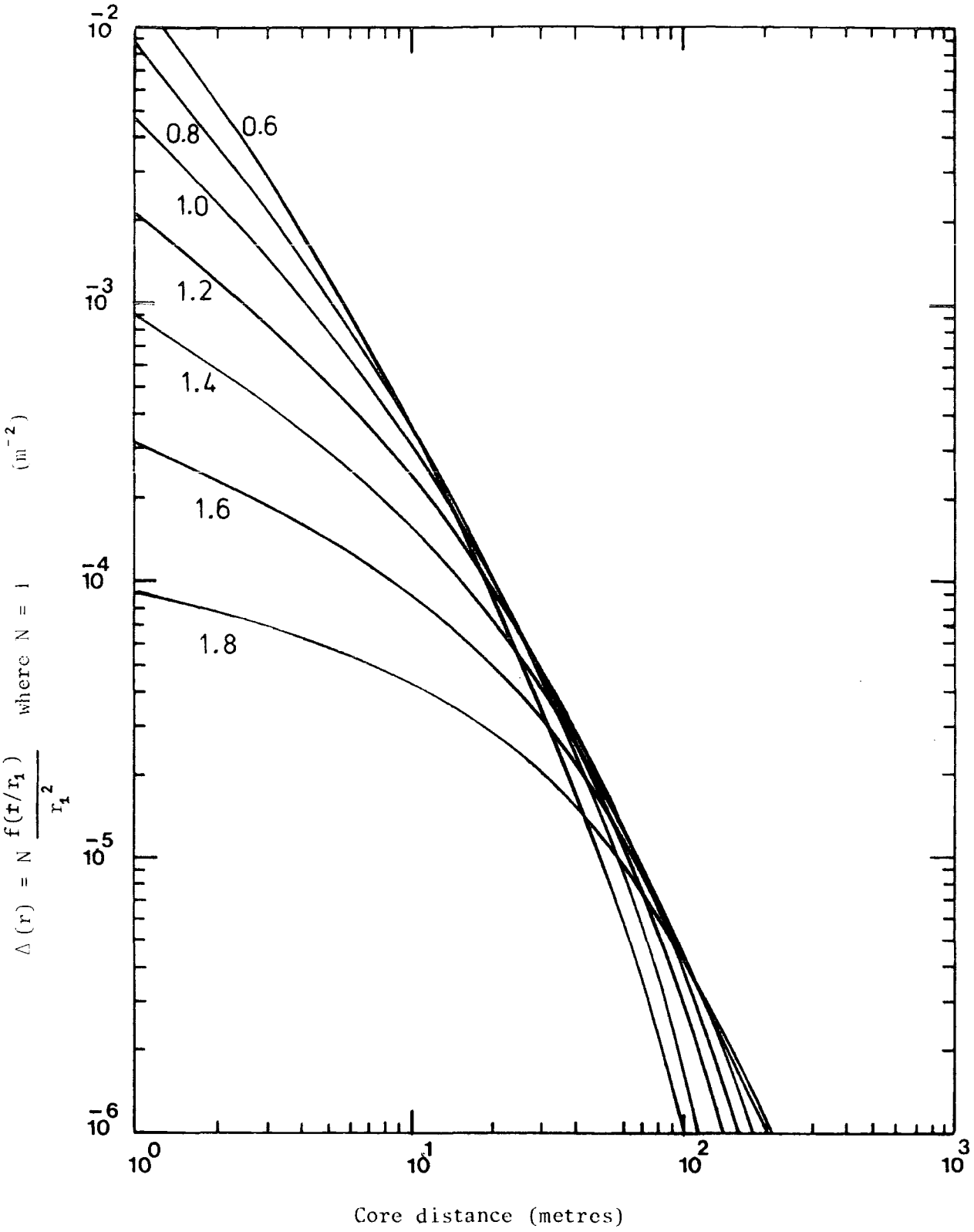

Figure 5.5: The lateral distribution of electrons in showers of unit size in air at level (r_o = 79m). The number attached to each curve is the age parameter (s) of the shower.

Chapter Six

Development of a computer program to simulate extensive air showers generated by high energy protons

6.1 INTRODUCTION

The Monte-Carlo method was used to calculate the distribution and the average of the total number of electrons at sea level in extensive air showers initiated by high energy cosmic ray protons with a given primary energy between 10^{12}-10^{19}eV. This simulation was carried out by a program named 'MC007' which simulates one dimensional propagation of a given number of extensive air showers (e.g. 1000 trials), all initiated by protons having the same primary energy. The program then gives the average behaviour of these showers. The most important result of this program was the determination of the relation between the energy of the primary cosmic ray protons and the size of the extensive air shower at sea level, which could be used to derive the energy spectrum from the measured size spectrum. To overcome the complexity of the program, a number of smaller programs were produced to help building up the final program. One of these small programs was to test and to understand the random number generator.

The Monte-Carlo method of solving numerically problems arising in Mathematics, Physics and other sciences, by constructing for each problem a random process whose parameters are equal to the required quantities and on which observations can be made by

ordinary computational means. From these observations, made on the random process, an estimate is made of the required parameters. In the probabilistic type of problem the actual random processes are simulated by suitably chosen random numbers and the required information is obtained from a sufficiently large number of observations using these numbers.

6.2 Dealing with random numbers

The random numbers needed for the simulation is provided by NAG (numerical algorithms group) which is in the FORTRAN library for subroutines and functions. Random numbers (or pseudo-random numbers) are produced by calling the G05CAF function. This function produces 16-figure random numbers, uniformly distributed between 0 and 1, using a multiplicative congruential method :-

$$N = 13^{13}\ N \bmod(2^{59}),$$

where N is a variable whose value is preserved between calls of the routine. Its initial value is $123456789(2^{32} + 1)$, but this may be altered by a call to G05CBF or G05CCF. These random number generators have a finite cycle length before the sequence repeats itself. The cycle is 2^{57} ($= 1.4412 \times 10^{17}$). The maximum number of random numbers used is the square root of the cycle length, which is about 3.8×10^{8}. In the present work, the longest sequence of random numbers used is about 1.3×10^{4}.

Program RG001 demonstrates how the NAG library function G05CAF is used . Figure 6.1 lists the program and its outputs. To test the uniformity of these random numbers between Zero and 1, the program DS02 was written, and the list of the program and its

outputs are shown in Figures 6.2 and 6.3. The outputs confirm the uniformity of the distribution between zero and 1.

6.3 Simulation of the free path

The free path of a high energy proton is the distance, in g cm^{-2}, travelled by this proton before it undergoes an inelastic interaction. The distribution of the free path of high energy cosmic ray protons in the atmosphere is an exponential one, with mean free path of 80 g cm^{-2}. In other words, if we have N protons each travelling x g cm^{-2} before interacting, the cumulative distribution of these free paths will has the form :

$$F(x) = N\, e^{-(x/L)} \qquad \text{Eq.(6.1)}$$

where L is the mean free path. To sample numbers which exponentialy distributed to represent the free path, we use the the following formula:

$$x = - L \ln(z) \qquad \text{Eq.(6.2)}$$

where z is a random number with uniform distribution between zero and 1. See Appendix D for the proof. The program DST03, which is listed in Figure 6.4 uses this theorem, to generate exponentialy distributed free paths using Eq.(6.2), where z is a random number between 0 and 1. The program constructs the cumulative frequency table and plots this table together with Eq.(6.1). The results of this program is shown in Figure 6.5. It is clear that the free path simulation is correct.

The next step was to simulate the number of interactions that a cosmic ray proton makes as it propagates through the atmosphere to sea level. This was achieved by the program 'MC001'. In this

program, we assume an incident cosmic rays proton undergoes a number of interactions until it reaches the sea level, and the free path between two successive interactions is sampled as in the previous program (DST03), then this is repeated for a given number of times. The program produces a bar-graph for the distribution of the number of interactions, and plots with it the expected Poisson distribution with the form:

$$P(n) = \frac{e^{-z} \; z^{n}}{n!} \qquad \text{Eq.(6.3)}$$

where n is the number of interactions and z is equal to 12.9 which is the expected average number of interactions, obtained by dividing the atmospheric depth (1030 g cm^{-2}) by the mean free path (80 g cm^{-2}). The program is listed in Figure 6.6, and Figure 6.7 is the graphical output of this program.

6.4 The model used in the simulation program.

In this model we adopted the theory of the extensive air showers which was discussed in the previous chapter. Properties of the model can be summarized as follows:

(1) High energy protons lose on average half of their energy in each collision and have an interaction mean free path in the atmosphere of 80 g cm^{-2}, both these quantities being independent of energy.

(2) All secondary particles are pions, and the fraction of energy lost by a proton which does not appear as pions is negligible. There being on average equal numbers of each of the three kinds of pions (positive, negative and neutral) produced.

(3) The multiplicity of secondary pion, n_s, is given by :

$$n_s = 3.0\ E_p^{\frac{1}{4}} \quad , \qquad \text{Eq.6.4}$$

with E_p in GeV.

(4) Pion interactions are assumed to differ from nucleon interactions in that they are catastrophic with interaction length of 120 g cm^{-2}. The energy spectrum of the pions produced in pion interactions is taken to be that given by the same relation as for protons but with K = 1.

The character of interactions assumed in this model is as follows: A proton with energy E_p entering the atmosphere suffers nuclear collisions with mean free path of 80 g cm^{-2}. The integral distribution of the free path is described by Eq 6.1 . However, the proton is not lost in an inelastic collision: it emerges as a proton or neutron with half of its initial energy. The rest of energy (E_p) is spent in the production of secondary particles all of which are pions as all other particles are ignored in this model. Positive, negative, and neutral pions which are appearing in this interaction, have equal numbers. The number of pions produced is given in Eq 6.4, and the average energy of each pion is: $\frac{1}{6} E^{3/4}$ (Eq 6.5), which is found by dividing $\frac{1}{2}E$ by the total number of pions. The neutral pions immediately decay into pairs of photons. It is clear that the number of these photons is twice the number of neutral pions producing them, and the average energy of the photons is equal to half the average energy of the pions. Each of these photons starts a photon-electron cascade at this point of the

atmosphere. The expression given by Greisen (1956) and discussed in the previous chapter is used here to describe the development of these cascades. The charged pions which are produced in the collision travel 120 g cm^{-2} before they interact with air nuclei. However, not all charged pions survive to interact. The number of surviving pions, N , is

$$N = N_o \; e^{-d/D} \qquad \text{Eq(6.6)}$$

where N_o is the original number of pions and D is the "decay length". The decay length of a charged pion with energy E is

$$D = \gamma \, cT_o$$

$$D = \frac{E}{m_\pi c^2} \; c \; T_o \qquad \text{Eq(6.7)}$$

where $m_\pi c^2$ =0.14 GeV, c = 3 x 10^8 m/s, and T_o= 2.6 x 10^{-8}. Then one may write

$$D = 0.056 \; E \quad \text{km} \qquad \text{Eq(6.8)}$$

with E in GeV. Notice that for this calculation the distance travelled by the charged pion between two collisions, d , should be in km, not in g cm^{-2}. To convert the depth in g cm^{-2} to altitude in km, the relation given by Rossi (1952), for the standard atmosphere is adopted. The graph he gave is consistent with the analytical description

$$\left.\begin{aligned} Z &= 6.38 \log\left(\frac{1300}{x}\right) \quad \text{km, for } 0 < x < 224 \text{ g cm}^{-2} \\ Z &= 12.95 \; (3.56 - x^{0.183}) \quad \text{km, for } 224 < x < 1035 \text{ g cm}^{-2} \end{aligned}\right\} \qquad \text{Eq(6.9)}$$

where Z is the altitude in km, and x is the depth in g cm^{-2}.

The surviving charged pions interact with air nuclei consuming all their energy to produce a new generation of pions of the three kinds in equal quantities, and the number of them is given by Eq 6.4, for each parent pion, and the energy is assumed to be distributed equally among the produced pions. Each of the neutral pions decay to a pair of photons which in turn initiate photon-electron cascades, in the same way as the photons created by neutral pions produced in the nuclear interaction discussed above. The charged pions of this generation repeat the role played by the parent charged pions until eventually their average energy is not enough to produce new pions, or they reach sea level. All that is for the first collision of the cosmic ray proton with an air nucleus, but the proton will make a number of collisions before it reaches sea level. The collisions of protons and charged pions are accounted for as long as the particle energy is > 1GeV. Each nuclear collision produces a number of photon-electron cascades. All these cascades add together to form the extensive air shower.

6.5 The Simulation Programs

The simulation program was done in three stages. First, a program simulates the part of the shower produced by neutral pions only (program MC004), second, the program MC006 which looks at the number of electrons produced by charged pions only, and finally, the two programs were combined together into one program which

takes the problem as a whole. Now we will write about each of these program.

MC004

This program simulates the average number of electrons arriving at different atmospheric depths produced by neutral pion production only as a primary nucleon propagates through the atmosphere assuming the model which has been described in section 6.4. A list of this program is given in Figure 6.8 and its flowchart is shown in Figure 6.9. The program MC004 could be understood by the following logical steps:

1. Initialisation of the variables, lines 16-33. In which the primary energy and number of trials are set as the user requires.
2. At line (35) the program starts its main loop which will be repeated for the number of trials set in line number 19. Y is set to be 0 where Y is the atmospheric depth where the proton last interacted. Variable J is set to be equal the primary energy. The array SL is reserved for the number of electrons at sea level.
3. Statement labelled 10 at line number 41 starts the simulation for one shower. The program at this step calls the function GO5CAF to generate a random number uniformly distributed between 0 and 1 as discussed in program RG001. The next line changes the random number Z to be chosen from exponential distribution as it has been done before in program DS03, to simulate the path length of the proton; then this value is added to Y to give the depth of the collision in the atmosphere.

4. The depth Y is compared with the depth of the atmosphere at sea level which is taken in this program to be 1000 g cm^{-2}. If the depth of collision is deeper than the atmosphere then the program will end the simulation for this shower, otherwise the program will resume its simulation.
5. The program calculates in line number 47, the number of neutral pions only "FPI0" using equation 6.4 of the adopted model, taking in account that the neutral pions are one third of the total produced pions. At line number 48 the average energy for each pion is computed using relation Eq 6.5 .
6. The number of photons and the average energy of each of them are calculated in lines 49 and 50.
7. The program assumes that each of the produced photons initiates a photon-electron cascade. The program computes the number of electrons at 100 points of the atmosphere (10, 20, ... 1000), produced by all photons. However the value of the cascades for all points before the interaction is zero. Each of these values is stored at the relevant element of the array "A". For each point the small loop calls the FUNCTION ANUM which needs two arguments, the first is the the energy of the photon "EG", and the second "TX" is the thickness of the air between the position of interaction "Y" and the required point "X". The FUNCTION ANUM is the same as FUNCTION ANUM used in the program EQ02 discussed in the previous chapter.
8. The energy of the proton "E" is reduced by one half in line number 59, and in line number 60 the program decides whether to continue the simulation for this shower in case that "E" is

greater than 10^9 eV, by going to statement 10 (at line number 41), or else, the program starts the simulation for a new shower by doing a new turn in the main loop, which means that the program will return to the beginning of step 2.

9. When the main loop finishes, the two dimensional array "A" will contain the information about the development of the extensive air shower. An element A(i,j) of this array, contains the summation of the number of electrons due to all collision numbers j in all simulated showers at depth (10.i) g cm^{-2}.
10. To find the average number of electrons at different depths for each nuclear collision, each element of the array is divided by the number of showers simulated (= NTRIAL), that is done in the loop starting at line number 64.
11. To find the average electron number as a function of depth, the averages produced by all interactions are added for all points of the atmosphere and is performed in the loop in lines 69 to 71.
12. A call to the GR2 SUBROUTINE draws the total number of electrons in the shower as a function of depth.
13. The average number of electrons due to each one of the interactions is drawn by calling to GR2 for each curve, within the loop in lines 74 to 79.
14. The program does some statistics after the main routine of the program for the number of electrons at sea level and prints tables as discussed below in the discussion about the outputs of the program.

The program produces two graphs, the first shows the average behaviour of a shower initiated by a cosmic ray proton of a given energy; and also on the same graph the contribution of each of the nuclear interactions are drawn. The second graph is a histogram showing the distribution of the quantity $\log_{10}$ of the number of the electrons at sea level. The program also produces tables, the first group of tables gives the average number of electrons at different points of the atmosphere (100, 200, ... ,1000 g cm^{-2}) for each interaction and the last one of this group is for all the shower. The program then gives the mean and the standard deviation of the number of electrons at sea level, and the mean and the standard deviation of the $\log_{10}$ of the number of electrons at sea level. The program also prints the frequency table of the $\log_{10}$ of the electron number at sea level. Only one example of printed output is given here, Table 6.1, for simulated showers initiated by a proton of energy 10^{15} eV. The graphical outputs are given in Figures 6.10.1 to 6.10.9.

MC006

As mentioned before in section 6.4, each time the proton makes a collision it produces all kinds of pions in equal numbers. This program simulates the average number of electrons arriving at different atmospheric depths produced by the pion cascade originating from the charged pions produced as a primary nucleon propagates through the atmosphere assuming the model described in section 6.4. The program is listed in Figure 6.11, and the flowchart of it is shown in Figure 6.12. The program in general is

similar to MC004 which deals with the neutral pions only, but there is a difference which is that for charged pions the program should trace the charged pions while they make a number of interactions. For each interaction the program calculates the number of the new generated pions of all kinds and then finds the photon-electron cascades due to those that are neutral. The following is a description of program MC006:

1. Initialisation of the variables (lines number 18 to 35).
2. The main loop starts at line number 39 which ends with statement labelled as 300 at line number 89. Each turn of this loop simulates one shower. At the beginning of each turn the program sets the depth of the interaction, Y , to be zero, the counter, J ,which counts the number of the interaction is also initialised to zero, and the energy of the proton reset to the value of the primary energy stored in the variable "ENERGY".
3. The program in lines 44 to 47 samples the depth of the collision as discussed in the description of program MC001.
4. If the depth of the collision calculated in step 3 is $\geq$1000 g cm^{-2} (line 48) the program will assume that the proton has reached sea level and hence it will go to the end of the loop (label 300).
5. The program computes the depth of the charged pions, W2 , by adding 120 to the depth of the nuclear collision Y. And translates these two depths to altitudes by the FUNCTION ALTI, which uses the relation between depth and altitude that is discussed in section 6.4, (Eq 6.9).
6. The number of charged pions created in the proton collision and

the average energy of each of them, are calculated in lines 55 and 56. The program computes in lines 57 to 58, the number of charged pions surviving to interact after 120 g cm^{-2}.

7. With the number of charged pions and the average energy of them, the program enters a small loop which starts at statement labelled 120 and ends at statement labelled 200.

Line 60 computes the number of neutral pions, and line 61 computes the average energy of the neutral pions. As it was assumed that each neutral pion decays to a pair of photons, each carries half of the pion energy. These photons initiate photon-electron cascades and these cascades are calculated in lines 67 to 74 for 100 positions in the atmosphere. The same argument mentioned in step 7 of the description of program MC004 could be applied here. When calculation of the photon-electron cascade ends the program repeats this small loop for another pionic interaction until the charged pions have not enough energy to produce more pions, or those charged pions reach sea level. For each turn the number of electrons at different depths are accumulated to form at the end of this loop the contribution of charged pions produced in this proton collision ,ie collision number J.

8. By the end of the above loop the energy of the proton is reduced by one half, and if that energy is enough to generate pions, the program will go to statement 110 at line number 44 to simulate the next proton collision by repeating steps 3,4,5,6 and 7. This loop ends when the depth of the collision Y is greater than 1000 g cm^{-2} (see line 52), or the energy of the

proton becomes less than 10^9 eV (see line 87). By the end of the main loop the simulation of one extensive air shower is completed. The array A contains at this stage the share of each collision accumulated to all shares of collisions having the same order in the previous simulated showers for different depths.

9. The main loop is repeated for the next simulated shower, and repeated again until the trial number reaches the preset value.

The rest of the main routine is exactly the same as program MC004. The same discussion carried out in steps 9 to 14 of the description of program MC004 is applicable here. The program MC006 produces the same kinds of graphical and printed outputs as the ones produced by MC004. The graphical outputs are shown in Figures 6.13.1 to 6.13.9. Only an example of the output tables is given here for energy 10^{15}eV (Table 6.2).

MC007

MC007 is the final program in which the model that is proposed in section 6.4 is fully taken. The list of this program is shown in figure 6.14, and its flowchart is given in Figure 6.15. The program may be described in the following steps:

1. Initialization of variables in lines 16 to 34. The program user may set the value of the primary energy in line 19 as he requires. Also he may change the number of trials in line 20 to suit him. In line 22 the program calls the subroutine GR1 to prepare for the graphical output.

2. The program starts at line 37 and its main loop is repeated for each simulated shower. The end of this loop is labelled as 300 in line number 85.
3. In the beginning of each turn of the loop, the depth Y of the proton in the atmosphere is set to zero, the counter J of the collisions is also set to zero.
4. At line 42 (statement labelled 110) the program starts the calculation related to one nuclear collision. The program at this step samples a random free path for the proton by generating a random number Z between 0 and 1 using NAG Function G05CAF at line number 42, then z is changed to be a sampled free path from an exponential distribution in line number 43. The full discussion about sampling the free path is found in section 6.3. The program will continue if the value of Y which is the depth of the collision is less than 1000 g cm^{-2} which is the assumed thickness of the atmosphere.
5. This step is the core of the program, in which the program calls to the SUBROUTINE MC004 to compute the contribution of this nuclear interaction (number J), to the number of electrons produced by direct neutral pion production, and stores this information temporarily in the array A1, such that an element A1(i) contains the value of the number of the electrons obtained in this calculation for the depth (i.10) g cm^{-2}. The program then calls the SUBROUTINE MC006 to compute the contribution of this nuclear interaction (number J), in the number of electrons produced by the pion cascade originating from the charged pions and stores this information temporarily in the array A2 such

that an element A2(i) contains the value of the number of the electrons obtained in this calculation for the depth (i.10) g cm^{-2}. The program determines the share of this nuclear collision in the shower for different depths by adding the values of the two elements of the array A1 and A2 with the same subscript to the value of the element of the two-dimensional array A, that element which has the same subscript, and that is done for all elements of array A1 and array A2.

The Subroutines MC004 and MC006 have essentially the same idea as the programs MC004 and MC006 respectively.

6. The program then reduces the energy of the proton by 0.5 in line 56 and if that energy is greater than 1 GeV the program will resume to the beginning of step 4 for simulation of the next collision. The program accumulates the number of electrons for different collisions and different depths in the array A.
7. The above loop contains steps 4, 5, and 6, is repeated for a number of collisions until the depth of the interaction reaches sea level (line 47), or the energy of the proton becomes to be not enough for pion production (line 57)
8. In case the simulation for a shower ends as mentioned in step 7, the program repeats the main loop which contain steps 2 to 7, again and again until the number of simulated showers is equal to the number which is set by the user.
9. When the main loop finishes, the two dimensional array "A" will contain the information about the development of the extensive air showers in the atmosphere. An element A(i,j) of this array, should contain the summation of the number of electrons due to

all collisions numbered j in all simulated showers at depth (10.i) g cm^{-2}.

10. To find the average number of electrons at different depths for each nuclear collision, each element of the array is divided by the number of showers simulated (= NTRIAL), that is done in the loop which starts at line number 60.
11. The average number of electrons due to each one of the interaction is drawn by calling to SUBROUTINE GR2 for each curve, within the loop in lines 60 to 62.
12. To find the total average of electron numbers as a function of depth, the averages produced by all interactions are added for all points of the atmosphere and it is performed in the loop in lines 71 to 74, and that is stored in the array T.
13. A call to the GR2 SUBROUTINE draws the total number of electrons in the shower as a function of depth.
14. The program does some statistics at the end of the main routine of the program for the number of electrons at sea level and prints tables as discussed below in the discussion about the program outputs.

The program produces two graphs for each run, the first shows the average behaviour of a shower initiated by a cosmic ray proton of a given energy; and also on the same graph the contribution of each of the nuclear interactions are drawn. The second graph is a histogram showing the distribution of the quantity $\log_{10}$ of the number of the electrons at sea level, those graphs are given in Figures 6.16.1 to 6.16.9. The programs also

produce tables, the first group of tables gives the average number of electrons at different points of the atmosphere (100, 200, ... ,1000 g cm^{-2}) for each interaction and the last one of this group is for all the shower. The program then gives the mean and the standard deviation of the number of electrons at sea level, and the mean and the standard deviation of the $\log_{10}$ of the number of electrons at sea level. The program also prints the frequency table of the $\log_{10}$ of the electron number at sea level. Only an example of printed output is given here, for simulated showers initiated by a proton of energy 10^{15} eV, Table 6.3.

6.6 Results.

The programs MC004, MC006 and MC007 were run for primary energies 10^{12} to 10^{19} eV. Only the graphical outputs are presented because the produced tables are too long to be put in this thesis. The following are the interesting relations deduced by investigating the results of these runs.

1. The most important result is the relation between the primary energy of a cosmic ray proton and the average number of electrons at sea level for an extensive air shower initiated by that proton. In Table 6.4, the average number of electrons at sea level calculated for direct neutral pion production only (MC004) and the average number of electrons at sea level calculated for charged pion production only (MC006) and the average number of electrons at sea level calculated for all pion production (MC007) is given for primary energies in the range 10^{12} to 10^{19} eV. Also given in this table is the standard deviation of each of the

electron numbers at sea level. Figure 6.17 demonstrates the relation between the primary energy and the electron number at sea level, which were simulated by program MC007. On the same graph the same relation for electron number produced just by neutral pions from N-N collisions as calculated by MC004 and that which is just produced by charged pions from $\pi^{\pm}$-N collisions as calculated by MC006 are also drawn. The root mean square for each of the numbers of electrons was calculated from the mean and the standard deviation as shown in Table 6.5. Figure 6.18 shows the average number of electrons and the root mean square number of electrons as functions of the primary energy. Some experimental points are plotted for comparison, and the same two curves were drawn in Figure 6.19 with simulation results given by other workers. The empirical formula describing the dependence of the number of electrons at sea level on the primary energy is found to be

$$\log_{10}(N_e) = -21.27 + 2.22 \log_{10}E_p - 0.031 (\log_{10}E_p)^2$$

where N_e is the number of electron at sea level and E_p is the primary energy (eV) and it is plotted in Figure 6.20.

2. The dependance of the depth of shower maximum t_{max} on the primary energy E_p was also found and is plotted in Figures 6.21 where it is compared with some experimental data collected by Capdevielle and Gawin (1985). The relation between the depth of shower maximum and the number of electron at sea level is obtained and is shown in Figure 6.22 where the experimental points due to Inoue et al (1985) are shown for comparison.

3. The relation between the number of particles at shower maximum and the primary energy was obtained. La Pointe et al

(1968) suggested that, to 25% one may take 1.4 GeV per particle present at shower maximum , this is represented by dashed line in Figure 6.23 to be compared with the present simulation results , some experimental points are also plotted.

4. The shape of the developing of the shower size as it propagates through the atmosphere for energies 10^{16}eV, and 10^{17}eV is compared in Figure 6.24 with some observations. Notice that the observed points are not for the given energy but these points are for showers detected at a fixed rate.

6.7 Conclusion.

In this chapter, a FORTRAN program (MC007), which simulates extensive air showers generated by high energy protons, was described. Using the Monte-Carlo simulation method to solve the problem of the extensive air shower is easier than other mathematical methods. The program adopts a simple model which was discussed in section 4 of this chapter. In spite of the simplicity of the model used, it is seen that the results of the simulation program are very much in agreement with previous simulations and experimental results, as was shown in section 6.6. This infers that the model used is a reasonable model.

INITIAL ENERGY =1.0E+15 EV
NUMBER OF TRIALS = 1000

INTERACTION NUMBER 1

DEPTH ($g\ cm^{-2}$)	NE (*total number of electrons*)
100	1.53655E+03
200	2.51003E+04
300	9.29814E+04
400	1.58821E+05
500	1.68781E+05
600	1.30637E+05
700	8.06523E+04
800	4.20649E+04
900	1.92806E+04
1000	7.96937E+03

INTERACTION NUMBER 2

DEPTH	NE
100	2.16726E+02
200	5.73523E+03
300	2.84529E+04
400	6.07981E+04
500	7.85862E+04
600	7.29464E+04
700	5.36032E+04
800	3.30389E+04
900	1.77418E+04
1000	8.58378E+03

INTERACTION NUMBER 3

DEPTH	NE
100	2.68235E+01
200	1.20708E+03
300	8.10848E+03
400	2.18344E+04
500	3.42506E+04
600	3.74322E+04
700	3.16182E+04
800	2.20362E+04
900	1.31752E+04
1000	7.01991E+03

Table 6.1: Output of the program MC004 for proton of initial energy 10^{15} eV.

(to be continued).

INTERACTION NUMBER 4

DEPTH	NE
100	3.33563E+00
200	2.48405E+02
300	2.16214E+03
400	7.19821E+03
500	1.34911E+04
600	1.72980E+04
700	1.70226E+04
800	1.37114E+04
900	9.34408E+03
1000	5.49905E+03

INTERACTION NUMBER 5

DEPTH	NE
100	1.53330E-01
200	4.50183E+01
300	5.60106E+02
400	2.32279E+03
500	5.07768E+03
600	7.46596E+03
700	8.41254E+03
800	7.66288E+03
900	5.83547E+03
1000	3.84079E+03

INTERACTION NUMBER 6

DEPTH	NE
100	4.08551E-02
200	1.04847E+01
300	1.54700E+02
400	7.26314E+02
500	1.80694E+03
600	3.03258E+03
700	3.84943E+03
800	3.96996E+03
900	3.41384E+03
1000	2.48530E+03

Continuation of Table 6.1.

Output of the program MC004.

INTERACTION NUMBER 7

DEPTH	NE
100	1.47723E-02
200	2.74734E+00
300	3.08071E+01
400	1.99756E+02
500	6.31950E+02
600	1.19758E+03
700	1.67098E+03
800	1.89311E+03
900	1.81260E+03
1000	1.47875E+03

INTERACTION NUMBER 8

DEPTH	NE
100	0.0
200	1.18112E+00
300	8.72869E+00
400	5.45184E+01
500	2.01322E+02
600	4.45818E+02
700	6.98397E+02
800	8.67511E+02
900	9.08558E+02
1000	8.15500E+02

INTERACTION NUMBER 9

DEPTH	NE
100	0.0
200	1.70999E-01
300	2.21068E+00
400	1.35164E+01
500	5.53398E+01
600	1.49283E+02
700	2.80182E+02
800	3.99443E+02
900	4.54116E+02
1000	4.28575E+02

Continuation of Table 6.1.

Output of the program MC004.

INTERACTION NUMBER 10

DEPTH	NE
100	0.0
200	3.18241E-02
300	7.38256E-01
400	4.19960E+00
500	1.60556E+01
600	4.95969E+01
700	1.03652E+02
800	1.64854E+02
900	2.11019E+02
1000	2.19094E+02

INTERACTION NUMBER 11

DEPTH	NE
100	0.0
200	2.54404E-03
300	1.69432E-01
400	9.87364E-01
500	4.41675E+00
600	1.58122E+01
700	3.86630E+01
800	6.53365E+01
900	9.23145E+01
1000	1.06620E+02

INTERACTION NUMBER 12

DEPTH	NE
100	0.0
200	0.0
300	5.28506E-02
400	2.56045E-01
500	1.52628E+00
600	4.99130E+00
700	1.31789E+01
800	2.49267E+01
900	3.95603E+01
1000	4.84218E+01

Continuation of Table 6.1.

Output of the program MC004.

INTERACTION NUMBER 13

DEPTH	NE
100	0.0
200	0.0
300	0.0
400	2.86644E-02
500	2.44514E-01
600	1.45906E+00
700	4.62845E+00
800	9.00398E+00
900	1.52183E+01
1000	2.22075E+01

INTERACTION NUMBER 14

DEPTH	NE
100	0.0
200	0.0
300	0.0
400	3.09217E-03
500	9.18300E-02
600	3.32854E-01
700	1.35170E+00
800	3.32627E+00
900	5.59387E+00
1000	8.69383E+00

INTERACTION NUMBER 15

DEPTH	NE
100	0.0
200	0.0
300	0.0
400	0.0
500	2.98674E-03
600	6.63412E-02
700	4.55091E-01
800	1.18091E+00
900	2.27566E+00
1000	3.46147E+00

Continuation of Table 6.1.

Output of the program MC004.

INTERACTION NUMBER 16

DEPTH	NE
100	0.0
200	0.0
300	0.0
400	0.0
500	0.0
600	6.96416E-03
700	1.11549E-01
800	4.31473E-01
900	8.57805E-01
1000	1.39309E+00

INTERACTION NUMBER 17

DEPTH	NE
100	0.0
200	0.0
300	0.0
400	0.0
500	0.0
600	0.0
700	2.81590E-02
800	1.29674E-01
900	3.09478E-01
1000	5.41584E-01

INTERACTION NUMBER 18

DEPTH	NE
100	0.0
200	0.0
300	0.0
400	0.0
500	0.0
600	0.0
700	9.59808E-03
800	4.42011E-02
900	1.21039E-01
1000	1.84045E-01

Continuation of Table 6.1.

Output of the program MC004.

INTERACTION NUMBER 19

DEPTH	NE
100	0.0
200	0.0
300	0.0
400	0.0
500	0.0
600	0.0
700	3.50601E-03
800	1.03132E-02
900	4.15784E-02
1000	6.03608E-02

* T O T A L *

DEPTH	NE
100	1.78365E+03
200	3.23507E+04
300	1.32462E+05
400	2.51974E+05
500	3.02905E+05
600	2.70677E+05
700	1.97969E+05
800	1.25913E+05
900	7.23331E+04
1000	3.85317E+04

Continuation of Table 6.1.

Output of the program MC004.

INFORMATION ABOUT THE TOTAL NUMBER OF ELECTRONS AT SEA LEVEL

AVERAGE = 3.85297E+04
STANDARD DEVIATION = 4.12639E+04
AVERAGE OF LOG (N E) = 4.4025
STANDARD DEVIATION OF LOG(N E) = 0.3924

LOG (NUMBER OF ELECTRON)	FREQUENCY
3.40 -- 3.50	0.
3.50 -- 3.60	1.
3.60 -- 3.70	11.
3.70 -- 3.80	37.
3.80 -- 3.90	57.
3.90 -- 4.00	68.
4.00 -- 4.10	79.
4.10 -- 4.20	82.
4.20 -- 4.30	92.
4.30 -- 4.40	95.
4.40 -- 4.50	96.
4.50 -- 4.60	78.
4.60 -- 4.70	64.
4.70 -- 4.80	73.
4.80 -- 4.90	51.
4.90 -- 5.00	34.
5.00 -- 5.10	35.
5.10 -- 5.20	18.
5.20 -- 5.30	18.
5.30 -- 5.40	8.
5.40 -- 5.50	3.
5.50 -- 5.60	0.
5.60 -- 5.70	0.
5.70 -- 5.80	0.
LESS THAN 3.40000 =	0
GREATER THAN 5.80000 =	0

Continuation of Table 6.1.

Output of the program MC004.

INITIAL ENERGY=1.0E+15 EV
NUMBER OF TRIALS = 1000

INTERACTION NUMBER 1

DEPTH ($g\ cm^{-2}$)	NE (*total number of electrons*)
100	0.0
200	1.02778E+04
300	1.20800E+05
400	3.39777E+05
500	4.08426E+05
600	3.02196E+05
700	1.68164E+05
800	7.71842E+04
900	3.10065E+04
1000	1.13594E+04

INTERACTION NUMBER 2

DEPTH	NE
100	0.0
200	1.30833E+03
300	2.70641E+04
400	1.05689E+05
500	1.71506E+05
600	1.67300E+05
700	1.20454E+05
800	7.06230E+04
900	3.52915E+04
1000	1.56272E+04

INTERACTION NUMBER 3

DEPTH	NE
100	0.0
200	1.35506E+02
300	5.51209E+03
400	2.94834E+04
500	6.35350E+04
600	7.94824E+04
700	6.99208E+04
800	4.82891E+04
900	2.80148E+04
1000	1.39987E+04

Table 6.2: Output of the program MC006 for proton of initial energy 10^{15} eV.

(to be continued).

INTERACTION NUMBER 4

DEPTH	NE
100	0.0
200	1.30596E+01
300	1.05773E+03
400	7.46298E+03
500	2.06184E+04
600	3.20302E+04
700	3.44595E+04
800	2.89995E+04
900	2.01203E+04
1000	1.16813E+04

INTERACTION NUMBER 5

DEPTH	NE
100	0.0
200	1.33161E-01
300	1.80009E+02
400	1.83334E+03
500	6.33388E+03
600	1.16960E+04
700	1.49270E+04
800	1.48674E+04
900	1.18664E+04
1000	7.86338E+03

INTERACTION NUMBER 6

DEPTH	NE
100	0.0
200	0.0
300	3.56797E+01
400	4.52165E+02
500	1.79193E+03
600	3.88686E+03
700	5.82066E+03
800	6.68631E+03
900	6.25989E+03
1000	4.80439E+03

Continuation of Table 6.2.

Output of the program MC006.

INTERACTION NUMBER 7

DEPTH	NE
100	0.0
200	0.0
300	6.86935E+00
400	7.50333E+01
500	4.68289E+02
600	1.26627E+03
700	2.11618E+03
800	2.69832E+03
900	2.85096E+03
1000	2.52390E+03

INTERACTION NUMBER 8

DEPTH	NE
100	0.0
200	0.0
300	2.52966E+00
400	1.51746E+01
500	1.08292E+02
600	3.58900E+02
700	7.14600E+02
800	1.02609E+03
900	1.19818E+03
1000	1.18022E+03

INTERACTION NUMBER 9

DEPTH	NE
100	0.0
200	0.0
300	2.57003E-01
400	2.87658E+00
500	2.11317E+01
600	8.30523E+01
700	2.10725E+02
800	3.68135E+02
900	4.92544E+02
1000	5.16600E+02

Continuation of Table 6.2.

Output of the program MC006.

INTERACTION NUMBER 10

DEPTH	NE
100	0.0
200	0.0
300	2.22460E-02
400	5.77623E-01
500	4.04887E+00
600	1.72021E+01
700	5.56395E+01
800	1.08962E+02
900	1.69964E+02
1000	2.03997E+02

INTERACTION NUMBER 11

DEPTH	NE
100	0.0
200	0.0
300	0.0
400	3.58409E-02
500	5.56298E-01
600	3.04228E+00
700	1.18790E+01
800	2.94893E+01
900	4.92077E+01
1000	7.09512E+01

INTERACTION NUMBER 12

DEPTH	NE
100	0.0
200	0.0
300	0.0
400	1.96012E-02
500	6.93562E-02
600	6.00571E-01
700	1.91354E+00
800	6.18008E+00
900	1.18144E+01
1000	1.96122E+01

Continuation of Table 6.2.

Output of the program MC006.

INTERACTION NUMBER 13

DEPTH	NE
100	0.0
200	0.0
300	0.0
400	0.0
500	1.83607E-03
600	1.59453E-02
700	2.70509E-01
800	9.75324E-01
900	1.95411E+00
1000	3.74730E+00

INTERACTION NUMBER 14

DEPTH	NE
100	0.0
200	0.0
300	0.0
400	0.0
500	0.0
600	6.31849E-04
700	7.84944E-03
800	7.79868E-02
900	2.35194E-01
1000	4.17918E-01

INTERACTION NUMBER 15

DEPTH	NE
100	0.0
200	0.0
300	0.0
400	0.0
500	0.0
600	0.0
700	0.0
800	0.0
900	0.0
1000	0.0

Continuation of Table 6.2.

Output of the program MC006.

INTERACTION NUMBER 19

DEPTH	NE
100	0.0
200	0.0
300	0.0
400	0.0
500	0.0
600	0.0
700	0.0
800	0.0
900	0.0
1000	0.0

* T O T A L *

DEPTH	NE
100	0.0
200	1.17349E+04
300	1.54659E+05
400	4.84791E+05
500	6.72813E+05
600	5.98321E+05
700	4.16856E+05
800	2.50887E+05
900	1.37334E+05
1000	6.98536E+04

Continuation of Table 6.2.

Output of the program MC006.

INFORMATION ABOUT THE TOTAL NUMBER OF
ELECTRONS AT SEA LEVEL

AVERAGE = 6.98557E+04
STANDARD DEVIATION = 9.84871E+04
AVERAGE OF LOG (N E) = 4.5455
STANDARD DEVIATION OF LOG(N E) = 0.5113

LOG (NUMBER OF ELECTRON)	FREQUENCY
2.80 -- 2.90	0.
2.90 -- 3.00	0.
3.00 -- 3.10	0.
3.10 -- 3.20	0.
3.20 -- 3.30	0.
3.30 -- 3.40	1.
3.40 -- 3.50	2.
3.50 -- 3.60	9.
3.60 -- 3.70	25.
3.70 -- 3.80	35.
3.80 -- 3.90	39.
3.90 -- 4.00	51.
4.00 -- 4.10	42.
4.10 -- 4.20	74.
4.20 -- 4.30	67.
4.30 -- 4.40	70.
4.40 -- 4.50	61.
4.50 -- 4.60	76.
4.60 -- 4.70	76.
4.70 -- 4.80	52.
4.80 -- 4.90	62.
4.90 -- 5.00	52.
5.00 -- 5.10	60.
5.10 -- 5.20	32.
5.20 -- 5.30	32.
5.30 -- 5.40	28.
5.40 -- 5.50	20.
5.50 -- 5.60	12.
5.60 -- 5.70	14.
5.70 -- 5.80	5.
5.80 -- 5.90	2.
5.90 -- 6.00	1.
6.00 -- 6.10	0.
6.10 -- 6.20	0.
6.20 -- 6.30	0.
6.30 -- 6.40	0.
LESS THAN 2.80000 =	0
GREATER THAN 6.40000 =	0

Continuation of Table 6.2.

Output of the program MC006.

INITIAL ENERGY =1.0E+15 EV
NUMBER OF TRIALS = 1000

INTERACTION NUMBER 1

DEPTH ($g\ cm^{-2}$)	NE (*total number of electrons*)
100	1.53655E+03
200	3.53743E+04
300	2.13784E+05
400	4.98561E+05
500	5.77210E+05
600	4.32794E+05
700	2.48829E+05
800	1.19260E+05
900	5.02879E+04
1000	1.93281E+04

INTERACTION NUMBER 2

DEPTH	NE
100	2.16726E+02
200	7.04348E+03
300	5.55144E+04
400	1.66489E+05
500	2.50101E+05
600	2.40258E+05
700	1.74068E+05
800	1.03671E+05
900	5.30359E+04
1000	2.42071E+04

INTERACTION NUMBER 3

DEPTH	NE
100	2.68235E+01
200	1.34256E+03
300	1.36205E+04
400	5.13152E+04
500	9.77876E+04
600	1.16921E+05
700	1.01547E+05
800	7.03306E+04
900	4.11908E+04
1000	2.10163E+04

Table 6.3: Output of the program MC007 for proton of initial energy 10^{15} eV.

(to be continued).

INTERACTION NUMBER 4

DEPTH	NE
100	3.33563E+00
200	2.61464E+02
300	3.21977E+03
400	1.46612E+04
500	3.41056E+04
600	4.93268E+04
700	5.14817E+04
800	4.27119E+04
900	2.94619E+04
1000	1.71809E+04

INTERACTION NUMBER 5

DEPTH	NE
100	1.53330E-01
200	4.51513E+01
300	7.40111E+02
400	4.15603E+03
500	1.14116E+04
600	1.91607E+04
700	2.33360E+04
800	2.25273E+04
900	1.77018E+04
1000	1.17048E+04

INTERACTION NUMBER 6

DEPTH	NE
100	4.08551E-02
200	1.04847E+01
300	1.90378E+02
400	1.17845E+03
500	3.59878E+03
600	6.91945E+03
700	9.67019E+03
800	1.06565E+04
900	9.67394E+03
1000	7.28989E+03

Continuation of Table 6.3.

Output of the program MC007.

INTERACTION NUMBER 7

DEPTH	NE
100	1.47723E-02
200	2.74734E+00
300	3.76764E+01
400	2.74787E+02
500	1.10023E+03
600	2.46367E+03
700	3.78705E+03
800	4.59143E+03
900	4.66359E+03
1000	4.00264E+03

INTERACTION NUMBER 8

DEPTH	NE
100	0.0
200	1.18112E+00
300	1.12583E+01
400	6.96926E+01
500	3.09612E+02
600	8.04719E+02
700	1.41287E+03
800	1.89332E+03
900	2.10644E+03
1000	1.99544E+03

INTERACTION NUMBER 9

DEPTH	NE
100	0.0
200	1.70999E-01
300	2.46769E+00
400	1.63930E+01
500	7.64702E+01
600	2.32332E+02
700	4.90907E+02
800	7.67583E+02
900	9.46669E+02
1000	9.45189E+02

Continuation of Table 6.3.

Output of the program MC007.

INTERACTION NUMBER 10

DEPTH	NE
100	0.0
200	3.18241E-02
300	7.60502E-01
400	4.77721E+00
500	2.01045E+01
600	6.67987E+01
700	1.59285E+02
800	2.73812E+02
900	3.80983E+02
1000	4.23095E+02

INTERACTION NUMBER 11

DEPTH	NE
100	0.0
200	2.54404E-03
300	1.69432E-01
400	1.02320E+00
500	4.97303E+00
600	1.88544E+01
700	5.05419E+01
800	9.48195E+01
900	1.41511E+02
1000	1.77557E+02

INTERACTION NUMBER 12

DEPTH	NE
100	0.0
200	0.0
300	5.28506E-02
400	2.75647E-01
500	1.59563E+00
600	5.59184E+00
700	1.50923E+01
800	3.11067E+01
900	5.13746E+01
1000	6.80329E+01

Continuation of Table 6.3.

Output of the program MC007.

INTERACTION NUMBER 13

DEPTH	NE
100	0.0
200	0.0
300	0.0
400	2.86644E-02
500	2.46350E-01
600	1.47500E+00
700	4.89894E+00
800	9.97919E+00
900	1.71722E+01
1000	2.59542E+01

INTERACTION NUMBER 14

DEPTH	NE
100	0.0
200	0.0
300	0.0
400	3.09217E-03
500	9.18300E-02
600	3.33486E-01
700	1.35954E+00
800	3.40425E+00
900	5.82899E+00
1000	9.11150E+00

INTERACTION NUMBER 15

DEPTH	NE
100	0.0
200	0.0
300	0.0
400	0.0
500	2.98674E-03
600	6.63412E-02
700	4.55091E-01
800	1.18091E+00
900	2.27566E+00
1000	3.46147E+00

Continuation of Table 6.3.

Output of the program MC007.

INTERACTION NUMBER 16

DEPTH	NE
100	0.0
200	0.0
300	0.0
400	0.0
500	0.0
600	6.96416E-03
700	1.11549E-01
800	4.31473E-01
900	8.57805E-01
1000	1.39309E+00

INTERACTION NUMBER 17

DEPTH	NE
100	0.0
200	0.0
300	0.0
400	0.0
500	0.0
600	0.0
700	2.81590E-02
800	1.29674E-01
900	3.09478E-01
1000	5.41584E-01

INTERACTION NUMBER 18

DEPTH	NE
100	0.0
200	0.0
300	0.0
400	0.0
500	0.0
600	0.0
700	9.59808E-03
800	4.42011E-02
900	1.21039E-01
1000	1.84045E-01

Continuation of Table 6.3.

Output of the program MC007.

INTERACTION NUMBER 19

DEPTH	NE
100	0.0
200	0.0
300	0.0
400	0.0
500	0.0
600	0.0
700	3.50601E-03
800	1.03132E-02
900	4.15784E-02
1000	6.03608E-02

* T O T A L *

DEPTH	NE
100	1.78365E+03
200	4.40816E+04
300	2.87121E+05
400	7.36728E+05
500	9.75727E+05
600	8.68973E+05
700	6.14854E+05
800	3.76824E+05
900	2.09669E+05
1000	1.08379E+05

Continuation of Table 6.3.

Output of the program MC007.

INFORMATION ABOUT THE TOTAL NUMBER OF
ELECTRONS AT SEA LEVEL

AVERAGE = 1.08389E+05
STANDARD DEVIATION = 1.39399E+05
AVERAGE OF LOG (N E) = 4.7853
STANDARD DEVIATION OF LOG(N E) = 0.4618

LOG (NUMBER OF ELECTRON)	FREQUENCY
3.20 -- 3.30	0.
3.30 -- 3.40	0.
3.40 -- 3.50	0.
3.50 -- 3.60	0.
3.60 -- 3.70	0.
3.70 -- 3.80	0.
3.80 -- 3.90	6.
3.90 -- 4.00	16.
4.00 -- 4.10	36.
4.10 -- 4.20	51.
4.20 -- 4.30	57.
4.30 -- 4.40	52.
4.40 -- 4.50	83.
4.50 -- 4.60	70.
4.60 -- 4.70	81.
4.70 -- 4.80	77.
4.80 -- 4.90	85.
4.90 -- 5.00	57.
5.00 -- 5.10	70.
5.10 -- 5.20	55.
5.20 -- 5.30	62.
5.30 -- 5.40	35.
5.40 -- 5.50	32.
5.50 -- 5.60	28.
5.60 -- 5.70	18.
5.70 -- 5.80	13.
5.80 -- 5.90	11.
5.90 -- 6.00	2.
6.00 -- 6.10	3.
6.10 -- 6.20	0.
6.20 -- 6.30	0.
6.30 -- 6.40	0.
LESS THAN 3.20000 =	0
GREATER THAN 6.40000 =	0

Continuation of Table 6.3.

Output of the program MC007.

Primary energy eV	Average number of electrons at depth 1000 g cm^{-2}			The standard deviation of number of electrons at depth 1000 g cm^{-2}		
	π^oproduction from N-N collisions only	π^oproduction from $\pi^{\pm}$-N collisions only	All pionic production	π^oproduction from N-N collisions only	π^oproduction from $\pi^{\pm}$-N collisions only	All pionic production
10^{12}	7.043×10^{0}	1.260×10^{0}	8.304×10^{0}	2.705×10^{1}	1.138×10^{1}	3.782×10^{1}
10^{13}	1.261×10^{2}	8.567×10^{1}	2.118×10^{2}	2.322×10^{2}	2.338×10^{2}	4.624×10^{2}
10^{14}	2.358×10^{3}	3.370×10^{3}	5.728×10^{3}	3.597×10^{3}	6.830×10^{3}	1.039×10^{4}
10^{15}	3.853×10^{4}	6.985×10^{4}	1.084×10^{5}	4.126×10^{4}	9.849×10^{4}	1.394×10^{5}
10^{16}	6.044×10^{5}	1.185×10^{6}	1.790×10^{6}	4.781×10^{5}	1.310×10^{6}	1.782×10^{6}
10^{17}	9.077×10^{6}	1.832×10^{7}	2.739×10^{7}	5.247×10^{6}	1.630×10^{7}	2.146×10^{7}
10^{18}	1.267×10^{8}	2.613×10^{8}	3.880×10^{8}	5.237×10^{7}	1.894×10^{8}	2.403×10^{8}
10^{19}	1.640×10^{9}	3.514×10^{9}	5.154×10^{9}	4.659×10^{8}	2.064×10^{9}	2.504×10^{9}

Table 6.4: Summary of the outputs of the simulation programs MC004, MC006, and MC007.

Primary energy eV	Number of electrons at atmospheric depth of 1000 g cm^{-2}.		
	Average	Standard diviation	Root mean square
10^{12}	8.304×10^{0}	3.782×10^{1}	3.872×10^{1}
10^{13}	2.118×10^{2}	4.624×10^{2}	5.086×10^{2}
10^{14}	5.728×10^{3}	1.039×10^{4}	1.186×10^{4}
10^{15}	1.084×10^{5}	1.394×10^{5}	1.766×10^{5}
10^{16}	1.790×10^{6}	1.782×10^{6}	2.526×10^{6}
10^{17}	2.739×10^{7}	2.146×10^{7}	3.480×10^{7}
10^{18}	3.880×10^{8}	2.403×10^{8}	4.564×10^{8}
10^{19}	5.154×10^{9}	2.504×10^{9}	5.730×10^{9}

Table 6.5: The number of electrons at sea level and the standard diviation about the mean as calculated by simulation program MC007. The root mean square of the number of electrons at sea level was calculated from the average and the standard diviation for each primary energy.

Primary energy eV	Average number of electrons at depth 1000 gcm^{-2}	Depth of the maximum number of electrons	Number of electron at maximum
10^{12}	8.304×10^{0}	310	3.90×10^{2}
10^{13}	2.118×10^{2}	400	5.55×10^{3}
10^{14}	5.728×10^{3}	450	8.075×10^{4}
10^{15}	1.084×10^{5}	510	9.78×10^{5}
10^{16}	1.790×10^{6}	560	1.08×10^{7}
10^{17}	2.739×10^{7}	610	1.136×10^{8}
10^{18}	3.880×10^{8}	660	1.16×10^{9}
10^{19}	5.154×10^{9}	710	1.17×10^{10}

Table 6.6: The depth, in g cm^{-2}, of at which the number of electrons reach its maximum in the shower which represent the average behaviour of 1000 simulated showers, produced by the program MC007, and the maximum number of electrons at its maximum listed verses the primary energy and the simulated average number of electrons at sea level.

```
      1      CC  RG001
      2            REAL X
      3            INTEGER I
      4            DO 20 I=1,100
      5            X=G05CAF(X)
      6            WRITE(6,100)X
      7      100   FORMAT (F10.8)
      8      20    CONTINUE
      9            STOP
     10            END
```

```
0.79512399    0.22571719    0.37128025    0.22503501    0.87874478
0.04747330    0.18057132    0.43276554    0.03937023    0.57517058
0.95461273    0.62410277    0.63906831    0.68812144    0.20123965
0.88100594    0.34761631    0.49382067    0.30296952    0.10393000
0.78215247    0.87325287    0.08894348    0.05381407    0.03852082
0.02283794    0.40198863    0.62099230    0.89889300    0.42640996
0.87381119    0.95602226    0.23532397    0.62174314    0.63967115
0.44518042    0.86360115    0.12909335    0.47076118    0.87470543
0.60452759    0.46288848    0.48874527    0.42788202    0.13241076
0.11525756    0.60729104    0.00040439    0.02413317    0.71116203
0.82230616    0.62145132    0.92967409    0.43797737    0.48854434
0.53852296    0.03520143    0.36260426    0.56486058    0.38974392
0.61825085    0.41639310    0.96600115    0.00548277    0.71524531
0.45024961    0.41041726    0.36066073    0.51637822    0.16893232
0.98773694    0.65360135    0.51127499    0.28519839    0.58734363
0.84596372    0.04819425    0.04164308    0.19871217    0.20004016
0.86738992    0.03606553    0.66518325    0.04450495    0.30642903
0.62989277    0.18406785    0.88330603    0.27235836    0.07343459
0.04282685    0.86847538    0.75122631    0.51183146    0.77449095
0.03295543    0.54483920    0.39316416    0.20417696    0.06683731
```

Figure 6.1: List of the program RG001. The numbers shown are the sample of 100 random numbers generated by the program.

```
1     CCCCCCCCCCCCCCCCCCCCCCCCCCCCCCCCCCCCCCCCCCCCCCCCCCCCCCCCCCCCCC
2     C                                                               C
3     C        DST02                                                  C
4     C     This  program  generate " N "  random                     C
5     C   number uniformally distributed bettween                     C
6     C   0 & 1 . *NAG library  function is used.                     C
7     C   The " N " random number are distributed                     C
8     C   and both histogram and frequency  table                     C
9     C   are  optained .                                            C
10    C                                                               C
11    CCCCCCCCCCCCCCCCCCCCCCCCCCCCCCCCCCCCCCCCCCCCCCCCCCCCCCCCCCCCCC
12          DIMENSION F(50),RF(50)
13          DO 20 I=1,50
14      20  F(I)=0.0
15    CCCCCCC SET THESE TO SUIT DATA
16          N=10000
17          AMIN=0.0
18             K=10
19          AMAX=1.0
20          W= (AMAX - AMIN) / K
21    CCCCCCCCCCCCCCCCCCCCCCCCCCCCCCCCCC
22          KSAT=0
23          BIG=0.0
24    CCCCCCCC
25          DO 300 JJ=1,N
26          X = G05CAF(X)
27          IF(X .GT. AMAX) BIG=BIG+1.
28          IF(X .GT. AMAX)  GOTO 300
29          IF(X .EQ. AMAX) F(N)=F(N)+1
30          IF(X .EQ. AMAX) GOTO 300
31           I = ( X - AMIN ) / W  + 1
32           F(I)= F(I)+ 1
33    CCCCCCCCCCCCCCCCCCCCCCCC
34     300  CONTINUE
35    CCCCCCCCCCCCCCCCCCCCCCCC
36          DO 305 I=1,K
37          RF(I)=F(I)/N
38     305  CONTINUE
39    CCCCCCCCCCCCCCCCCCCCCCCC
40          WRITE (6,310)
41     310  FORMAT(45H INTERVAL        FREQUENCY       RELATIVE FREQ.)
42          DO 350 I=1,K
43          C = (I-1)*W
44          D = C+W
45          WRITE (6,340)C,D,F(I),RF(I)
46     340  FORMAT( F4.2,3H---,F4.2,4X,F5.0,12X,F8.6)
47     350  CONTINUE
48          WRITE(6,380)N
49     380  FORMAT(6H TOTAL,I6)
50           WRITE(6,392)BIG
51     392   FORMAT(18H GREATER THAN MAX=,F4.0)
52    CCCCCCCCCCCCCCC  CCCCC CCCCCCCCCCCCCCCCCCCCCCCCCCCCCC
53          XX=AMAX*0.55
54          CALL PAPER(1)
55          CALL PSPACE(0.1181,0.9055,0.1181,0.9055)
56          CALL MAP(0.0,AMAX,0.0,0.5)
57          CALL BORDER
58          CALL HISTGM(0.0,0.0,W,RF,1,K)
59          CALL PLOTCS(XX,.45,'TOTAL OF',8)
60          CALL PLOTNI(XX+.3,.45,N)
61          CALL SCALES
62          CALL GREND
63    CCCCCCCCCCCCCCCCCCCCCCCCCCCCCCCCCCCCCCCCCCCCCCCCCCCCCCCCCCCCCC
64          STOP
65          END
```

Figure 6.2: List of Program DST02.

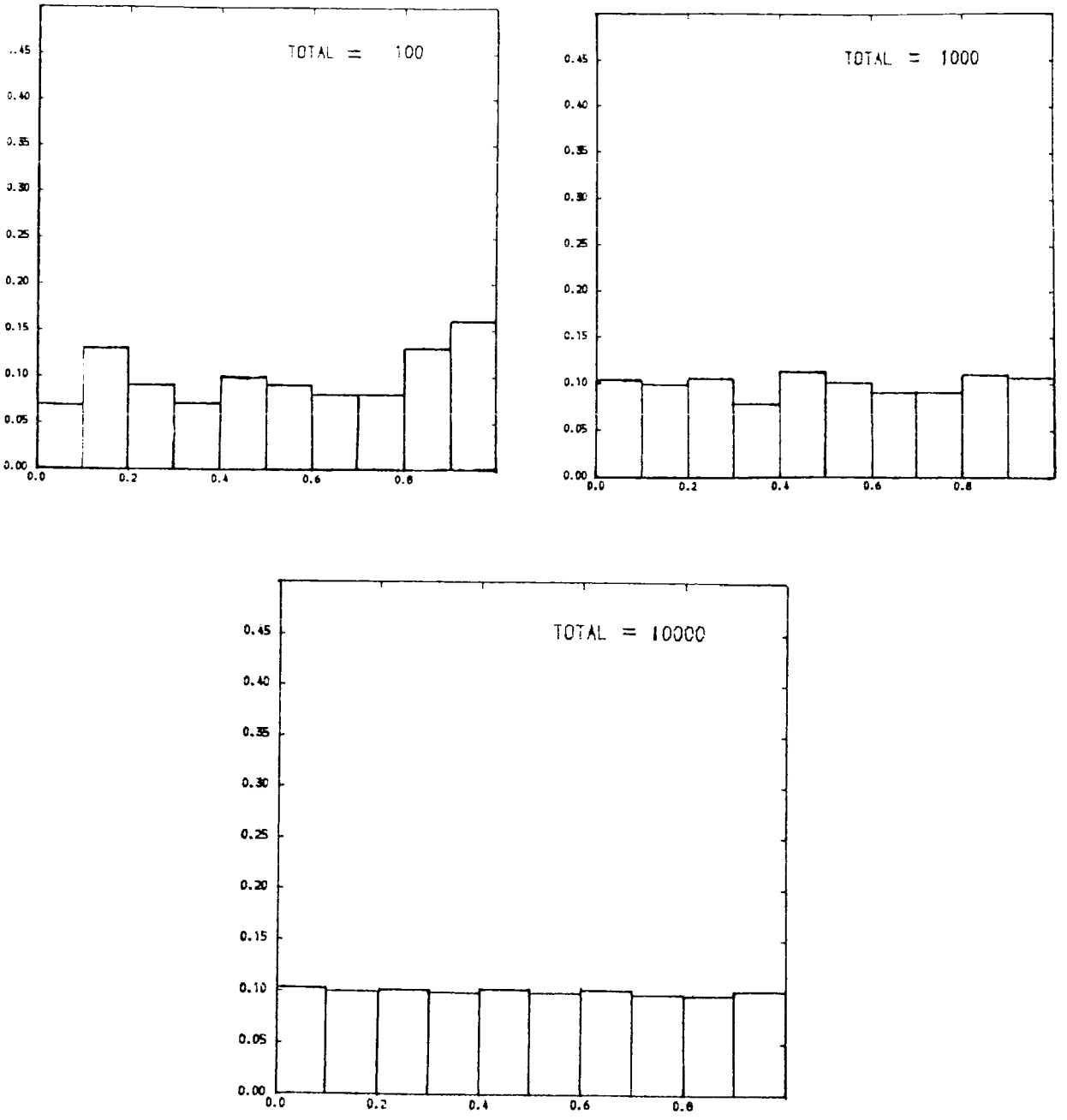

Figure 6.3: Three outputs of the program DS02. Each of them is a distribution of a sample of random numbers. The abscissa is the value of the random number, and the ordinate is the relative frequency of it. The size of the sample for each is written on the top right of each plot.

```
      CCCCCCCCCCCCCCCCCCCCCCCCCCCCCCCCCCCCCCCCCCCCCCCCCCCCCCCCCCCCCCCC
      C        DST03                                                  C
      C                                                               C
      C   This program generates " N "  random numbers using *NAG    C
      C  subroutine. Random number x takes values from 0-1 uniformally C
      C  distributed. This destribution is changed to exponential dis- C
      C  tribution  (  P(>X) = EXP (-X/80) )  by operating the inverse C
      C  function (i.e. X = -Log(x/80) ).                             C
      C                                                               C
      C                                                               C
      CCCCCCCCCCCCCCCCCCCCCCCCCCCCCCCCCCCCCCCCCCCCCCCCCCCCCCCCCCCCCCCC
            DIMENSION F(50),RF(50),FI(50),XZ(50),X9(101),Y9(101)
            DO 20 I=1,50
        20  F(I)=0.0
      CXXXX  N is the number of trailes, it could be changed
                  N=100
                  AMIN=0.0
      CXXXXX  K is the number of intervals
                  K = 20
                  KPLUS1 = K+1
            AMAX = 200.
            W= (AMAX - AMIN) / K
      CCCCCCCCCCCCCCCCCCCCCCCCCCCCCCCC
            KSAT = 0
            BIG  = 0.0
      CCCCCCCC
            DO 300 JJ=1,N
            X = G05CAF(X)
            X =-80. * ALOG(X)
            IF(X .GT. AMAX) BIG=BIG+1.
            IF(X .GT. AMAX)  GOTO 300
            IF(X .EQ. AMAX) F(N)=F(N)+1
            IF(X .EQ. AMAX) GOTO 300
             I = ( X - AMIN ) / W  + 1
             F(I)= F(I)+ 1
      CCCCCCCCCCCCCCCCCCCCCCCCCC
       300  CONTINUE
      CCCCCCCCCCCCCCCCCCCCCCCCCC
            FI(K+1)=BIG
            DO 304 J=1,K
            I=(K+1)-J
            FI(I) = FI(I+1) + F(I)
       304  CONTINUE
      CCCCCCCCCCCCCCCCCCCCCCCCCC
            DO 305 I=1,KPLUS1
            RF(I)=FI(I)/N
       305  CONTINUE
      CCCCCCCCCCCCCCCCCCCCCCCCCC
            WRITE (6,310)
       310  FORMAT(45H   X              FREQUENCY       RELATIVE FREQ.)
            DO 350 I=1,K
            C = (I-1)*W
            XZ(I)= C
            WRITE (6,340)C,FI(I),RF(I)
       340  FORMAT( F10.4,6X,F7.0,10X,F8.6)
       350  CONTINUE
             BIG1=BIG/N
             WRITE(6,340)AMAX,BIG,BIG1
      CCCCCCCCCCCCCCCCCCCCCCCCCCCCCCCCCCCCCCCCCCCCCCCCCCCCCCCCCCCCCCCC
            XX=AMAX*0.55
            DX=AMAX*0.90
            CALL PAPER(1)
            CALL PSPACE(0.1181,0.9055,0.1181,0.9055)
            CALL MAP(0.0,AMAX,0.0,1.0)
            CALL BORDER
            CALL CTRSET(4)
            CALL PTPLOT(XZ,RF,1,K,54)
            CALL CTRSET(1)
            CALL THICK(2)
            CALL PLOTCS(XX,.90,'TOTAL = ',8)
            CALL PLOTNI(DX,.90,N)
            CALL SCALES
            CALL THICK(1)
               DO 400 I=1,101
               X9(I)=((I-1) * AMAX ) / 100.0
               Y9(I)= EXP(-X9(I)/80.0)
       400     CONTINUE
            CALL CURVEO(X9,Y9,1,101)
            CALL GREND
      CCCCCCCCCCCCCCCCCCCCCCCCCCCCCCCCCCCCCCCCCCCCCCCCCCCCCCCCCCCCCCCC
             STOP
             END
```

Figure 6.4: List of Program DST03.

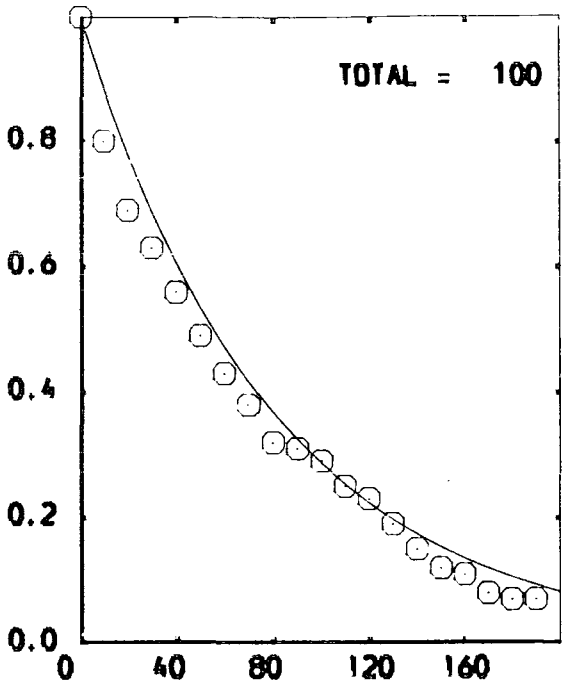

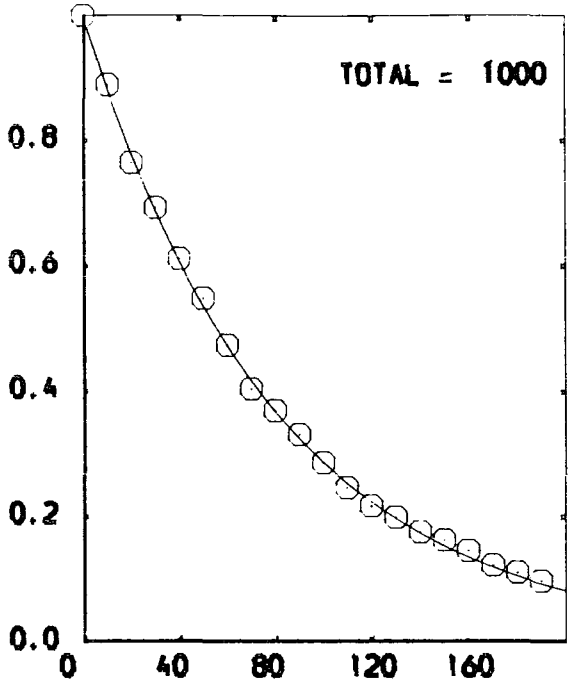

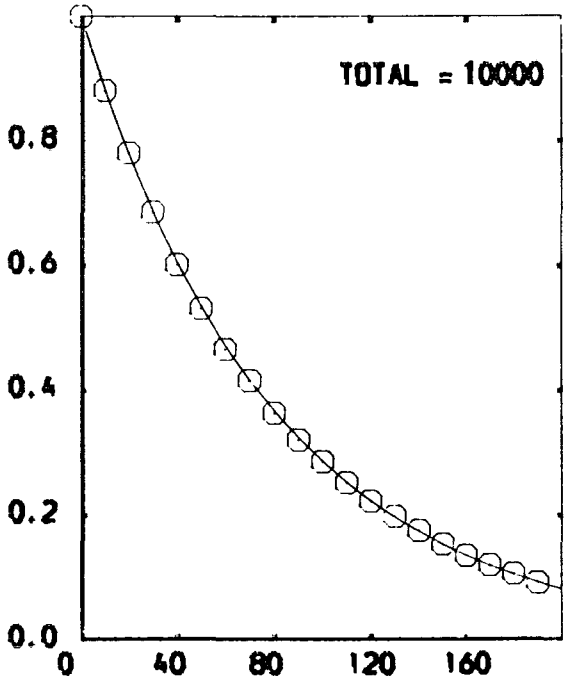

Figure 6.5

Three outputs of the program DS03. Each of them is an integral distribution of a sample of random numbers exponentialy distributed with the mean of 80. The abscissa is the value of the random number, and the ordinate is the integral relative frequency of it. The size of the sample for each is written on the top right of each plot.

Figure 6.6: List of the program MC001.

```
1     CCCCCCCCCCCCCCCCCCCCCCCCCCCCCCCCCCCCCCCCCCCCCCCCCCCCCCCCCCCCCCCC
2     C                    PROGRAM MC001                               C
3     C                                                                C
4     C  This program samples the number of interactions               C
5     C  made by high energy nucleon traversing the                    C
6     C  atmosphere assuming mean path is 80 gm / cm**2                C
7     C  The sample frequancy distribution is compared                 C
8     C  with expected Poisson distribution . *GHOST and               C
9     C  *NAG   FORTRAN library were used .                            C
10    C                                                                C
11    CCCCCCCCCCCCCCCCCCCCCCCCCCCCCCCCCCCCCCCCCCCCCCCCCCCCCCCCCCCCCCCC
12          DIMENSION F(27),RF(27),FTH(26),X2(26)
13          SUM=0.
14          SSQ=0.
15          DO 10 I=1,27
16          F(I)=0.0
17    10    CONTINUE
18    CCCCCCCCCCCCCCCCCCCCCCCCCCCCCCCCCCCCCCCCCCCCCCCCCCCCCCCCCCCCCCCC
19          M=1000
20          DO 50 I=1,M
21          N=0.0
22          YT=0.0
23    20    X=G05CAF(X)
24          Y=-80. * ALOG(X)
25          YT=YT+Y
26          IF ( YT .GE. 1030.) GOTO 25
27          N=N+1
28          GOTO 20
29    25    IF (N .GT. 25) F(27)=F(27)+1
30          IF (N .GE. 25) GOTO 30
31          J=N+1
32          F(J)=F(J)+1
33    30    SUM=SUM + N
34          SSQ=SSQ+(N*N)
35    50    CONTINUE
36    CCCCCCCCCCCCCCCCCCCCCCCCCCCCCCCCCCCCCCCCCCCCCCCCCCCCCCCCCCCCCCCC
37          FTH(1)=EXP(-12.875)
38          FCTR=1.
39          DO 60 I=1,25
40          FCTR =FCTR * I
41          FTH(I+1)=FTH(1) * 12.875**I /FCTR
42    60    CONTINUE
43    CCCCCCCCCCCCCCCCCCCCCCCCCCCCCCCCCCCCCCCCCCCCCCCCCCCCCCCCCCCCCCCC
44          AVE=SUM / M
45          SDV= SSQ/M - AVE*AVE
46          SDV=SQRT(SDV)
47    CCCCCCCCCCCCCCCCCCCCCCCCCCCCCCCCCCCCCCCCCCCCCCCCCCCCCCCCCCCCCCCCC
48          DO 65 I=1,27
49          RF(I)=F(I)/M
50     65   CONTINUE
51    CCCCCCCCCCCCCCCCCCCCCCCCCCCCCCCCCCCCCCCCCCCCCCCCCCCCCCCCCCCCCCCCC
```

```
52            WRITE (7,70)
53       70   FORMAT(53H   X      FREQUENCY     RELATIVE FREQ.    THE
     O. FREQ.)
54            DO 75  I=1,26
55            J=I-1
56            WRITE (7,73 )J,F(I),RF(I),FTH(I)
57       73   FORMAT( I3,4X,F7.0,10X,E11.5,7X,E11.5)
58       75   CONTINUE
59            WRITE (7,77)F(27)
60       77   FORMAT(3H>25,4X,F7.0)
61            WRITE(7,78)AVE
62       78   FORMAT(10HAVERAGE = ,F9.5)
63            WRITE(7,79)SDV
64       79   FORMAT(21HSTANDARD DEVIATION = ,F9.5)
65      CCCCCCCCCCCCCCCCCCCCCCCCCCCCCCCCCCCCCCCCCCCCCCCCCCCCCCCCCCC
66            CALL PAPER(1)
67            CALL PSPACE(.2,.9,.2,.9)
68            CALL MAP(0.0,28.,0.0,.14)
69            CALL BORDER
70            CALL MASK(0.0,28.0,0.0,0.003 )
71            CALL AXES
72            CALL UNMASK(0)
73            DO 80 I=1,26
74            X2(I)=I-1
75       80   CONTINUE
76            CALL CURVEO(X2,FTH,1,25)
77            DO 85 I=1,26
78            CALL POSITN(X2(I),RF(I))
79            CALL JOIN(X2(I),0.0)
80       85   CONTINUE
81            CALL PLOTCS(5.,-.015,'NUMBER OF INTERACTIONS',22)
82            CALL CTRMAG(10)
83            CALL PLOTCS(18.,.13,'NO. OF TRIAL =  ',16)
84            CALL TYPENI(M)
85            CALL PLOTCS(18.,.125,'AVE.   =  ',8)
86            CALL TYPENF(AVE,4)
87            CALL CTRMAG(15)
88            CALL CTRSET(4)
89            CALL PLOTCS(18.,.12,'S  ',3)
90            CALL CTRMAG(10)
91            CALL TYPECS('= ',2)
92            CALL TYPENF(SDV,4)
93            CALL CTRSET(1)
94            CALL CTRMAG(20)
95            CALL CTRORI(1.)
96            CALL PLOTCS(-3.,0.02,'RELATIVE FREQUENCY',18)
97            CALL GREND
98       CCCCCCCCCCCCCCCCCC
99            STOP
100           END
```

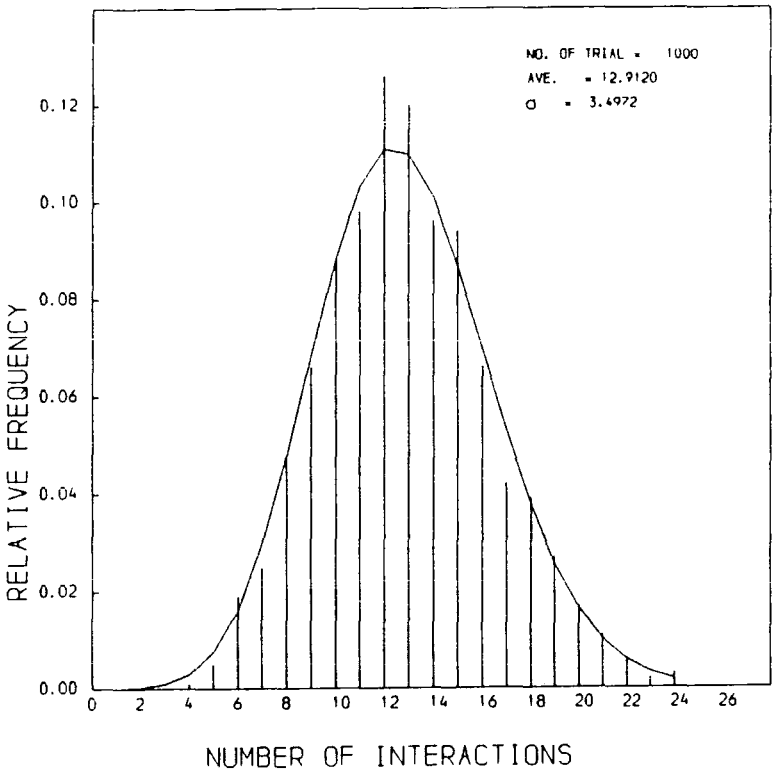

Figure 6.7: The graphical output of the program MC001, (bars). It shows the frequency distribution of the number of interactions which a cosmic ray proton with mean free path of 80 g cm^{-2}, undergoes before it reaches the sea-level. The simulation done for 1000 protons. The solid curve is the expected Poisson distribution.

Figure 6.8 : List of MC004.

```
CCCCCCCCCCCCCCCCCCCCCCCCCCCCCCCCCCCCCCCCCCCCCCCCCCCCCCCCCCCCCCC
C                                                  01.04.86        C
C NAME: MC004                                                      C
C                                                                  C
C Simulation of the average number of electrons arriving C
C at different atmospheric depths produced by pi-zero     C
C meson production only as a primary nucleon propagates  C
C through the atmosphere assuming,                        C
C L(N) = 80 g/cm**2                                       C
C K(N)= 0.5                                               C
C n(s)= 3*E**(1/4)                                        C
C with E in GeV .                                         C
C                                                         C
CCCCCCCCCCCCCCCCCCCCCCCCCCCCCCCCCCCCCCCCCCCCCCCCCCCCCCCCCCCCCCC
C
      DIMENSION T(100),A(100,40),XG(100),FREQ(40),SL(1000)
      COMMON NTRIAL , ENERGY
      ENERGY = 1.0E+12
      NTRIAL = 1000
      CALL GR1
      JMAX=((ALOG10(ENERGY)-ALOG10(2.0E+9))/ALOG10(2.))+1
      DO 5 I=1,100
      T ( I ) = 0.0
      DO 5 J=1,JMAX
 5    A ( I , J ) = 0.0
      ISMSL=0
      IBGSL=0
      SUM=0.0
      SSQ=0.0
      SUMLG=0.0
      SSQLG=0.0
      DO 7 I=1,40
7      FREQ(I) = 0
C*****
      DO 40 NEV=1,NTRIAL
      Y = 0
      J = 0
      E = ENERGY
      SL(NEV)=0.0
C**
 10   Z=G05CAF(Z)
      Z=-80 * ALOG(Z)
      Y=Y+Z
      J=J+1
          IF (J .GT. JMAX  )    GOTO 40
          IF (Y .GE. 1000.0) GOTO 40
      FPI0 = (E/1.E9)**0.25
      EPI0 = .17 * (E/1.E9)**0.75 *1.E9
      FG   = 2.0 * FPI0
      EG   = 0.5 * EPI0
```

```
      DO 35 I=1,100
      X = I * 10.0
      TX = X -Y
      IF (TX .LE. 0.0) GOTO 35
      AX = ANUM(EG,TX) * FG
      A(I,J) = A(I,J) + AX
35    CONTINUE
      SL(NEV) = AX + SL(NEV)
      E = E / 2.
      IF (E .LE. 1.E+9 ) GOTO 40
      GOTO 10
40    CONTINUE
C*****
      DO 50 I=1,100
      DO 50 J=1,JMAX
      A(I,J) = A(I,J) / NTRIAL
50    CONTINUE
C*****
      DO 60 I=1,100
      DO 60 J=1,JMAX
60    T(I) = T(I) + A(I,J)
      CALL GR2(T)
C*****
      DO 66 J=1,JMAX
      DO 65 I=1,100
      XG(I) = A(I,J)
65    CONTINUE
      CALL GR2(XG)
66    CONTINUE
      CALL GREND
C*****
      DO 70 I=1,NTRIAL
      SUM = SUM + SL(I)
      SSQ = SSQ + (SL(I) * SL(I) )
70    CONTINUE
      AVE=SUM / NTRIAL
      SDV=SSQ / NTRIAL - AVE*AVE
      SDV=SQRT(SDV)
C*
      DO 72 I=1,NTRIAL
      SLX = ALOG10(SL(I))
      SUMLG = SUMLG + SLX
      SSQLG = SSQLG + SLX*SLX
72    CONTINUE
      AVELG = SUMLG / NTRIAL
      SDVLG = SSQLG / NTRIAL -AVELG*AVELG
      SDVLG = SQRT(SDVLG)
C*
      WD = .2
      IF (ENERGY .GT. 1.0E13) WD = 0.1
```

```
      IF (ENERGY .GT. 1.0E16) WD = 0.05
      AMIN = INT((AVELG - 2.5*SDVLG)/ WD) * WD
      AMAX = INT((AVELG + 3.7*SDVLG)/ WD) * WD
      NBIN = (( AMAX - AMIN ) / WD ) +0.0001
      DO 74 I=1,NTRIAL
      XSL = ALOG10(SL(I))
      IF (XSL .GT. AMAX) IBGSL=IBGSL+1
      IF (XSL .GT. AMAX) GOTO 74
      IF (XSL .LT. AMIN) ISMSL=ISMSL+1
      IF (XSL .LT. AMIN) GOTO 74
      INDEX=((XSL-AMIN)/ WD )+1
      FREQ(INDEX) =  FREQ(INDEX) + 1
74    CONTINUE
      CALL HISTO(FREQ,NBIN,AMIN,AMAX,WD,AVELG,SDVLG)
C*****
      WRITE(6,75)ENERGY
75    FORMAT(//  ' INTIAL ENERGY =',1PE7.1,3H EV)
      WRITE(6,76)NTRIAL
76    FORMAT(' NUMBER OF TRIALS = ',I4)
      WRITE(6,88)
      DO 80 J=1,JMAX
      WRITE(6,82)J
      WRITE(6,84)
      DO 78 I=10,100,10
      IX = 10 * I
78    WRITE(6,86)IX,A(I,J)
      WRITE(6,88)
80    CONTINUE
82    FORMAT(20H INTERACTION NUMBER ,I3)
84    FORMAT(20H   DEPTH          NE)
86    FORMAT(3X,I4,10X,1PE11.5)
88    FORMAT(30H ------------------------------//)
      WRITE(6,89)
89    FORMAT(20H       * T O T A L *)
      WRITE(6,84)
      DO 90 I=10,100,10
      IX = 10 * I
90    WRITE(6,86)IX,T(I)
      WRITE(6,92)
92    FORMAT(30H ------------------------------////)
C*****
      WRITE(6,105)
      WRITE(6,106)
105   FORMAT (38H INFORMATION ABOUT THE TOTAL NUMBER OF)
106   FORMAT (22H ELECTRON AT SEE LEVEL/)
      WRITE(6,110) AVE
110   FORMAT (11H AVERAGE = ,1PE11.5)
      WRITE(6,112) SDV
112   FORMAT (22H STANDARD DEVIATION = ,1PE11.5)
      WRITE(6,114) AVELG
```

```
      114   FORMAT (23H AVERAGE OF LOG (N E) =,F7.4)
            WRITE(6,116) SDVLG
      116   FORMAT (34H STANDARD DEVIATION OF LOG(N E) = ,F7.4//)
            WRITE(6,120)
      120   FORMAT (42H   LOG ( NUMBER OF ELECTRON )    FREQUENCY/)
            DO 130 I=1,NBIN
            XX1=(I-1)* WD + AMIN
            XX2=XX1 + WD
      130   WRITE(6,131)XX1,XX2, FREQ(I)
      131   FORMAT (5X,F5.2,' -- ',F5.2,13X,F5.0)
            WRITE(6,132)AMIN,ISMSL
      132   FORMAT (1X,14H LESS    THAN ,F8.5,' = ',I6)
            WRITE(6,134)AMAX,IBGSL
      134   FORMAT (1X,14H GREATER THAN ,F8.5,' = ',I6)
      C*****
            CALL TB3(T)
            STOP
            END
      CCCCCCCCCCCCCCCCCCCCCCCCCCCCCCCCCCCCCCCCCCCCCCCCCCCCCCCC
      C1
            FUNCTION ANUM(W,X)
            BETA=ALOG(W/84.2E+6)
            T=X/37.7
            S=3*T/(T+2*BETA)
            ANUM=0.31*EXP(T*(1.-1.5*ALOG(S)))
            ANUM=ANUM/SQRT(BETA)
            RETURN
            END
      C2
            SUBROUTINE GR1
            COMMON NTRIAL , ENERGY
            YU = 7.0
            IF (ENERGY .GT. 1.0E+15) YU = 11.
            CALL PAPER(1)
            CALL PSPACE(0.2,0.75,0.35,0.95)
            CALL MAP(0.0,1100.,-1.,YU)
            CALL BORDER
            CALL CTRMAG(12)
            Y = .95 *YU
            CALL PLOTCS(50.,Y,'NUMBER OF TRIALS = ',19)
            CALL TYPENI(NTRIAL)
            CALL PLOTCS(700.,Y,'ENERGY = 10',11)
            NENG = ALOG10(ENERGY)+.01
            CALL SUPFIX
            CALL TYPENI(NENG)
            CALL CTRMAG(12)
            CALL CTRSET(2)
            CALL PLOTCS(960.,Y, ' E',2)
            CALL CTRSET(1)
            CALL TYPECS('V',1)
```

```
201           CALL SCALSI(100.,1.)
202           CALL CTRMAG(15)
203           Y = -.2833 * YU
204           CALL PLOTCS(300.,Y,'A',1)
205           CALL CTRSET(2)
206           CALL PLOTCS(300.,Y,' TMOSPHERIC DEPTH ( G CM  )',27)
207           CALL CTRMAG(10)
208           Y = -.26667 * YU
209           CALL PLOTCS(900.,Y,'-2',2)
210           CALL CTRMAG(15)
211           CALL CTRORI(1.)
212           Y = .33333 * YU
213           CALL PLOTCS(-100.,Y,' OG N',5)
214           CALL CTRSET(1)
215           CALL PLOTCS(-100.,Y,'L',1)
216           CALL CTRMAG(10)
217           CALL CTRSET(2)
218           CALL PLOTCS(-70.,Y,'    10',8)
219           CALL PLOTCS(-80.,Y,'       E',10)
220           RETURN
221           END
222      C3
223           SUBROUTINE GR2(Z)
224           DIMENSION X(100),Y(100),Z(100)
225           M=1
226           DO 880 I=1,100
227      880  Y(I)=Z(I)
228           DO 900 I=1,100
229           X(I)=I*10.0
230           IF (Y(I) .EQ. 0.0) GOTO 890
231           Y(I)=ALOG10(Y(I))
232           GOTO 900
233      890  M=I+1
234      900  CONTINUE
235            IF (M .GT. 99) GOTO 905
236           CALL CURVEO(X,Y,M,100)
237      905  RETURN
238           END
239      C4
240           SUBROUTINE HISTO(F,N,XMIN,XMAX,WD,AVE,SD)
241           COMMON NTRIAL,ENERGY
242           DIMENSION F(30)
243           XU = XMAX -XMIN
244           YU = 200.
245           CALL PAPER(1)
246           CALL PSPACE(.2,.7,.35,.95)
247           CALL MAP(XMIN,XMAX,0.0,YU)
248           CALL BORDER
249           CALL CTRSET(1)
250           CALL CTRORI(0.0)
```

```
251           CALL CTRMAG(10)
252           CALL SCALSI((2*WD),20.)
253     CC
254           CALL HISTGM(XMIN,0.0,WD,F,1,N)
255           X=XMIN + XU * .2
256           Y=-0.1 * YU
257           CALL CTRMAG(15)
258           CALL CTRSET(2)
259           CALL PLOTCS(X,Y,' OG    UMBER OF  LCTRONS )',26)
260           CALL CTRSET(1)
261           CALL PLOTCS(X,Y,'L   ( N          E          ',26)
262           X = X + XU*0.06
263           Y = Y - YU*0.04
264           CALL CTRMAG(10)
265           CALL PLOTCS(X,Y,'10',2)
266           CALL CTRORI(1.)
267           CALL CTRMAG(15)
268           X=XMIN -XU *.15
269           Y= YU / 3.
270           CALL PLOTCS(X,Y,'FREQUENCY',9)
271           CALL CTRORI(0.0)
272           CALL CTRSET(1)
273           CALL CTRMAG(12)
274           X= XMIN + XU * .1
275           Y= YU * .95
276           CALL PLOTCS(X,Y,'INITIAL ENERGY = 10',19)
277           NG   = ALOG10(ENERGY) + .1
278           CALL SUPFIX
279           CALL TYPENI(NG)
280           CALL SUFFIX
281           CALL CTRSET(2)
282           CALL CTRMAG(12)
283           CALL TYPECS(' E',2)
284           CALL CTRSET(1)
285           CALL TYPECS('V',1)
286           CALL CTRSET(2)
287           X=XMIN + XU * .4
288           Y=YU * .9
289           CALL PLOTCS(X,Y,' UMBER OF  RIALS =',16)
290           CALL CTRSET(1)
291           CALL PLOTCS(X,Y,'N          T       ',18)
292           CALL TYPENI(NTRIAL)
293           Y=YU * .86
294           CALL PLOTCS(X,Y,'M',1)
295           CALL CTRSET(2)
296           CALL TYPECS('EAN =',5)
297           CALL CTRSET(1)
298           CALL TYPENE(AVE,6)
299           CALL CTRSET(4)
300           Y=YU * .82
```

```
      CALL CTRMAG(20)
      CALL PLOTCS(X,Y,' S ',3)
      CALL CTRSET(1)
      CALL CTRMAG(12)
      CALL PLOTCS(X,Y,'      =',6)
      CALL TYPENE(SD,6)
      CALL GREND
      RETURN
      END
C**
      SUBROUTINE TB3(T)
      DIMENSION T(100)
      COMMON NTRIAL,ENERGY
      WRITE(7,605)ENERGY
605   FORMAT('  100                 |  INTIAL ENERGY =',1PE7.1,' EV |')
610   FORMAT(3X,F6.0,10X,1PE11.5)
      DO 615 I=1,100
       X = 10 * I
615   WRITE(7,610) X,T(I)
      RETURN
      END
```

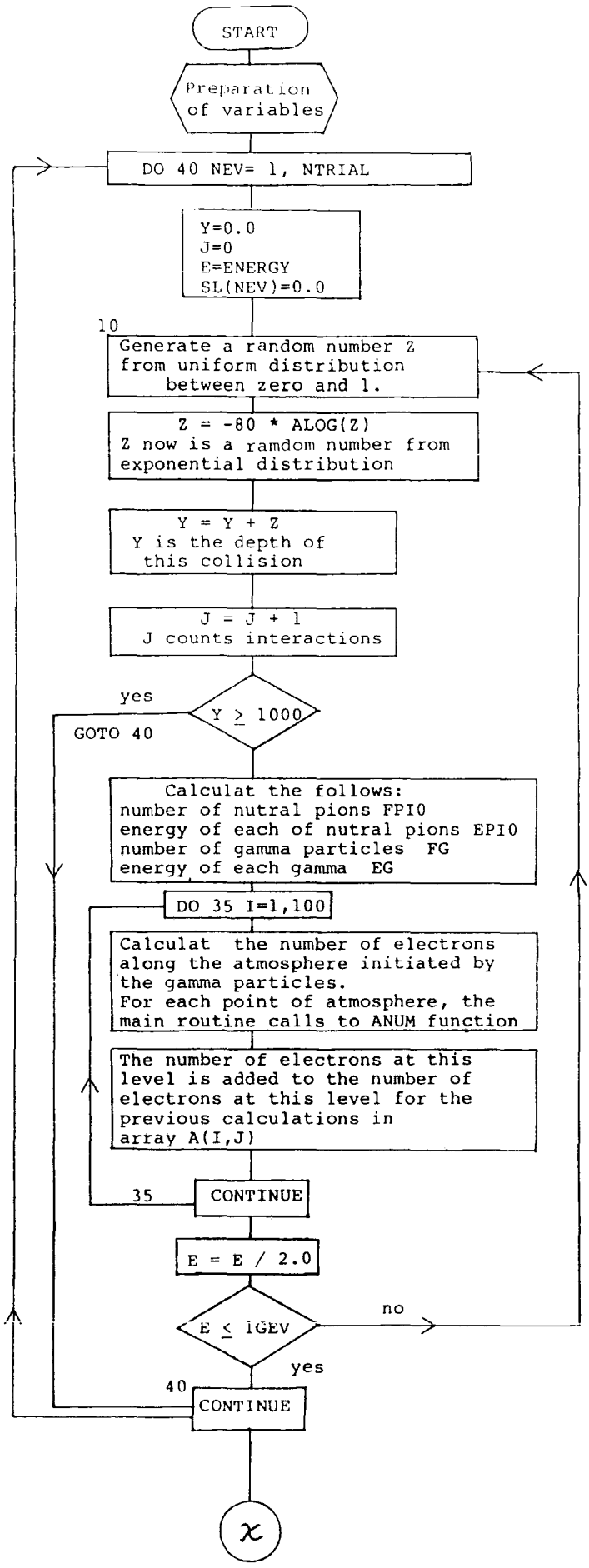

Figure 6.9:

Flowchart of MC004.

FIGURE 6.10

Outputs of Program MC004.

Figures 6.10a.1 to 6.10a.8

Outputs of the program MC004. the simulation of the average number of electrons arriving at different atmospheric depths produced by neutral pion production only as a primary proton propagates through the atmosphere. The upper most curve is the average of the total of the number of electrons in the shower, the other curves are for the average of the electron number contributed by each protonic collision. Each Figure is for a given proton initial energy which is written on the top of the plot.

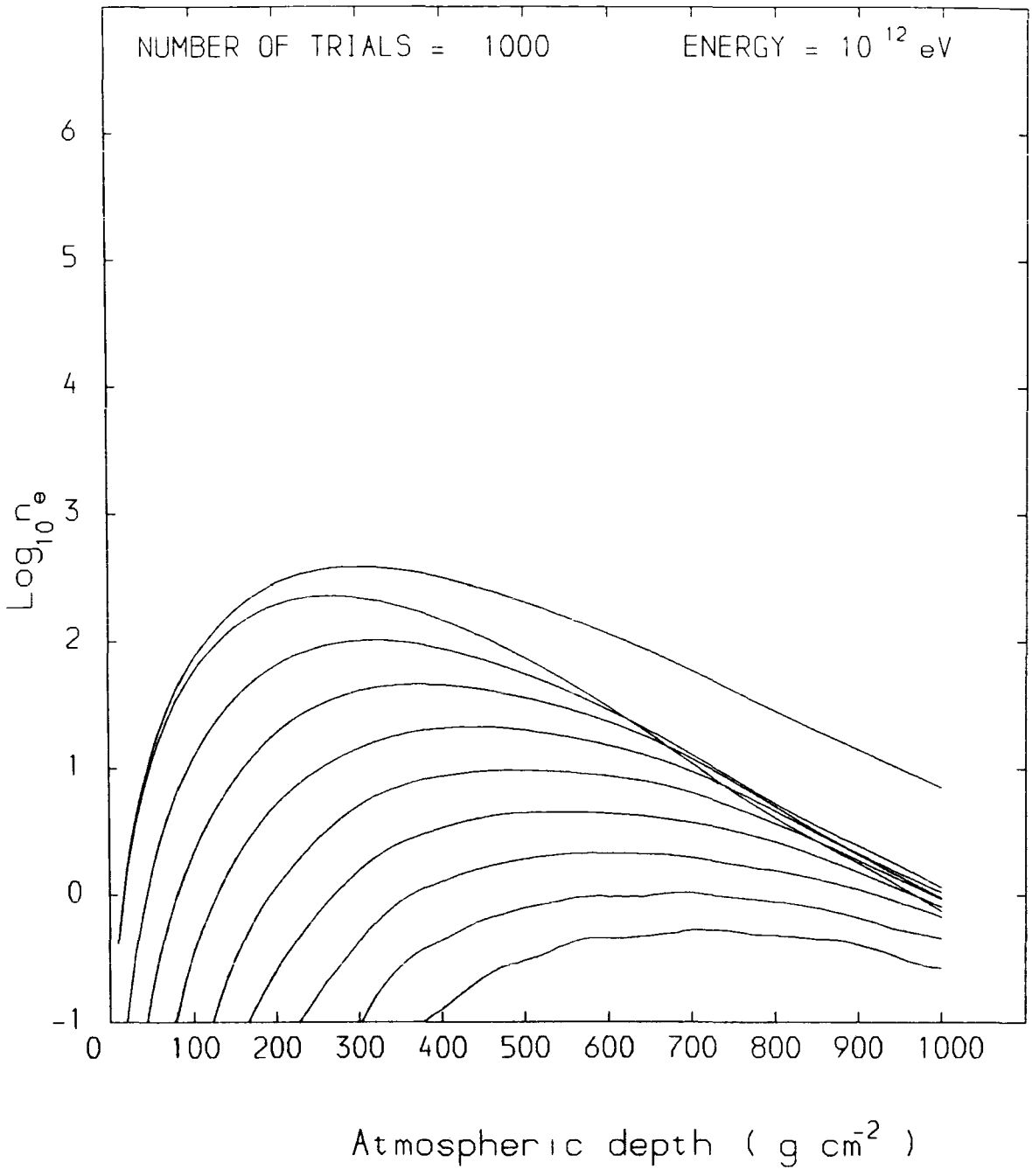

Figure 6.10a.1: See the heading page for caption.

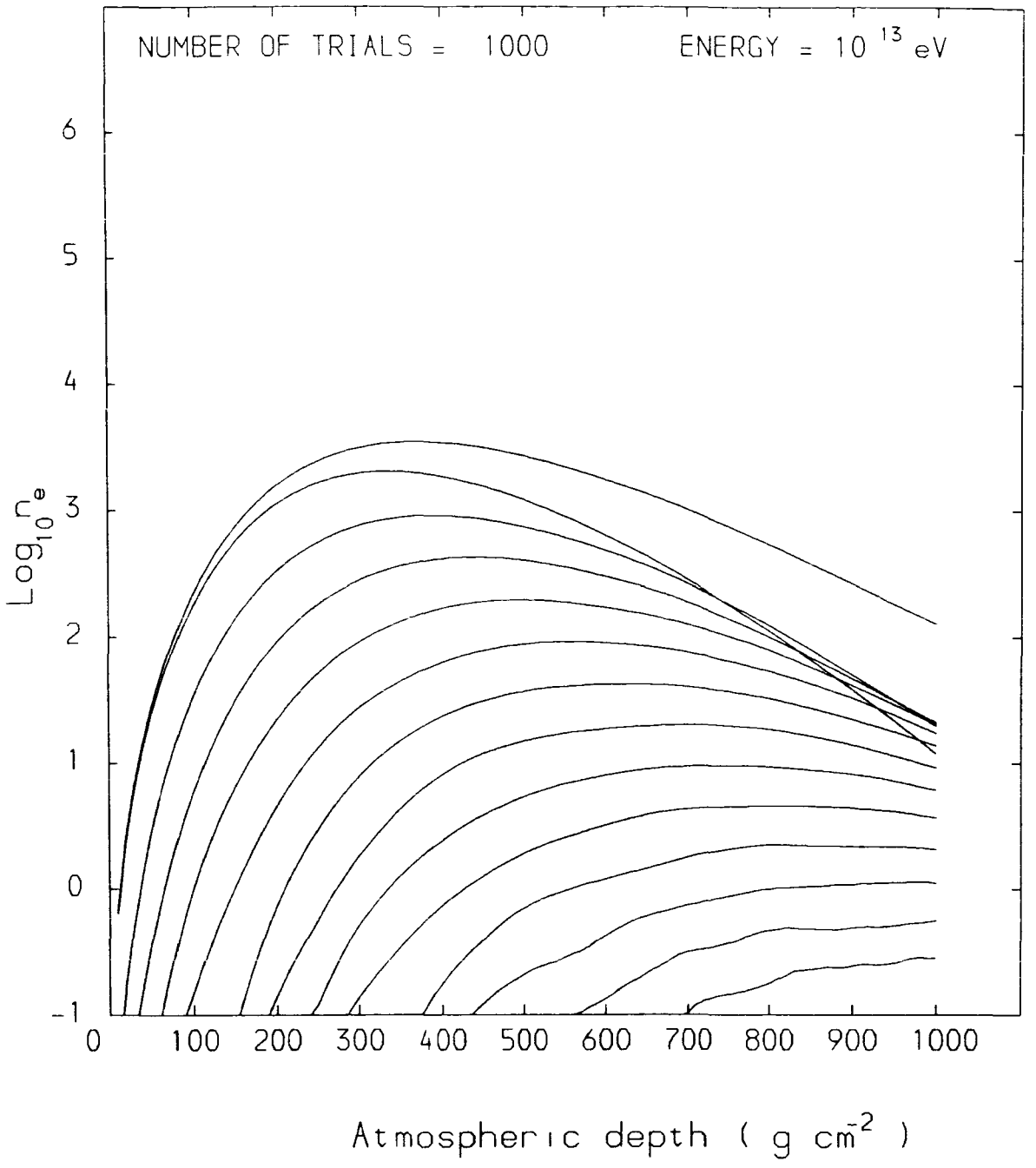

Figure 6.10a.2: See the heading page for caption.

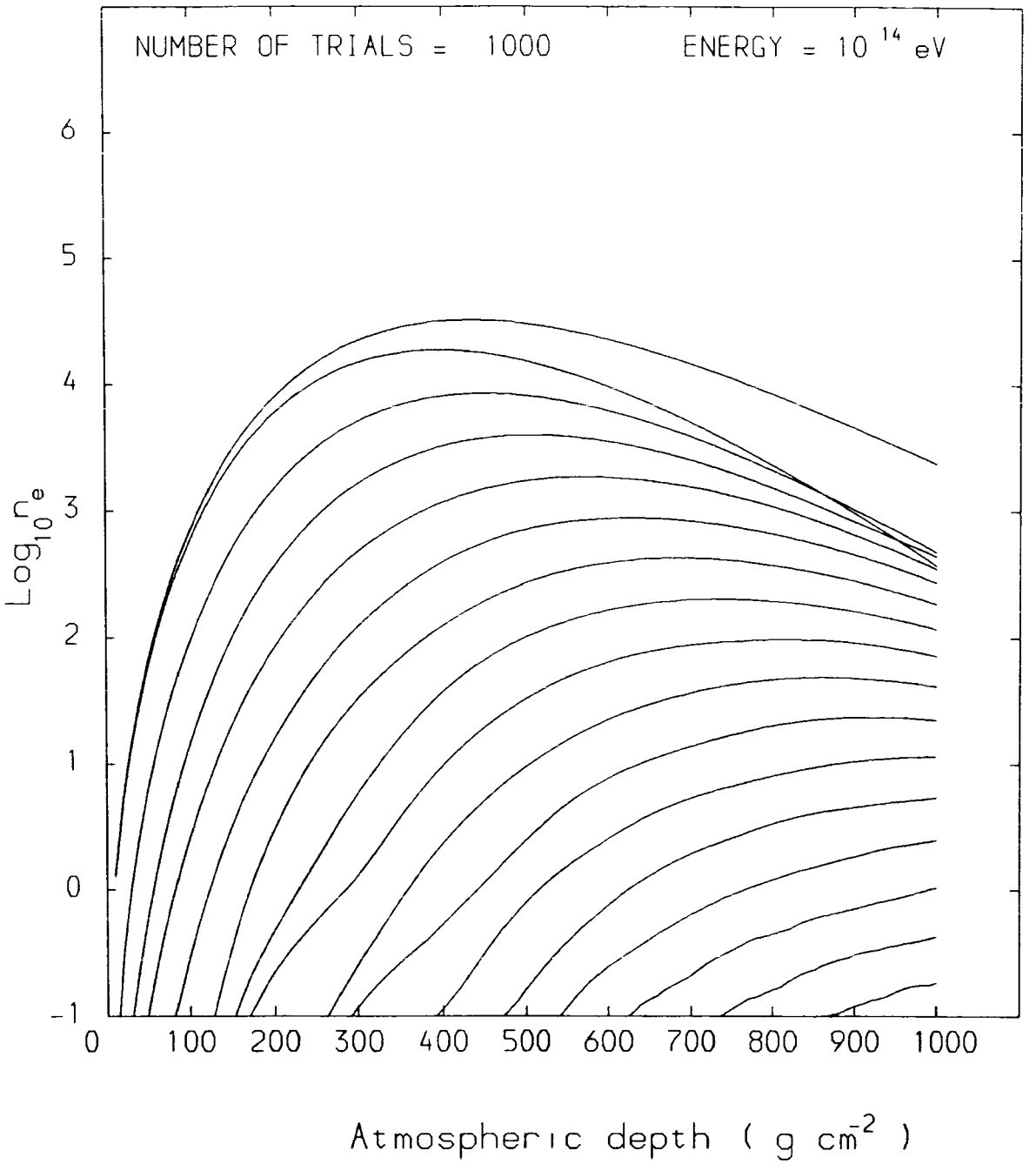

Figure 6.10a.3: See the heading page for caption.

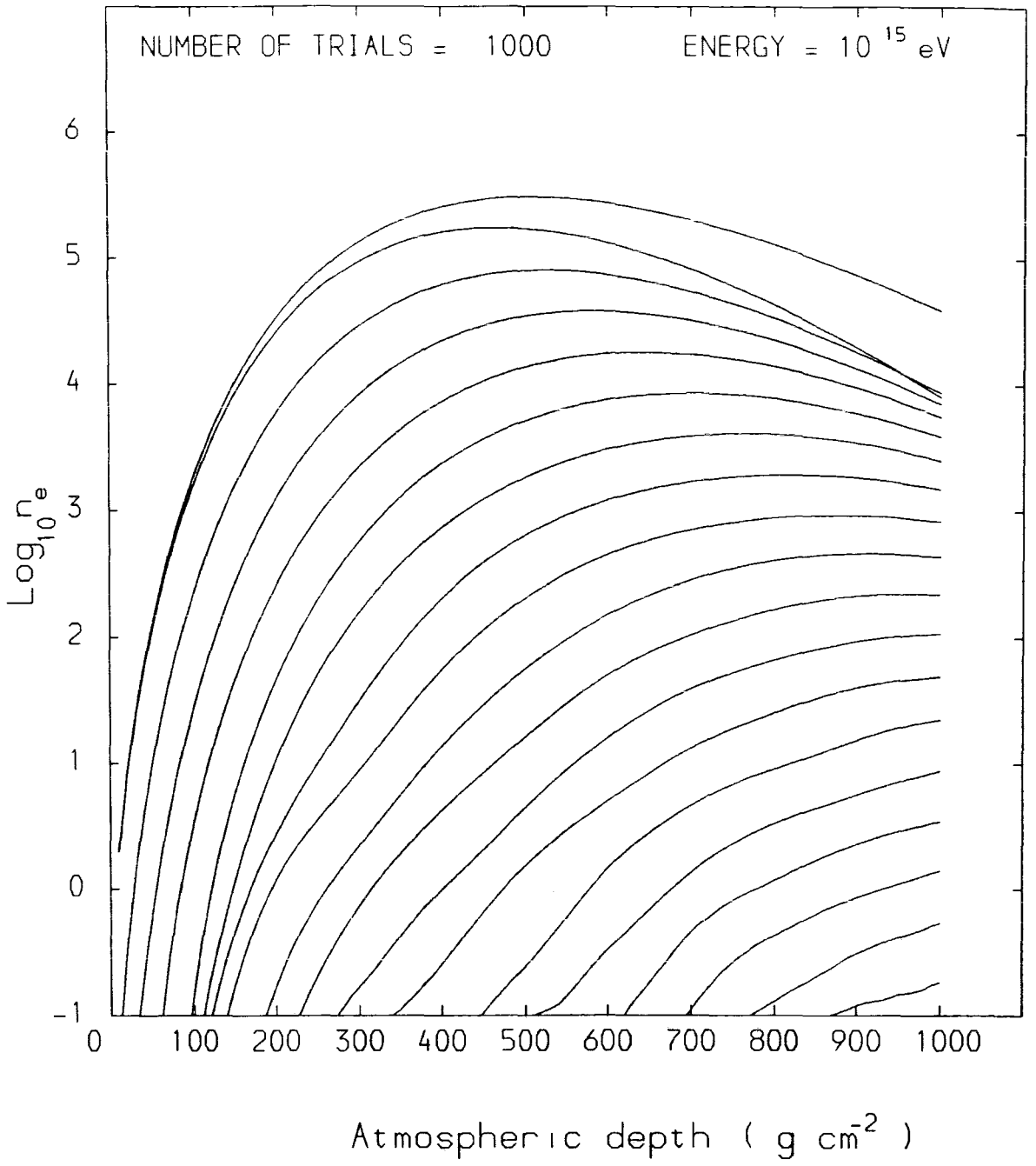

Figure 6.10a.4: See the heading page for caption.

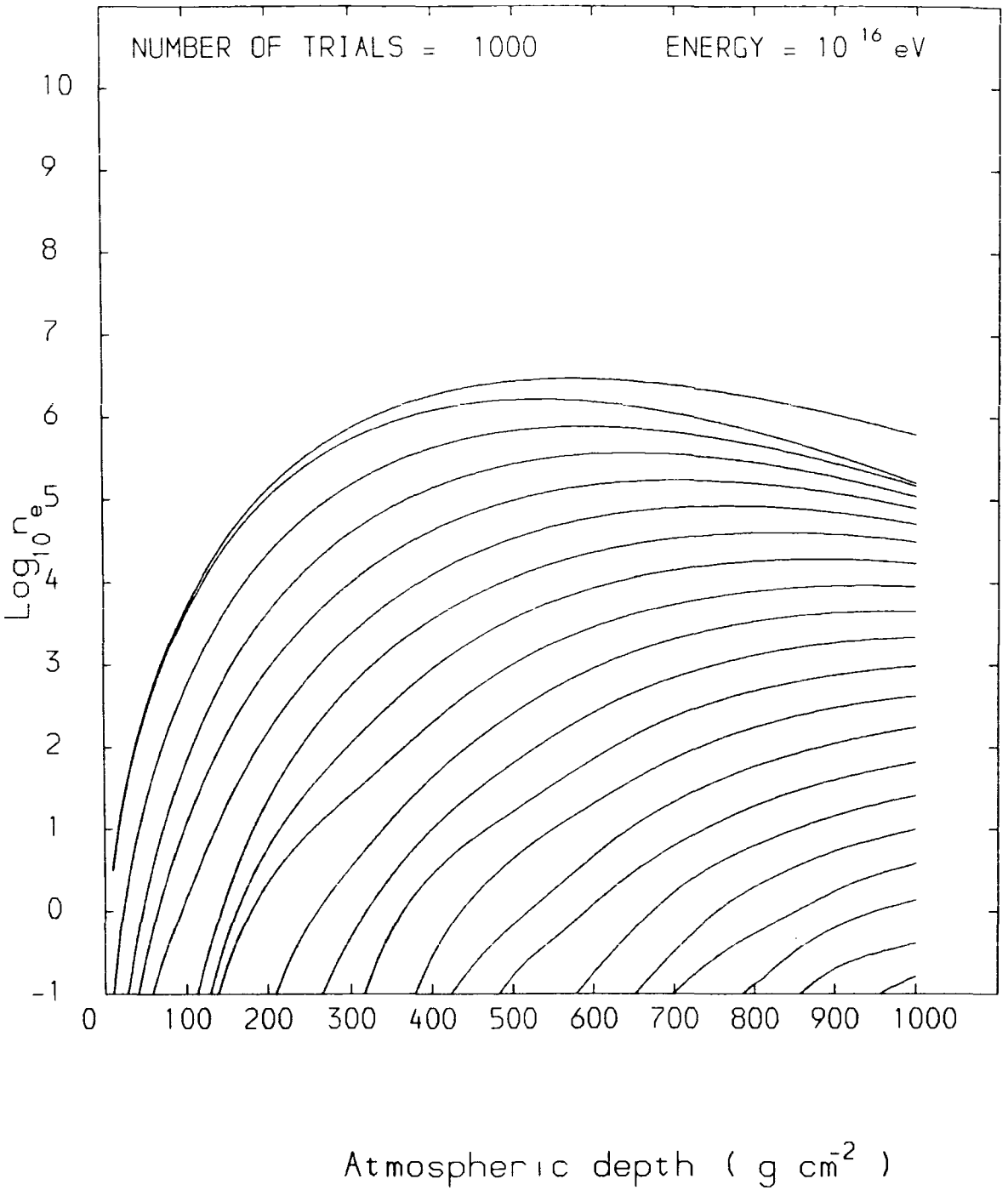

Figure 6.10a.5: See the heading page for caption.

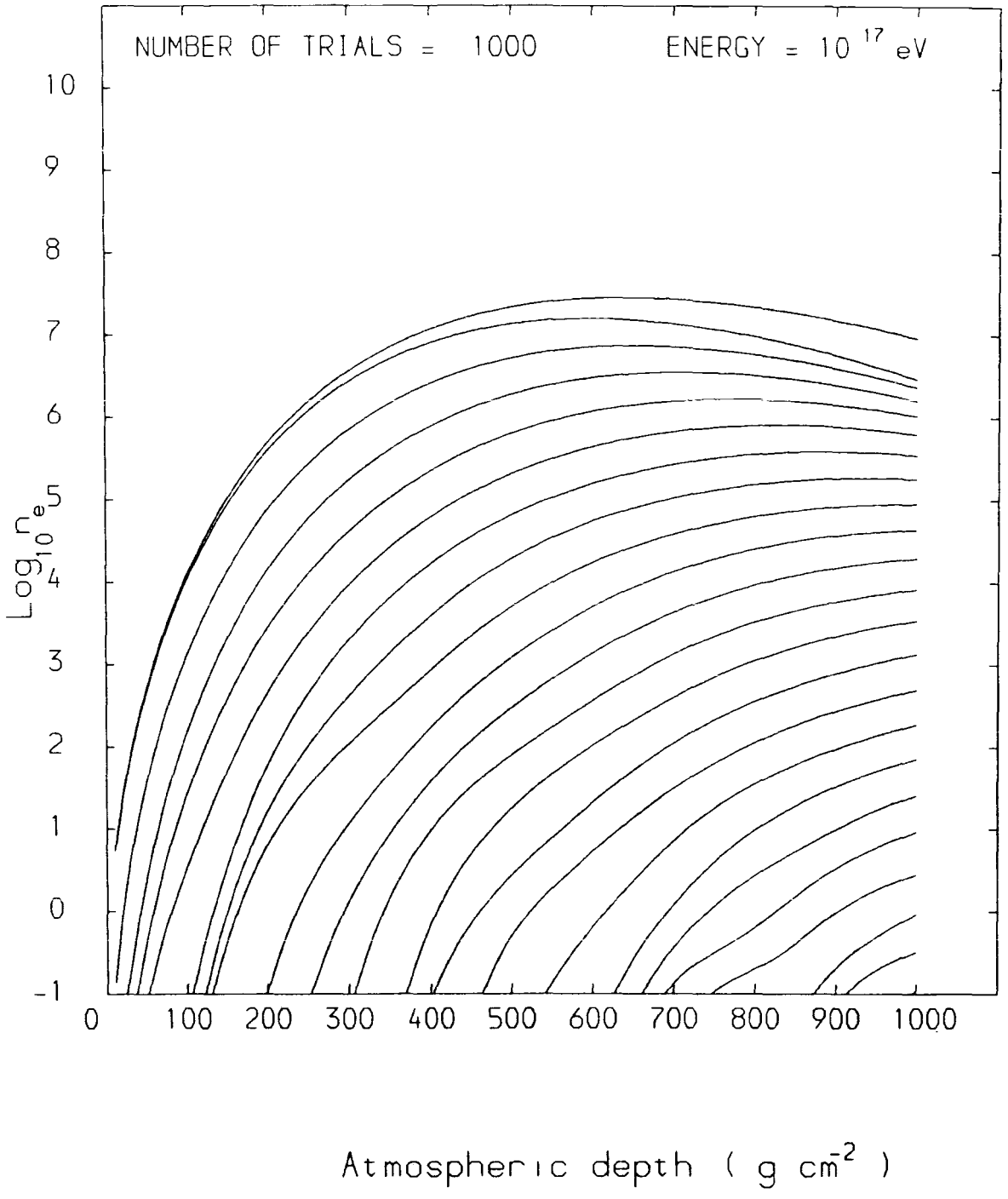

Figure 6.10a.6: See the heading page for caption.

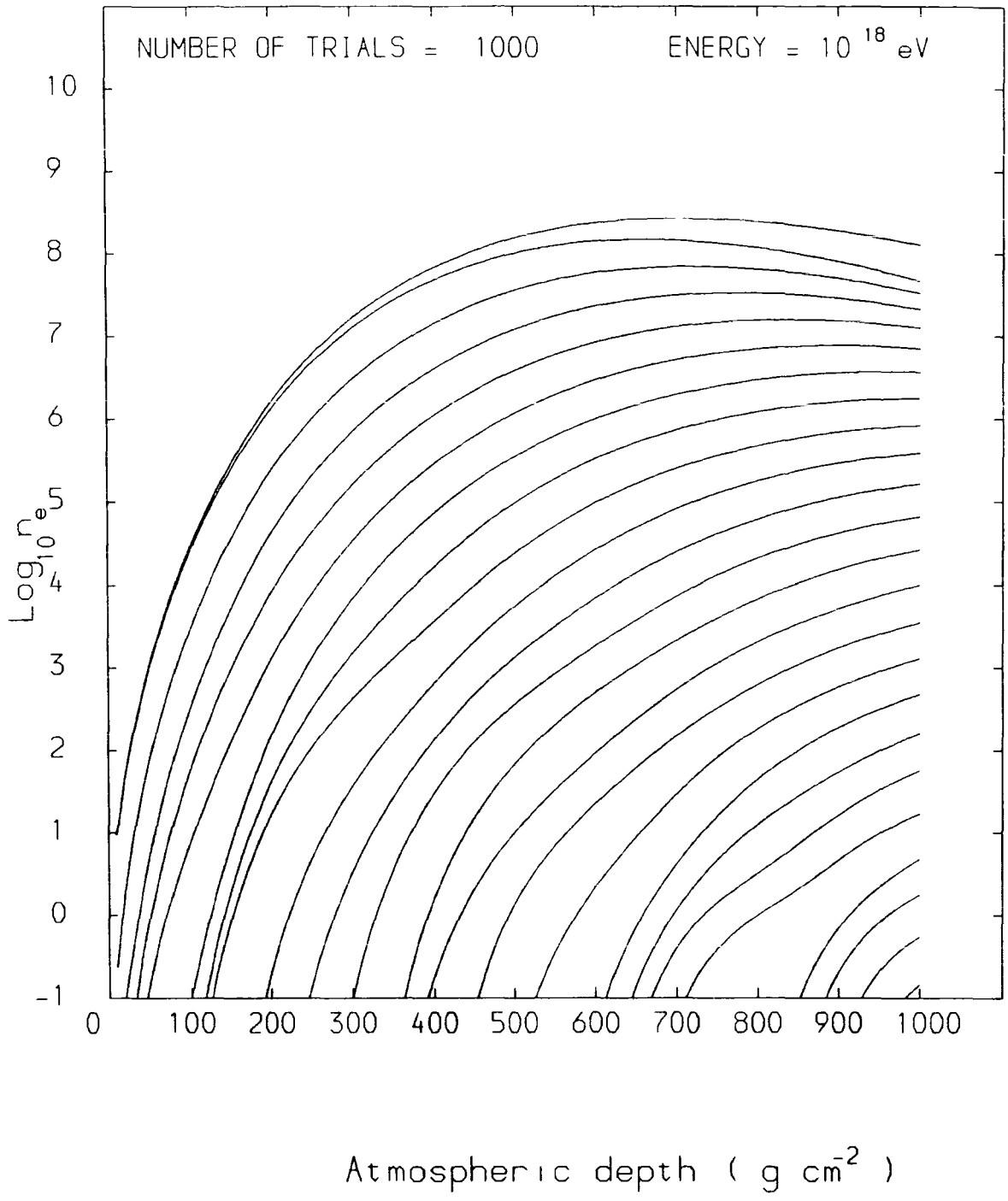

Figure 6.10a.7: See the heading page for caption.

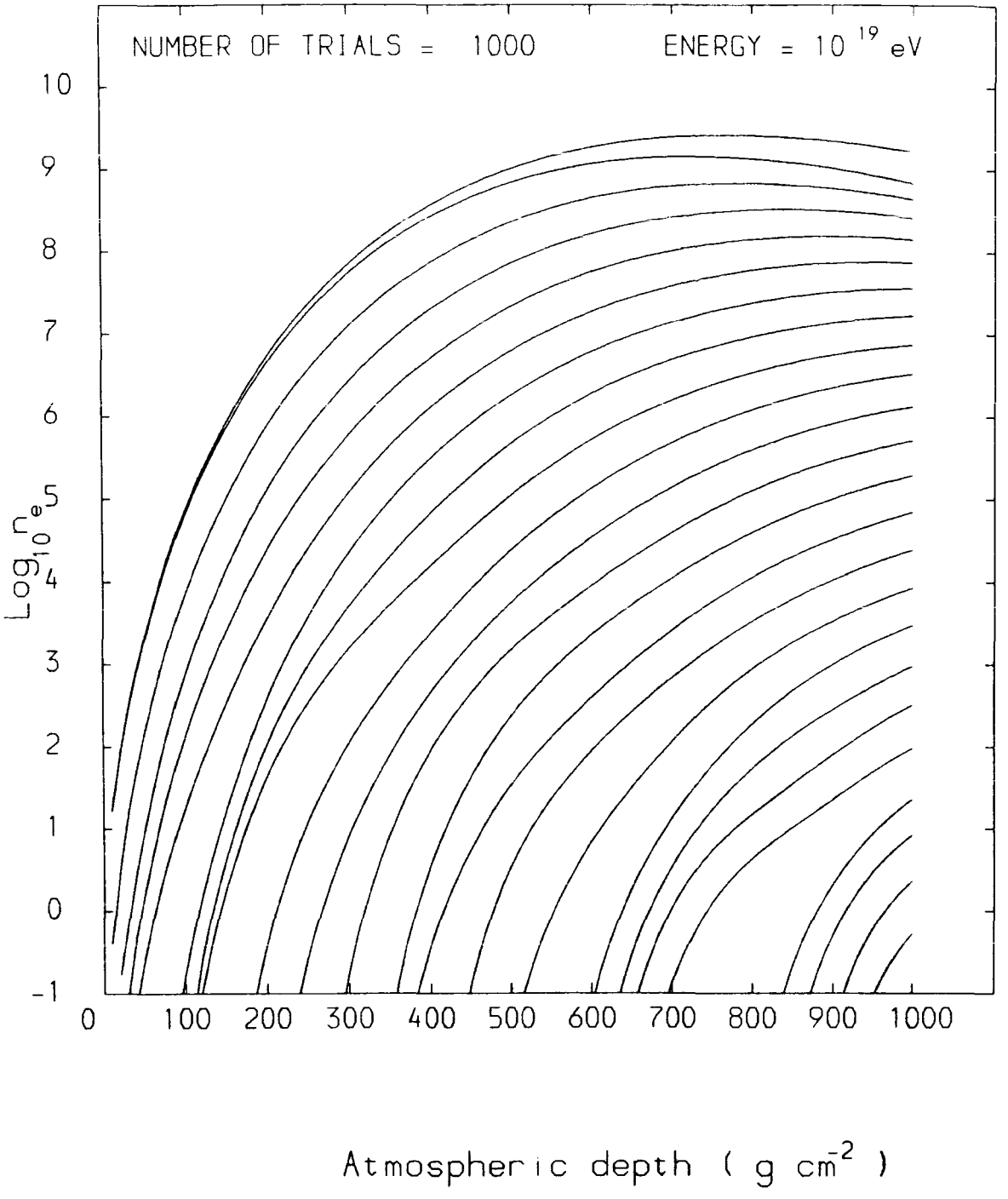

Figure 6.10a.8: See the heading page for caption.

Figures 6.10b.1 to 6.10b.8

The distribution of the $\log_{10}$ of number of electrons at sea-level as it was calculated by the program MC004. Each distribution is for a given proton initial energy which is written on the top of the plot.

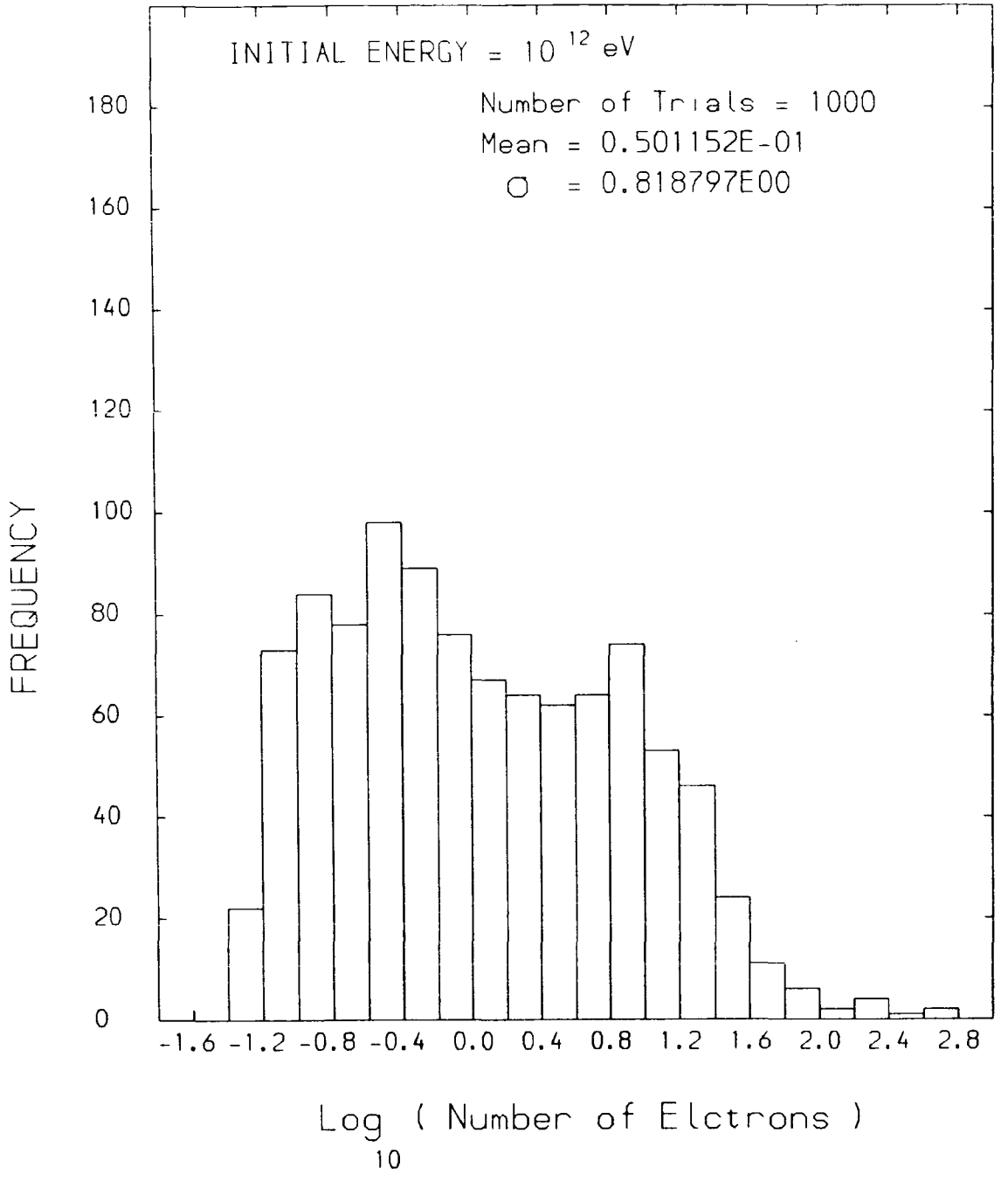

Figure 6.10b.1: See the heading page for caption.

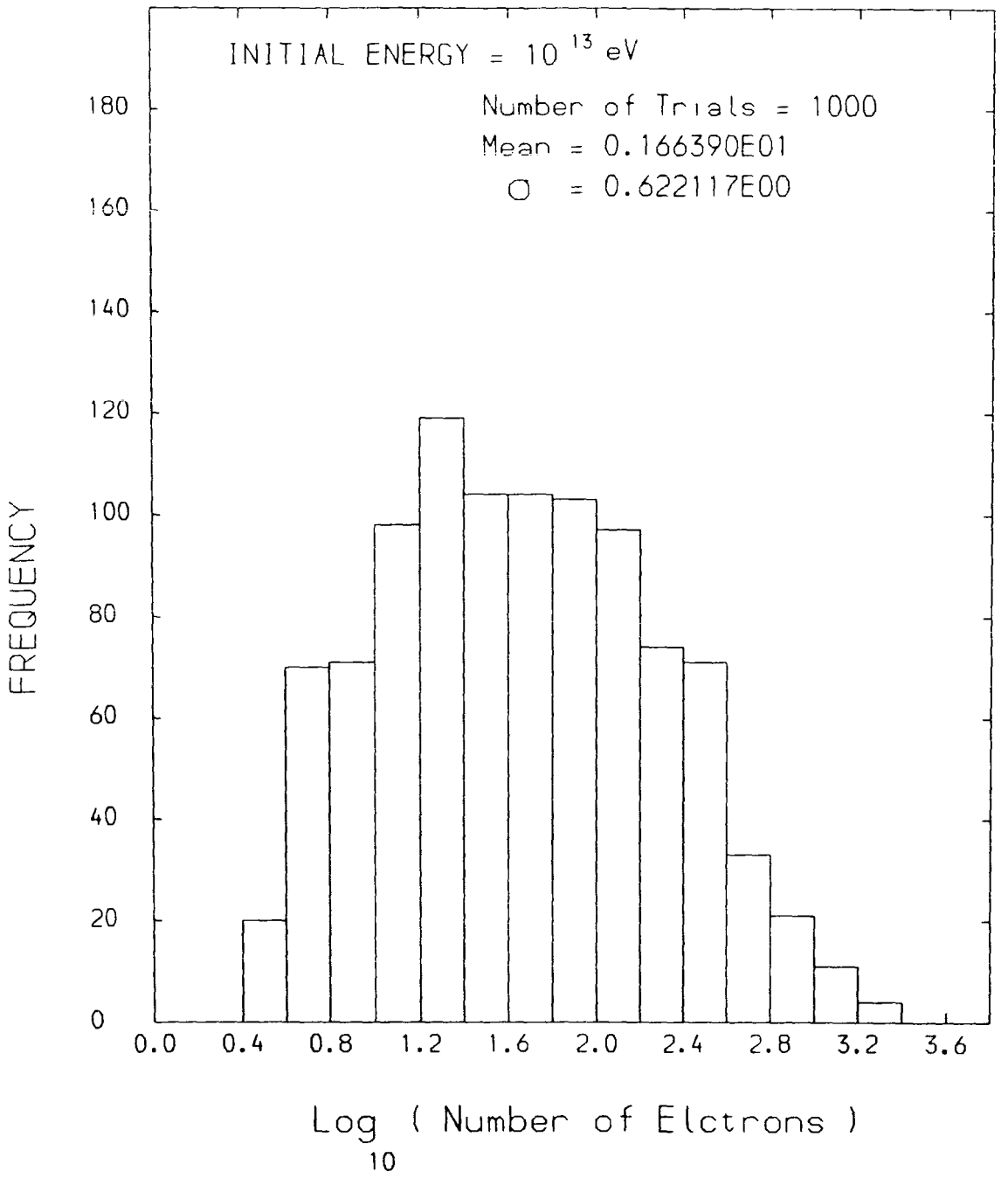

Figure 6.10b.2: See the heading page for caption.

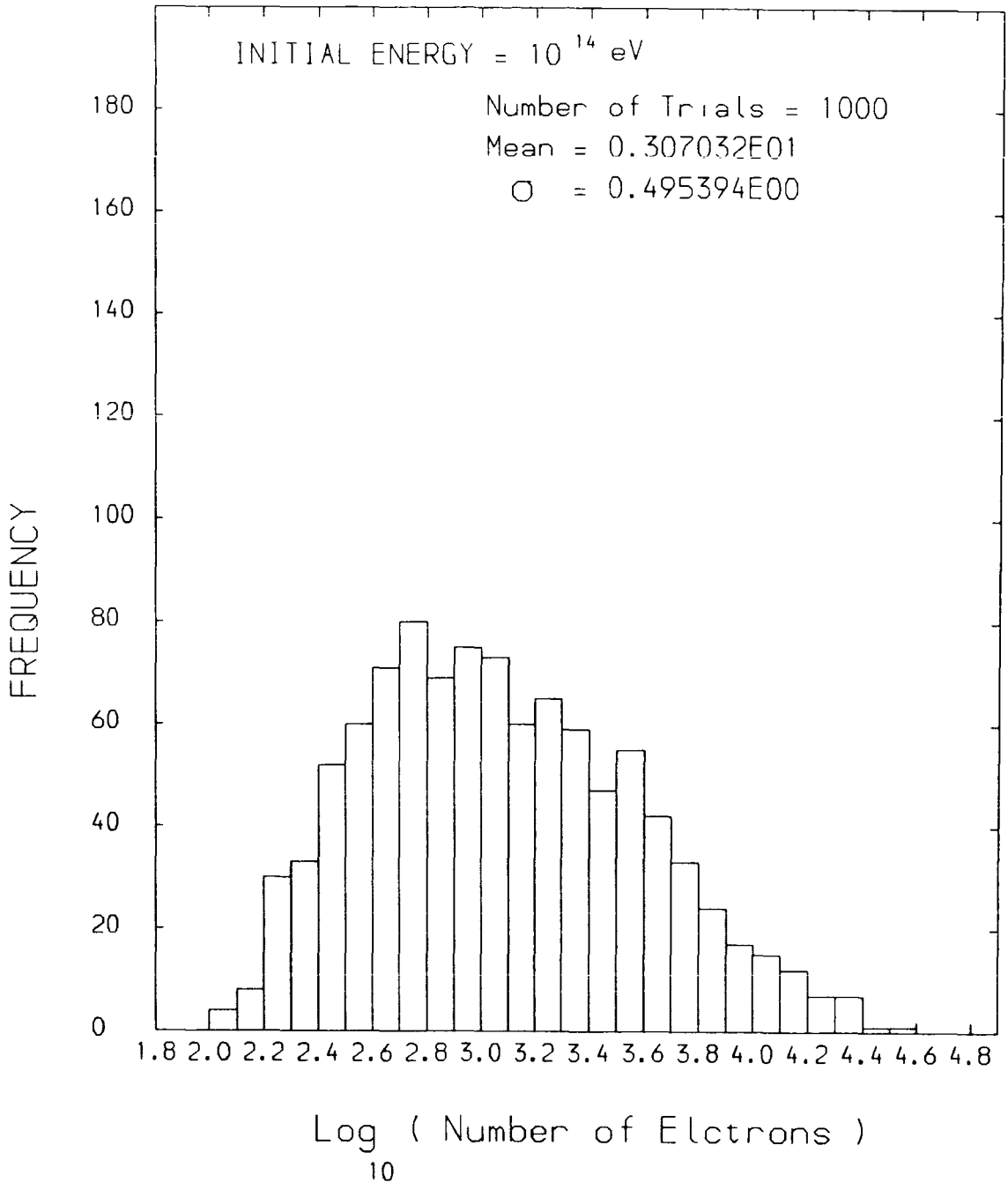

Figure 6.10b.3: See the heading page for caption.

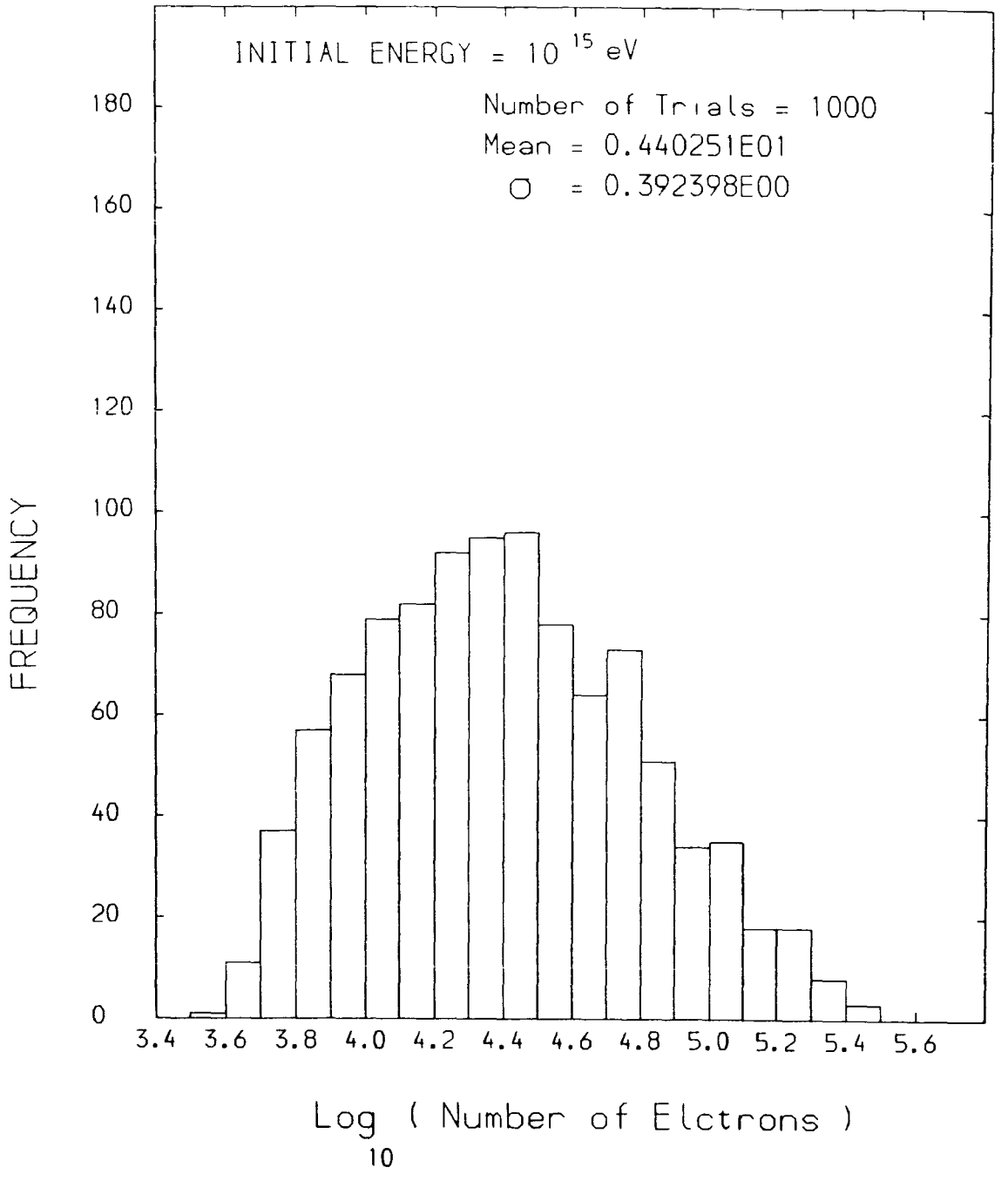

Figure 6.10b.4: See the heading page for caption.

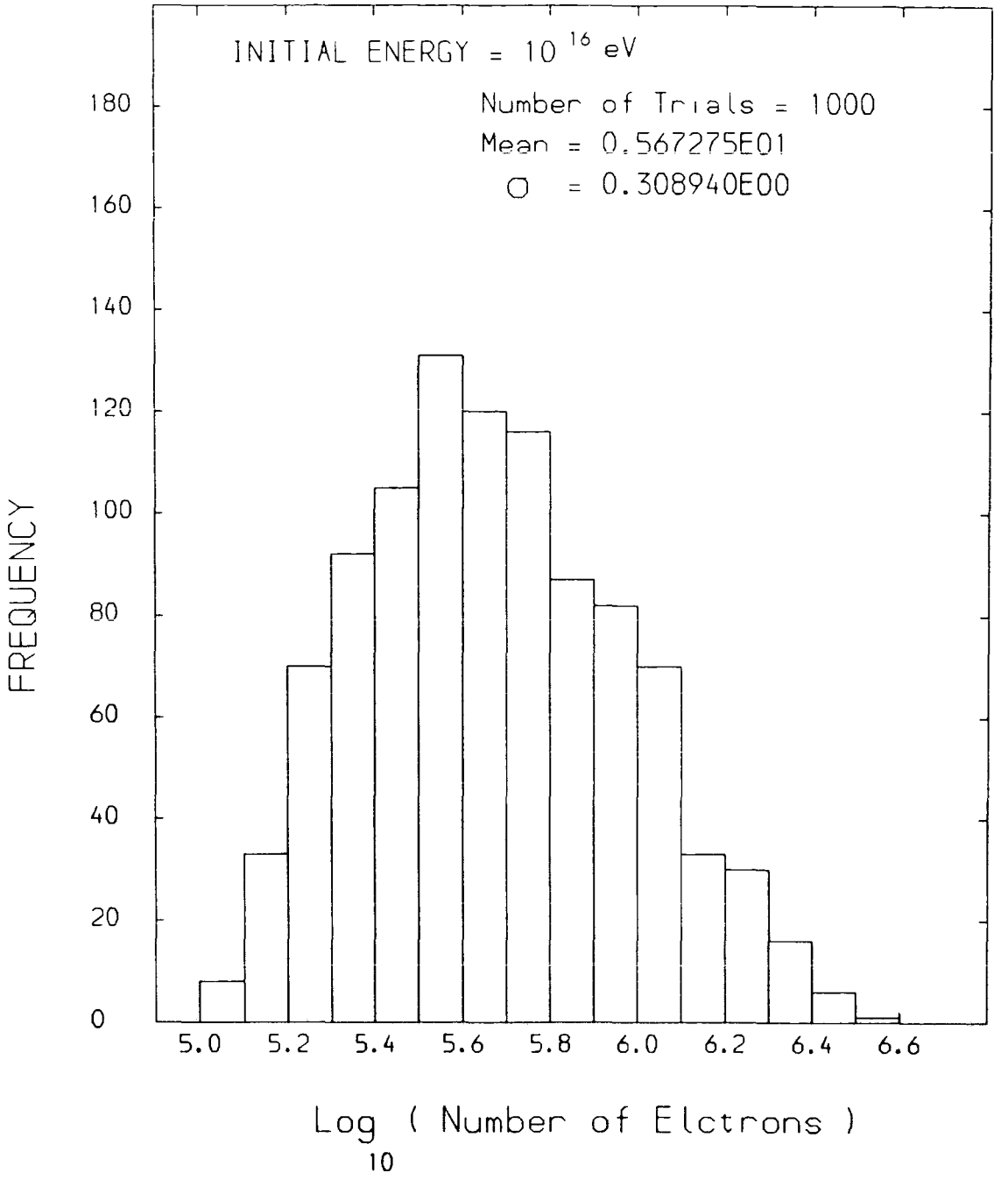

Figure 6.10b.5: See the heading page for caption.

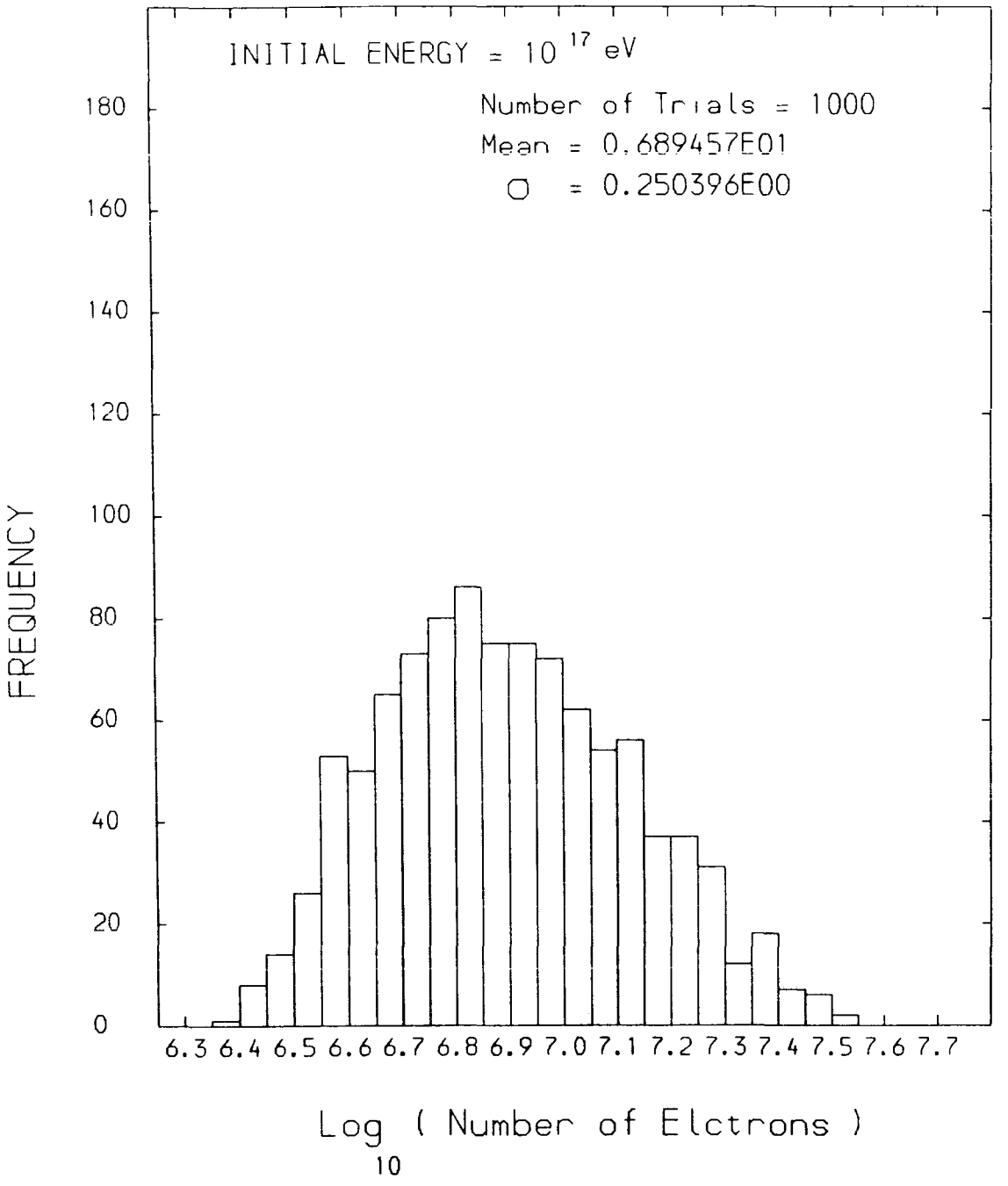

Figure 6.10b.6: See the heading page for caption.

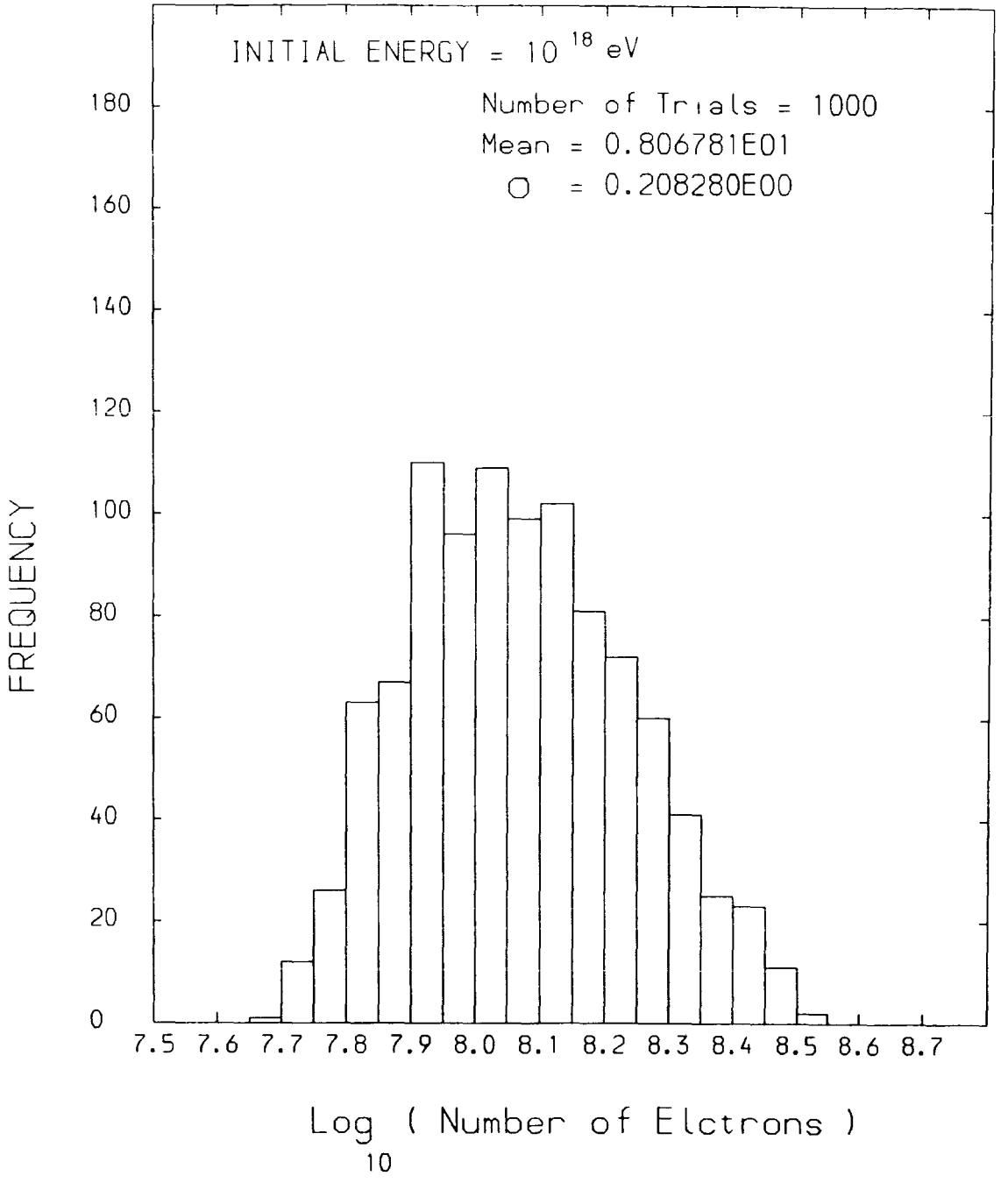

Figure 6.10b.7: See the heading page for caption.

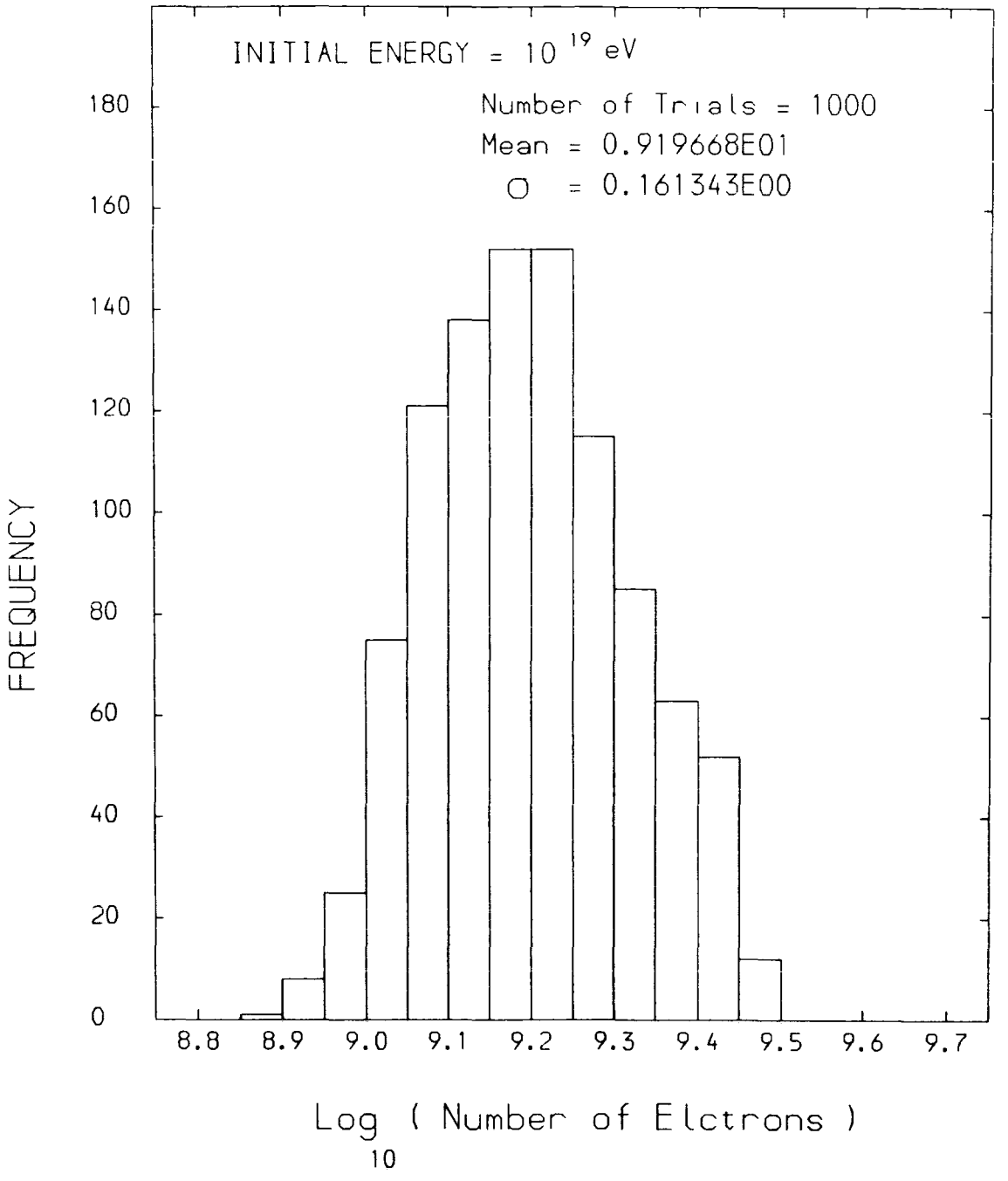

Figure 6.10b.8: See the heading page for caption.

Figure 6.11: List of MC006.

```
1     C-------------------------------------------------------C
2     C                                          17.06.86     C
3     C NAME: MC006                                           C
4     C                                                       C
5     C Simulation of the average number of electrons arriving C
6     C at different atmospheric depths produced  by the  pion C
7     C cascade orignating from  the charged pions produced as C
8     C a primary nucleon  propagates  through  the atmosphere C
9     C assuming ;                                            C
10    C L(N)  = 80   g/cm**2                                  C
11    C K(N)  = 0.5                                           C
12    C L(pi) = 120  g/cm**2                                  C
13    C K(pi) = 1.0                                           C
14    C n(s)= 3*E**(1/4)     with E in GeV .                  C
15    C                                                       C
16    C-------------------------------------------------------C
17    C
18          DIMENSION T(100),A(100,40),XG(100),FREQ(40),SL(1000)
19          COMMON NTRIAL,ENERGY
20          ENERGY = 1.0E+12
21          NTRIAL = 1000
22          JMAX=((ALOG10(ENERGY)-ALOG10(2.0E+9))/ALOG10(2.))+1
23          CALL GR1
24          ISMSL = 0
25          IBGSL = 0
26          SUM = 0.0
27          SSQ = 0.0
28          SUMLG = 0.0
29          SSQLG = 0.0
30          DO 60 I=1,40
31     60   FREQ(I) = 0.0
32    101   DO 105 I=1,100
33          T(I) = 0.0
34          DO 105 J=1,JMAX
35    105   A(I,J) = 0.0
36    C
37    C-----------------------------------------
38    C
39          DO 300 NEV=1,NTRIAL
40          Y = 0.0
41          J = 0
42          E = ENERGY / 1.E9
43    C**
44    110   Z = G05CAF(Z)
45          Z = -80. * ALOG(Z)
46          Y = Y + Z
47          J = J + 1
48          IF(Y .GE. 1000.) GOTO 300
49          IF(J .GT. JMAX ) GOTO 300
50          W1 = Y
```

```
      W2 = W1 +120.
      IF ( W2 .GE. 1000 ) GOTO 200
      L1 = ALTI(W1)
      L2 = ALTI(W2)
      FPIC = 2. * E** .25
      EPIC = 0.17 * E ** .75
      D = 0.056 * EPIC
      FPIC = FPIC * EXP(-(L1-L2) / D )
C
120   FPI0 = FPIC * EPIC**0.25
      EPI0 =(1.0/3.0) * EPIC**0.75
      IF (EPI0 .LT. 1.0) GOTO 200
      FPIC = 2. * FPI0
      EPIC = EPI0
      D    = 0.056  * EPIC
C
      EG = 0.5 * EPI0 *1.E9
      DO 140 I=1,100
      X  = I * 10.0
      TX = X - W2
      IF ( TX .LE. 0.0 ) GOTO 140
      AX = ANUM (EG,TX) * 2 * FPIC
      A(I,J) = A(I,J) + AX
140   CONTINUE
      SL(NEV) = AX + SL(NEV)
C
      W3 = W2 + 120.
      IF ( W3 .GE. 1000) GOTO 200
      L3 = ALTI(W3)
      FPIC = FPIC * EXP(-(L2-L3) / D )
      EPIC = EPI0
      L2 = L3
      W2 = W3
      GOTO 120
C
200   E= 0.5 * E
      IF ( E .GT. 1.0 ) GOTO 110
C
300   CONTINUE
C
C-------------------------------------------------
C
      DO 320 J=1,JMAX
      DO 320 I=1,100
320   A(I,J) = A(I,J) / NTRIAL
C
      DO 360 J=1,JMAX
      DO 350 I=1,100
      XG(I) = A(I,J)
350   CONTINUE
```

```
101           CALL GR2(XY)
102     360   CONTINUE
103     C
104           DO 370 I=1,100
105           DO 370 J=1,JMAX
106     370   T(I) = T(I) + A(I,J)
107           CALL GR2(T)
108           CALL GREND
109     C****
110           DO 470 I=1,NTRIAL
111           SUM = SUM + SL(I)
112           SSQ = SSQ + (SL(I) * SL(I) )
113     470   CONTINUE
114           AVE=SUM / NTRIAL
115           SDV=SSQ / NTRIAL - AVE*AVE
116           SDV=SQRT(SDV)
117     C*
118           DO 472 I=1,NTRIAL
119           SLX = ALOG10(SL(I))
120           SUMLG = SUMLG + SLX
121           SSQLG = SSQLG + SLX*SLX
122     472   CONTINUE
123           AVELG = SUMLG / NTRIAL
124           SDVLG = SSQLG / NTRIAL -AVELG*AVELG
125           SDVLG = SQRT(SDVLG)
126     C*
127           WD = .2
128           IF (ENERGY .GT. 1.0E13) WD = 0.1
129           IF (ENERGY .GT. 1.0E16) WD = 0.05
130           AMIN = INT((AVELG - 3.4*SDVLG)/ WD) * WD
131           AMAX = INT((AVELG + 3.7*SDVLG)/ WD) * WD
132           NBIN = (( AMAX - AMIN ) / WD ) +0.0001
133           DO 474 I=1,NTRIAL
134           XSL = ALOG10(SL(I))
135           IF (XSL .GT. AMAX) IBGSL=IBGSL+1
136           IF (XSL .GT. AMAX) GOTO 474
137           IF (XSL .LT. AMIN) ISMSL=ISMSL+1
138           IF (XSL .LT. AMIN) GOTO 474
139           INDEX=((XSL-AMIN)/ WD )+1
140           FREQ(INDEX) =  FREQ(INDEX) + 1
141     474   CONTINUE
142           CALL HISTO(FREQ,NBIN,AMIN,AMAX,WD,AVELG,SDVLG)
143     C*****
144           WRITE(6,475)ENERGY
145     475    FORMAT(//  ' INTIAL ENERGY =',1PE7.1,3H EV)
146           WRITE(6,476)NTRIAL
147     476    FORMAT(' NUMBER OF TRIALS = ',I4)
148           WRITE(6,488)
149           DO 480 J=1,JMAX
150           WRITE(6,482)J
```

```
151           WRITE(6,484)
152           DO 478 I=10,100,10
153           IX = 10 * I
154      478  WRITE(6,486)IX,A(I,J)
155           WRITE(6,488)
156      480  CONTINUE
157      482  FORMAT(20H INTERACTION NUMBER ,I3)
158      484  FORMAT(20H   DEPTH          NE)
159      486  FORMAT(3X,I4,10X,1PE11.5)
160      488  FORMAT(30H ----------------------------//)
161           WRITE(6,489)
162      489  FORMAT(20H       * T O T A L *)
163           WRITE(6,484)
164           DO 490 I=10,100,10
165           IX = 10 * I
166      490  WRITE(6,486)IX,T(I)
167           WRITE(6,492)
168      492  FORMAT(30H ----------------------------////)
169      C*****
170           WRITE(6,505)
171           WRITE(6,506)
172      505  FORMAT (38H INFORMATION ABOUT THE TOTAL NUMBER OF)
173      506  FORMAT (22H ELECTRON AT SEE LEVEL/)
174           WRITE(6,510) AVE
175      510  FORMAT (11H AVERAGE = ,1PE11.5)
176           WRITE(6,512) SDV
177      512  FORMAT (22H STANDARD DEVIATION = ,1PE11.5)
178           WRITE(6,514) AVELG
179      514  FORMAT (23H AVERAGE OF LOG (N E) =,F7.4)
180           WRITE(6,516) SDVLG
181      516  FORMAT (34H STANDARD DEVIATION OF LOG(N E) = ,F7.4//)
182           WRITE(6,520)
183      520  FORMAT (42H   LOG ( NUMBER OF ELECTRON )    FREQUENCY/)
184           DO 530 I=1,NBIN
185           XX1=(I-1)* WD + AMIN
186           XX2=XX1 + WD
187      530  WRITE(6,531)XX1,XX2, FREQ(I)
188      531  FORMAT (5X,F5.2,' -- ',F5.2,13X,F5.0)
189           WRITE(6,532)AMIN,ISMSL
190      532  FORMAT (1X,14H LESS    THAN ,F8.5,' = ',I6)
191           WRITE(6,534)AMAX,IBGSL
192      534  FORMAT (1X,14H GREATER THAN ,F8.5,' = ',I6)
193           CALL TB3(T)
194      C*****
195           STOP
196           END
```

All "SUBROUTINE"s in this program are the same ones used in program MC007 .

```
FUNCTION ALTI(X)
FUNCTION ANUM(W,X)
SUBROUTINE GR1
SUBROUTINE GR2(Z)
SUBROUTINE HISTO(F,N,XMIN,XMAX,WD,AVE,SD)
SUBROUTINE TB3(T)
```

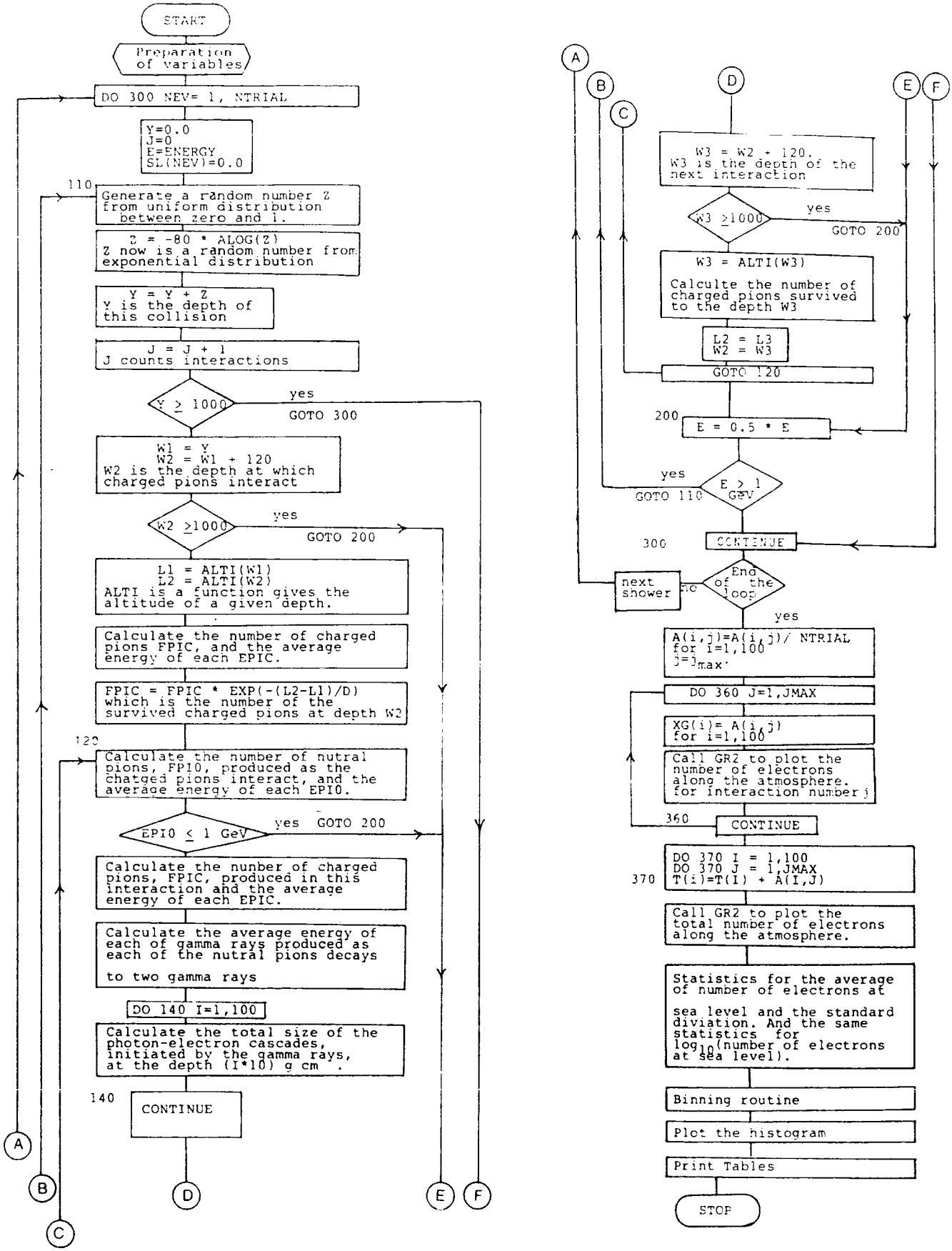

Figure 6.12: Flowchart of MC006.

FIGURE 6.13

Outputs of Program MC006.

Figures 6.13a.1 to 6.13a.8

Outputs of the program MC006. The simulation of the average number of electrons arriving at different atmospheric depths produced by the pion cascade orignating from the charged pions produced as a primary nucleon propagates through the atmosphere. The uper most curve is the average of the total of the number of elctrons in the shower, the other curves are for the average of the electron number contributed by each protonic collision. Each Figure is for a given proton initial energy which is written on the top of the plot.

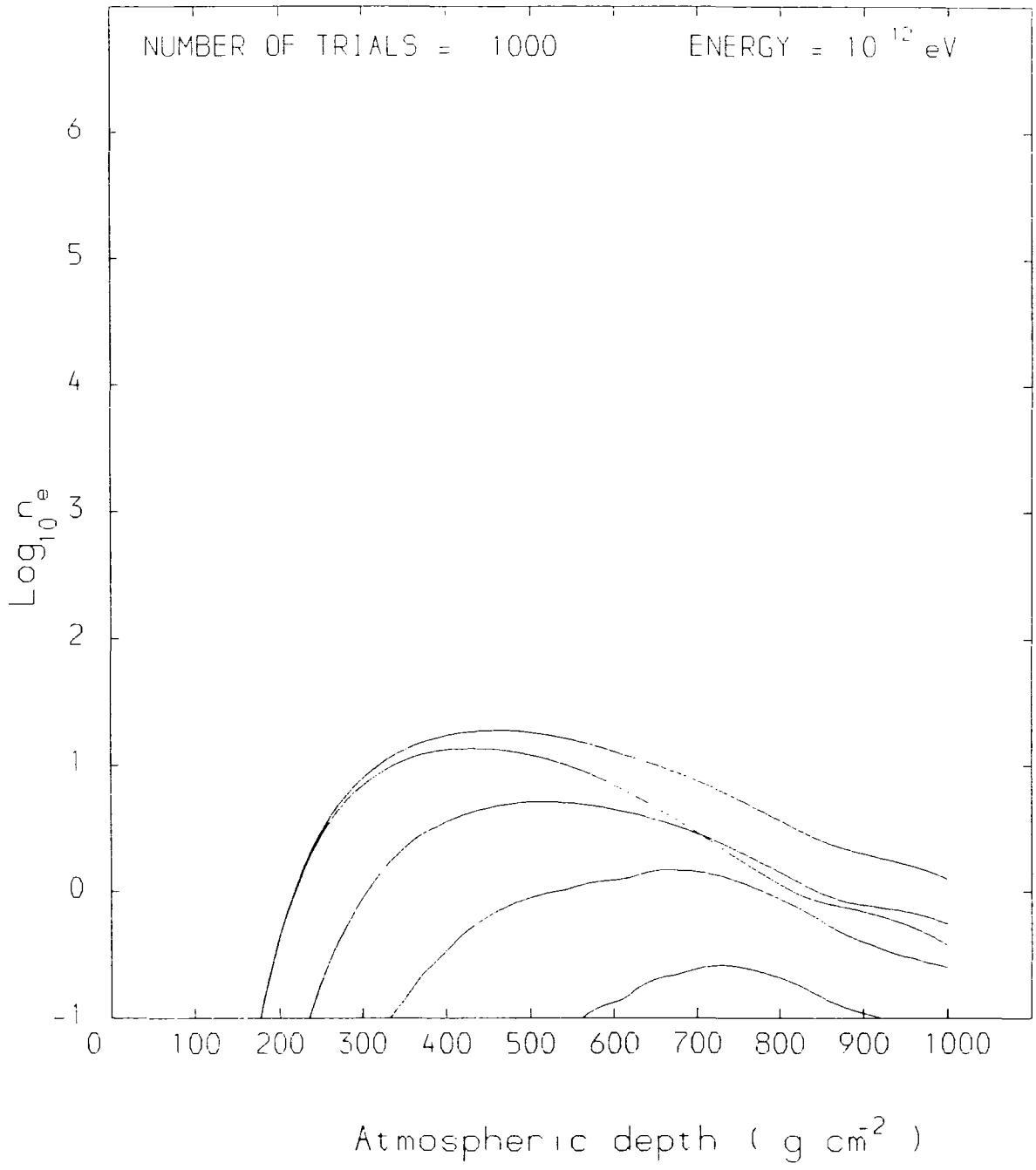

Figure 6.13a.1: See the heading page for caption.

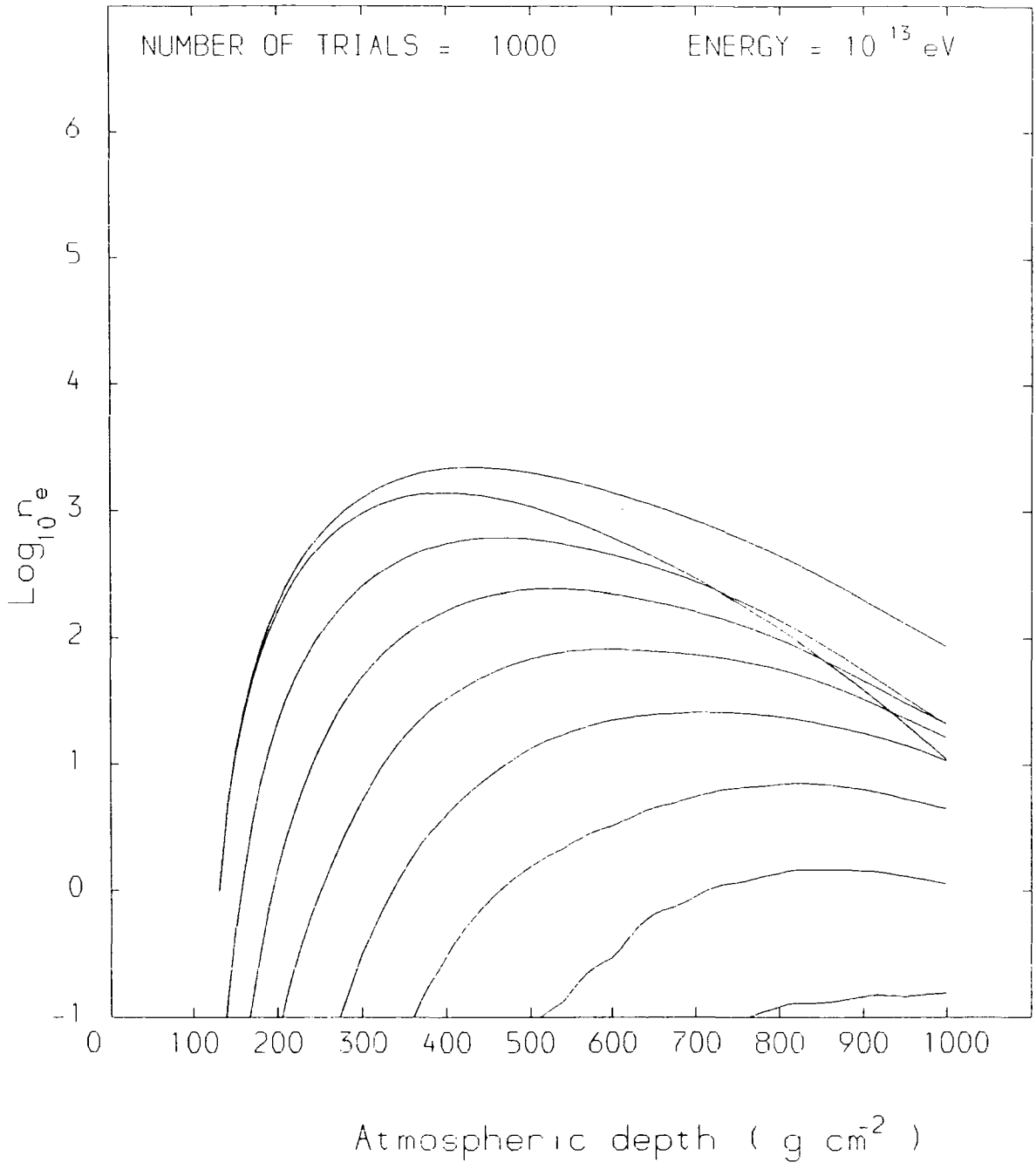

Figure 6.13a.2: See the heading page for caption.

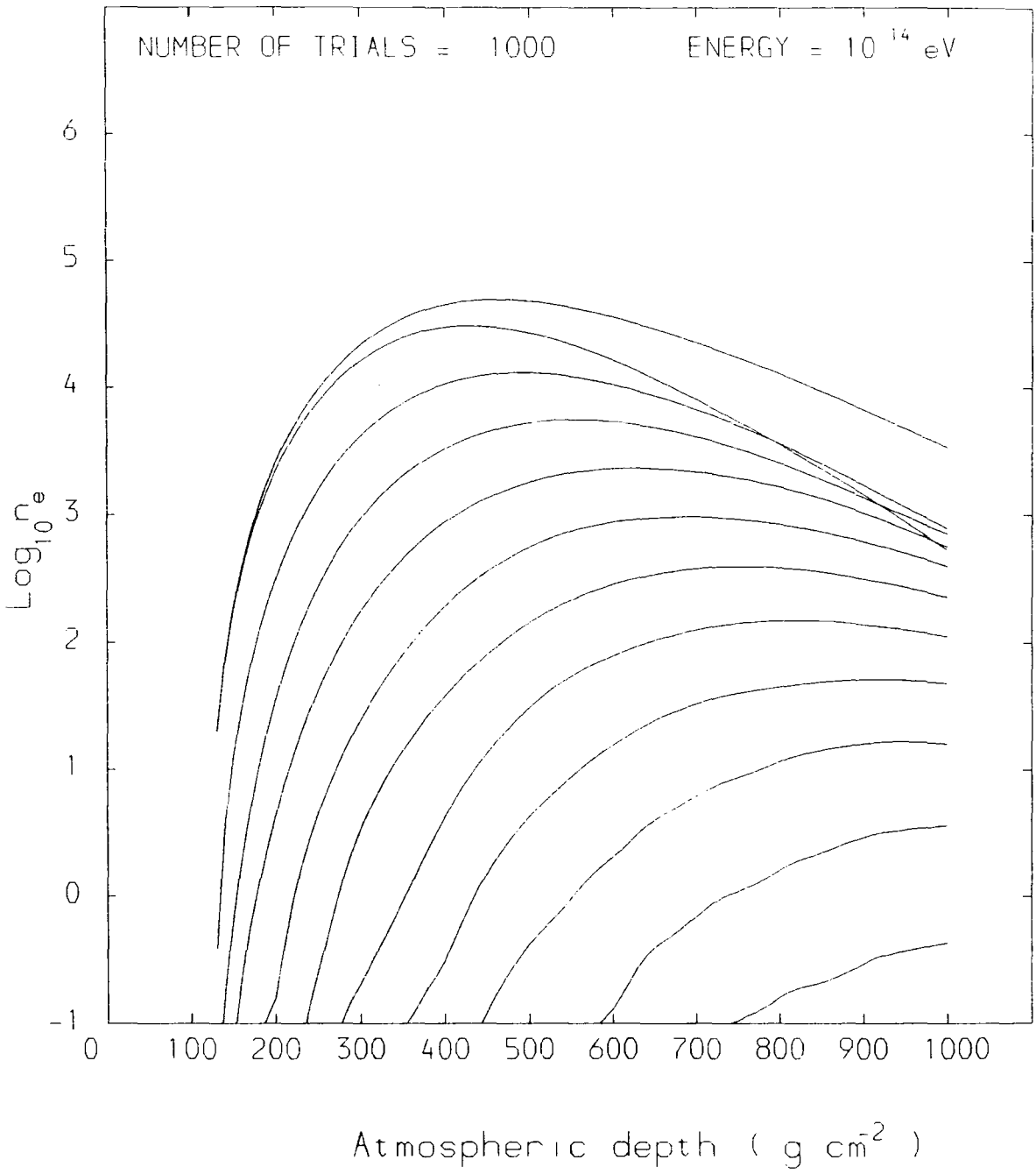

Figure 6.13a.3: See the heading page for caption.

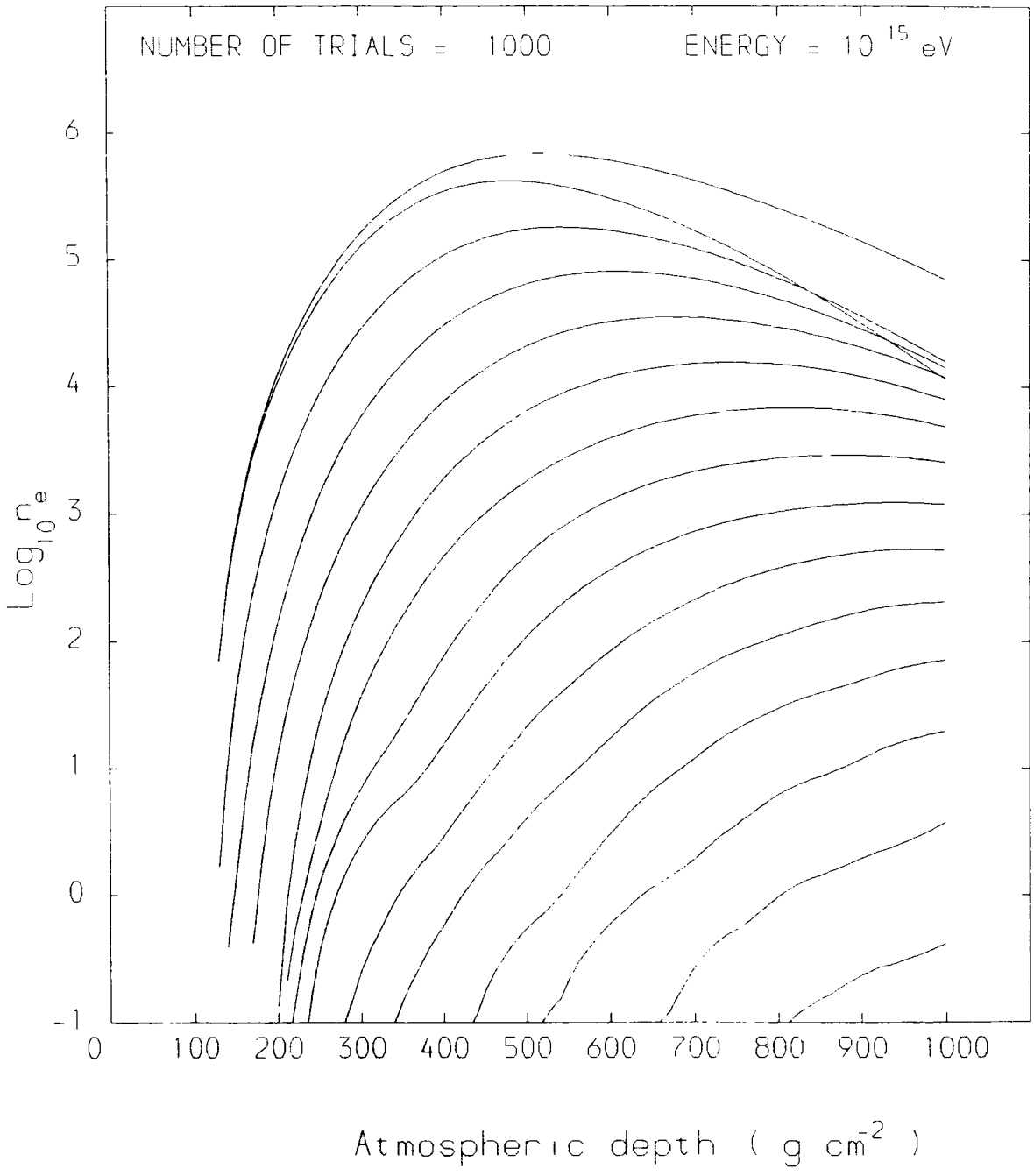

Figure 6.13a.4: See the heading page for caption.

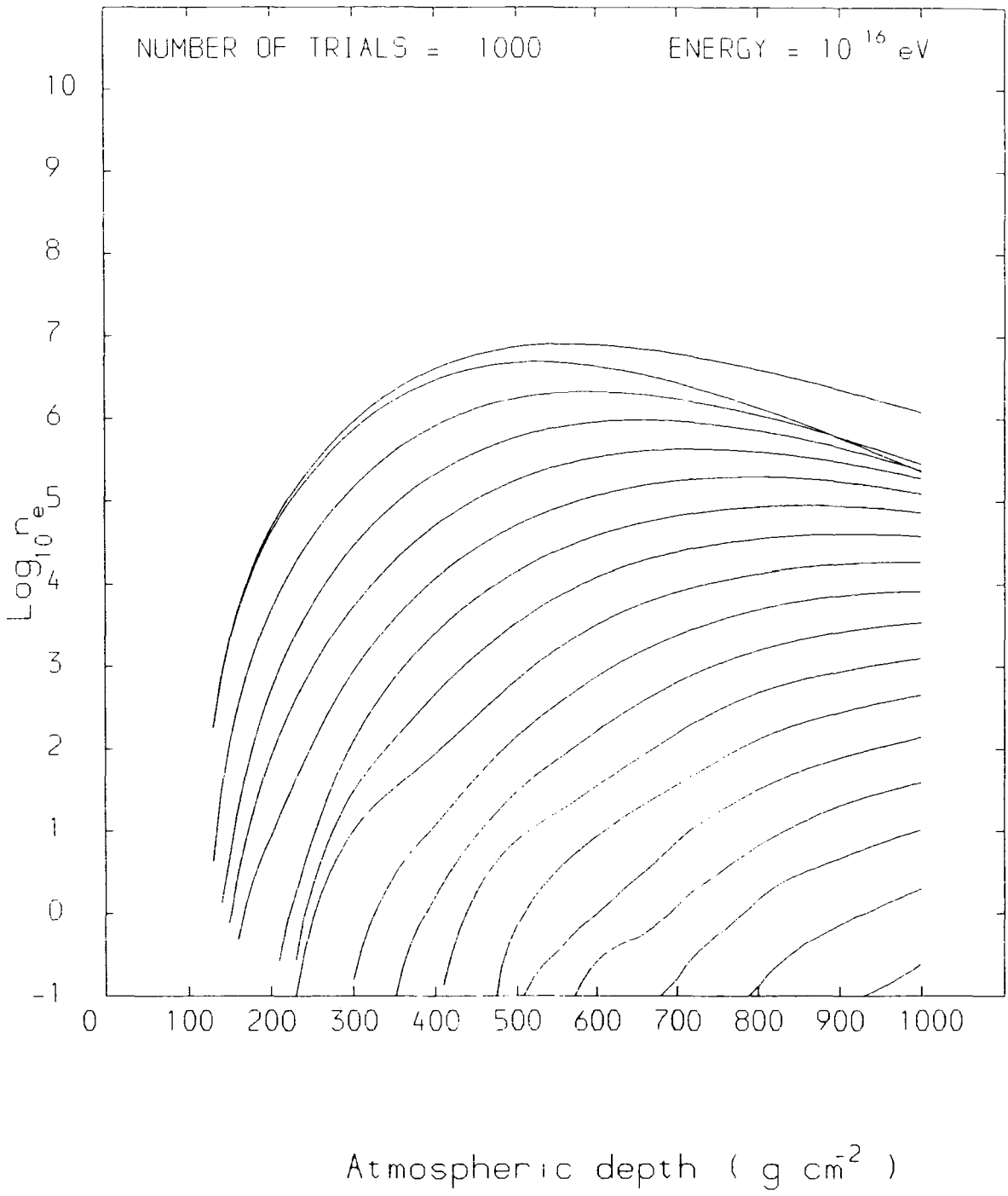

Figure 6.13a.5: See the heading page for caption.

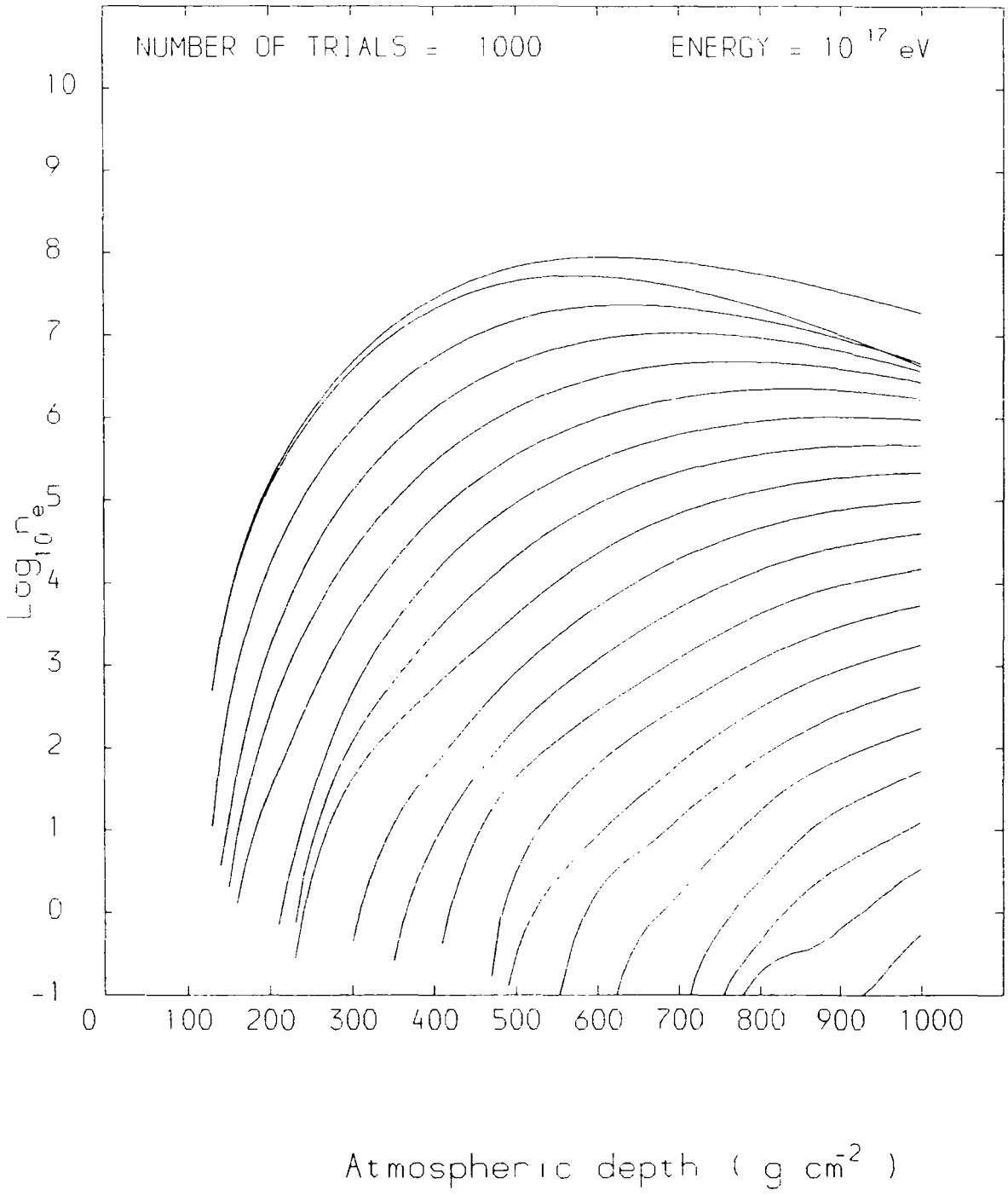

Figure 6.13a.6: See the heading page for caption.

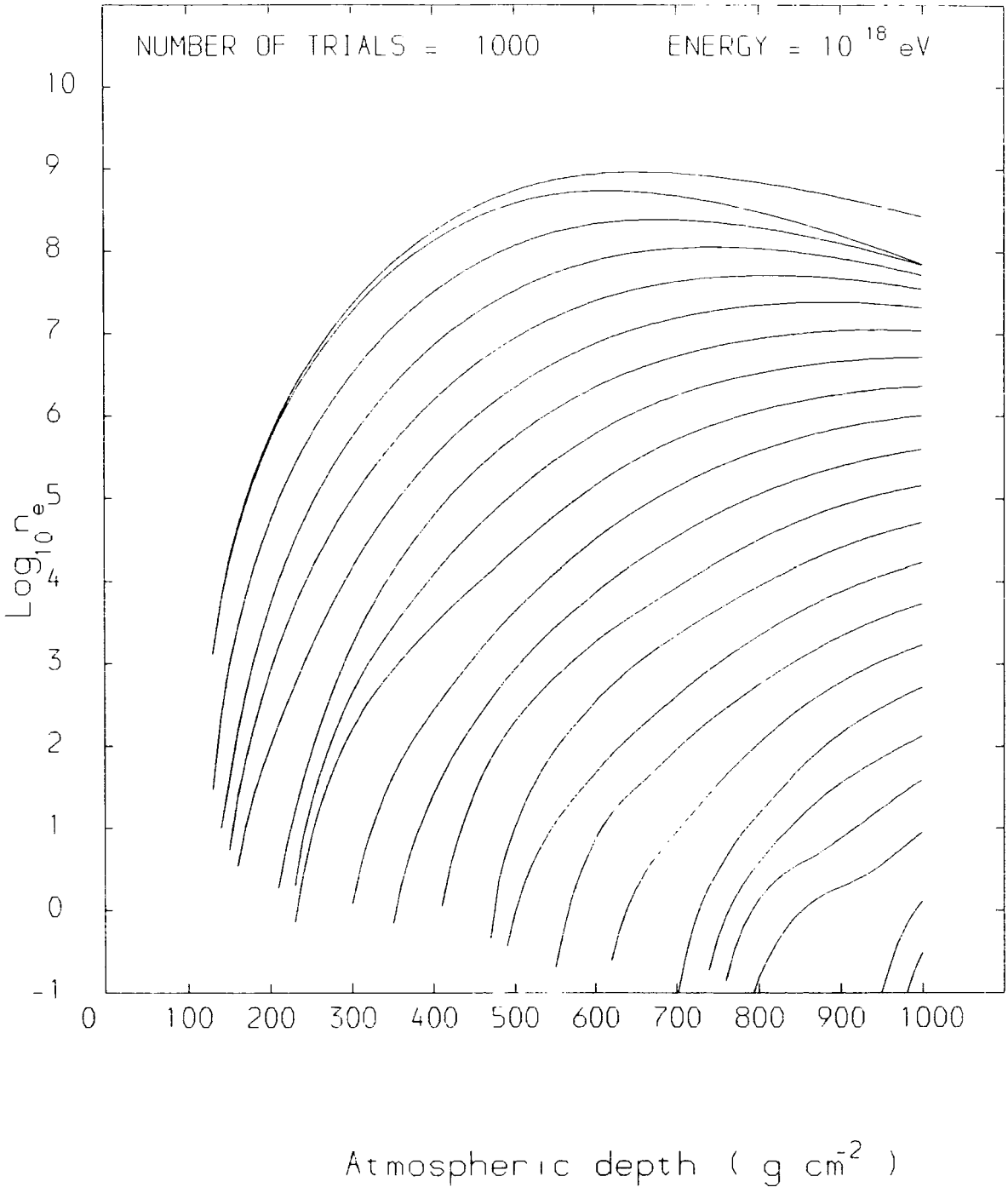

Figure 6.13a.7: See the heading page for caption.

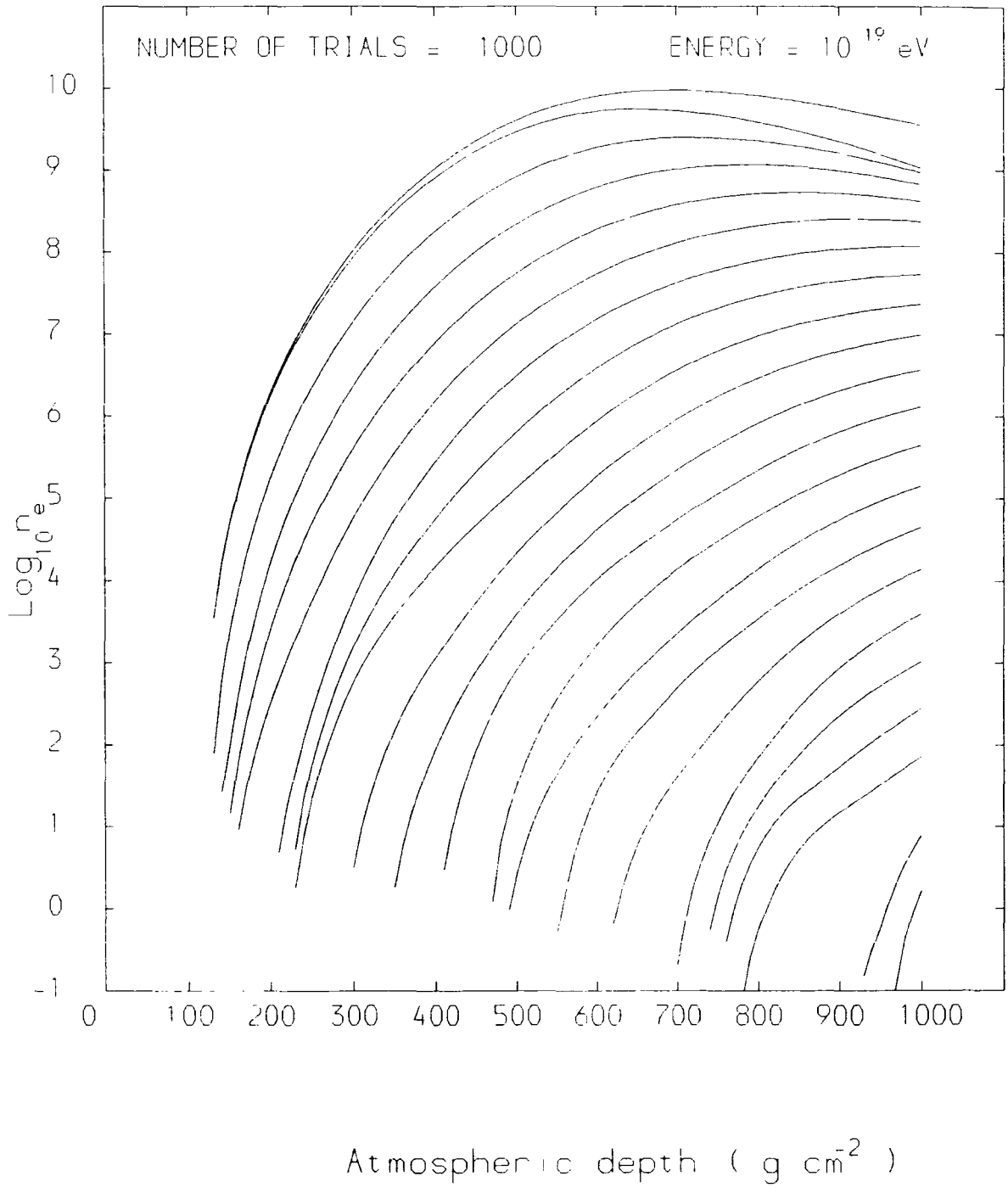

Figure 6.13a.8: See the heading page for caption.

Figures 6.13b.1 to 6.13b.8

The distribution of the $\log_{10}$ of number of electrons at sea-level as it was calculated by the program MC006. Each distribution is for a given proton initial energy which is written on the top of the plot.

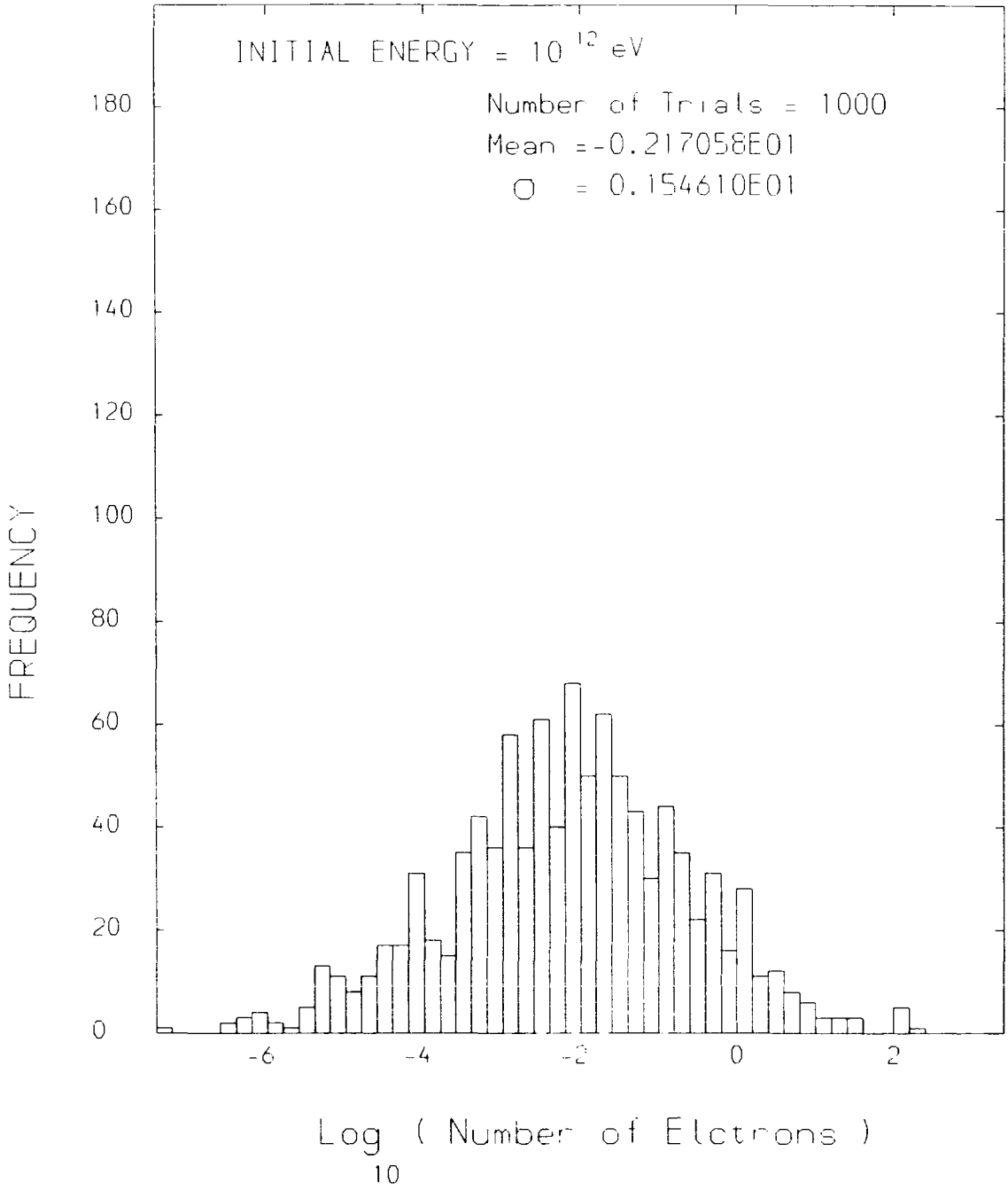

Figure 6.13b.1: See the heading page for caption.

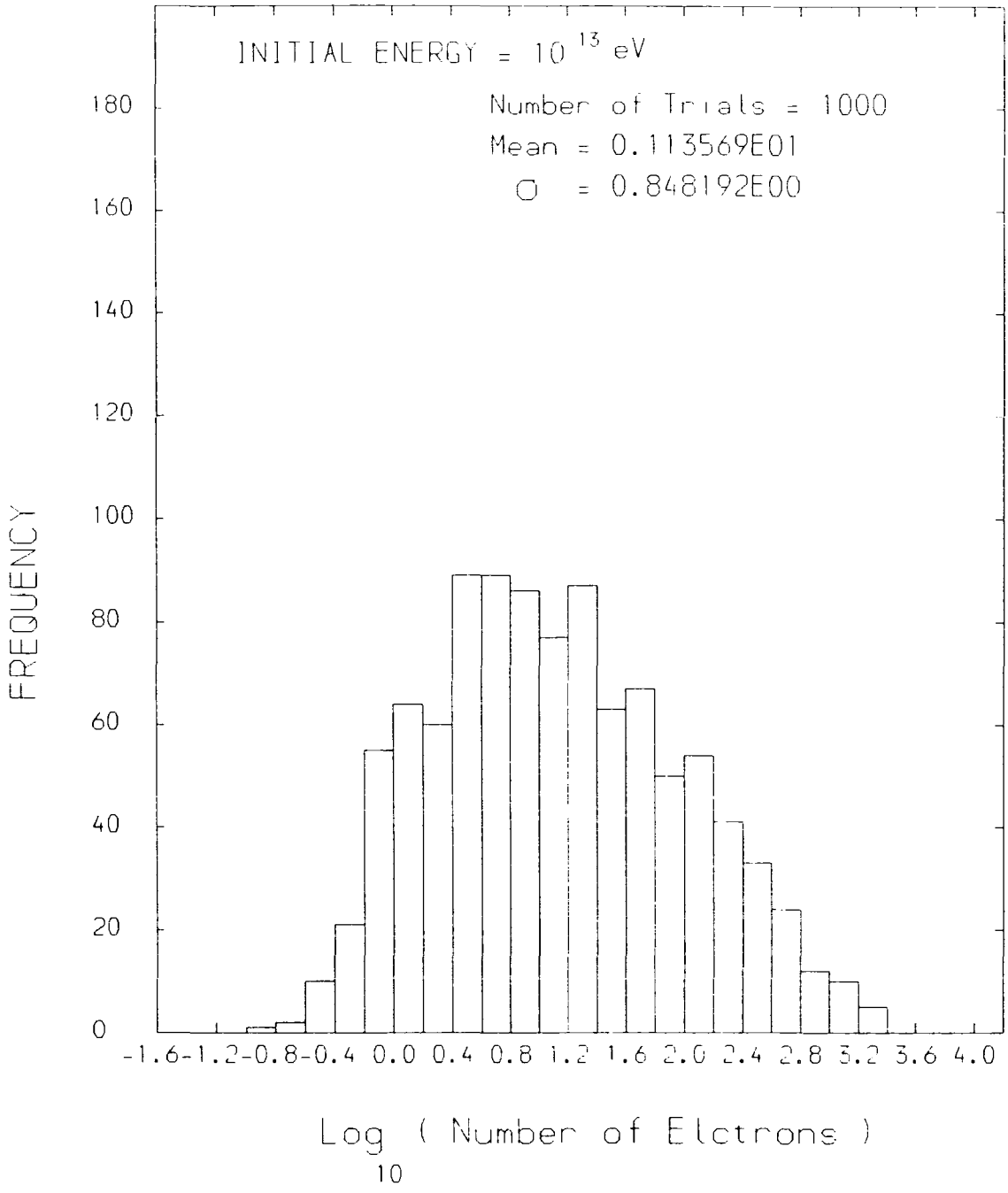

Figure 6.13b.2: See the heading page for caption.

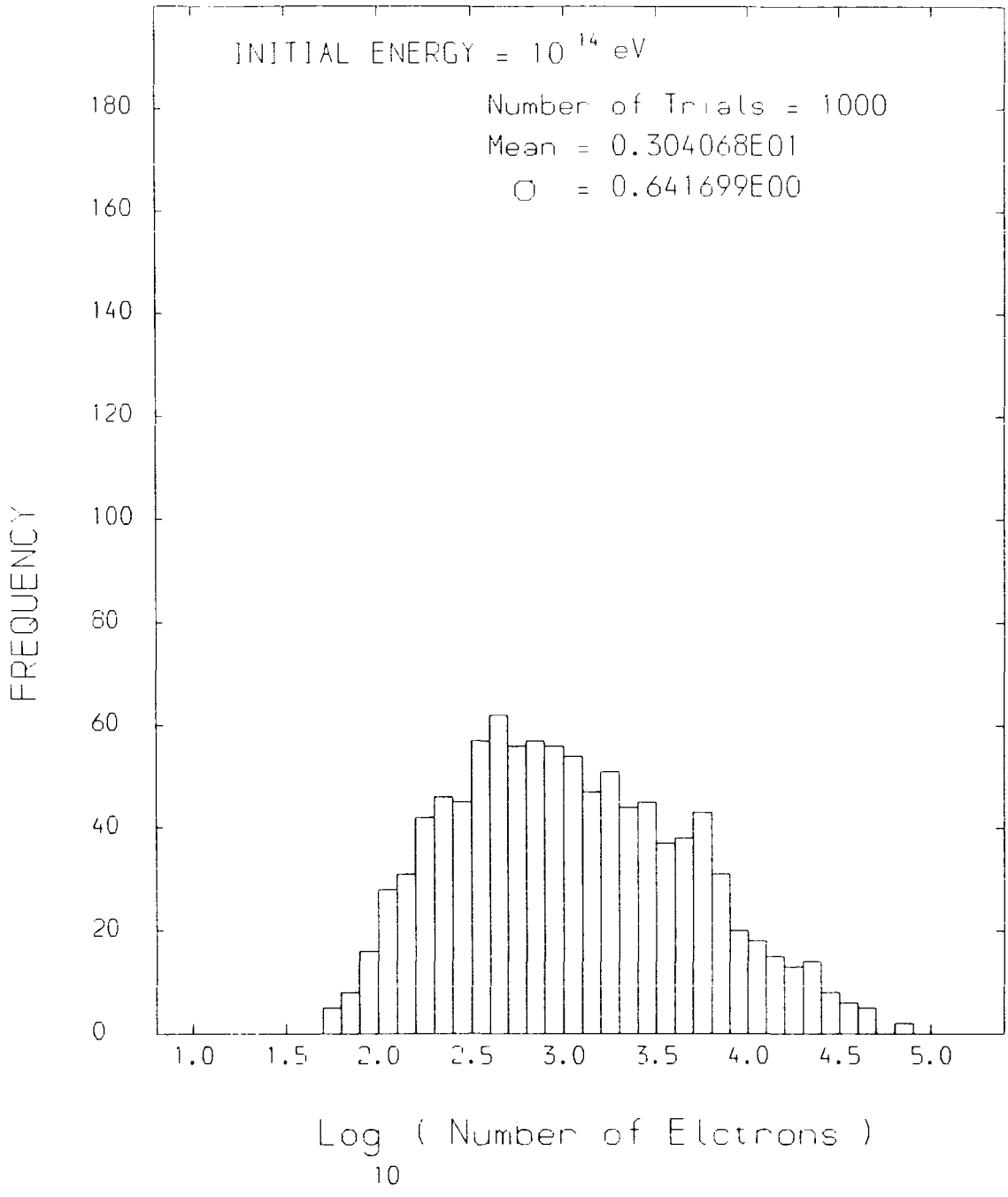

Figure 6.13b.3: See the heading page for caption.

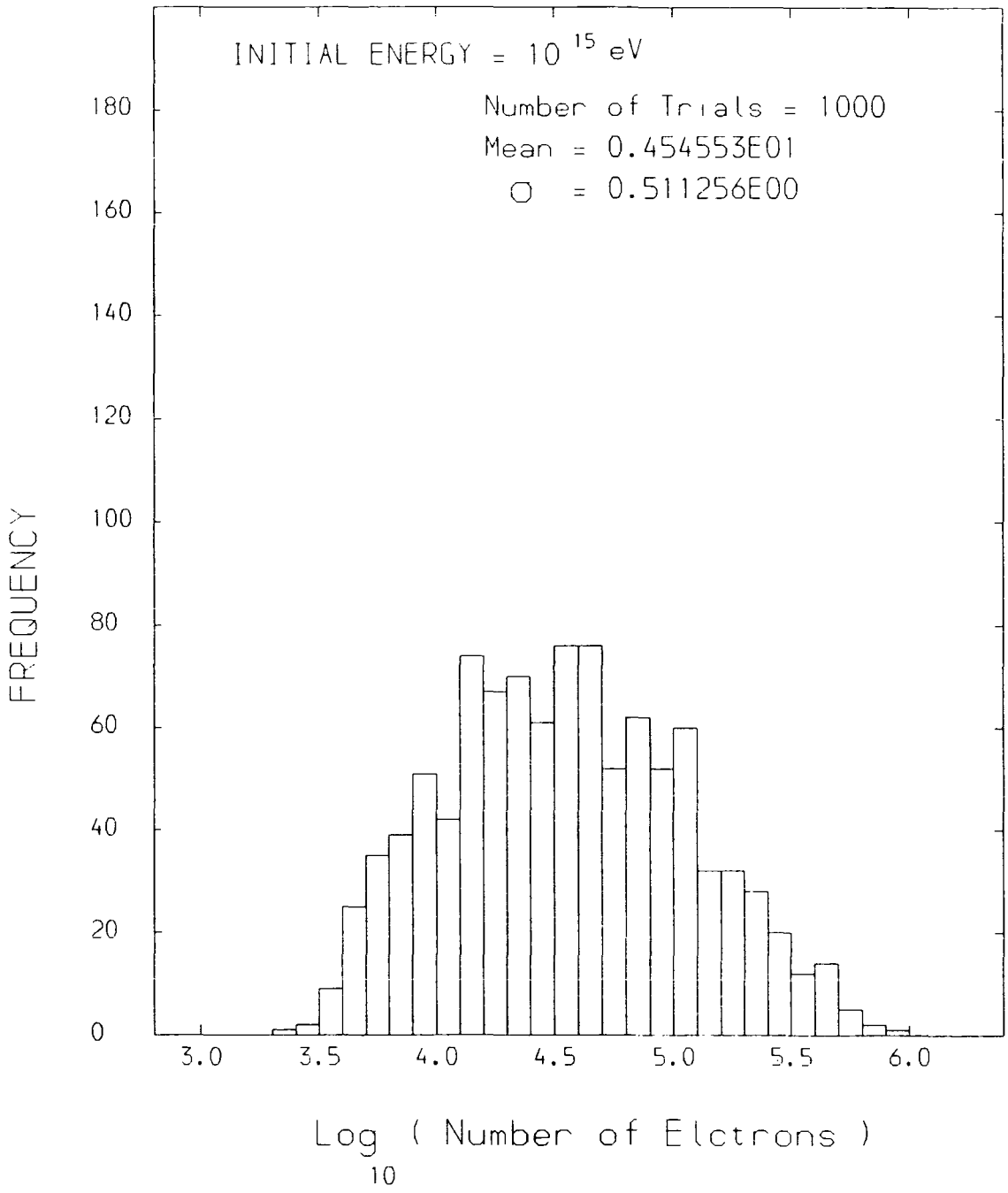

Figure 6.13b.4: See the heading page for caption.

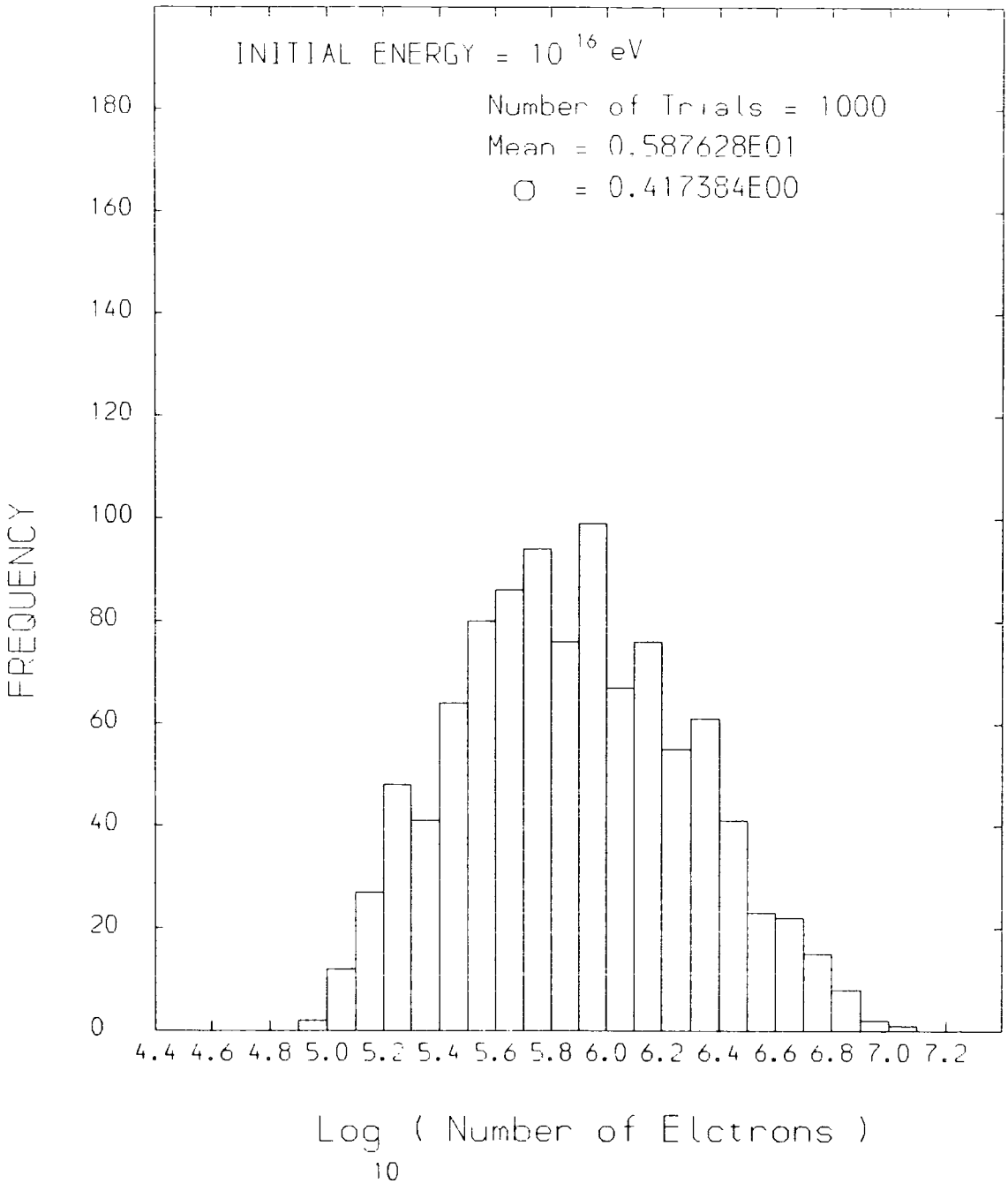

Figure 6.13b.5: See the heading page for caption.

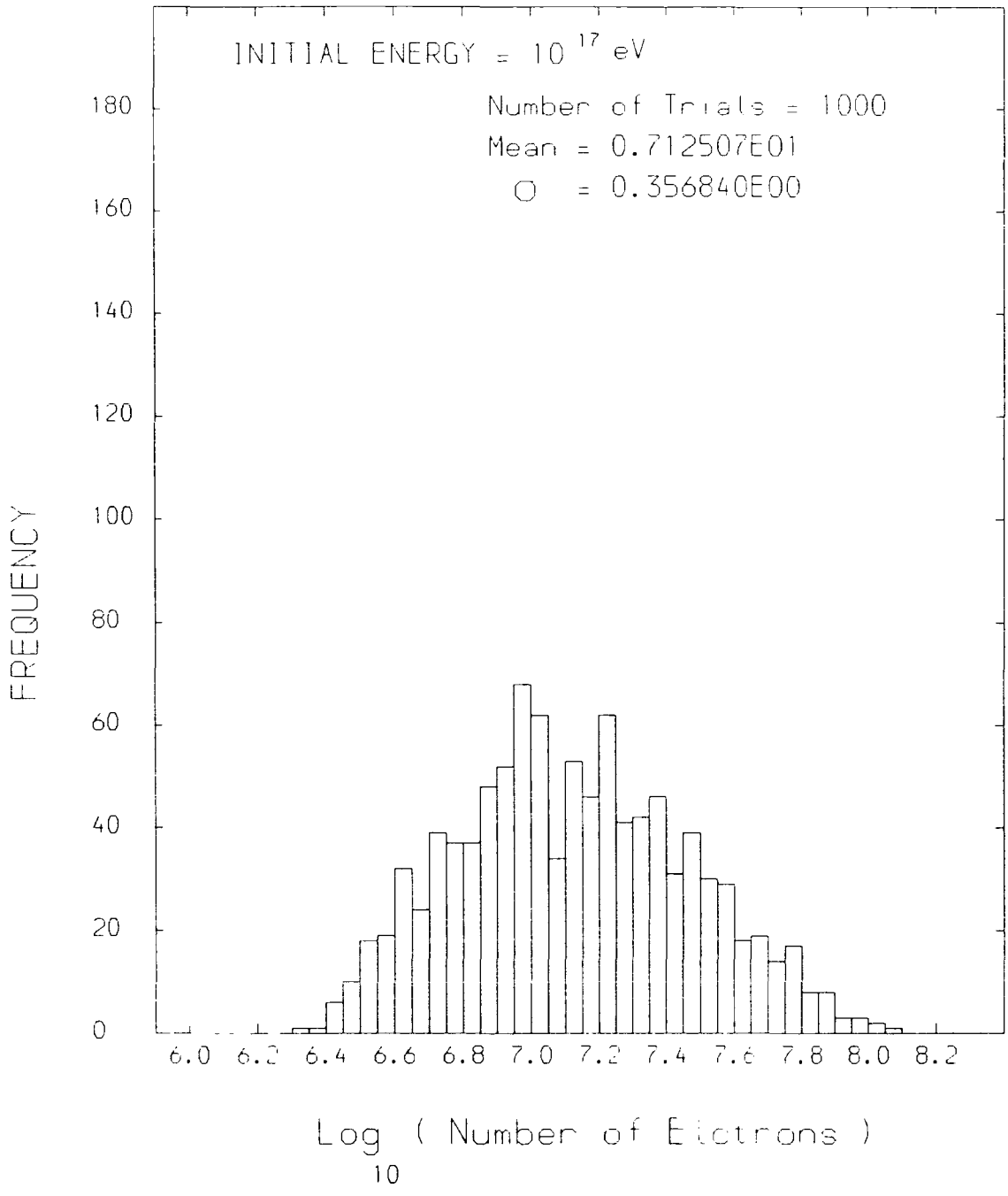

Figure 6.13b.6: See the heading page for caption.

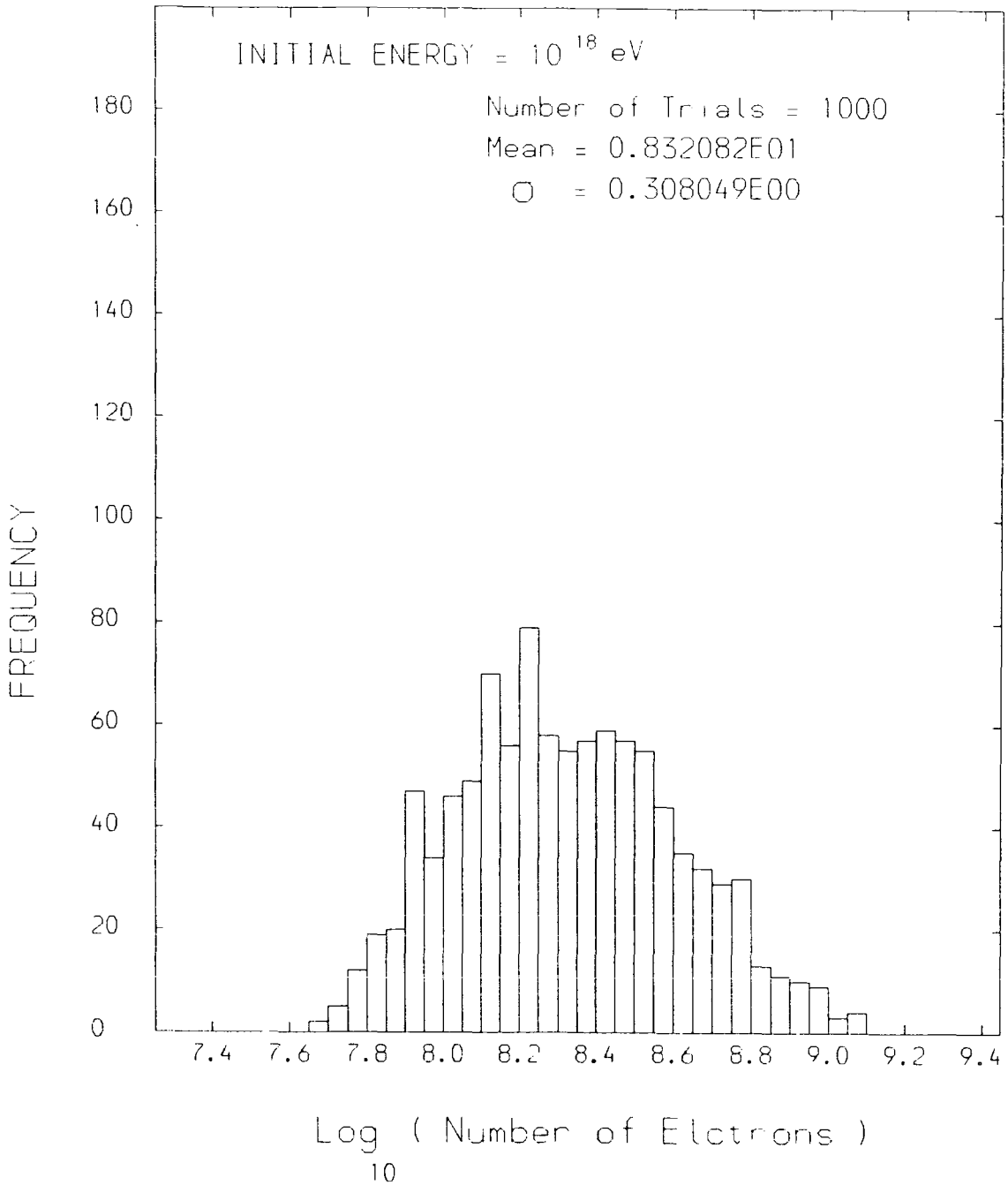

Figure 6.13b.7: See the heading page for caption.

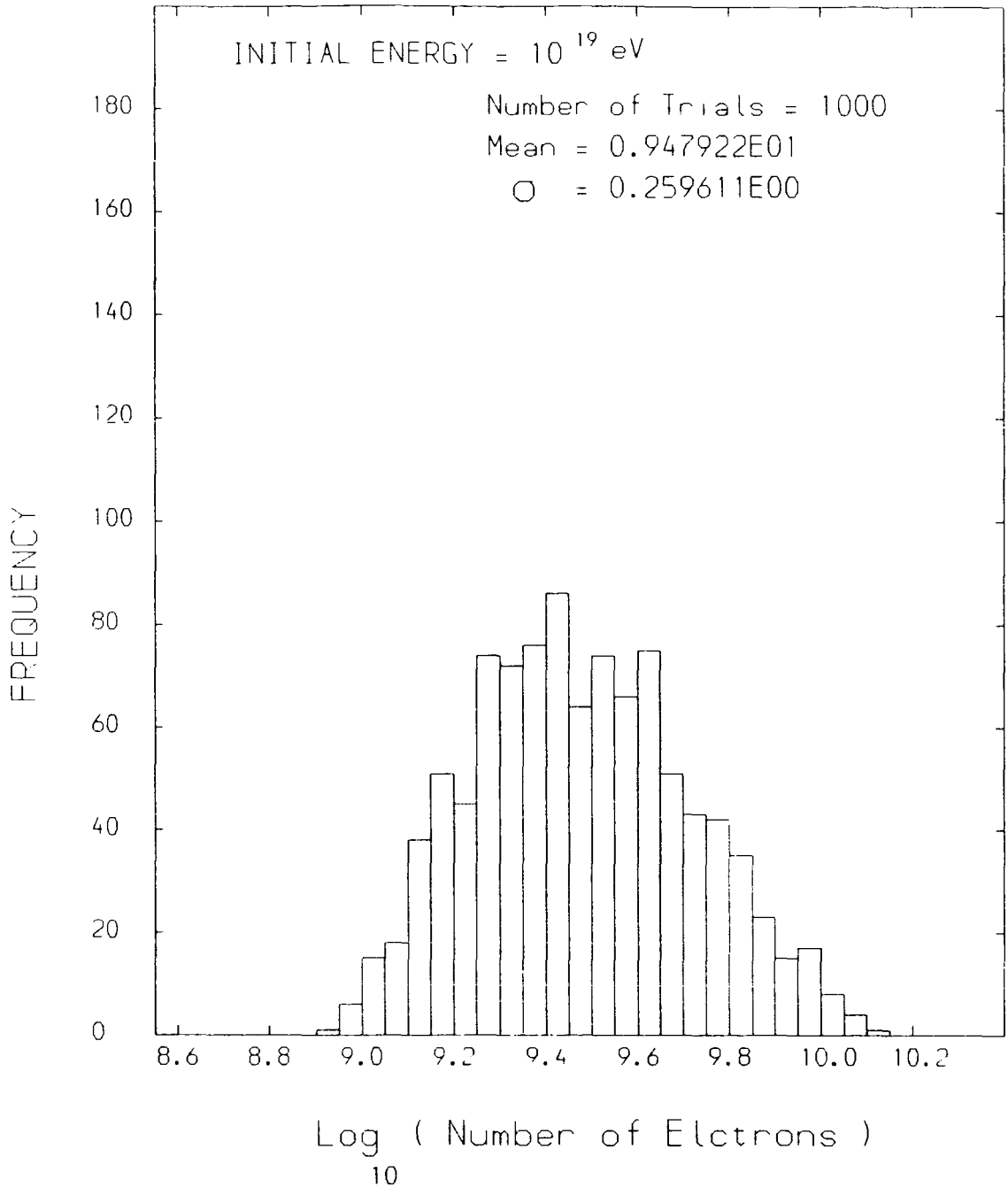

Figure 6.13b.8: See the heading page for caption.

Figure 6.14: List of MC007.

```
C-------------------------------------------------------C
C                                          08.07.1986   C
C NAME: MC007                                           C
C                                                       C
C Simulation of the average number of electrons arriving C
C at different atmospheric depths produced  as a primary C
C nucleon  propagates  through the atmosphere assuming ; C
C L(N)  = 80   g/cm**2                                  C
C K(N)  = 0.5                                           C
C L(pi) = 120  g/cm**2                                  C
C K(pi) = 1.0                                           C
C n(s)= 3*E**(1/4)     with E in GeV .                  C
C                                                       C
C-------------------------------------------------------C
C
      DIMENSION A(100,40),A1(100),A2(100)
      DIMENSION T(100),XG(100),FREQ(50),SL(1000)
      COMMON NTRIAL,ENERGY
      ENERGY = 1.00E+15
      NTRIAL = 1000
      JMAX=((ALOG10(ENERGY)-ALOG10(2.0E+9))/ALOG10(2.))+1
      CALL GR1
      ISMSL = 0
      IBGSL = 0
      SUM = 0.0
      SSQ = 0.0
      SUMLG = 0.0
      SSQLG = 0.0
      DO 60 I=1,50
 60   FREQ(I) = 0.0
101   DO 105 I=1,100
      T(I) = 0.0
      DO 105 J=1,JMAX
105   A(I,J) = 0.0
C-----------------------------------------
C
      DO 300 NEV=1,NTRIAL
      Y = 0.0
      J = 0
      E = ENERGY / 1.E9
```

```
41      C**
42      110   Z = G05CAF(Z)
43            Z = -80. * ALOG(Z)
44            Y = Y + Z
45            J = J + 1
46            IF (J .GT. JMAX  )  GOTO 300
47            IF (Y .GE. 1000. )  GOTO 300
48      C
49            SL1=0.0
50            SL2=0.0
51            CALL MC004(E,Y,A1,SL1)
52            CALL MC006(E,Y,A2,SL2)
53            DO 200 I=1,100
54      200   A(I,J) = A(I,J) + A1(I) + A2(I)
55            SL(NEV) = SL(NEV) + SL1 + SL2
56            E = .5 * E
57            IF (E .GT. 1.0  )   GOTO 110
58      300   CONTINUE
59      C-------------------------------------------------
60            DO 320 J=1,JMAX
61            DO 320 I=1,100
62      320   A(I,J) = A(I,J) / NTRIAL
63      C
64            DO 360 J=1,JMAX
65            DO 350 I=1,100
66            XG(I) = A(I,J)
67      350   CONTINUE
68            CALL GR2(XG)
69      360   CONTINUE
70      C
71            DO 370 I=1,100
72            DO 370 J=1,JMAX
73      370   T(I) = T(I) + A(I,J)
74            CALL GR2(T)
75            CALL GREND
76      C----
```

```
77          DO 470 I=1,NTRIAL
78          SUM = SUM + SL(I)
79          SSQ = SSQ + (SL(I) * SL(I) )
80    470   CONTINUE
81          AVE=SUM / NTRIAL
82          SDV=SSQ / NTRIAL - AVE*AVE
83          SDV=SQRT(SDV)
84    C*
85          DO 472 I=1,NTRIAL
86          SLX = ALOG10(SL(I))
87          SUMLG = SUMLG + SLX
88          SSQLG = SSQLG + SLX*SLX
89    472   CONTINUE
90          AVELG = SUMLG / NTRIAL
91          SDVLG = SSQLG / NTRIAL -AVELG*AVELG
92          SDVLG = SQRT(SDVLG)
93    C----
94          WD = .2
95          IF (ENERGY .GT. 1.0E13) WD = 0.1
96          IF (ENERGY .GT. 1.0E16) WD = 0.05
97          AMIN = INT((AVELG - 3.4*SDVLG)/ WD) * WD
98          AMAX = INT((AVELG + 3.7*SDVLG)/ WD) * WD
99          NBIN = (( AMAX - AMIN ) / WD ) +0.0001
100         DO 474 I=1,NTRIAL
101         XSL = ALOG10(SL(I))
102         IF (XSL .GT. AMAX) IBGSL=IBGSL+1
103         IF (XSL .GT. AMAX) GOTO 474
104         IF (XSL .LT. AMIN) ISMSL=ISMSL+1
105         IF (XSL .LT. AMIN) GOTO 474
106         INDEX=((XSL-AMIN)/ WD )+1
107         FREQ(INDEX) =  FREQ(INDEX) + 1
108   474   CONTINUE
109         CALL HISTO(FREQ,NBIN,AMIN,AMAX,WD,AVELG,SDVLG)
110         CALL TB1(JMAX,A,T)
111         CALL TB2(AVE,SDV,AVELG,SDVLG,NBIN,WD,AMIN,AMAX,
112        $ FREQ,ISMSL,IBGSL)
113         CALL TB3(T)
114         STOP
115         END
116   CCCCCCCCCCCCCCCCCCCCCCCCCCCCCCCCCCCCCCCCCCCCCCCCCCCCCCCCCCC
```

```
117     C**1
118           SUBROUTINE MC004(E,Y,A,SL)
119           DIMENSION A(100)
120           DO 100 I=1,100
121     100   A(I) = 0.0
122           SL = 0.0
123           FPI0 = E **0.25
124           EPI0 = .17 * E**0.75
125           FG   = 2.0 * FPI0
126           EG   = 0.5 * EPI0
127           EG = EG * 1.E+9
128           DO 35 I=1,100
129           X = I * 10.0
130           TX = X -Y
131           IF (TX .LE. 0.0) GOTO 35
132           AX = ANUM(EG,TX) * FG
133           A(I)   = A(I)   + AX
134     35    CONTINUE
135           SL = AX
136           RETURN
137           END
```

```
C**2
      SUBROUTINE MC006(E,Y,A,SL)
      DIMENSION A(100)
      DO 100 I=1,100
100   A(I) = 0.0
      SL = 0.0
      W1 = Y
      W2 = W1 +120.
      IF ( W2 .GE. 1000.) GOTO 200
      L1 = ALTI(W1)
      L2 = ALTI(W2)
      FPIC = 2. * E** .25
      EPIC = 0.17 * E ** .75
      D = 0.056 * EPIC
      FPIC = FPIC * EXP(-(L1-L2) / D )
C
120   FPI0 = FPIC * EPIC**0.25
      EPI0 =(1.0/3.0) * EPIC**0.75
      IF(EPI0 .LT. 1.) GOTO 200
      FPIC = 2. * FPI0
      EPIC = EPI0
      D    = 0.056  * EPIC
      EG   = 0.5 * EPI0

C
      EG = EG *1.E9
      DO 140 I=1,100
      X  = I * 10.0
      TX = X - W2
      IF ( TX .LE. 0.0 ) GOTO 140
      AX = ANUM (EG,TX) * 2 * FPIC
      A(I)   = A(I)   + AX
140   CONTINUE
      SL = AX + SL
C
      W3 = W2 + 120.
      IF ( W3 .GE. 1000) GOTO 200
      L3 = ALTI(W3)
      FPIC = FPIC * EXP(-(L2-L3) / D )
      EPIC = EPI0
      L2 = L3
      W2 = W3
      GOTO 120
200   RETURN
      END
```

```
C**3
      FUNCTION ALTI(X)
      IF ( X .GT. 224. ) GOTO 10
      ALTI = 6.38 * ALOG(1300/X)
      GOTO 20
10    ALTI = 12.95 * (3.56 - X ** 0.183)
20    RETURN
      END
C**4
      FUNCTION ANUM(W,X)
      BETA=ALOG(W/84.2E+6)
      T=X/37.7
      S=3*T/(T+2*BETA)
      ANUM=0.31*EXP(T*(1.-1.5*ALOG(S)))
      ANUM=ANUM/SQRT(BETA)
      RETURN
      END
```

```
200     C**5
201           SUBROUTINE GR1
202           COMMON NTRIAL , ENERGY
203           YU = 7.0
204           IF (ENERGY .GT. 1.0E+15) YU = 11.
205           CALL PAPER(1)
206           CALL PSPACE(0.2,0.75,0.35,0.95)
207           CALL MAP(0.0,1100.,-1.,YU)
208           CALL BORDER
209           CALL CTRMAG(12)
210           Y = .95 *YU
211           CALL PLOTCS(50.,Y,'NUMBER OF TRIALS = ',19)
212           CALL TYPENI(NTRIAL)
213           CALL PLOTCS(700.,Y,'ENERGY = 10',11)
214           NENG = ALOG10(ENERGY)+.01
215           CALL SUPFIX
216           CALL TYPENI(NENG)
217           CALL CTRMAG(12)
218           CALL CTRSET(2)
219           CALL PLOTCS(960.,Y, ' E',2)
220           CALL CTRSET(1)
221           CALL TYPECS('V',1)
222           CALL SCALSI(100.,1.)
223           CALL CTRMAG(15)
224           Y = -.2833 * YU
225           CALL PLOTCS(300.,Y,'A',1)
226           CALL CTRSET(2)
227           CALL PLOTCS(300.,Y,' TMOSPHERIC DEPTH ( G CM  )',27)
228           CALL CTRMAG(10)
229           Y = -.26667 * YU
230           CALL PLOTCS(900.,Y,'-2',2)
231           CALL CTRMAG(15)
232           CALL CTRORI(1.)
233           Y = .33333 * YU
234           CALL PLOTCS(-130.,Y,' OG N',5)
235           CALL CTRSET(1)
236           CALL PLOTCS(-130.,Y,'L',1)
237           CALL CTRMAG(10)
238           CALL CTRSET(2)
239           CALL PLOTCS(-100.,Y,'    10',8)
240           CALL PLOTCS(-110.,Y,'       E',10)
241           RETURN
242           END
```

```
C**6
      SUBROUTINE GR2(Z)
      DIMENSION X(100),Y(100),Z(100)
      M=1
      DO 880 I=1,100
880   Y(I)=Z(I)
      DO 900 I=1,100
      X(I)=I*10.0
      IF (Y(I) .EQ. 0.0) GOTO 890
      Y(I)=ALOG10(Y(I))
      GOTO 900
890   M=I+1
900   CONTINUE
       IF (M .GT. 99) GOTO 905
      CALL CURVEO(X,Y,M,100)
905   RETURN
      END

C**7
      SUBROUTINE HISTO(F,N,XMIN,XMAX,WD,AVE,SD)
      COMMON NTRIAL,ENERGY
      DIMENSION F(30)
      XU = XMAX -XMIN
      YU = 200.
      CALL PAPER(1)
      CALL PSPACE(.2,.7,.35,.95)
      CALL MAP(XMIN,XMAX,0.0,YU)
      CALL BORDER
      CALL CTRSET(1)
      CALL CTRORI(0.0)
      CALL CTRMAG(10)
      CALL SCALSI((4*WD),20.)
CC
      CALL HISTGM(XMIN,0.0,WD,F,1,N)
      X=XMIN + XU * .2
      Y=-0.1 * YU
      CALL CTRMAG(15)
      CALL CTRSET(2)
      CALL PLOTCS(X,Y,' OG    UMBER OF  LCTRONS )',26)
      CALL CTRSET(1)
      CALL PLOTCS(X,Y,'L   ( N         E         ',26)
      X = X + XU*0.06
      Y = Y - YU*0.04
      CALL CTRMAG(10)
      CALL PLOTCS(X,Y,'10',2)
      CALL CTRORI(1.)
      CALL CTRMAG(15)
      X=XMIN -XU *.15
      Y= YU / 3.
      CALL PLOTCS(X,Y,'FREQUENCY',9)
      CALL CTRORI(0.0)
      CALL CTRSET(1)
      CALL CTRMAG(12)
      X= XMIN + XU * .1
      Y= YU * .95
```

```
297           CALL PLOTCS(X,Y,'INITIAL ENERGY = 10',19)
298           NG   = ALOG10(ENERGY) + .1
299           CALL SUPFIX
300           CALL TYPENI(NG)
301           CALL SUFFIX
302           CALL CTRSET(2)
303           CALL CTRMAG(12)
304           CALL TYPECS(' E',2)
305           CALL CTRSET(1)
306           CALL TYPECS('V',1)
307           CALL CTRSET(2)
308           X=XMIN + XU * .4
309           Y=YU * .9
310           CALL PLOTCS(X,Y,' UMBER OF  RIALS =',18)
311           CALL CTRSET(1)
312           CALL PLOTCS(X,Y,'N         T       ',18)
313           CALL TYPENI(NTRIAL)
314           Y=YU * .86
315           CALL PLOTCS(X,Y,'M',1)
316           CALL CTRSET(2)
317           CALL TYPECS('EAN =',5)
318           CALL CTRSET(1)
319           CALL TYPENE(AVE,6)
320           CALL CTRSET(4)
321           Y=YU * .82
322           CALL CTRMAG(20)
323           CALL PLOTCS(X,Y,' S ',3)
324           CALL CTRSET(1)
325           CALL CTRMAG(12)
326           CALL PLOTCS(X,Y,'     =',6)
327           CALL TYPENE(SD,6)
328           CALL GREND
329           RETURN
330           END
```

```
C**8
      SUBROUTINE TB1(JMAX,A,T)
      DIMENSION A(100,40),T(100)
      COMMON NTRIAL,ENERGY
      WRITE(6,475)ENERGY
475    FORMAT(//  ' INTIAL ENERGY =',1PE7.1,3H EV)
      WRITE(6,476)NTRIAL
476    FORMAT(' NUMBER OF TRIALS = ',I4)
      WRITE(6,488)
      DO 480 J=1,JMAX
      WRITE(6,482)J
      WRITE(6,484)
      DO 478 I=10,100,10
      IX = 10 * I
478   WRITE(6,486)IX,A(I,J)
      WRITE(6,488)
480   CONTINUE
482   FORMAT(20H INTERACTION NUMBER ,I3)
484   FORMAT(20H   DEPTH          NE)
486   FORMAT(3X,I4,10X,1PE11.5)
488   FORMAT(30H ------------------------------//)
      WRITE(6,489)
489   FORMAT(20H       * T O T A L *)
      WRITE(6,484)
      DO 490 I=10,100,10
      IX = 10 * I
490   WRITE(6,486)IX,T(I)
      WRITE(6,492)
492   FORMAT(30H ------------------------------////)
      RETURN
      END
```

```
C**9
      SUBROUTINE TB2(AVE,SDV,AVELG,SDVLG,NBIN,WD,AMIN,AMAX,
     $ FREQ,ISMSL,IBGSL)
      DIMENSION FREQ(40)
      WRITE(6,505)
      WRITE(6,506)
505   FORMAT (38H INFORMATION ABOUT THE TOTAL NUMBER OF)
506   FORMAT (22H ELECTRON AT SEE LEVEL/)
      WRITE(6,510) AVE
510   FORMAT (11H AVERAGE = ,1PE11.5)
      WRITE(6,512) SDV
512   FORMAT (22H STANDARD DEVIATION = ,1PE11.5)
      WRITE(6,514) AVELG
514   FORMAT (23H AVERAGE OF LOG (N E) =,F7.4)
      WRITE(6,516) SDVLG
516   FORMAT (34H STANDARD DEVIATION OF LOG(N E) = ,F7.4//)
      WRITE(6,520)
520   FORMAT (42H   LOG ( NUMBER OF ELECTRON )    FREQUENCY/)
      DO 530 I=1,NBIN
      XX1=(I-1)* WD + AMIN
      XX2=XX1 + WD
530   WRITE(6,531)XX1,XX2, FREQ(I)
531   FORMAT (5X,F5.2,' -- ',F5.2,13X,F5.0)
      WRITE(6,532)AMIN,ISMSL
532   FORMAT (1X,14H LESS    THAN ,F8.5,' = ',I6)
      WRITE(6,534)AMAX,IBGSL
534   FORMAT (1X,14H GREATER THAN ,F8.5,' = ',I6)
      RETURN
      END
C**10
      SUBROUTINE TB3(T)
      DIMENSION T(100)
      COMMON NTRIAL,ENERGY
      WRITE(7,605)ENERGY
605   FORMAT('  100                 |  INTIAL ENERGY =',1PE7.1,' EV |')
610   FORMAT(3X,F6.0,10X,1PE11.5)
      DO 615 I=1,100
       X = 10 * I
615   WRITE(7,610) X,T(I)
      RETURN
      END
```

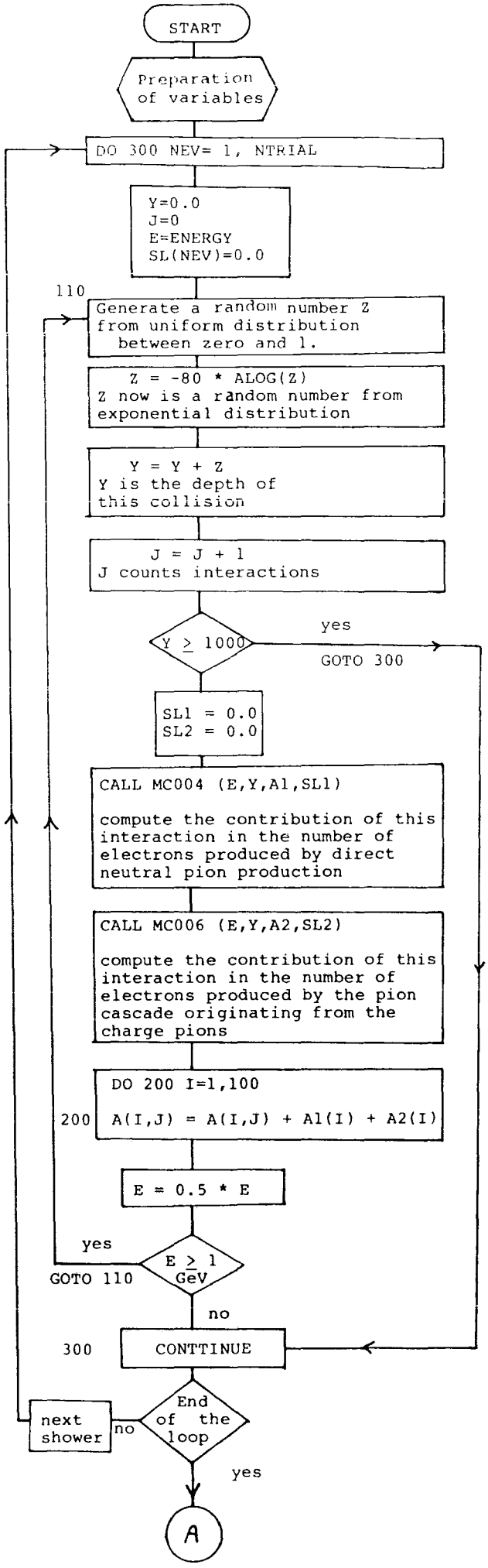

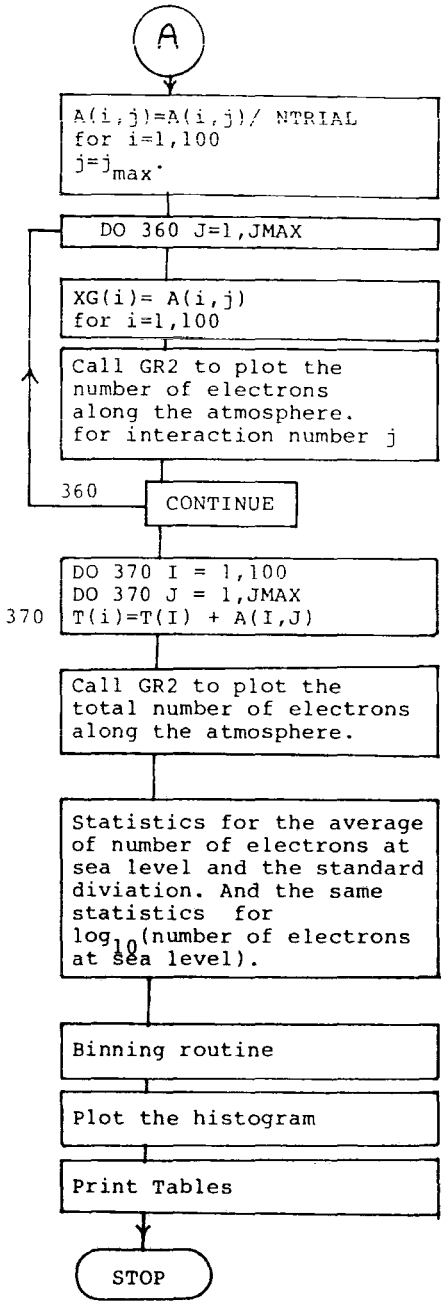

Figure 6.15:

Flowchart of MC007.

FIGURE 6.16

Outputs of Program MC007.

Figures 6.16a.1 to 6.16a.8

Outputs of the program MC007. The simulation of the average number of electrons arriving at different atmospheric depths produced as a primary nucleon propagates through the atmosphere. The uper most curve is the average of the total of the number of elctrons in the shower, the other curves are for the average of the electron number contributed by each protonic collision. Each Figure is for a given proton initial energy which is written on the top of the plot.

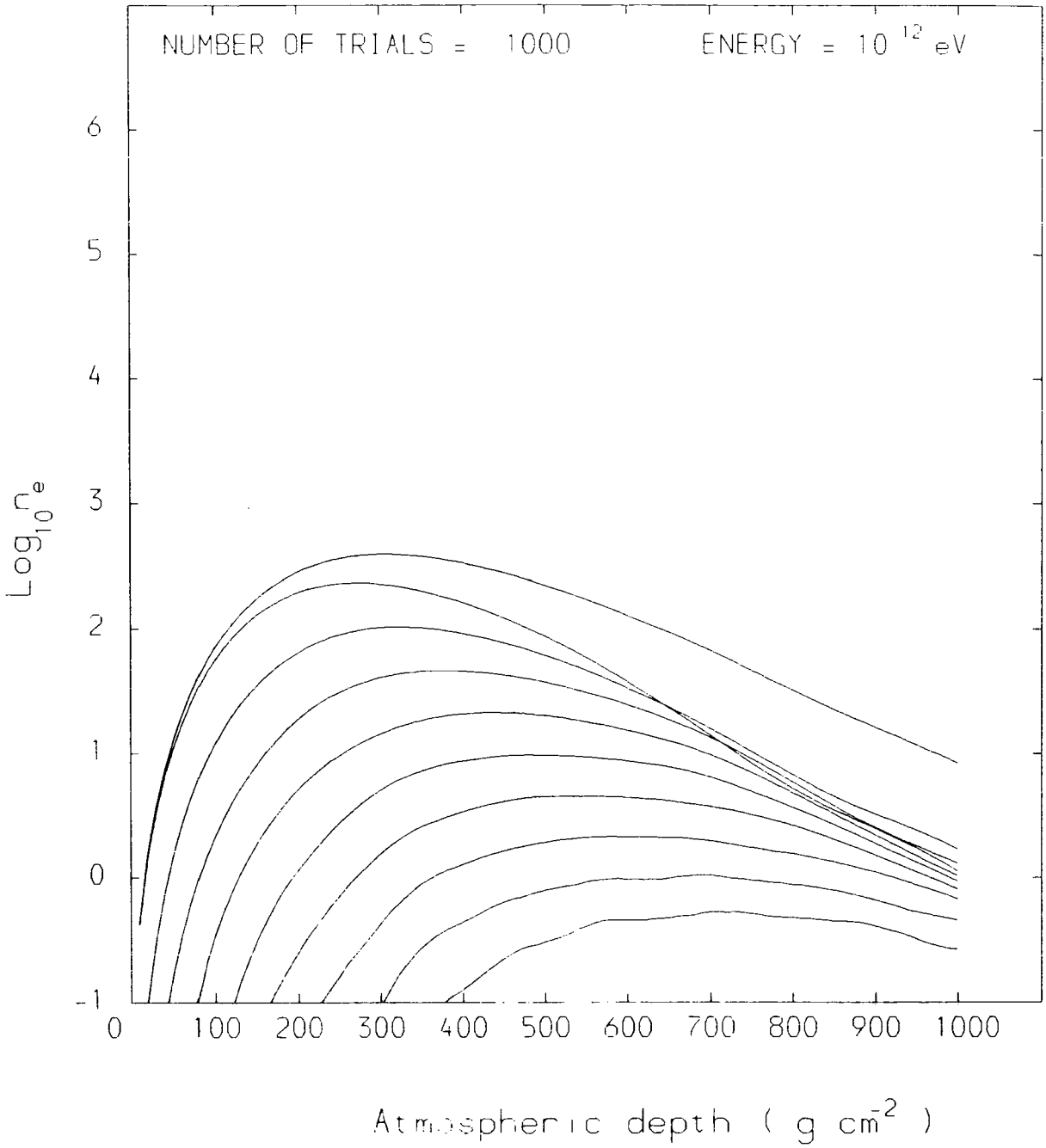

Figure 6.16a.1: See the heading page for caption.

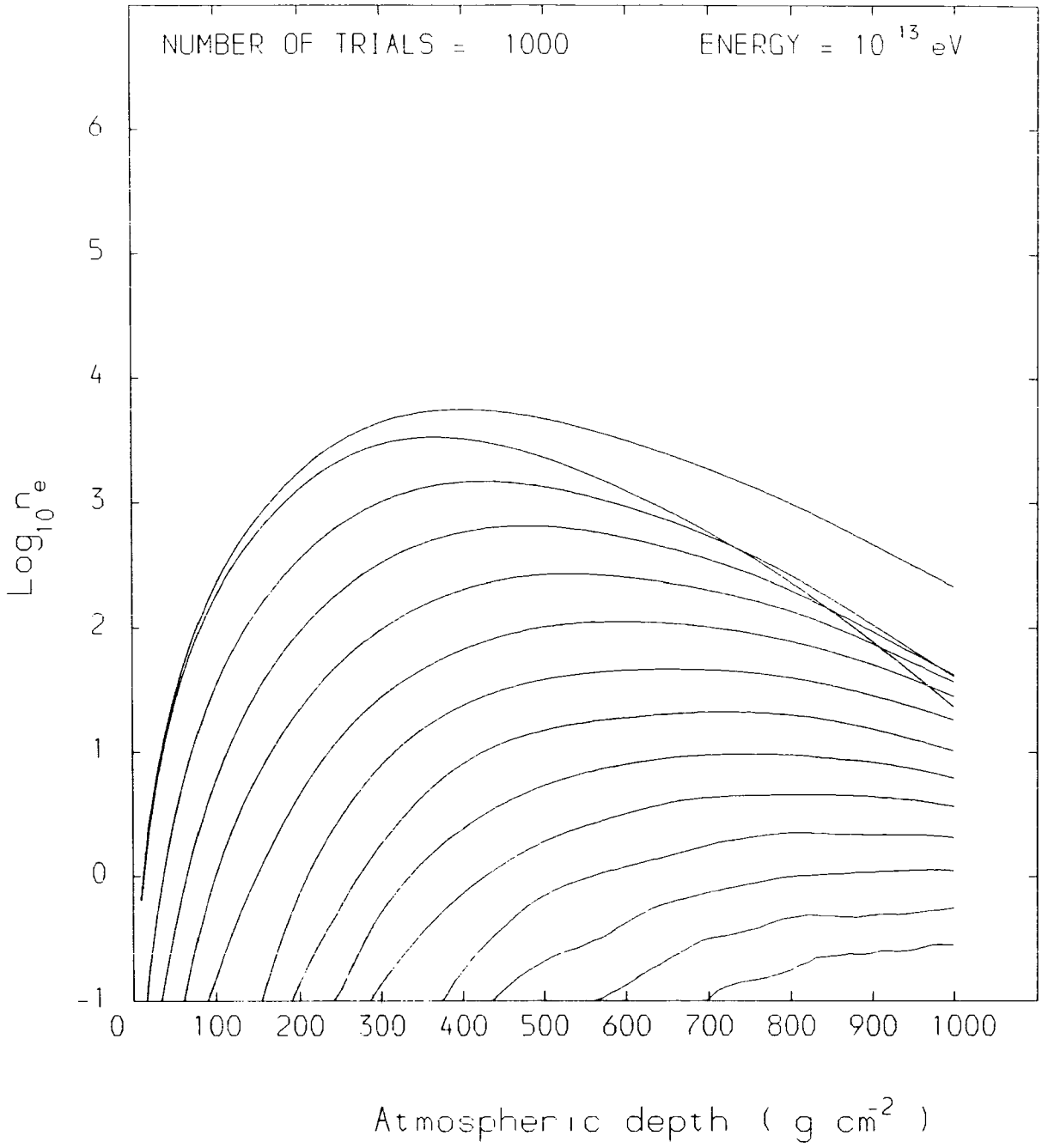

Figure 6.16a.2: See the heading page for caption.

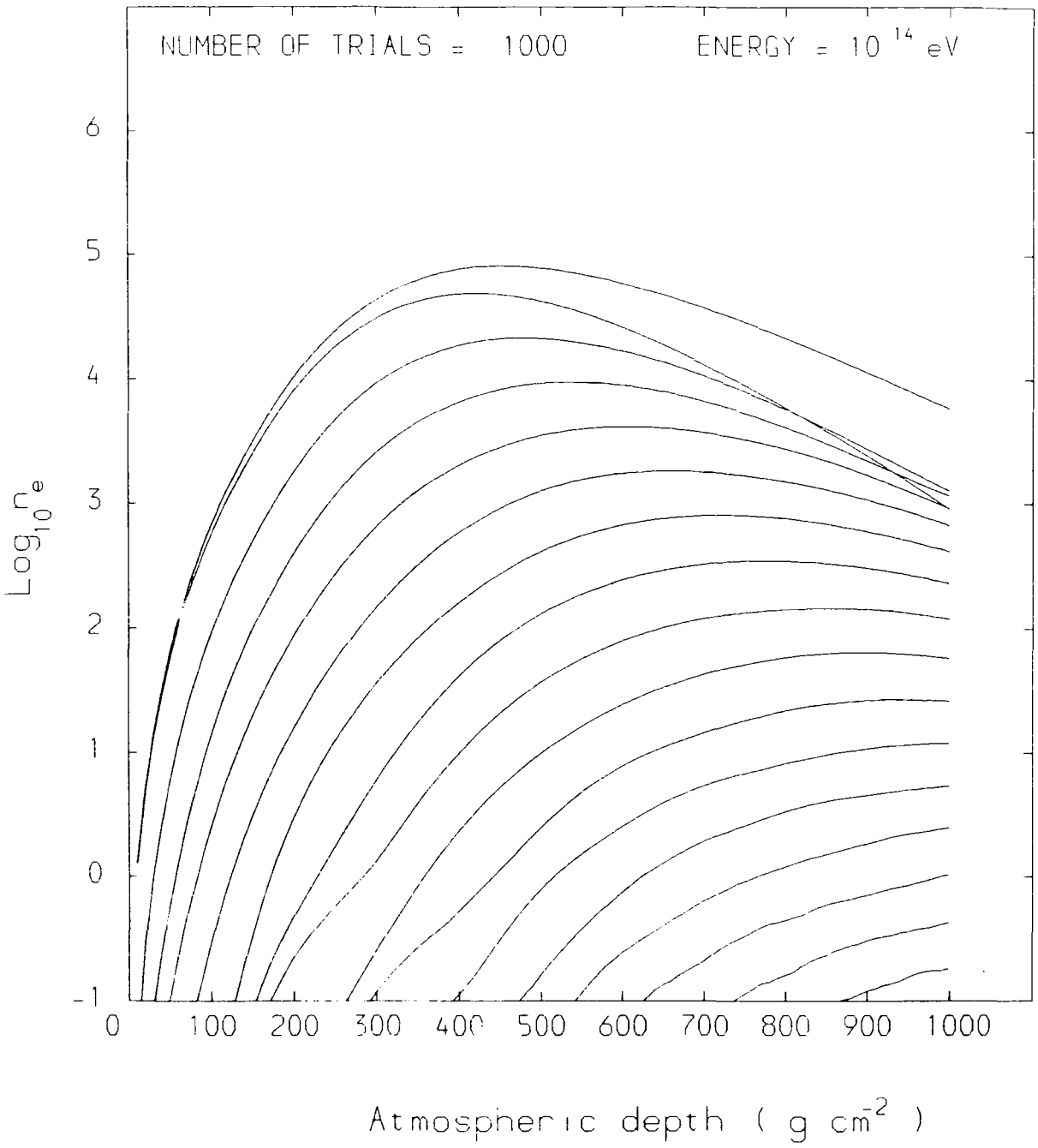

Figure 6.16a.3: See the heading page for caption.

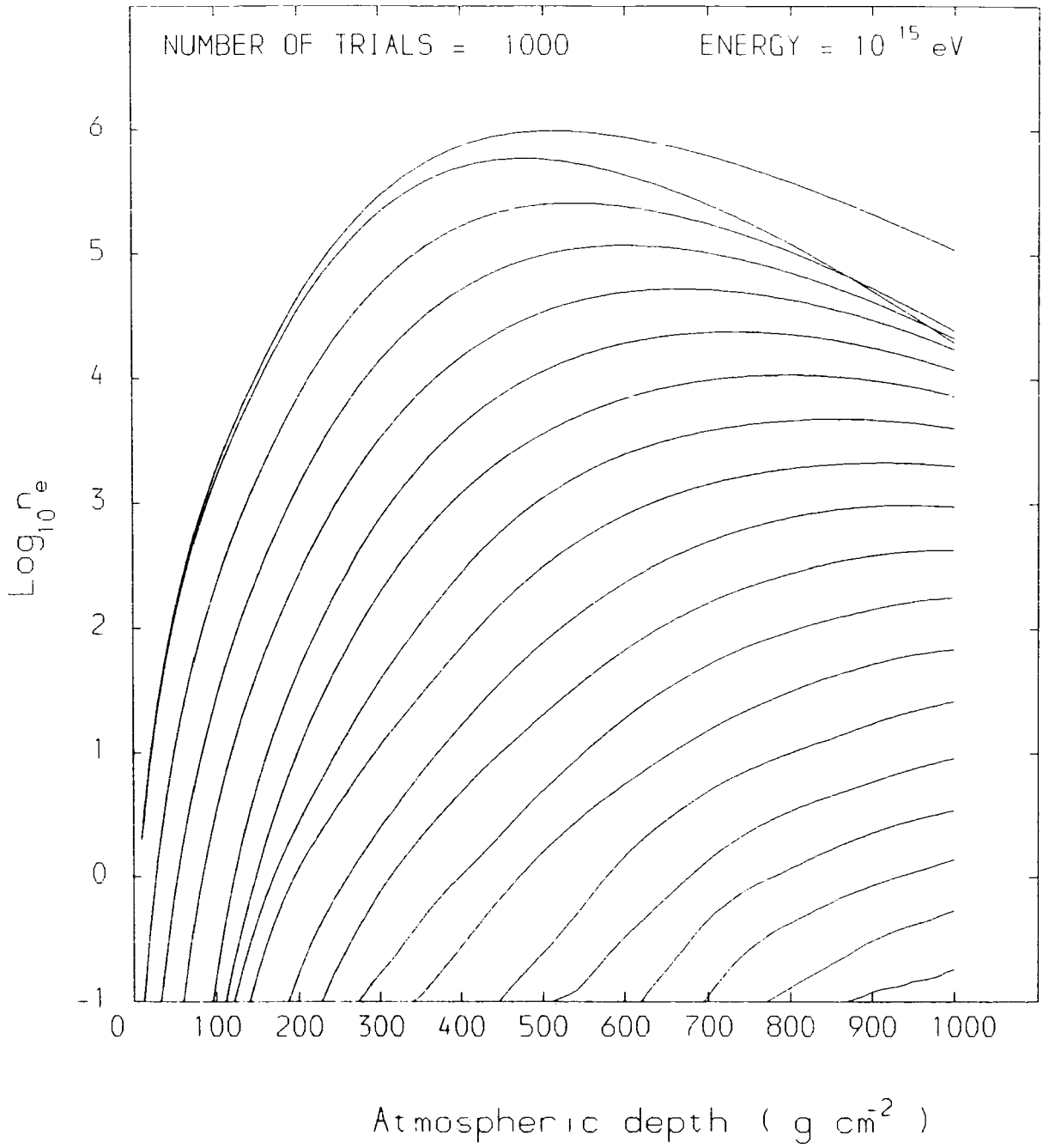

Figure 6.16a.4: See the heading page for caption.

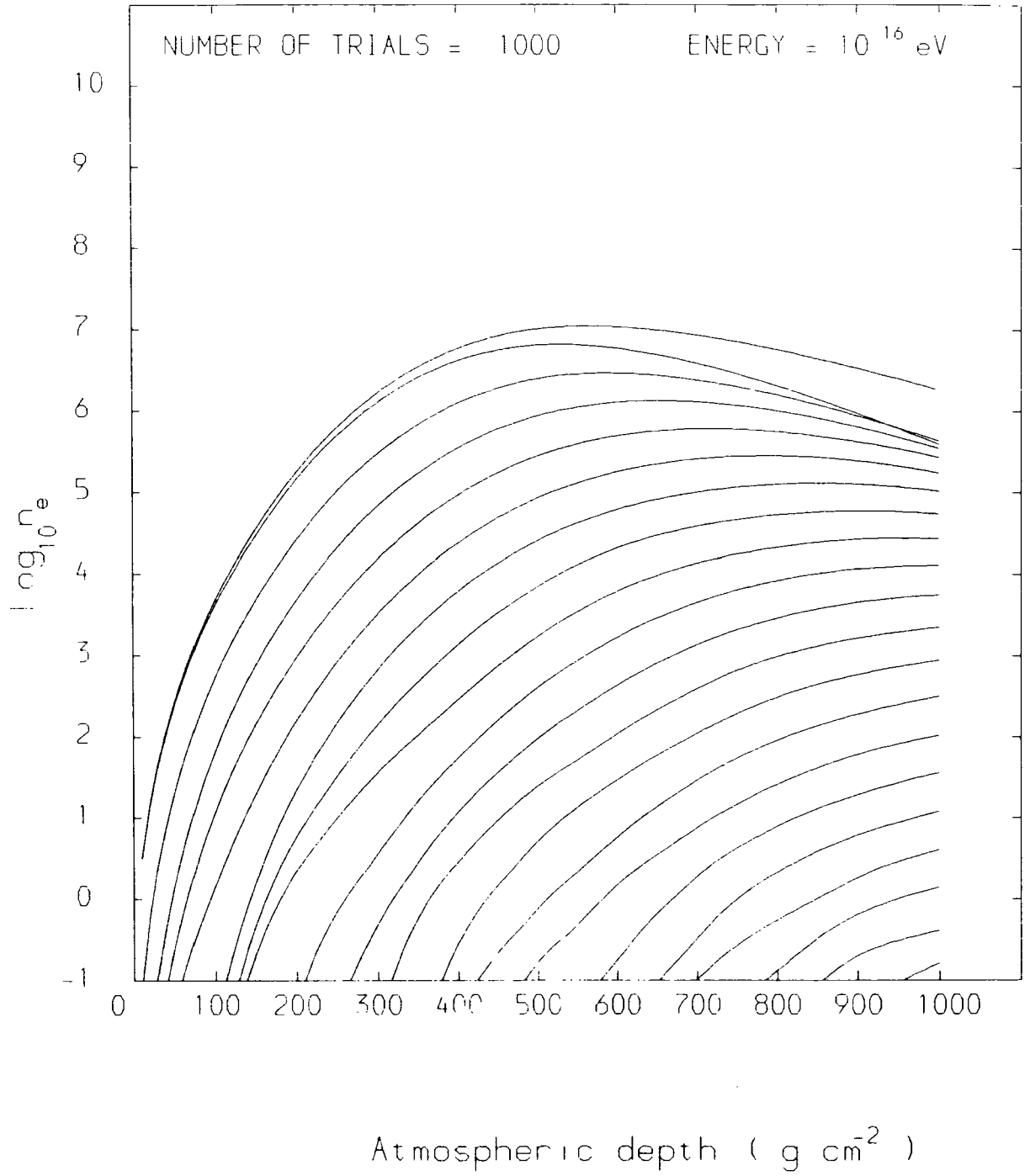

Figure 6.16a.5: See the heading page for caption.

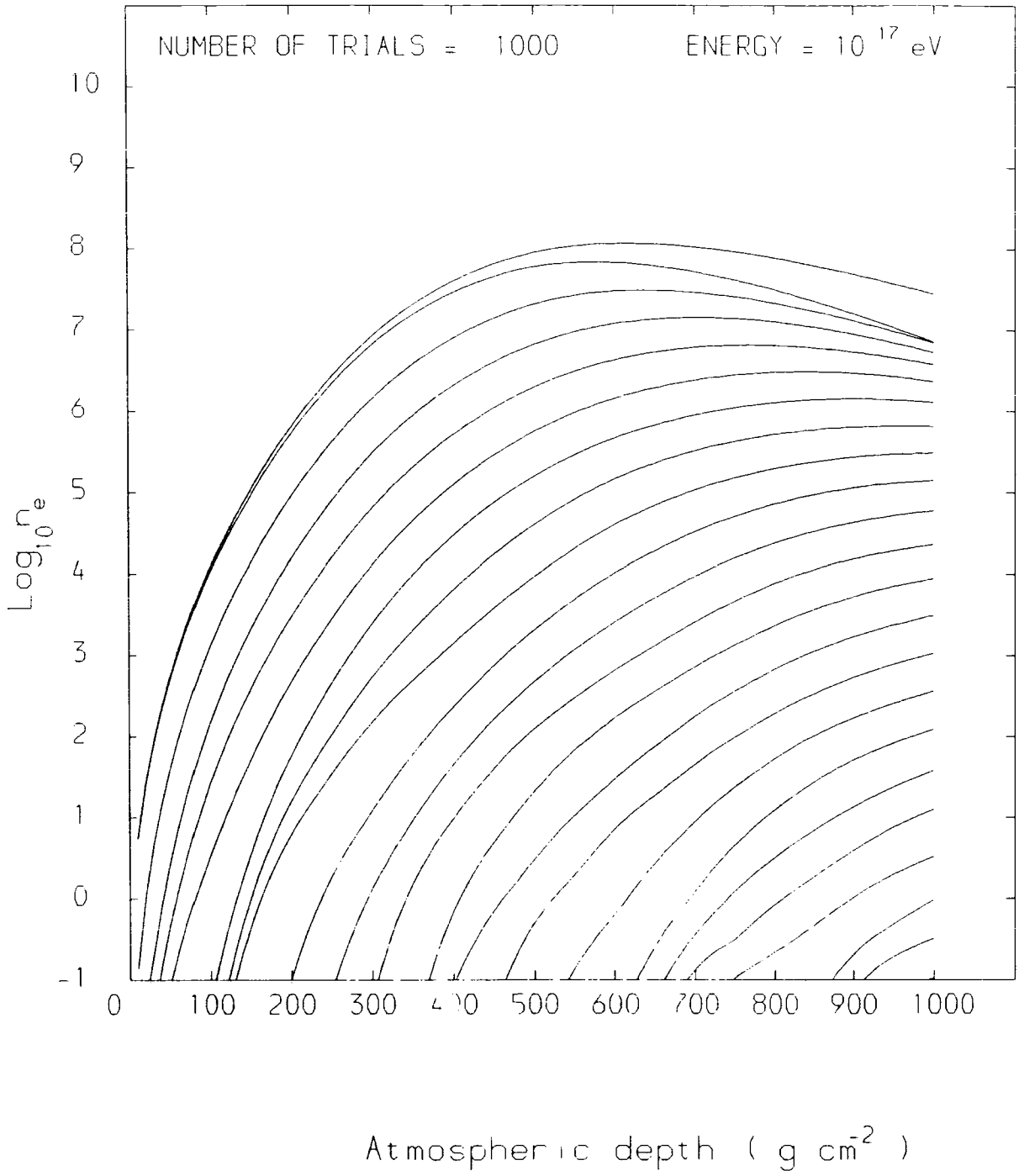

Figure 6.16a.6: See the heading page for caption.

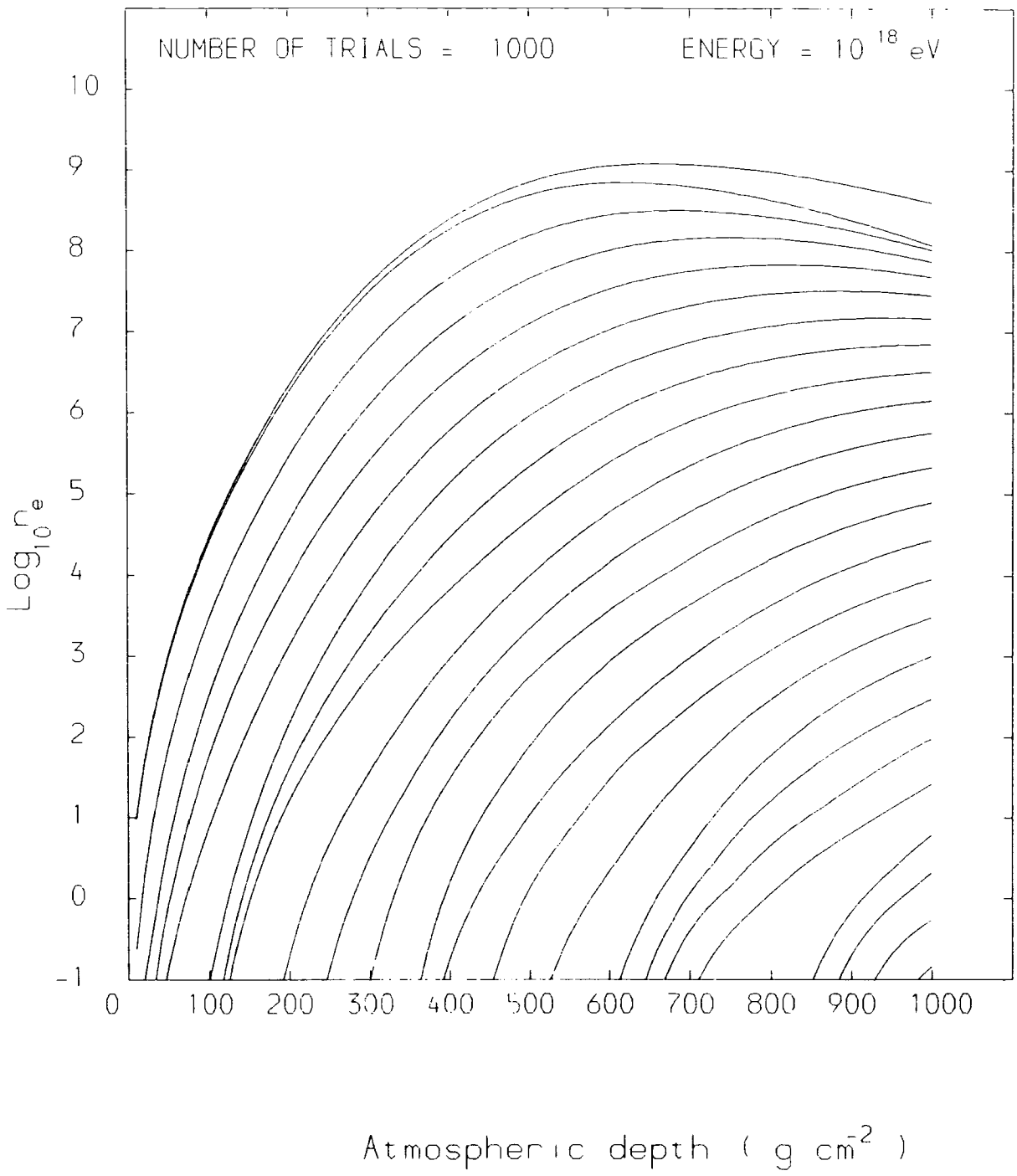

Figure 6.16a.7: See the heading page for caption.

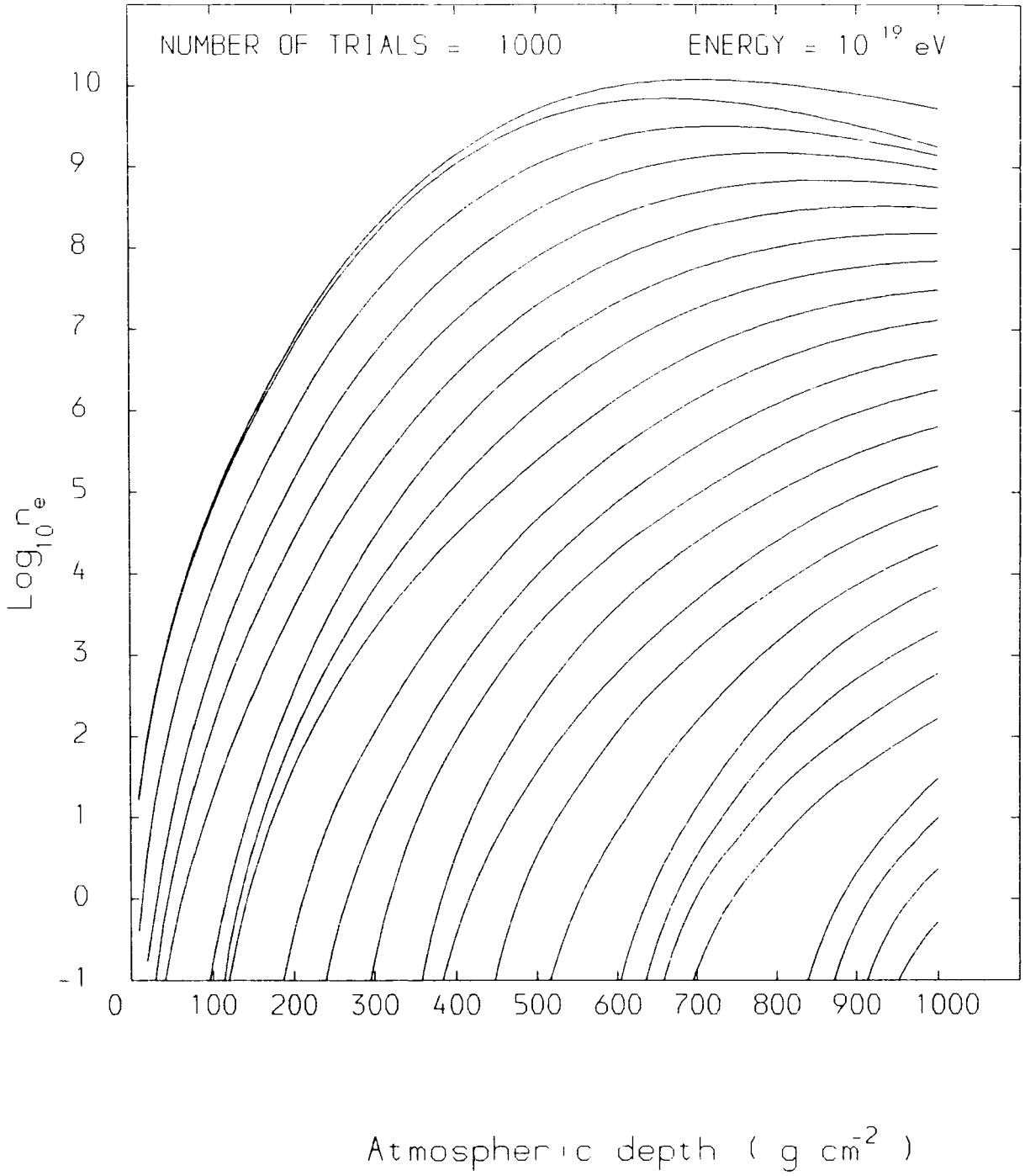

Figure 6.16a.8: See the heading page for caption.

Figures 6.16b.1 to 6.16b.8

The distribution of the $\log_{10}$ of number of electrons at sea-level as it was calculated by the program MC007. Each distribution is for a given proton initial energy which is written on the top of the plot.

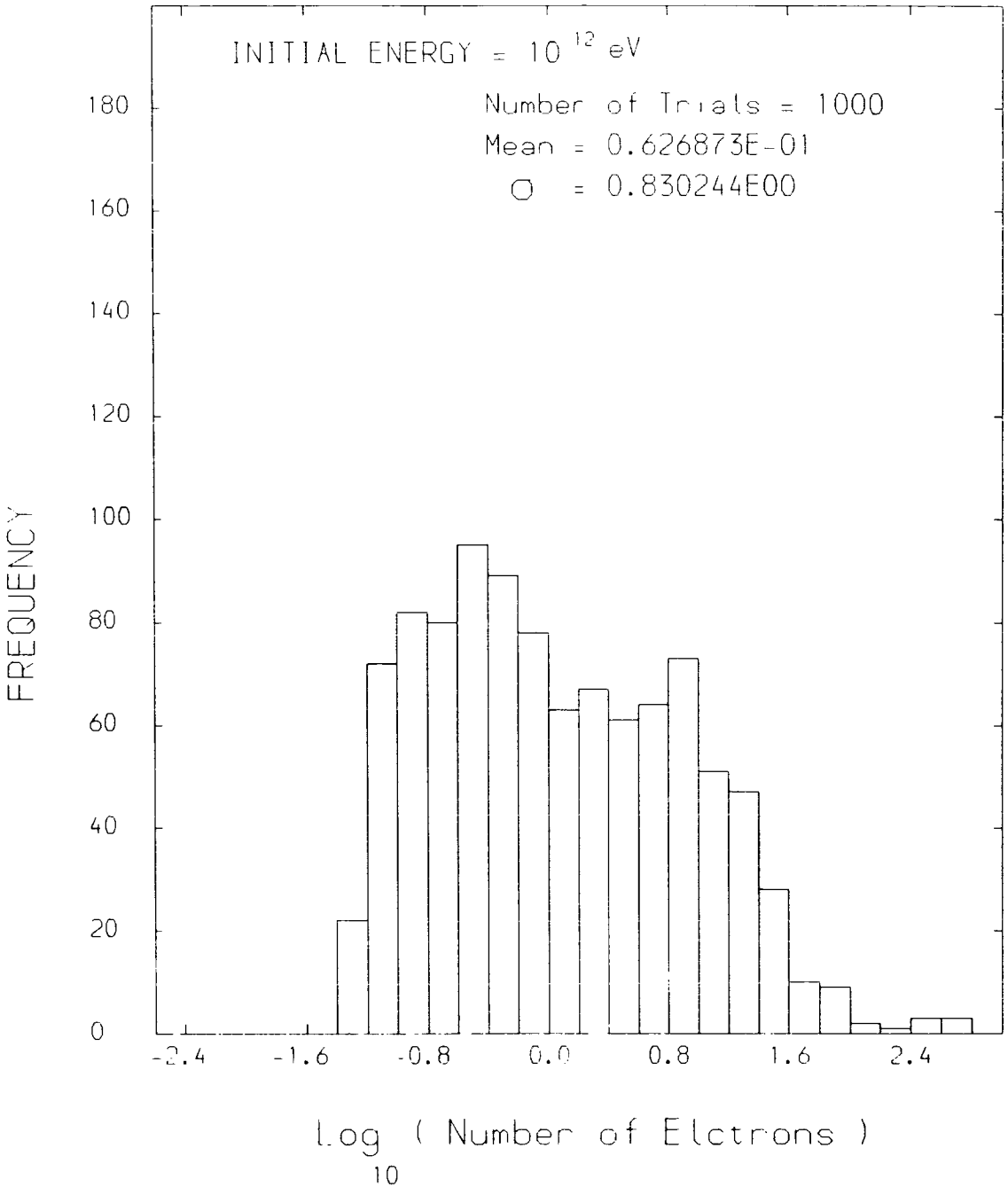

Figure 6.16b.1: See the heading page for caption.

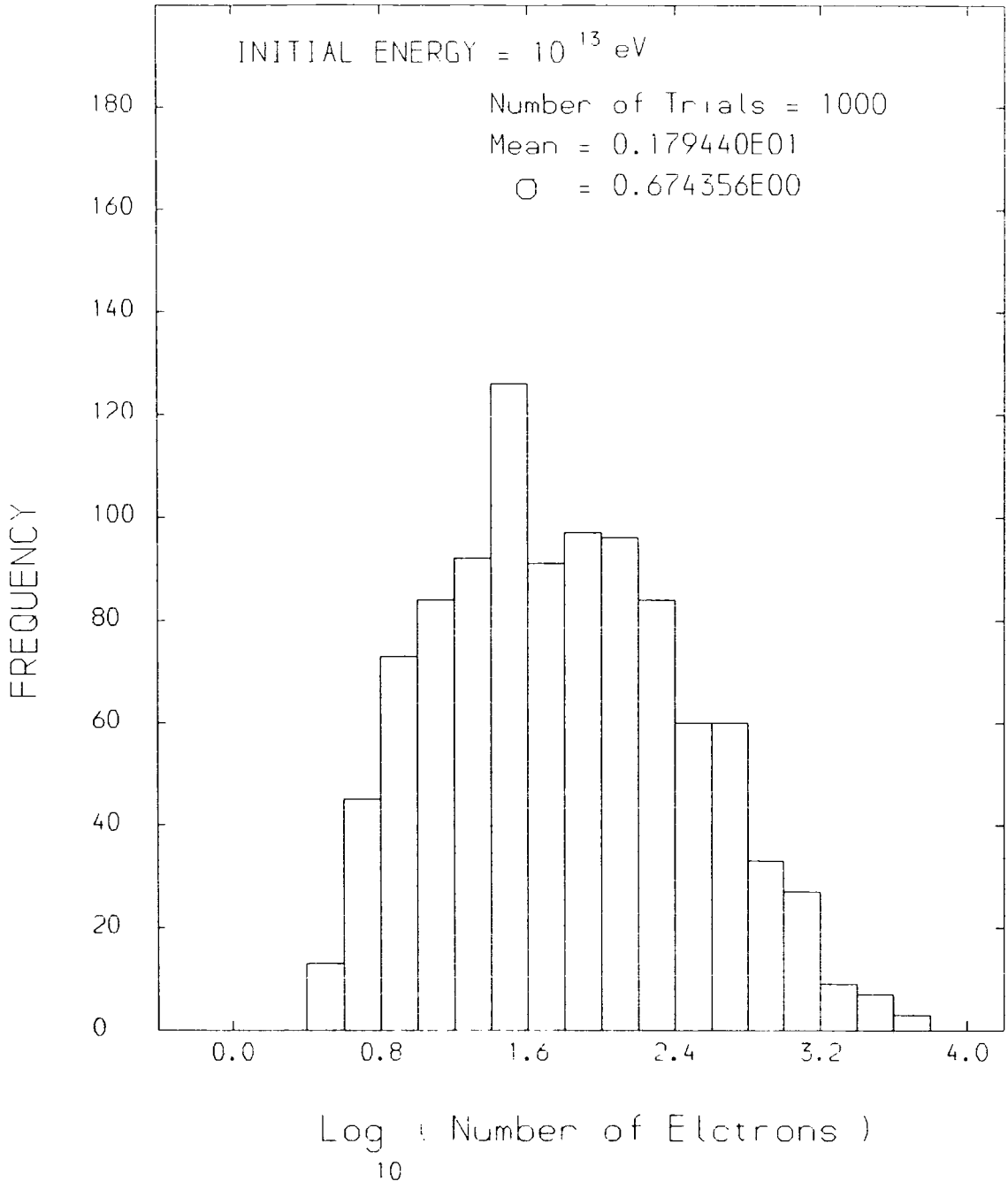

Figure 6.16b.2: See the heading page for caption.

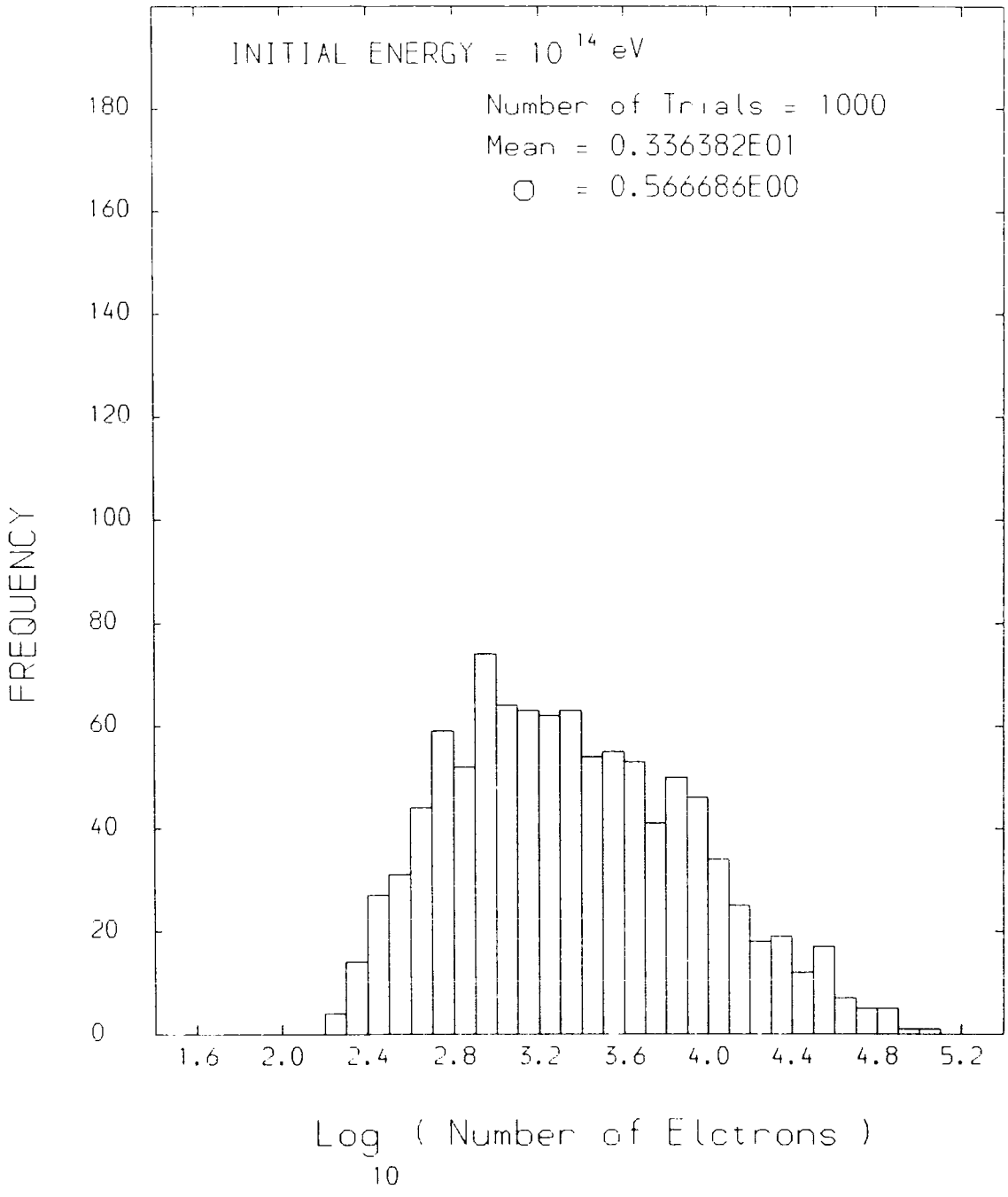

Figure 6.16b.3: See the heading page for caption.

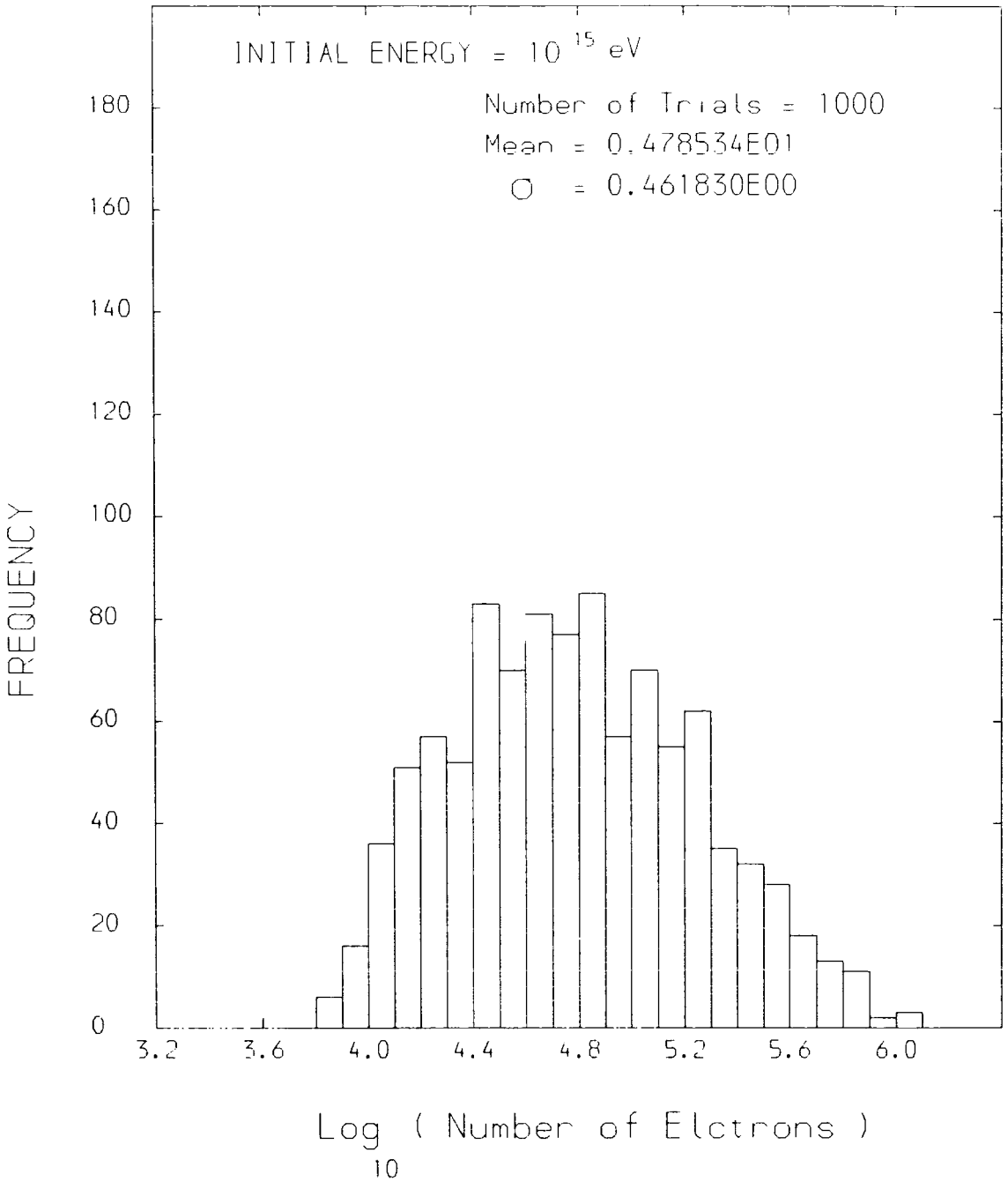

Figure 6.16b.4: See the heading page for caption.

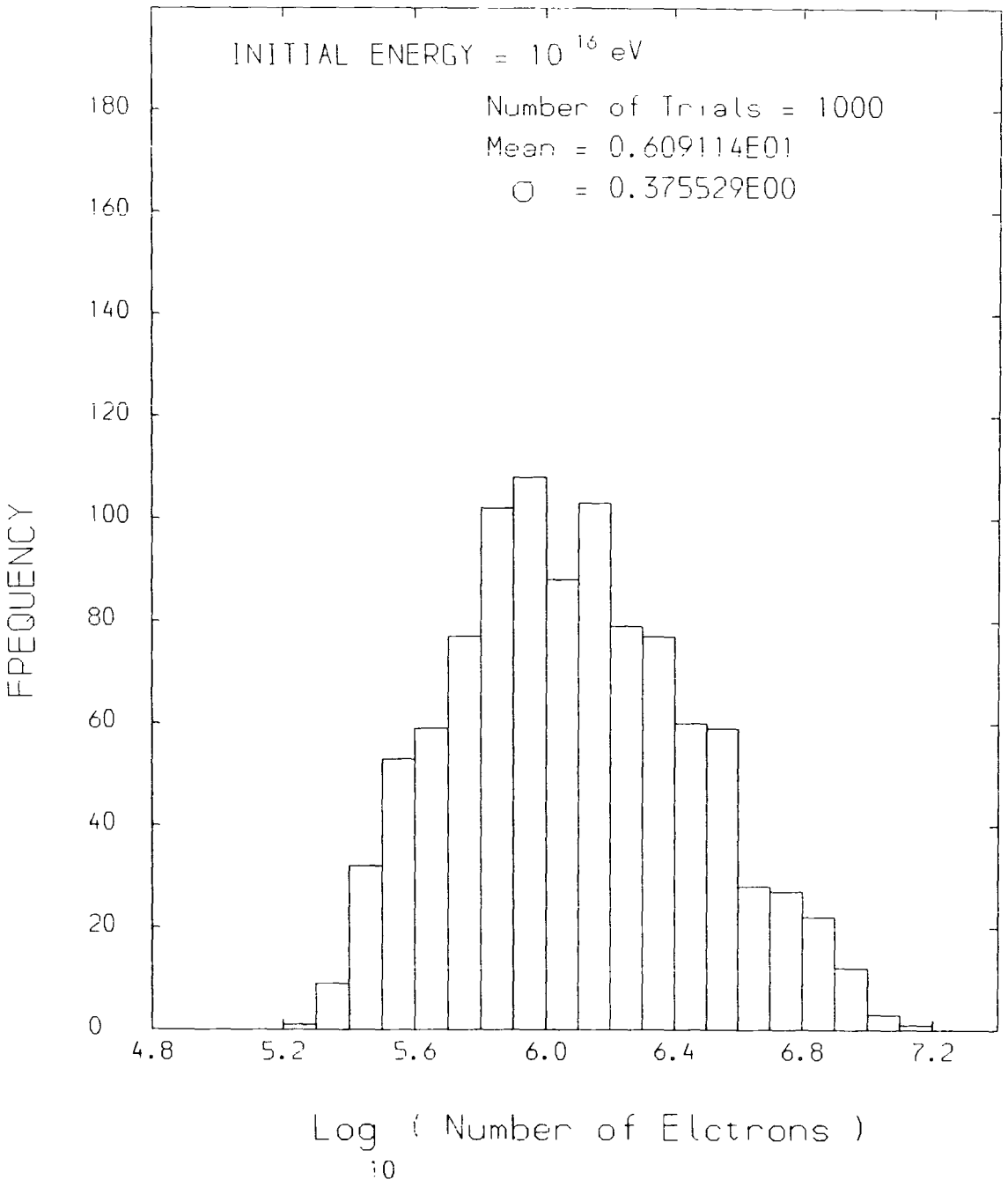

Figure 6.16b.5: See the heading page for caption.

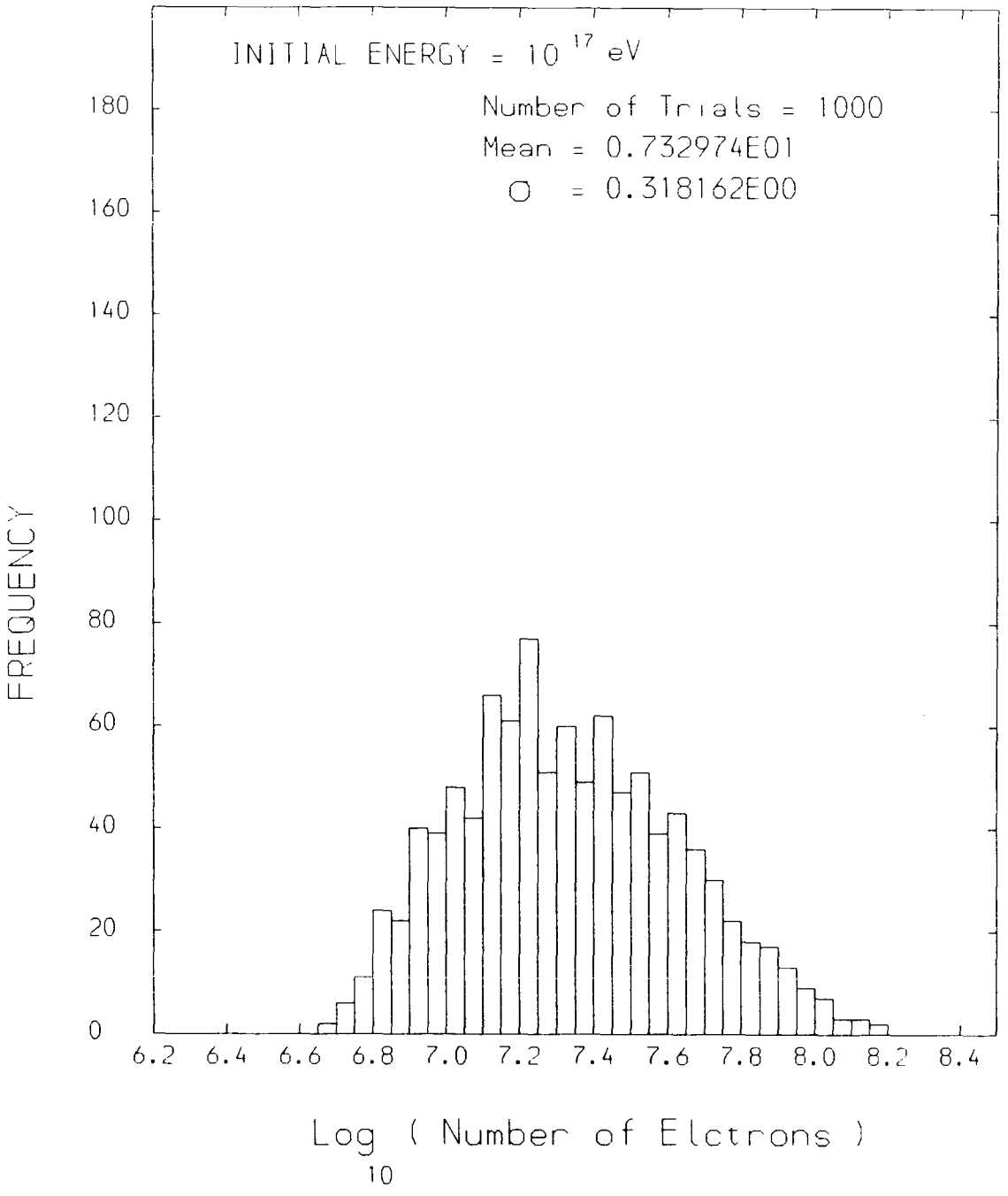

Figure 6.16b.6: See the heading page for caption.

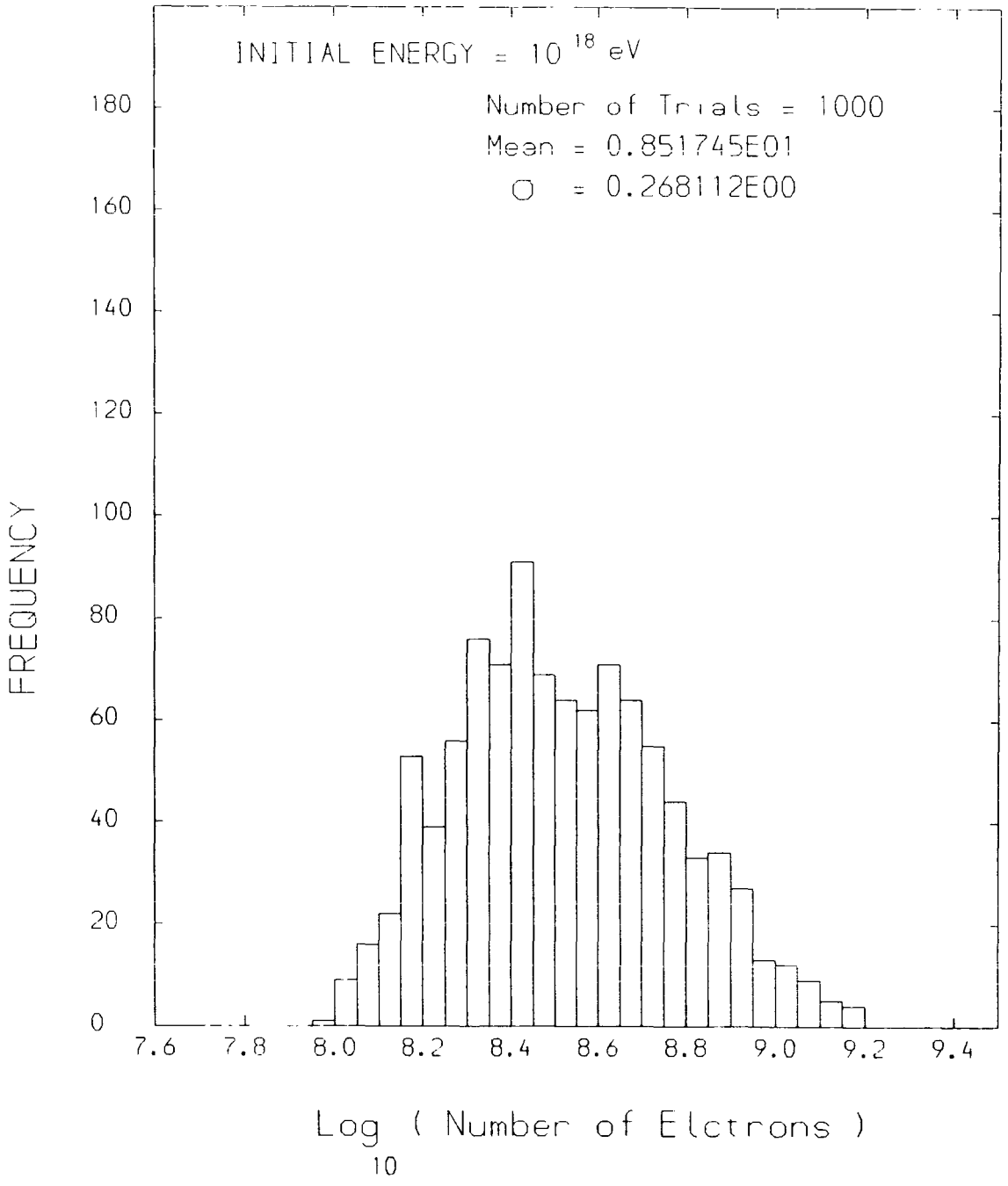

Figure 6.16b.7: See the heading page for caption.

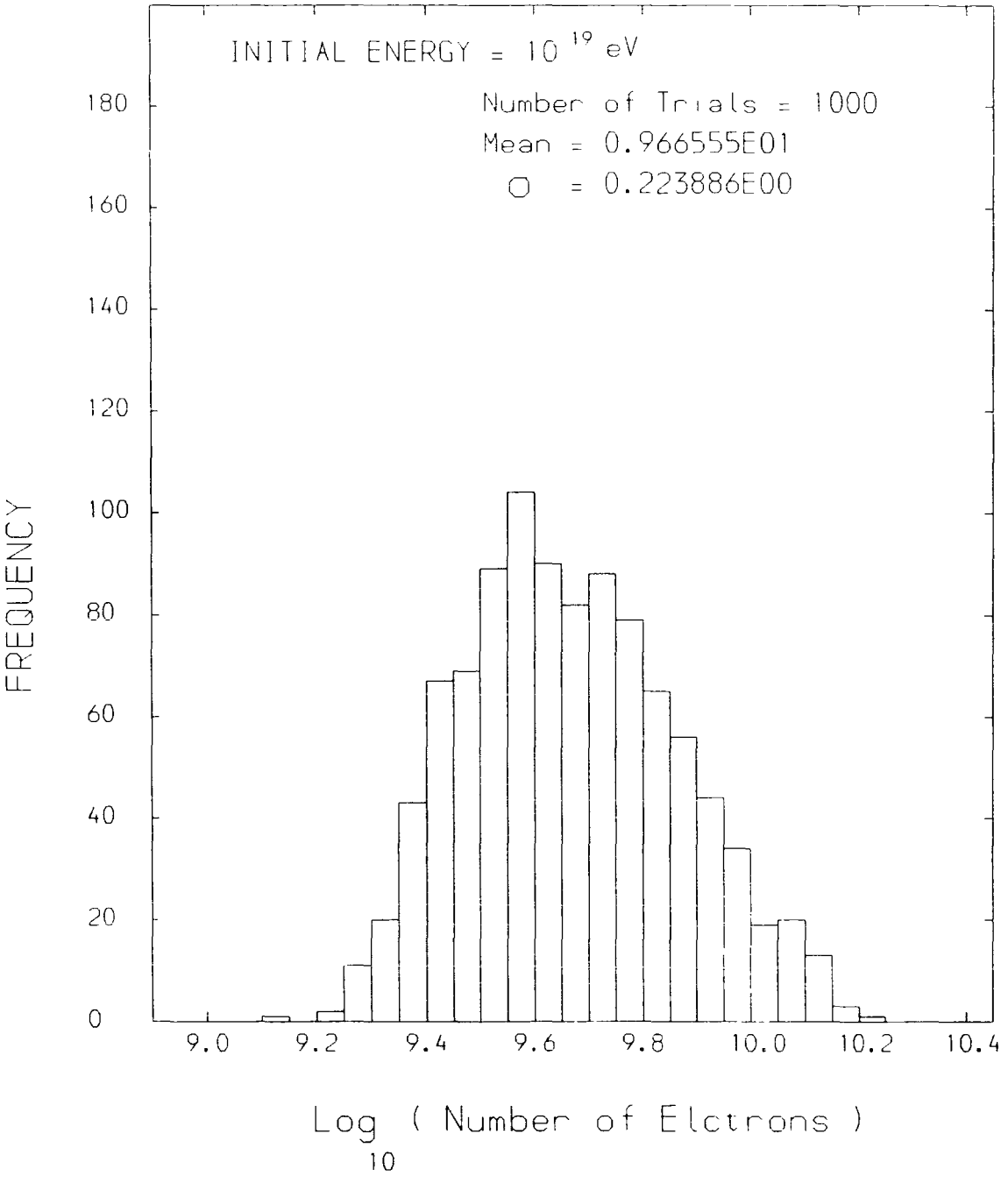

Figure 6.16b.8: See the heading page for caption.

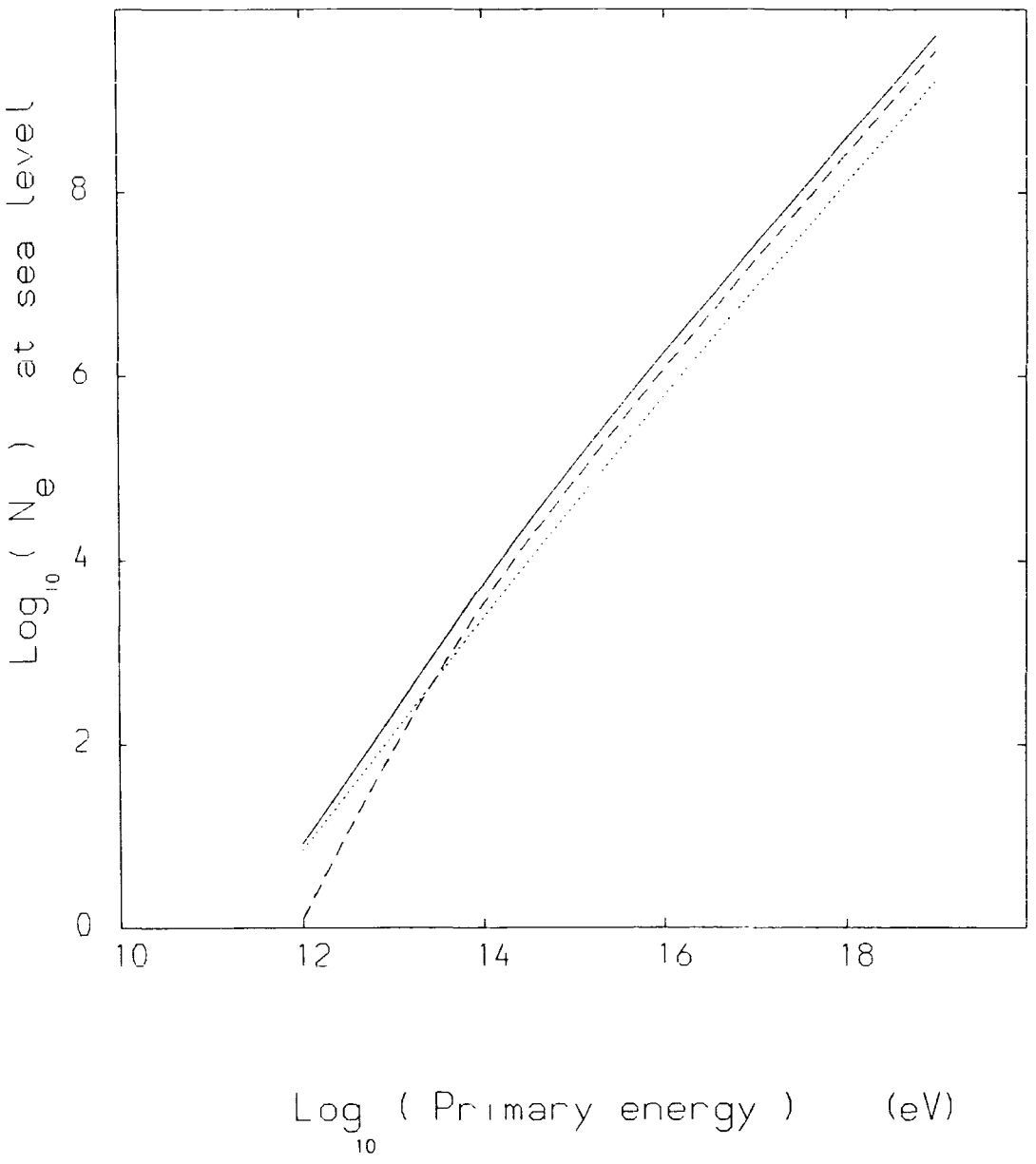

Figure 6.17: Average size of showers at sea level as a function of the primary proton energy, calculated by simulation. Solid curve is the simulation by program MC007. Dashed curve is the simulation by MC006 (number of electrons produced by pion cascade orignating from charged pions). Dotted curve is the simulation by MC004 (number of electrons produced by neutral pion production only)

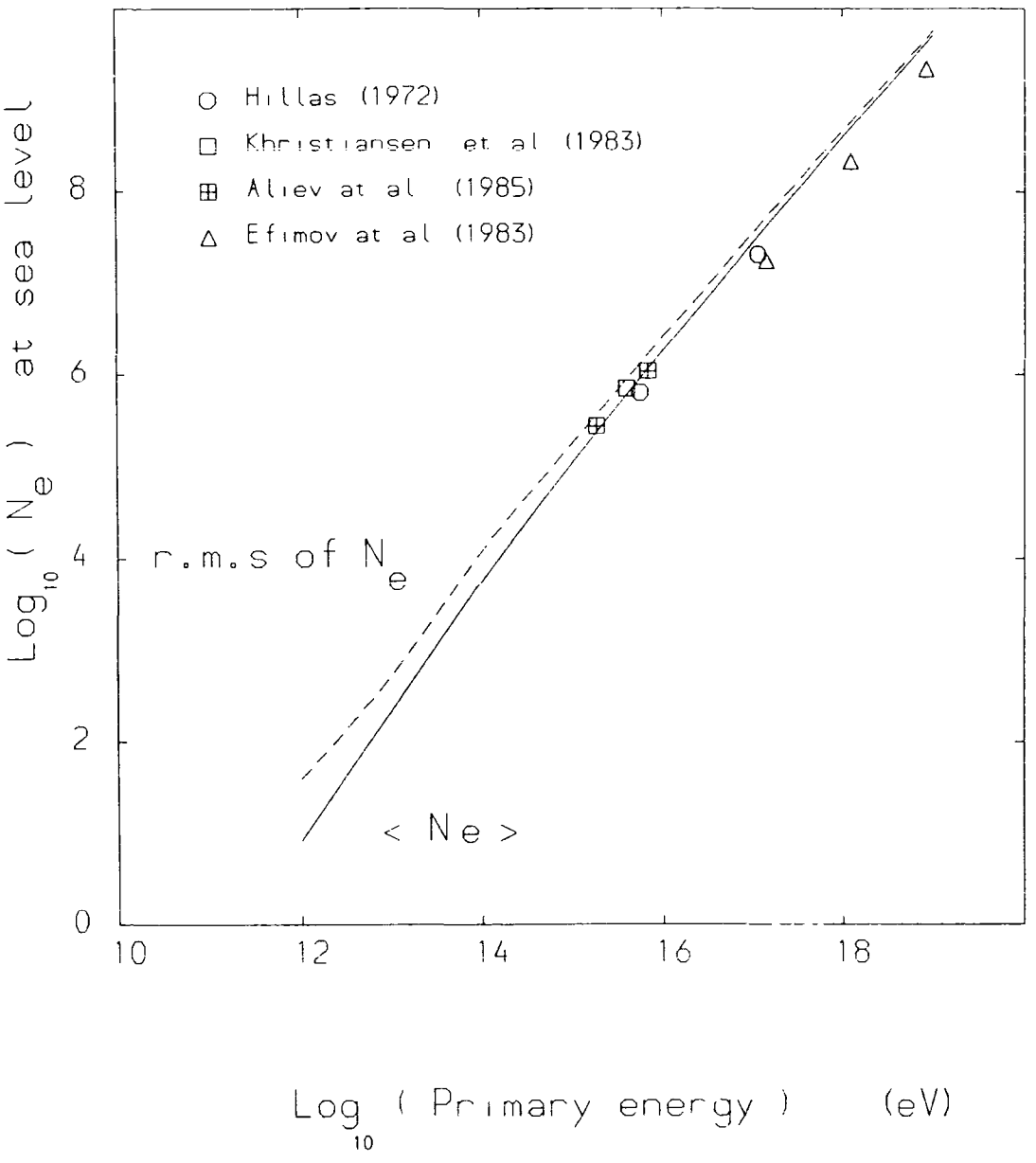

Figure 6.18: Average size of showers at sea level as a function of the primary proton energy, calculated by simulation program MC007. The solid curve is the averave of 1000 simullated results and the dashed curve is the root mean squares of the same sample. Some experimental data are plotted for comparison.

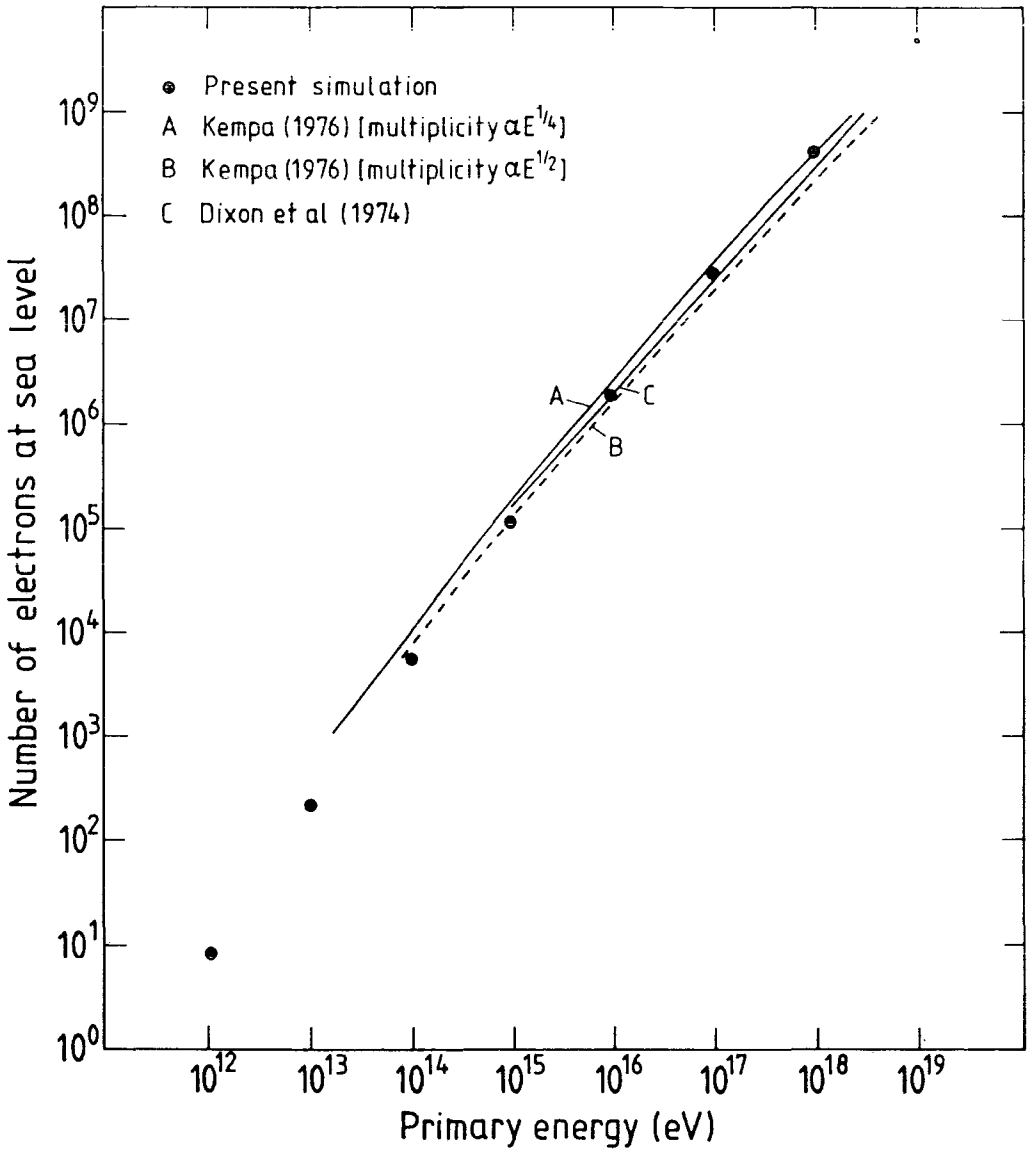

Figure 6.19: Average size of showers at sea level as a function of the primary proton energy, calculated by simulation. The present simulation (solid circles) is compared with some previous works.

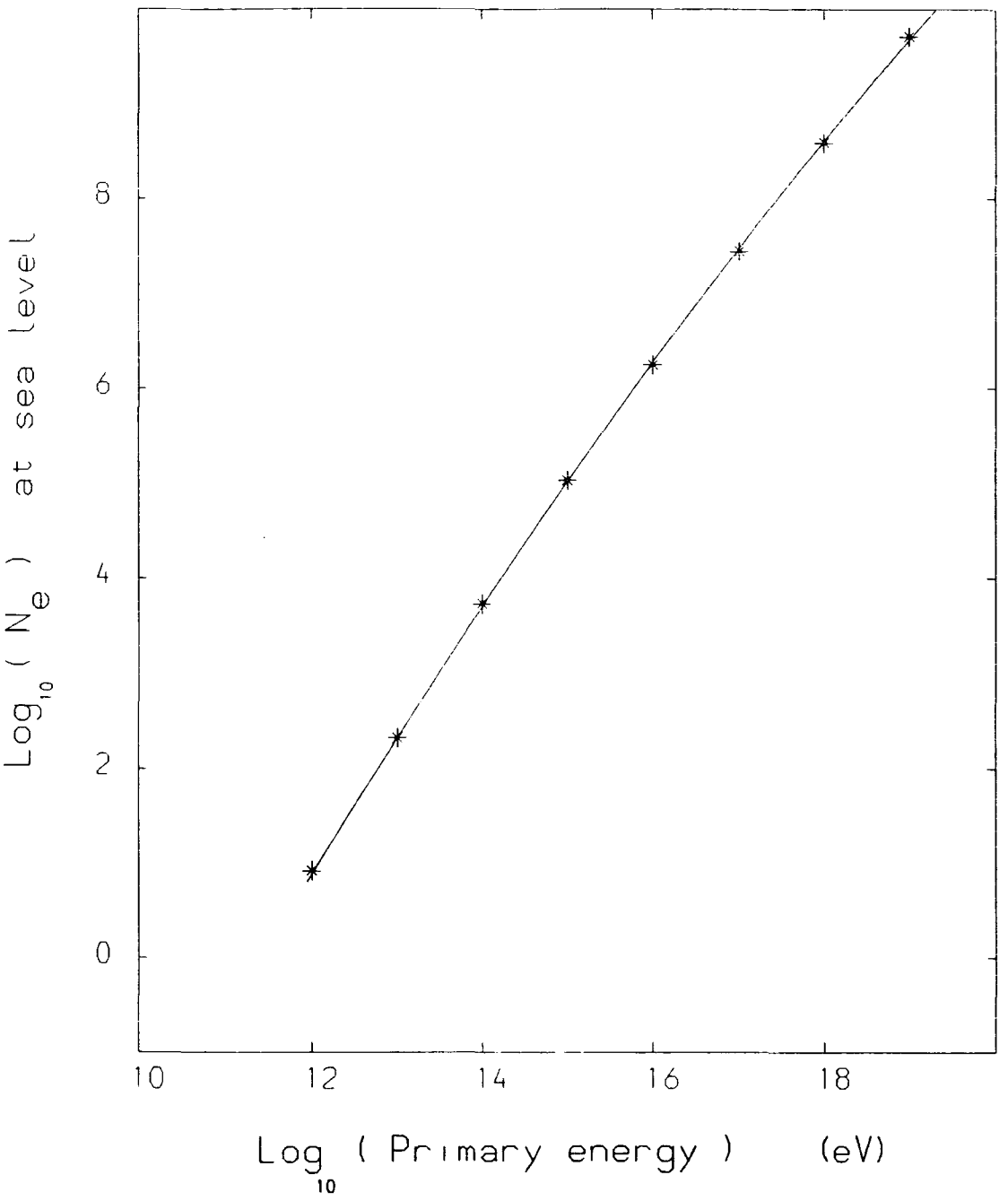

Figure 6.20: The best fit (solid curve) of the average simulated shower size at sea level as a function of the primary proton energy, simulated by the program MC007 (stars). The curve is discribed by:

$\log_{10}(N_e) = -21.27 + 2.22 \log_{10}E_p - 0.031 (\log_{10}E_p)^2$

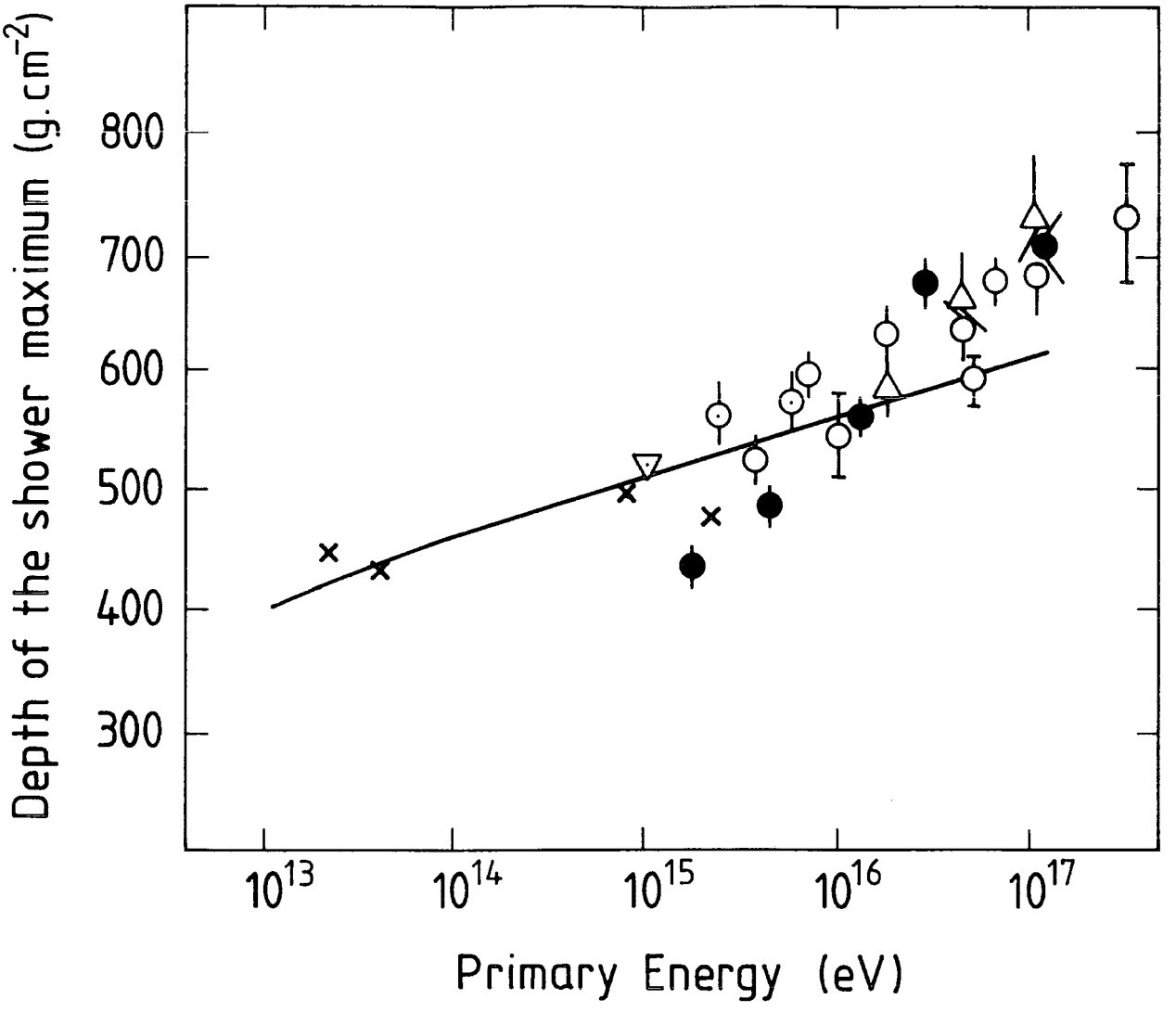

Figure 6.21: The depth of shower size maximum as a function of primary nucleon energy. It is the depth at which the average longitudinal development of electron number reaches its maximum. Some experimental data collected by Capdevielle and Gawin (1985) are compared with the result of the present simulation.

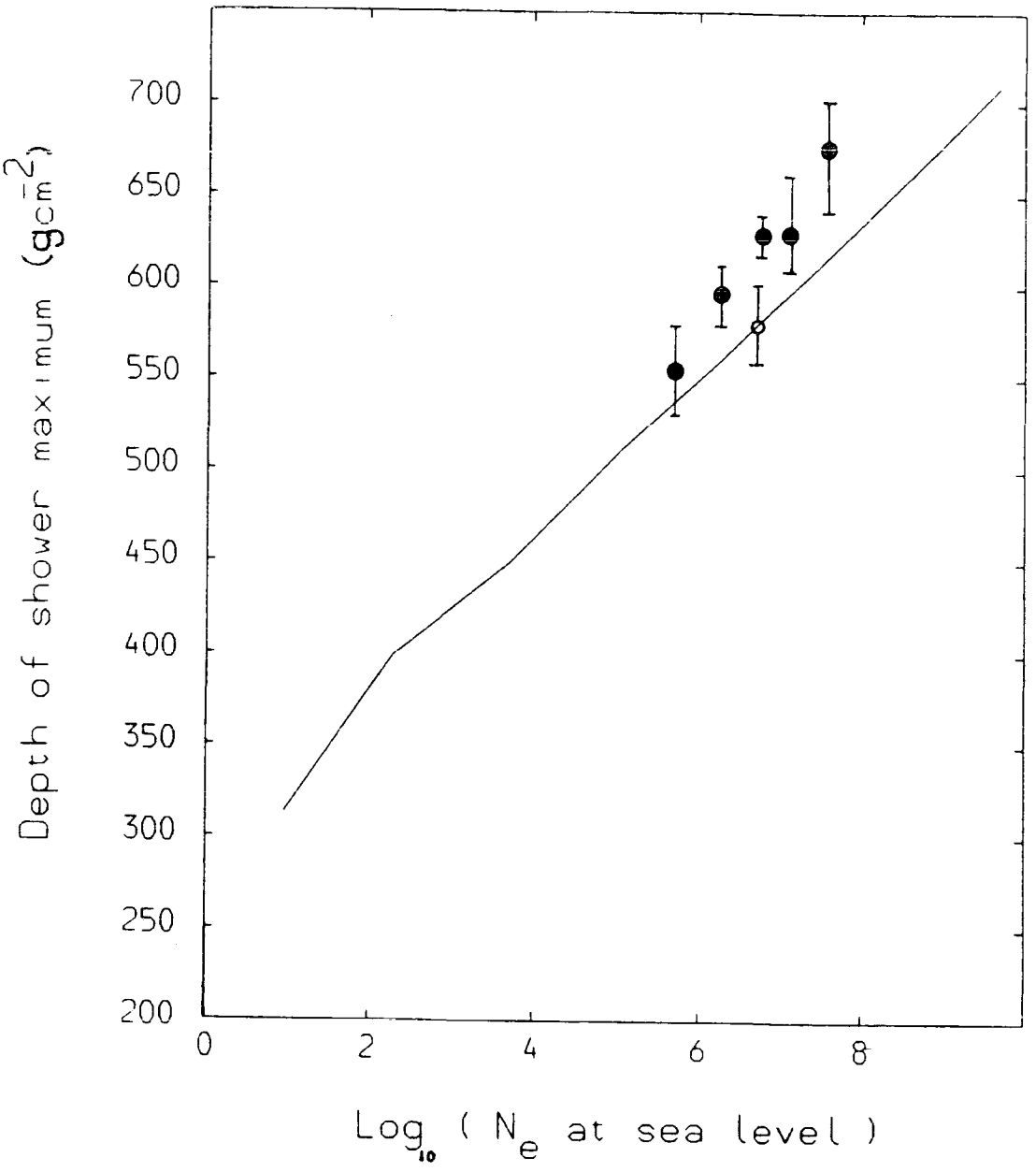

Figure 6.22: The depth of shower size maximum as a function of shower size at sea level. It is the depth at which the avearge longitudinal development of electron number reaches its maximum. Experimental points, due to Inoue et al.(1985) are plotted with the present simulation result.

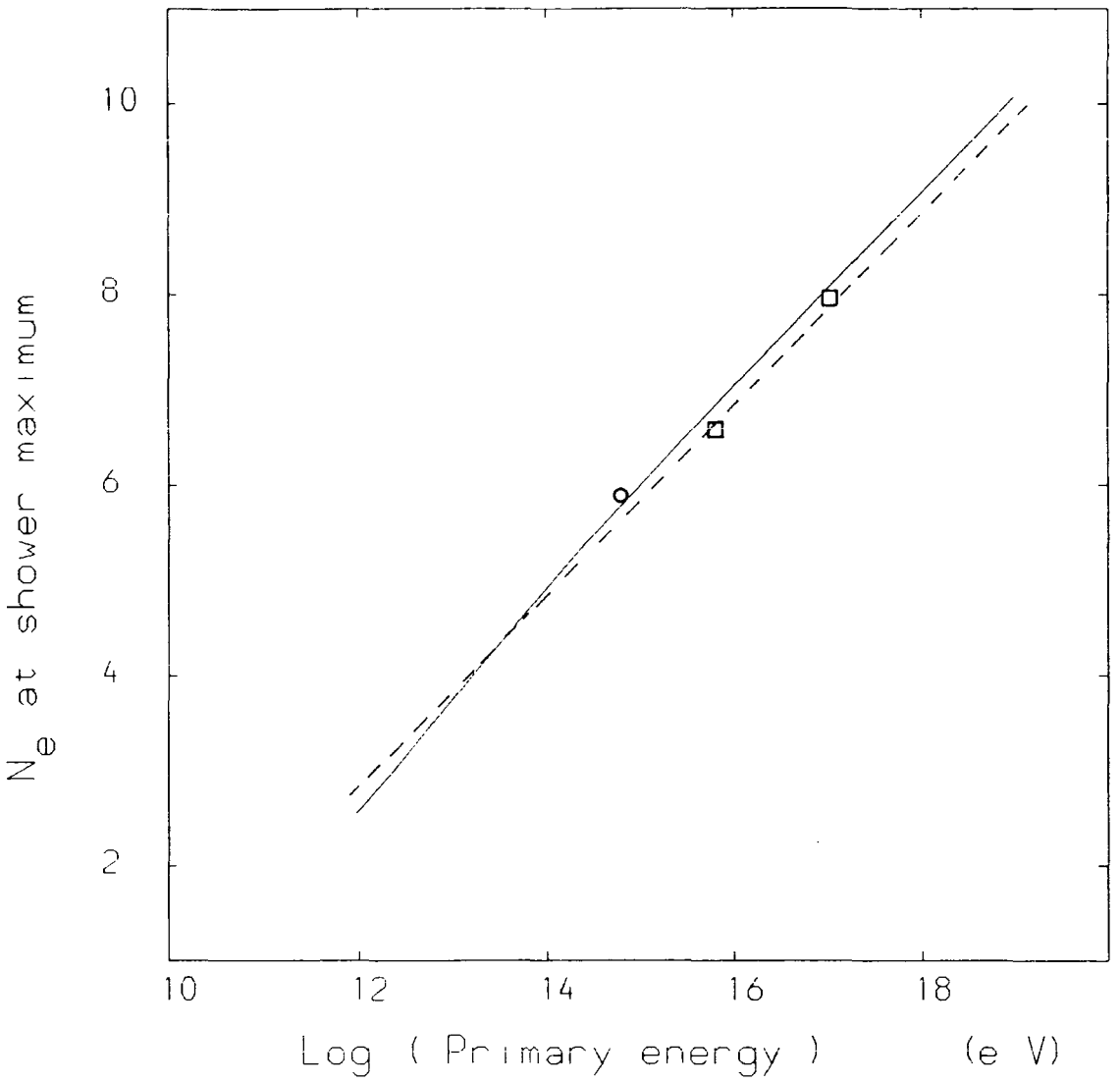

Figure 6.23: The shower size at the maximum of development curve represents the average behaviour of 1000 simulated showers (MC007), as a function of the primary energy. The dashed line is $N_e = E_p / 1.4$ with E_p in GeV as La Pointe (1968) suggested. The circle is derived from Nikolski (1962) and the squares are from Hillas (1972).

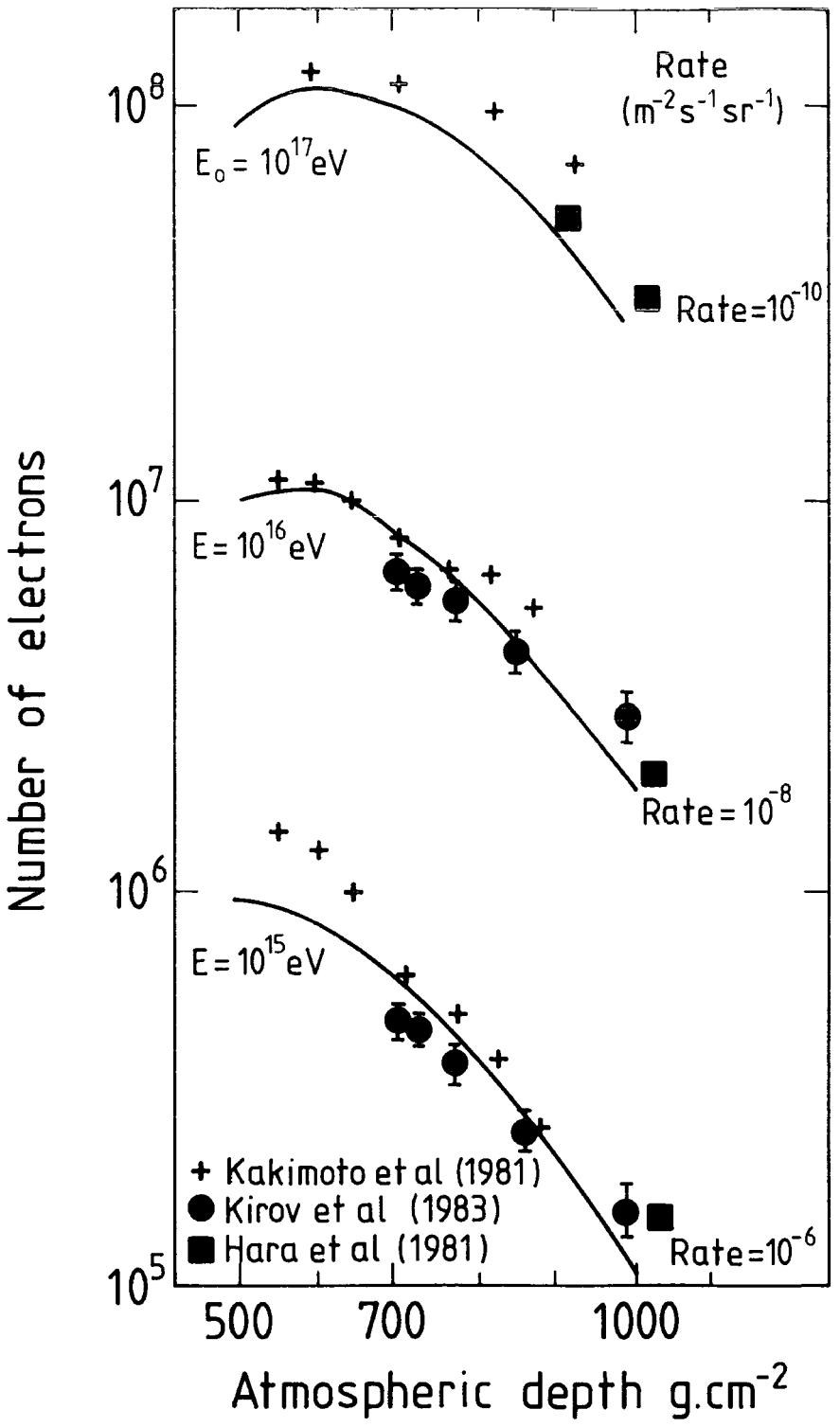

Figure 6.24: The shower size as it propagates through the atmosphere. The curves represent the simulation carried out by MC007 and the primary energy of each is written on each curve. The experimental data is plotted, but for given rate rather than primary energy.

Chapter Seven

Derivation of the primary energy spectrum from the sea level number spectrum

In Chapter 4 (Figure 4.18) an estimate was obtained for the integral size spectrum measured in the zenith direction from the measured sea level density spectrum. Using the relation between primary energy and average number of electrons arriving at sea level found by Monte Carlo calculation (Figure 6.20 of Chapter 6) an estimate has been made of the integral primary energy spectrum in the range 10^{14}-10^{16}eV. In Figure 7.1 the result is compared with the survey of Kempa et al (1974) where it is seen that the present result does not support the existence of a 'bump' supposedly produced by primary particles accelerated by pulsars in the energy range 10^{14}-10^{15}eV. However it should be noted that the Monte Carlo calculation carried out by the author assumed constant inelastic interaction lengths of 80 g cm^{-2} and 120 g cm^{-2} for the interaction of nucleons and pions with air nuclei. In fact both of these interaction lengthes decrease with increasing energy for $E > 10^{12}$ eV and the effect of this would be to decrease somewhat the expected average number of electrons at sea level produced by primary protons of a given energy. Such calculations need carrying out before the sea level number spectrum can be confidently related to the primary proton spectrum.

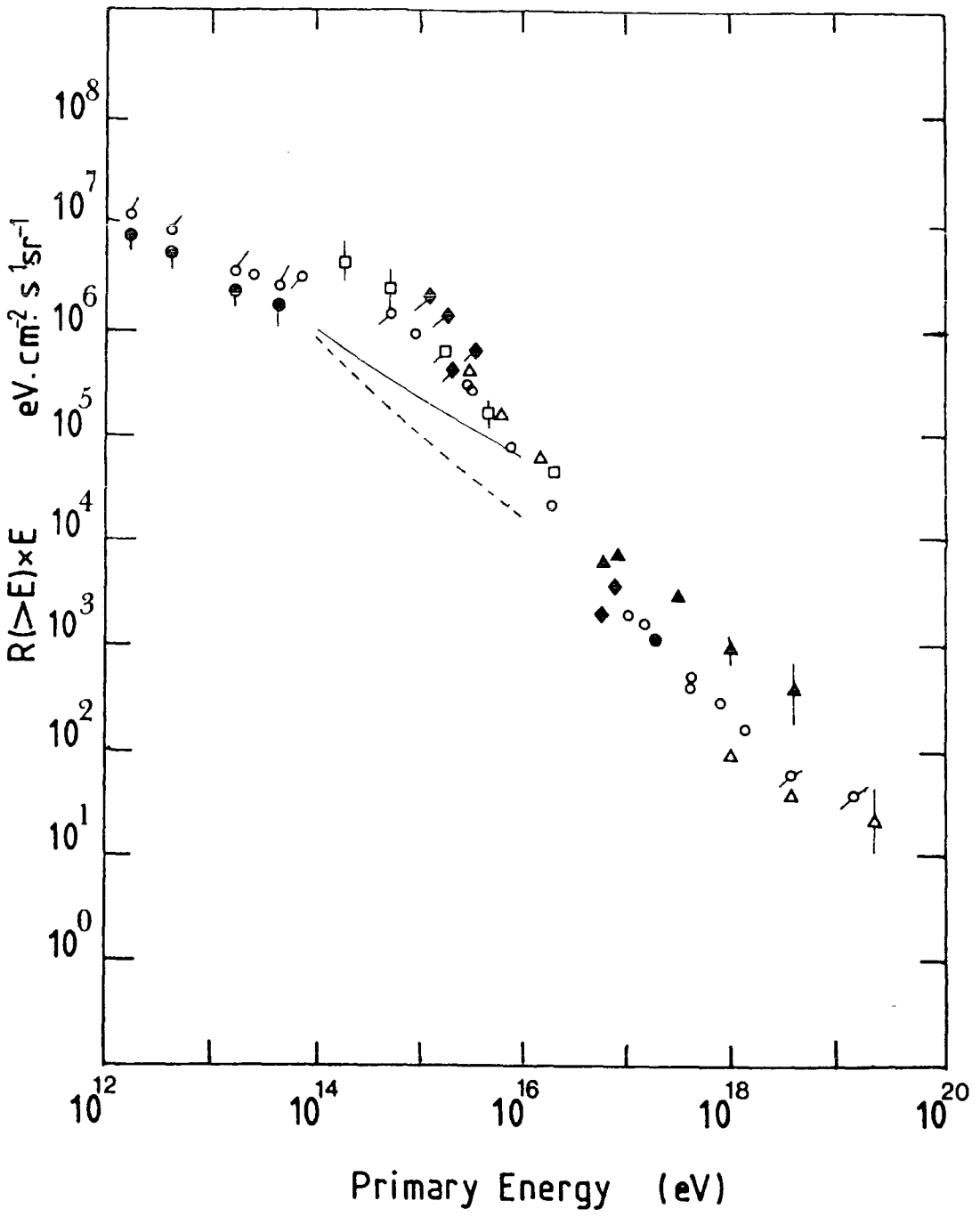

Figure 7.1: The primary energy spectrum derived from size spectrum obtained from the density spectrum measured by the author in the extperiment discussed in Chapter 4 (see Figure 4.18). the solid curve is the energy spectrum derived from the size spectrum which was obtained by scaling to work done by Ashton et al (1975), and the dashed curve is derived form the size spectrum obtained from the measured density spectrum by the program MC.DENSITY01 which simulates the experiment. The experimental data is the survey by Kempa et al (1974).

Chapter Eight

Conclusion

A computerised 8-channel data acquisition unit constructed by the Durham University Microprocessor Unit has been used successfully to record scintillation counter pulse heights with decay times of a few microseconds. This has been found to be a considerable improvement on the previous technique of photographing pulses displayed on an oscilloscope sweep using the appropriate number of delay lines even though precise pulse shape information is not available. Using two scintillation counters each of area 0.4 m^2 in coincidence, the integral density spectrum of electrons at sea level over the density range $20m^{-2}$ to $600m^{-2}$ has been measured. The result has been used to calculate the integral number spectrum of extensive air showers in the zeinth direction over the size range 10^4- $5x10^5$ particles at sea level. To interpret this result Monte Carlo calculations have been carried out to determine the relationship between the average number of particles at sea level produced by primary protons of a given energy. Knowing this relationship the sea level integral size spectrum has been converted into an integral primary energy spectrum. No evidence for a bump in the primary energy spectrum in the energy range 10^{14}-10^{15} eV has been found.

Appendix A

Electronics

Circuit diagrams for the electronics units used for experiments described are shown in this appendix. Unless otherwise stated all values of resistance are quoted in KΩ, all values of capacitance are quoted in μF, and all transistors used were of the type OC171.

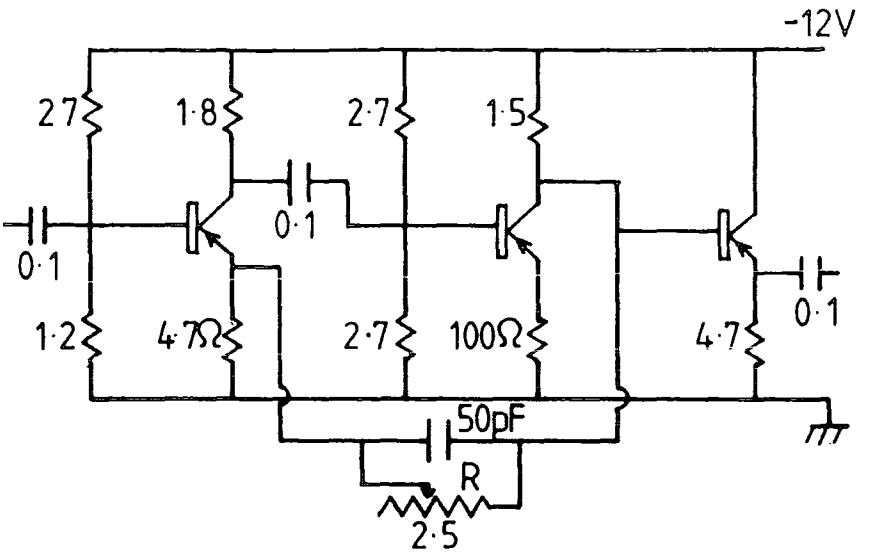

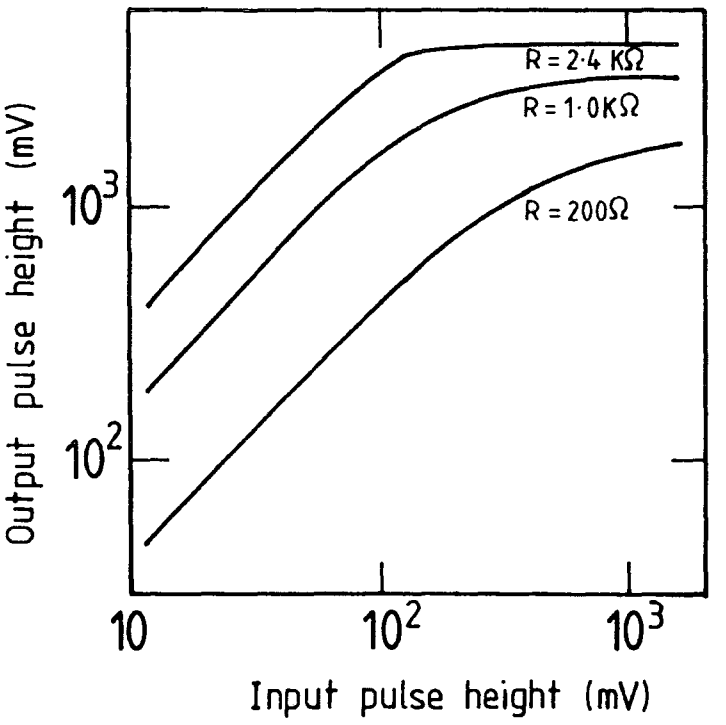

Figure A.1: The Voltage amplifier and its characteristics for various values of feedback resistance, R.

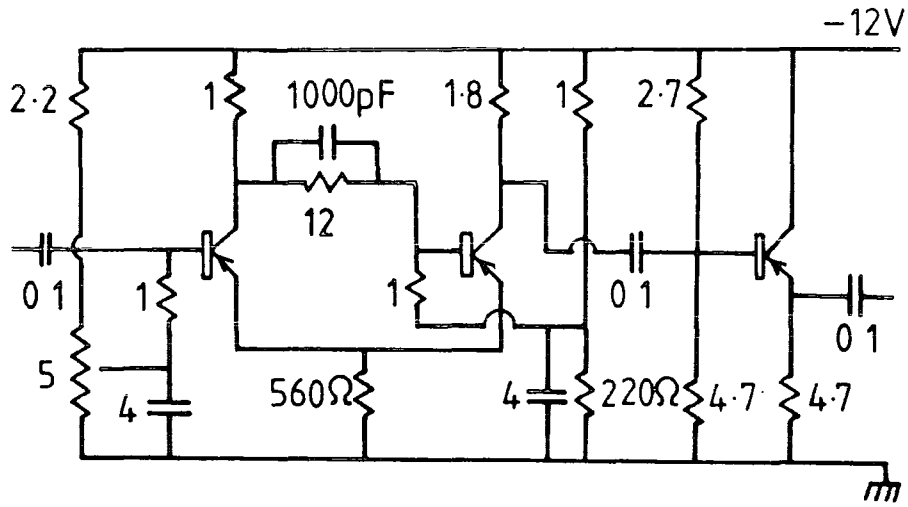

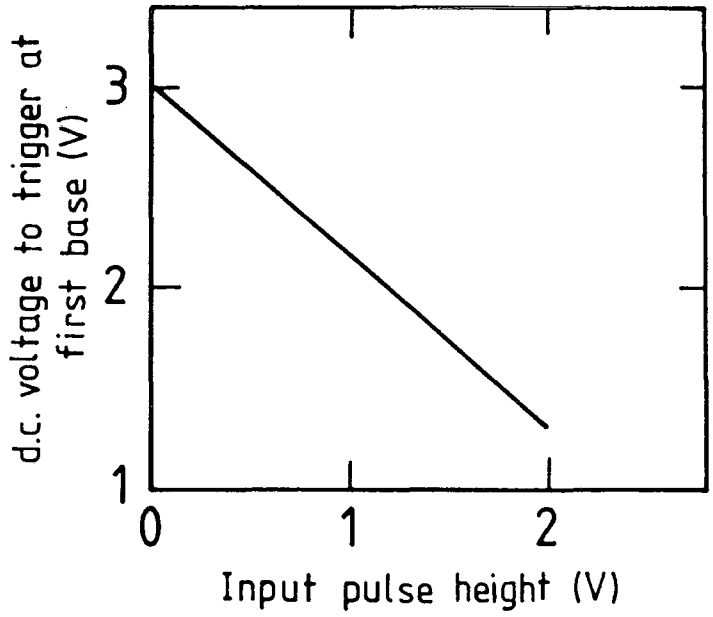

Figure A.2: The discriminator circuit and its relationship between the d.c. level on the first transistor and the minimum input pulse height required to trigger the circuit.

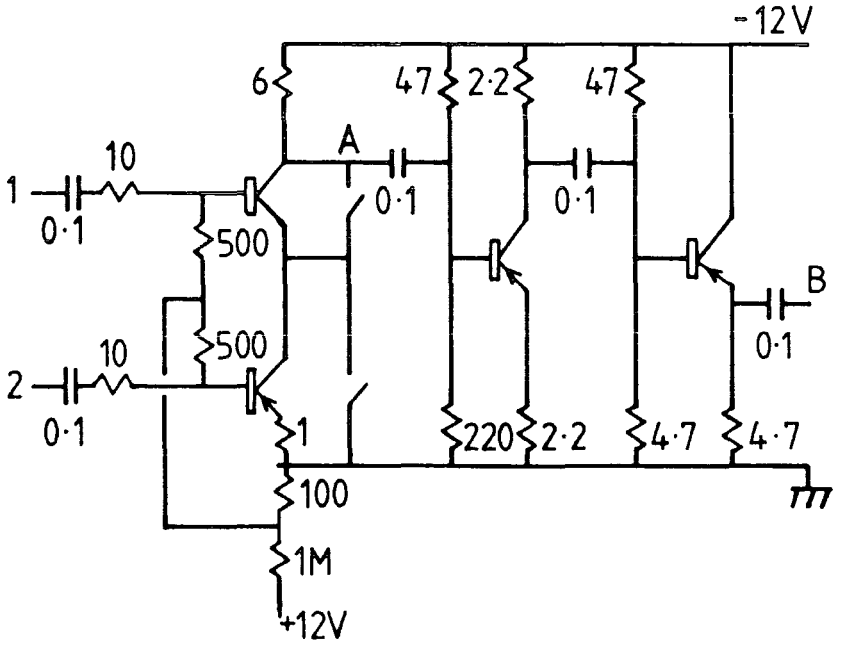

	Input from Discrimination	Output at A		Output at B		
		1 fold	2 fold	1 fold	2 fold	pulse width
Channel 1	-5V	+0·15V	+5·4V	-0·05V	-4·1V	1μs
Channel 2	-5V	+0·02		-0·04		1μs

Figure A.3: A twofold coincidence unit.

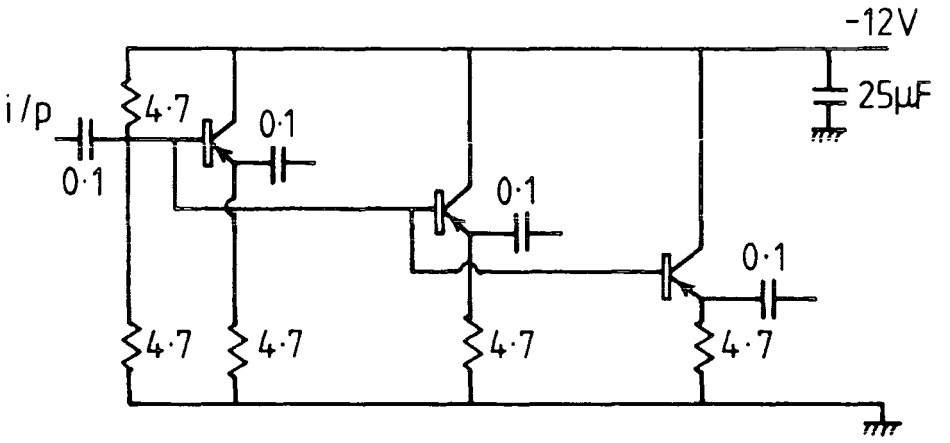

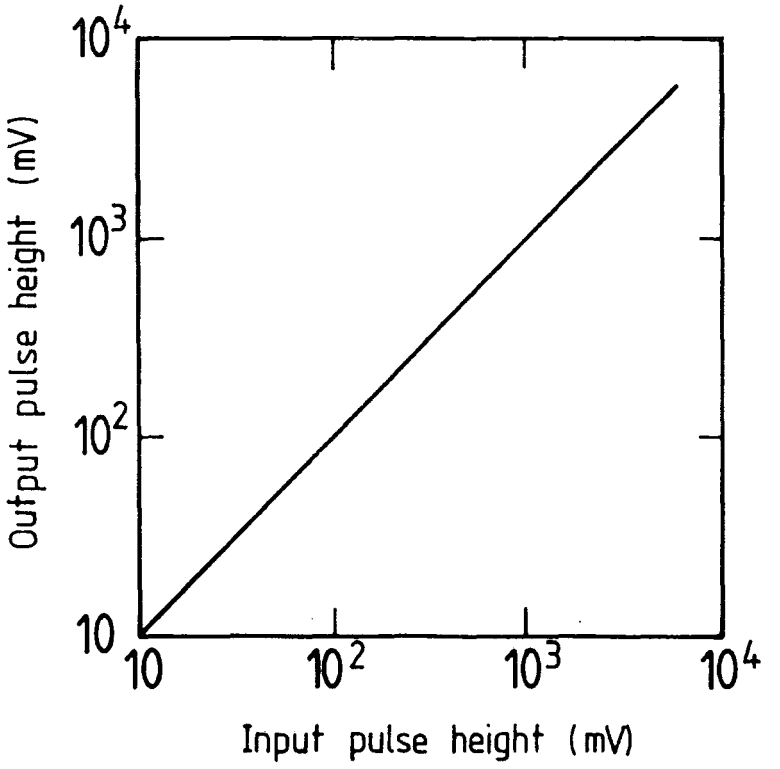

Figure A.4: The fan-out and its input-output characteristics.

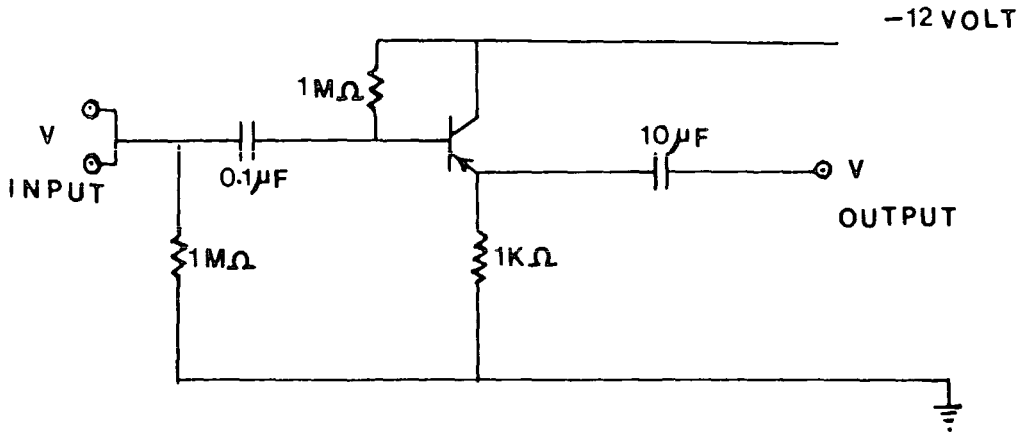

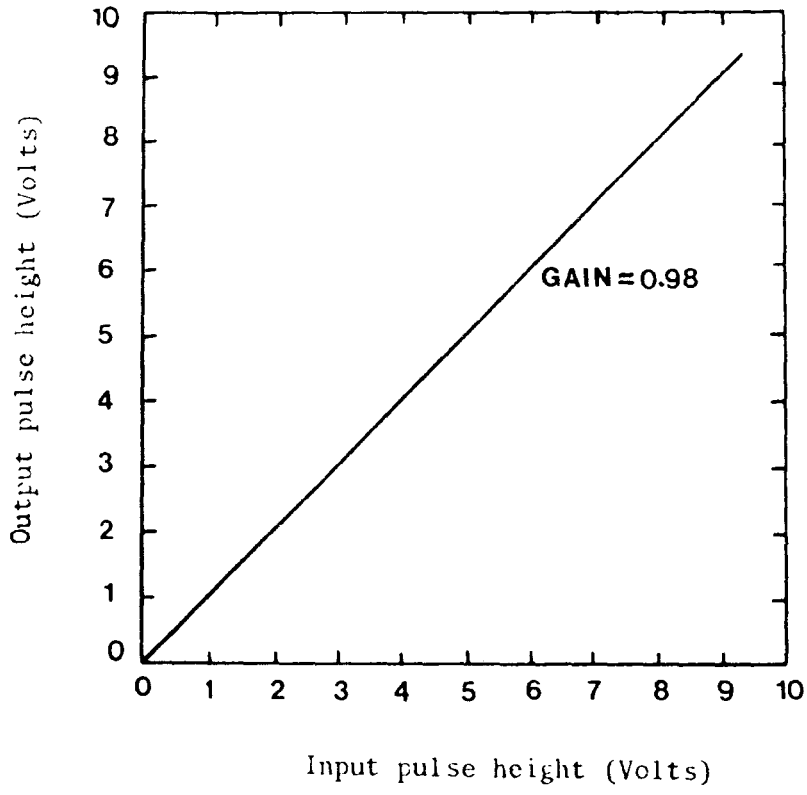

Figure A.5: Circuit diagram and response of head unit.

Appendix B

List of the program CALIBRATION

```
      CCCCCCCCCCCCCCCCCCCCCCCCCCCCCCCCCCCCCCCCCCCCCCCCCCCCCCCCCCCCCCCCCCCC
      C                                                                    C
      C                          CALIBRATION                               C
      C     This program reads the value of the pulse hieghs as were      C
      C     read by PET, and then corrects them.                           C
      C                                                                    C
      CCCCCCCCCCCCCCCCCCCCCCCCCCCCCCCCCCCCCCCCCCCCCCCCCCCCCCCCCCCCCCCCCCCC
            DIMENSION X(11),Y(11)
            DATA X/40.,70.,80.,100.,120.,150.,200.,250.,300.,350.,400./
            DATA Y/25.,30.,35.,45.,60.,105.,190.,295.,435.,500.,670./
       100  FORMAT(3F10.2)
      CCCCCCCCCCCCCCCCCCCCCCCCCCCCCCCCCCCCCCCCCCCCCCCCCCCCCCCCCCCCCCCCCCCC
        50   READ (5,100) A,B,C
             IF(A .EQ. 0.0) GOTO 50
      CCC  A  CCC
             IF(A .EQ. 9999.9) GOTO 999
             IF(A .GT. 7345.) GOTO 110
             IF(A .GE. 500. ) GOTO 120
             DO 105 J=1,10
             IF(A .EQ. Y(J)) GOTO 130
             IF(A .GT. Y(J) .AND. A .LT. Y(J+1)) GOTO 140
       105   CONTINUE
       110   AC= - A
             GOTO 200
       120   AC=(A+486.39)/2.7826
             GOTO 200
       130   AC=X(J)
             GOTO 200
       140   S=(Y(J)-Y(J+1))/(X(J)-X(J+1))
             YO=Y(J)-S*X(J)
             AC=(A-YO)/S
       200   CONTINUE
      CCC  B   CCC
             IF (B .GT. 7345.) GOTO 210
             IF (B .GE. 500. ) GOTO 220
             DO 205 J=1,10
             IF (B .EQ. Y(J) ) GOTO 230
             IF (B .GT. Y(J) .AND. B .LT. Y(J+1)) GOTO 240
       205   CONTINUE
       210   BC=-B
             GOTO 300
       220   BC=(B+486.39)/ 2.7826
             GOTO 300
       230   BC = X(J)
             GOTO 300
       240   S=(Y(J)-Y(J+1)) / (X(J)-X(J+1))
             YO=Y(J) - S*X(J)
             BC=(B-YO)/S
       300   CONTINUE
```

```
50      CCC   C   CCCCCCCCCCCCCCCCCCCCCC
51            IF (C .GT. 150.0 ) GOTO  330
52            CC = ( C/ 0.0855) ** ( 1. / 1.452 )
53            GOTO 400
54       330  IF (C .GT. 5400.0) GOTO 340
55            CC = (5.5 / 14.0) * (C + 360.)
56            GOTO 400
57       340  CC   = -1 * C
58       400  CONTINUE
59      CCCCCCCCCCCCCCCCCCCCCCCCCCCCCCCCCCCCCCCCCCC
60              WRITE(6,100)CA,CB,CC
61            GOTO 50
62      CCCCCCCCCCCCCCCCCCCCCCCCCCCCCCC
63      999     A=9999.9
64              WRITE(6,100)A,A,A
65               STOP
66                END
```

Appendix C

List of the program INTGDST04

```
      CCCCCCCCCCCCCCCCCCCCCCCCCCCCCCCCCCCCCCCCCCCCCCCCCCCCCCCCCCCCCCC
      C                                                               C
      C                          INTGDST04                            C
      C  This program reads corrected readings in terms of            C
      C density of particles on scint. A & B, and produces            C
      C the density integral distrbution.                             C
      C                                                               C
      CCCCCCCCCCCCCCCCCCCCCCCCCCCCCCCCCCCCCCCCCCCCCCCCCCCCCCCCCCCCCCC
            DIMENSION DELTA(19)
            DIMENSION A(1000),B(1000)
            INTEGER DELTA
            DATA DELTA/10,20,30,40,50,60,70,80,100,120,140,160,180
           $,200,240,300,340,400,500/
      C*************************************************************
            I=1
      50    READ(5,75)A(I),B(I)
      75    FORMAT(2F10.2)
            IF (A(I) .EQ. 9999.9) GOTO 80
            IF (A(I) .LT. 0.0 ) A(I)=2000.0
            IF (B(I) .LT. 0.0 ) B(I)=2000.0
            I=I+1
            GOTO 50
      80    N=I-1
      C*************************************************************
            KSUM=0
            WRITE(6,99)
      99    FORMAT(22HDELTA   COUNTS > DELTA)
      C*************************************************************
      C
            DO 200 I=1,17
      C
               DO 100 J=1,N
                  IF (A(J) .LT. DELTA(I) ) GOTO 100
                  IF (B(J) .LT. DELTA(I) ) GOTO 100
                  KSUM=KSUM + 1
      100      CONTINUE
      C
            WRITE (6,177) DELTA(I) , KSUM
      177   FORMAT(I4,5X,I4)
            KSUM = 0
      200   CONTINUE
      C*************************************************************
            STOP
            END
```

APPENDIX D

Generating individual sample from a given distribution using random numbers with a flat distribution

Suppose a source of random numbers x with a flat distribution is available, the random numbers being unformly distributed in range 0 to 1.

Consider an exponential distribution $f(y)=\frac{1}{k}e^{-(y/k)}$ which is normalised to unity $\int_0^\infty f(y)\,dy = 1$

In principle the following device works. Equate the cumulative probability distribution F(y) of the distribution f(y) to the cumulative probability distribution of a flat distribution and solve for y (Hamming 1973 page 142).

Cumulative probability distribution of normalised flat distribution is

$$\int_0^x 1 \,.\, dx = [x]_0^x = x \qquad (1)$$

Cumulative probability distribution of normalised exponential distribution is

$$\int_0^y \frac{1}{k} e^{-(y/k)}\, dy = \frac{1}{k}\left[\frac{e^{-(y/k)}}{-(1/k)}\right]_0^y = 1 - e^{-(y/k)} \qquad (2)$$

Equating (1) and (2) $\quad x = 1 - e^{-(y/k)}$

$$y = - k \ln(1-x) \qquad (3)$$

As x is a random number uniformaly distributed betwen 0 and 1, (1-x) will be a random number uniformly distributed between 0 and 1. An equally good method to (3) for sampling numbers from an exponential distribution, is to write

$$y = - k \ln x \qquad \text{Q.E.D.}$$

REFERENCES

(PICCR = Proceeding of International Confernce of Cosmic Rays)

Alexeenko, V.V., et al (1981), PICCR, Paris, **2**, 146-49

Aliev, et al (1985), PICCR, La Jolla, **7**, 191

Allkofer, O.C., et al (1970),Proc. 16 Interamerican Seminar on cosmic rays (universidad Mayor de San Anders),**6**,1930

Alvarez, L.W. and Compton, A.H. (1933), Phys. Rev., **43**,835

Anderson, C.D. (1933), Phys. Rev.,**43**, 491-494

Anderson, C.D. and Neddermeyer, S. (1938), Phys. rev., **54**, 88

Antonov, R.A. et al (1985), PICCR, La Jolla,**7**, 52

Ashton, F. et al (1972), Nuovo. Cim., **9B**, 344-350

Ashton, F. and Parvaresh, A. (1975), PICCR, Munich, **8**, 2719-2724

Ashton, F. et al (1979), PICCR, Kyoto, **13**, 243

Ashton, F. et al (1983), PICCR, Bangalore, **9**, 428-431

Auger,P. & Ehrenfest, P. Jr. (1937), J. de Physique,**8**,204-206

Aurela, A.M. and Wolfendale, A.W. (1967), Ann. Acad. Sci. Fenn. **A6**, 226

Ayre, C.A. et al (1971), J.Phys. A:Gen Phys.**4**,L89

de Beer J.F. et al (1966), Proc. Phys. Soc.,**89**, 567

Bjorklund R. et al (1950), Phys. Rev., **77**, 213-218

Bhabha, H.J. and Heitler, W. (1937), Proc. Roy. Soc. **A159**, 432

Capdevielle, J.N. and Gawin J. (1985), PICCR, La Jolla, **7**, 20

Carlson, J.F. and Oppenheimer, J.R. (1937), Phys. Rev. **51**, 220

Carlson A.G. et al (1950), Phil Mag., **41**, 701-724

Catz, Ph. et al (1975), PICCR, Munich, **12**, 4329.

Cheney, W. and Kincaid, D. (1980), "Numerical Mathematics and Computing", Brooks/Cole.

Crookes, J.N. and Rastin, B. (1971), PICCR, Tasmania, **4**, 1325.

Crouch, P.C. et al (1981), Nucl. Instr. and Meth., **179**, 467

Dixon, H.E., et al (1974), Proc. Roy. Soc. London, A, **337**, 133

Dzikowski, T. et al (1983), PICCR, Bangalore, **2**, 132-135

Efimov, N.N. et al (1983), PICCR, Bangalore, **6**, 176-179

Euler, H. and Heisenberg, W. (1938) Ergeb.d.exakt. Naturwiss, **17**, 1

Fermi, E. (1949a), Phys.Rev., **75**, 1196-1174

Fermi, E. (1949b), "Nuclear Physics", Chicago University Press.

Garciz-Munoz, M., et al (1977). Astrophysics J., **217**, 859

Gemesy, T., et al (1964), Nukleonika, **9**, 365

Greisen, K.I. (1942), Phys.Rev., **61**, 212-219

Greisen, K.I. (1956), "Prog. in Cosmic ray Physics",Vol. **III**, (Amesterdam: North Holland), p. 1

Greisen, K.I. (1960), Ann. Rev. Nucl. Sci., **10**, 63

Greisen, K.I. (1966), Phys.Rev. letters, **16**, 748-751

Grigorov, N.L. et al (1970) Sov. J.Nucl. Phys., **11**, 588

Hamming, R.W. (1973), "Numerical Methods for Scientists and Engineers", McGraw-Hill

Hara, T. et al (1981), PICCR, Paris,**11**,250

Hayashida, N., et al (1981), PICCR, Paris, **9**, 9-12

Heitler, W. (1948), "Quantum Theory of radiation", Oxford University Press.

Hess V.F. (1912) Physik Zeits.,**13**,1084, also (1913) Phys Zeits.,**14**,610

Hillas, A.M. (1970) Acta. Phys. Hung., **29**, Suppl.**3**, 355

Hillas, A.M. (1972) "Cosmic Rays", Pergamon Press

Hillas, A.M. (1979), PICCR, Kyoto, **8**, 7

Hillas, A.M. (1984), Ann. Rev. Astron. Astrophys., **22**, 425-444

Inoue, N. et al (1985), J. Phys. G: Nucl Phys., **11**,657-668

Johnson, T.H. (1933), Phys.Rev., **43**, 834

Kakimoto, F. et al (1981), PICCR, Paris,**11**, 254

Kempa, J. et al (1974), J. phys. A, **7**,1213.

Kempa, J. (1976), Nuov. cim., **31A**, 568

Khristiansen G.B. et al (1983), PICCR, Bangalore, **11**, 391-393

Kirov, I.N. et al (1983), PICCR, Bangalore, **6**, 15

Knuth, D.E. (1981),"The Art of Computer Programming, Vol.2", Addison Wesley.

Kolhorster, W. (1914), Deutsch. Phys. Gesell. Verh. **16**,719

Lambert, A., et al (1983), PICCR, Banglore, **9**, 219

LaPointe, M. et al (1968), Can. J. Phys., **46**,S68.

Lattes et el C.M.G (1947), Nature, **159**, 694

Longair, M.S. (1981), "High Energy Astrophysics", Cambridge

Lund, N. (1984), Adv. space Res., **4**, No. 2-3, 5-14

Luorui, S. and Winn, M.M. (1984), Nucl. Instr. and Meth. **223**, 173-179

MacKeown, P.K & Weekes, T.C. (1985), Scientific Am., Nov., **253**, No.5, 40-49

McCaugha, J.B.J. et al (1965), PICCR, London, **2**,720

Messel, H. and Grawford, D.F. (1970), "Electron-Photon Shower Distribution Function", (Pergamon Press).

Millikan, R.A. and Cameron G.H. (1926) Phys. Rev. **28**, 851

Nikolski S.I. (1963) Soviet USP., **5**, 849, sited Parvaresh (1975)

Nishimura, J. and Kamata, K. (1952), Prog. Theo. Phys., **1**,185

Nishimura, J. and Kamata, K. (1958), J.Suppl. Prog. Theo. Phys., **6**, 93

Norman, R.J. (1956), Proc. Phys. Soc., **69A**, 804

Parvaresh, A. (1975), Ph.D Thesis, Durham University.

Prescott, J.R. (1956), Proc. Phys. Soc.,**69A**, 870

Rochester, G.D. and Butler, C.C. (1947) Nature, **160**, 855

Reid, R.J. et al (1961), Proc. Phys. Soc., **78**, 103

Reid, R.J. (1962), J. Phys. Soc. Japan,**AIII**, Suppl.,**17**,234

Rossi, B. and Greisen,K.(1942),Phys.Rev.,**61**,121

Rossi. B. (1948), Rev. Mod. Phys.,**20**, 537-583

Rossi, B. (1952), "High energy particles", New York; Prentice-Hall.

Samorski M. and Stamm W. (1983), Ap. J. Lett. **268**,L17-22

Skobelzyn, D. (1929) Z. Phys., **54**, 686

Street, J.C. and Stevenson, E.C. (1937) Phys. Rev., **52**, 1003

Watson, A.A. (1984), Adv. Space Res. **4**, No. 2-3, 35-44.

Watson, A.A. (1986), Sci. Prog. Oxf. **70**, 1-5

Wdowlzyk, J. And Wolfendale, A.W. (1979), PICCR, Kyoto, **2**, 154

Webber, W.R. and Quenby, J.J. (1959), Phil. Mag., **4**,654

Wolfendale, A.W. (1978), "Cosmic Ray Astrophysics",Univ. Hong Hong